Exploration of Anti-Malarial Chemical Space and Bisquinolines and Quinazoline Hybrids as Potential Anti-Tubercular and Anti-Malarial Agents

THESIS

Submitted in partial fulfilment of the requirements for the degree of

DOCTOR OF PHILOSOPHY

by

Amritansh Bhanot

ID. No. 2018PHXF0040P

Under the supervision of

Dr. Sandeep Sundriyal

BIRLA INSTITUTE OF TECHNOLOGY & SCIENCE, PILANI

Pilani Campus

Pilani 333031, Rajasthan, India

2023

BIRLA INSTITUTE OF TECHNOLOGY & SCIENCE, PILANI

CERTIFICATE

This is to certify that the thesis entitled **"Exploration of anti-malarial chemical space and bisquinolines and quinazoline hybrids as potential anti-tubercular and anti-malarial agents"** submitted by Amritansh Bhanot, ID No. **2018PHXF0040P**, for award of Ph.D degree of the Institute, embodies original work done by him under my supervision.

Signature (Supervisor):

Name (Supervisor): Dr. Sandeep Sundriyal

Designation: Assistant Professor
                    Department of Pharmacy
                    BITS Pilani, Pilani Campus

Date:

TABLE OF CONTENTS

Acknowledgments

Words fall short to express my gratitude to people who not only encouraged me during this rough patch of my life but also contributed both directly and indirectly to completing the thesis of my doctoral degree. To begin with, I shall thank my almighty for making me believe in myself and also always pushing me towards my extreme limits and right path. Next, I would like to thank my parents, **Mr. Narender Bhanot** and **Mrs. Mridula Bhanot** and my wife **Mrs. Jasleen Bhanot** for constantly persuading me in completing my thesis, giving me beneficial words of advice and bearing with me during my hard times. I thank them for trusting in me regarding all the decisions I have taken so far including joining PhD.

Next and most importantly, I am immensely thankful and grateful to my supervisor **Dr. Sandeep Sundriyal** for his guidance, trust, patience, and support. This PhD journey would not have been memorable, insightful and knowledgeable if it wasn't for my supervisor. I will remain forever indebted to the trust he bestowed upon me during the times when I had completely lost faith in myself.

I am grateful to **Prof. Sudhirkumar Barai,** Director, **Prof. V Ramgopal Rao,** Vice-Chancellor, BITS Pilani, and **Prof. A.K Sarkar,** Former-Director, BITS Pilani, Pilani Campus for permitting me to pursue my research work in the Institute. I also express my sincere thanks to **Prof. Shamik Chakraborty**, Associate Dean AGSRD, and **Prof. Jitendra Panwar**, former Associate Dean, AGSRD for their motivation, constant support and encouragement.

I am greatly thankful to my Doctoral approval committee (DAC) members **Prof. Hemant R. Jadhav** Professor, Department of Pharmacy and **Prof. S Murugesan** Associate Professor, Department of Pharmacy, Pilani Campus for their words of advice and suggestions and also for evaluating my thesis. I would like to acknowledge **Prof. Anil Jindal**, Convener and **Prof. Deepak Chitkara** former Convener, Departmental Research Committee, Department of Pharmacy, BITS Pilani, Pilani Campus for providing valuable comments.

A special vote of thanks to the head of the Department of Pharmacy, **Prof. Gaikwad Anil Bhanudas** who has constantly encouraged and motivated me during my PhD tenure. I am

LIST OF ABBREVIATIONS

Ar	Aromatic rings
3D7	Chloroquine sensitive plasmodium strain
ABC	ATP binding cassette
ACT	Artemisinin-based Combination Therapy
AMR	Antimicrobial resistance
AQ	Amodiaquine
ASAM	Advanced stage antimalarials
ATP	Adenosine triphosphate
BCG	Bacille Calmette-Guerin
BHCD	β-hematin crystal docking
BHIA	β-hematin inhibition assay
BLI	Biolayer Interferometry
BPaL	Bedaquiline, pretomanid, linezolid
BPaLM	BPaL regime + moxifloxacin
Clp	Caseinolytic protease
clogP	Calculated partition coefficient
CMI	Cell-mediated immune
CQ	Chloroquine
CQR	Chloroquine resistant
CQS	Chloroquine sensitive
CRISPR	Clustered regularly interspaced short palindromic repeats
CymA	Cyclomarin A
DAQ	Diaminoquinazoline
DCM	Dichloromethane
Dd2	Chloroquine resistant plasmodium strain
DIEA	N,N-Diisopropylethylamine
DILI	Drug-induced liver injury
DNA	Deoxyribonucleic acid
DNMT	DNA methyl transferase
DprE1	Decaprenylphosphoryl-β-d-ribose 2'-epimerase
DV	Digestive vacuole
EGFR	Endothelial growth factor receptor
ELISA	Enzyme linked immunosorbent assay
FDA	Food and Drug Administration
Fe^{3+}PPIX	Ferritoprotoporphyrin IX
FITC	Fluorescein isothiocyanate
Fsp^3	Fraction of sp3 carbon
G6PD	Glucose-6-phosphate dehydrogenase
GAPDH	Glyceraldehyde-3-phosphate dehydrogenase
GSH	Reduced glutathione
HA	Highly active
HAT	Histone acetyl transferase
HBA	Hydrogen bond acceptor
HBD	Hydrogen bond donor
HD	Heme docking studies
HDAC	Histone deacetylase

HEPES	4- (2-hydroxyethyl)-1-piperazineethanesulfonic acid
HIV	Human immunodeficiency virus
HKMT	Histone lysine methyl transferases
HPLC	High performance liquid chromatography
HRG	histidine-rich glycoprotein
HRP	Histidine Rich protein
HTS	High throughput screening
Hz	Hemozoin
IN	Inactive
IPTG	Isopropyl β-D-1-thiogalactopyranoside
IP	Ion pair
logD	Distribution coefficient
LAM	Lipoarabinomannan
MA	Moderately active
MDR	Multidrug resistant
MDR-TB	Multidrug resistant tuberculosis
MIC	Minimum inhibitory concentration
MM/GBSA	Molecular Mechanics/Generalized Born Surface Area
Mtb	*Mycobacterium tuberculosis*
MTDL	Multitarget-directed ligands
MTT	3-(4,5-dimethylthiazol-2-yl)-2,5-diphenyltetrazolium bromide
MW	Molecular weight
Ni-NTA	Nickel-nitriloacetic acid
NLD	Neutral lipid droplets
NMR	Nuclear magnetic resonance
NTD	N-terminal domain
ORF	Open reading frame
O-BHIA	Oxidized β-hematin inhibition assay
PCR	Polymerase chain reaction
***Pf*ATP4**	*P. falciparum* ATPase4
***Pf*CRT**	*P. falciparum* chloroquine resistance transporter
***Pf*GR**	*P. falciparum* glutathione reductase
***Pf*K13**	*P. falciparum* Kelch 13
PPD	Purified protein derivative
PPR	Pattern recognition receptors
PQ	Primaquine
Prx	1-Cys peroxiredoxin
PTM	Post-translational modifications
RAP	Research antiplasmodial
RB	Rotatable bonds
RBC	Red blood cells
R-BHIA	Reduced β-hematin inhibition assay
RHZE	Rifampin, isoniazid, pyrazinamide, and ethambutol
RMSD	Root mean square deviation
Ro5	Rule of five
RT	Retention time
SAHA	Suberoylanilidehydroxamic acid
SAR	Structure activity relationship
SDS	Sodium dodecyl sulfate

SNLD	Synthetic neutral lipid droplet
TB	Tuberculosis
TDR-TB	Totally drug-resistant tuberculosis
THF	Tetrahydrofuran
TLC	Thin layer chromatography
TLR	Toll-like receptors
TMV	Tobacco mosaic virus
TNF	Tumor necrosis factor
TPSA	Topological polar surface area
TrxR	Thioredoxin reductase
TV	Transport vesicle
WHO	World Health Organization
XDR-TB	Extensively drug-resistant tuberculosis

LIST OF FIGURES/SCHEMES

LIST OF TABLES

ABSTRACT

This thesis entitled "**Exploration of anti-malarial chemical space and bisquinolines and quinazoline hybrids as potential anti-tubercular and anti-malarial drugs**" has been divided into 5 chapters and discusses the potential of bisquinolines and quinazolines combined in the form of hybrids as novel antimalarial and antitubercular drugs. Chapter 1 consists of introduction to the diseases and the basis of our work. Chapter 2 explains the use of cheminformatics to explore novel antimalarials. Chapter 3 includes synthesis of hybrid compounds and their evaluation as antimalarial agents. Chapter 4 consists discusses synthesis of potent compounds that act against *Mycobacterium tuberculsosis* (Mtb) by targeting ClpC1.

In chapter 2, to understand the property space of antimalarials, we collated a large dataset of research antiplasmodial (RAP) molecules with known *in vitro* potencies and advanced stage antimalarials (ASAMs) with established oral bioavailability. While RAP molecules are "non-druglike", ASAM molecules display properties closer to Lipinski's and Veber's thresholds. Comparison within the different potency groups of RAP molecules indicates that the *in vitro* potency is positively correlated to the molecular weight, the calculated octanol-water partition coefficient (clog P), aromatic ring counts (#Ar), and hydrogen bond acceptors. Despite both categories being bioavailable, the ASAM molecules are relatively larger and more lipophilic, have a lower polar surface area, and possess a higher count of heteroaromatic rings than oral drugs. Also, antimalarials are found to have a higher proportion of aromatic (#ArN) and basic nitrogen (#BaN) counts, features implicitly used in the design of antimalarial molecules but not well studied hitherto. We also propose using descriptors scaled by the sum of #ArN and #BaN (SBAN) to define

an antimalarial property space. Together, these results may have important applications in the identification and optimization of future antimalarials.

The emergence of drug resistant strains against ACT the gold standard for treatment of malaria has caused alarming concern about the treatment options available. New drugs are required urgently, this warrants the design and synthesis of novel antimalarial agents active against multiple targets. To achieve this the most efficient strategy could be to combine known scaffolds active against malaria therefore combining quinazoline scaffold with other anti-malarial pharmacophores such as quinolines could yield potent anti-plasmodial agents active against resistant *Plasmodium* strains. Therefore, in chapter 3 a total of 29 compounds were synthesized and tested against artemisinin sensitive and resistant strains of plasmodium. To check the mechanism of action the compounds were tested against BHIA and these showed significant activity against the beta hematin pathway. The most potent compounds are AB123, AB103, AB205, AB68 and AB210.

The emergence of drug-resistant strains of *Mycobacterium tuberculosis* (Mtb), the causative agent of tuberculosis (TB) in humans, is a primary reason for treatment failure. Currently, only limited options are available for the management of multi-drug resistant TB, warranting the design of novel anti-TB drugs by exploiting newer targets. One of the caseinolytic protease (Clp) machinery components, an unfoldase known as ClpC1, has emerged as a distinct anti-TB drug target owing to its essential role in the pathogen's survival. The naturally occurring cyclic peptides targeting the Mtb ClpC1, exhibit potent antimycobacterial activity. However, the large, complex, and poor synthetic tractability of these peptides limit their clinical application. Identification of small molecule inhibitors of Mtb ClpC1 will be useful for future drug development. Here in chapter 4, we report the discovery of a bisquinoline chemotype from the screening of a small molecule chemical library against Mtb ClpC1. The hit molecule binds with ClpC1 and exhibits dose-

dependent inhibition of its enzymatic activity by direct binding. The *in vitro* growth of Mtb is inhibited by the hit molecule at a minimum inhibitory concentration of 12.5 μM. Investigation of the structure–activity relationship by chemical synthesis underlines the requirement of the two quinoline rings, 9/10 carbon linker, and the importance of basic ring nitrogen for its inhibitory activity. To our knowledge, this is the first report on the systematic analysis of small molecule inhibitors of Mtb ClpC1.

Chapter 1

Introduction

1.1 ANTIMICROBIALS AND ANTIMICROBIAL RESISTANCE

Antimicrobials are drugs used for the treatment of infections caused by parasites, viruses, bacteria, and fungi. These organisms stop responding to medications over time due to mutations. So, there is an increased risk of severe illness and disease spread by superbugs. This situation is termed as antimicrobial resistance (AMR).[1] The problem of AMR is exacerbated due to biological and chemical pollution caused due to human activities like manufacturing, improper disposal of unused or expired antimicrobials, unmetabolized antimicrobials excreted from urine and faeces, use of disinfectants, microplastics[2–8] and use of herbicides in agriculture contaminating soil and water (**Figure 1.1**).[1]
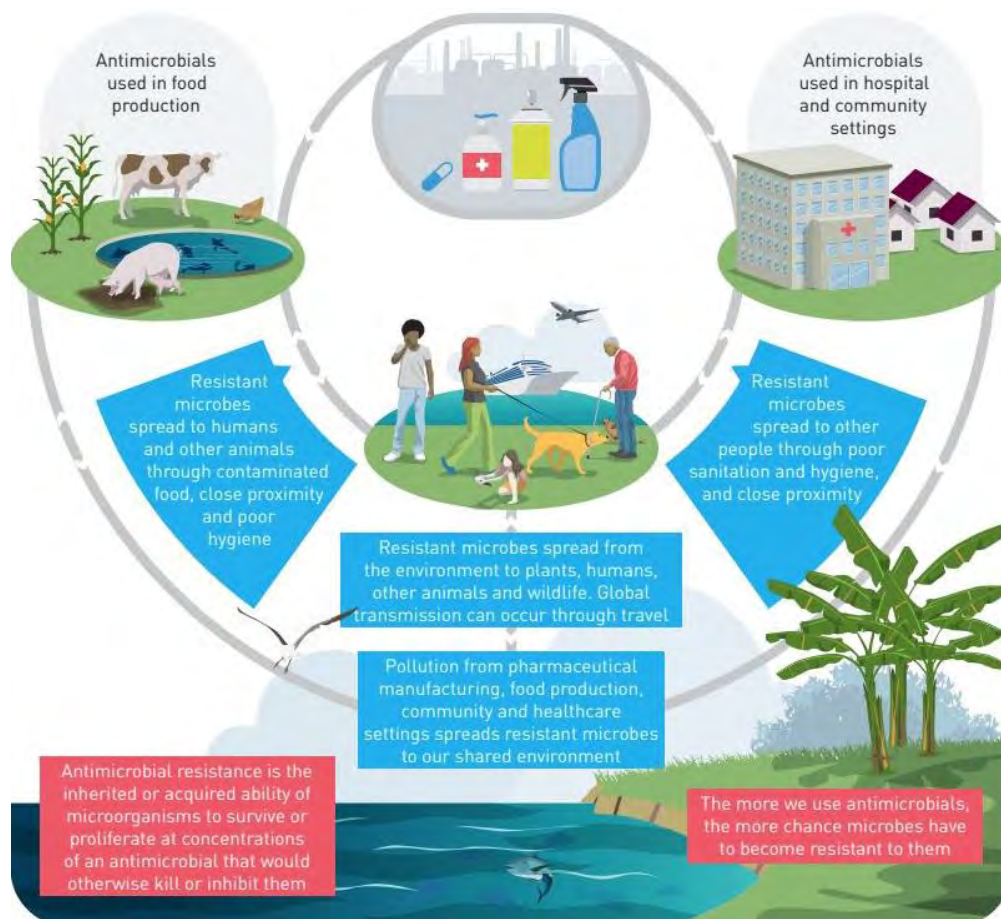
Figure 1.1. Spread of antimicrobial resistance[1]

Moreover, climate changes and excessive use of antimicrobials also contribute to increased AMR risk.[9–11] This is a global health concern manifested due to emergence of antibiotic

resistance gene through spontaneous mutations in microbes, horizontal gene transfer or transmission through mobile genetic elements. As per recent reports, it is estimated that AMR along with shortage of new antimicrobials in the pipeline may lead to approximately 10 million deaths by 2050 (**Figure 1.2**).[12,13] Moreover, it is predicted that Asia and Africa will be the most affected continents due to AMR (**Figure 1.3**).[14]
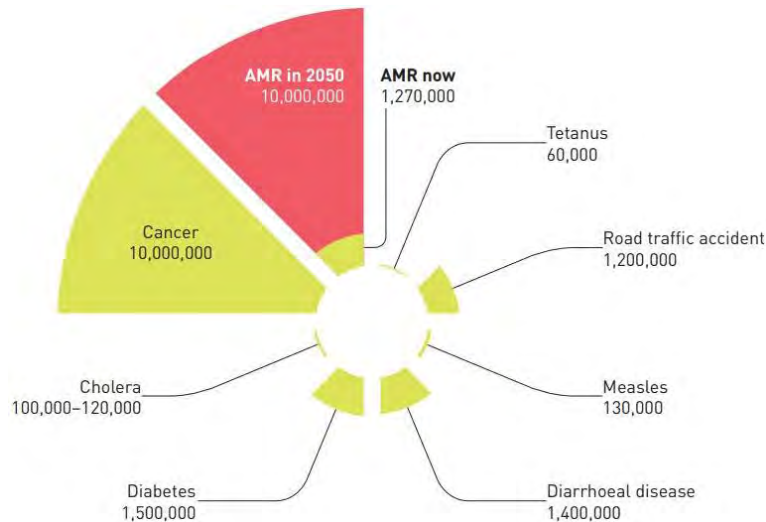
Figure 1.2. Predicted mortality due to AMR in comparison to other causes by year 2050[12,13]

Further, AMR could lead to a substantial economic impact resulting in extreme poverty by the next decade. Therefore, preventive measures are required to address the problem associated with AMR. In 2023, United Nations Environment Programme implemented the "One Health" approach, which recognizes that the health of humans, animals, plants, and the environment are interdependent.[1]
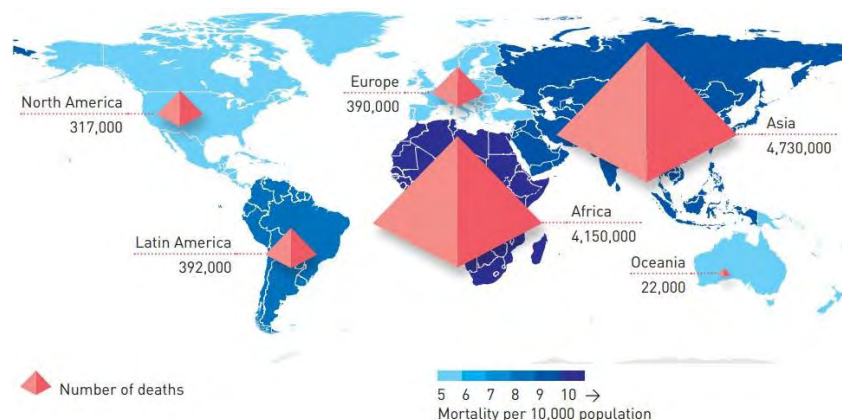
Figure 1.3. Deaths due to AMR predicted in 2050 around the globe[14]

Among all microbial infections, the most prevalent in the African and Indian subcontinent are malaria and tuberculosis (TB). Moreover, Artemisinin-combination therapy (ACT) the gold standard for treatment of malaria worldwide has also become ineffective due to emergence of resistance (**Figure 1.4**), which has led to increased morbidity and mortality. As per World Health Organization (WHO) reporting based on the studies conducted between 2001-2019, several ACT partner drugs have been rendered ineffective due to development of resistance in Cambodia, Lao People's Democratic Republic, Myanmar, Thailand and Vietnam. Furthermore, in some countries, development of resistance against sulfadoxine-pyrimethamine has also led to failure of artesunate-sulfadoxine-pyrimethamine combination. Important progress achieved in malaria control over years has been jeopardized due to the spread of resistance and further poses a major public health concern.[15]

Figure 1.4. Artemether-lumefantrine treatment failure to date globally

Besides, deaths attributable to resistance in TB are significantly higher when compared to other microbial diseases (**Figure 1.5**).[13] According to recent reports, there has been a sudden surge in the number of TB cases from the year 2020 to 2021, with around 3% increase in cases due to drug resistance.[16]
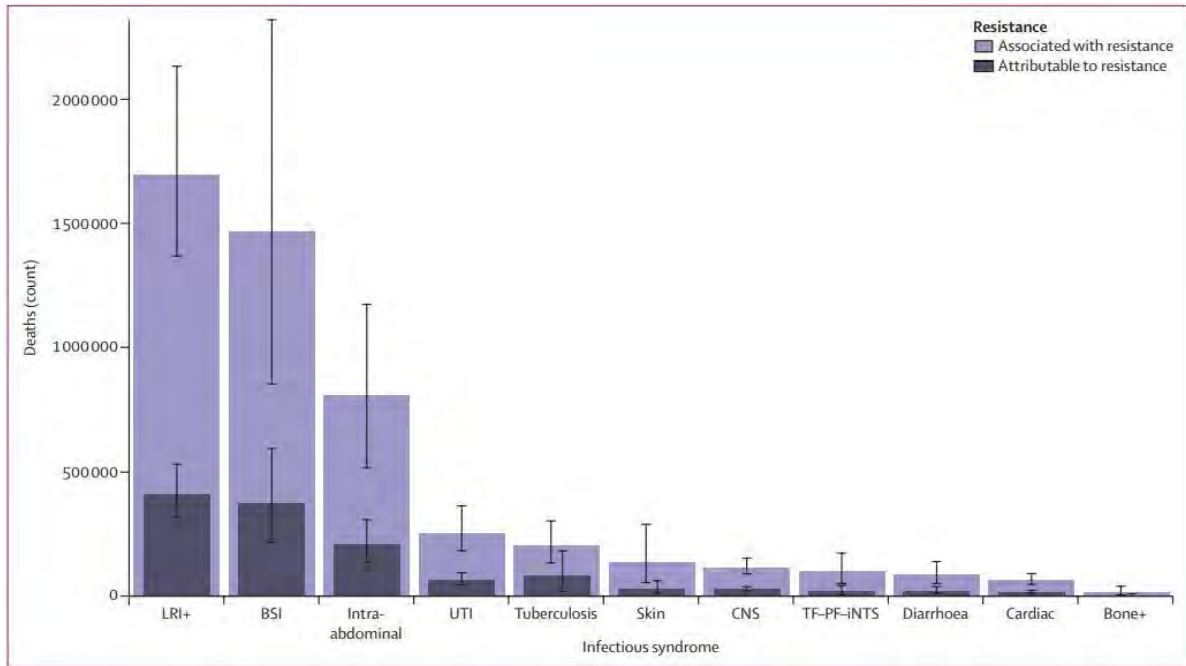
Figure 1.5. Number of deaths globally attributable to and associated with antimicrobial resistance in 2019. BSI: blood stream infections; cardiac: endocarditis and other cardiac infections; CNS: meningitis and other bacterial CNS infections; intra-abdominal: peritoneal and intra-abdominal infections; LRI+: lower respiratory infections and all related infections in the thorax; skin: bacterial infections of the skin and subcutaneous systems; TF-PF-iNTS: typhoid fever, paratyphoid fever, and invasive non-typhoidal *Salmonella spp.*; UTI: Urinary tract infections and pyelonephritis[1]

Antibiotic resistant Mtb strains have threatened the progress in containment of global TB epidemic. As per WHO estimates, around half a million new multidrug-resistant tuberculosis (MDR-TB) cases were globally identified in 2018. However, the majority of patients infected with MDR-TB went unreported. Moreover, only less than 60% of patients infected with MDR-TB could be cured successfully.[15]

Therefore, there is an urgent need to develop new drugs to combat the alarming situation of malaria and TB worldwide.

1.2 INTRODUCTION TO MALARIA

In Egyptian and Chinese writings dating back to 2700 B.C., malaria is depicted as an ancient human disease characterized by fatal periodic fevers and splenomegaly. Malaria had arrived in Rome around 200 B.C. and had engulfed Europe by the 12th century. By the 14th century, this malady had also spread to England. *Plasmodium malariae* and *Plasmodium vivax* were

believed to have been introduced to America by European explorers and colonists. By the early 1800s, malaria had expanded globally, coinciding with the importation of African slaves.[17] Malaria is endemic in more than 90 nations and affects more than 2.4 billion people.[18] According to the WHO, malaria is a life-threatening epidemic disease transmitted to humans by mosquitoes carrying *Plasmodium*, the malaria-causing parasite. *Plasmodium falciparum (P. falciparum), P. vivax, P. malariae, P. ovale,* and *P. knowlesi* are the five species that have the potential to cause malaria in humans.[18] However, *P. falciparum* and *P. vivax* pose the greatest hazard to humanity.

Dark or bloody urine

Extreme tiredness and fatigue

Difficulty breathing

Cerebral malaria, multiple convulsions, unconsciousness

Jaundice

Abnormal bleeding
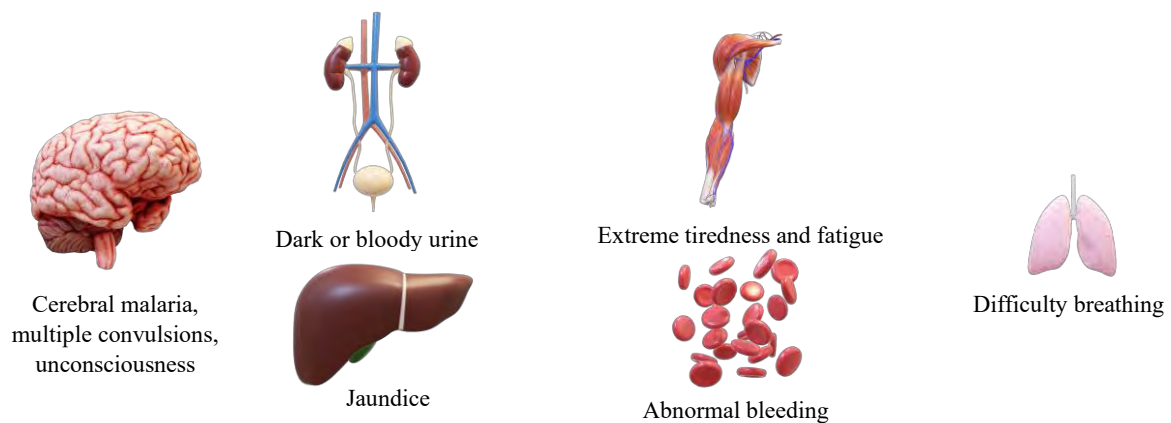
Figure 1.6. Severe symptoms of malaria

Malaria symptoms typically appear within 10 to 14 days of being bitten by an infected mosquito. The most prevalent initial symptoms of malaria are fever, headache, and chills. Symptoms vary in intensity from person to person. Some people may experience mild symptoms, particularly those who have had malaria before. Due to the possibility of non-specific symptoms, early testing is always advised. If not treated timely, malaria has been known to cause severe illness and death. In addition, infants, geriatric patients, expectant women, children under 5 years of age, and human immunodeficiency virus (HIV)-positive individuals are at a greater risk of contracting the disease's severe form, which manifests with symptoms such as dark or bloody urine, difficulty breathing, extreme tiredness and fatigue,

abnormal bleeding, jaundice, multiple convulsions, unconsciousness and cerebral malaria (**Figure 1.6**).[18]
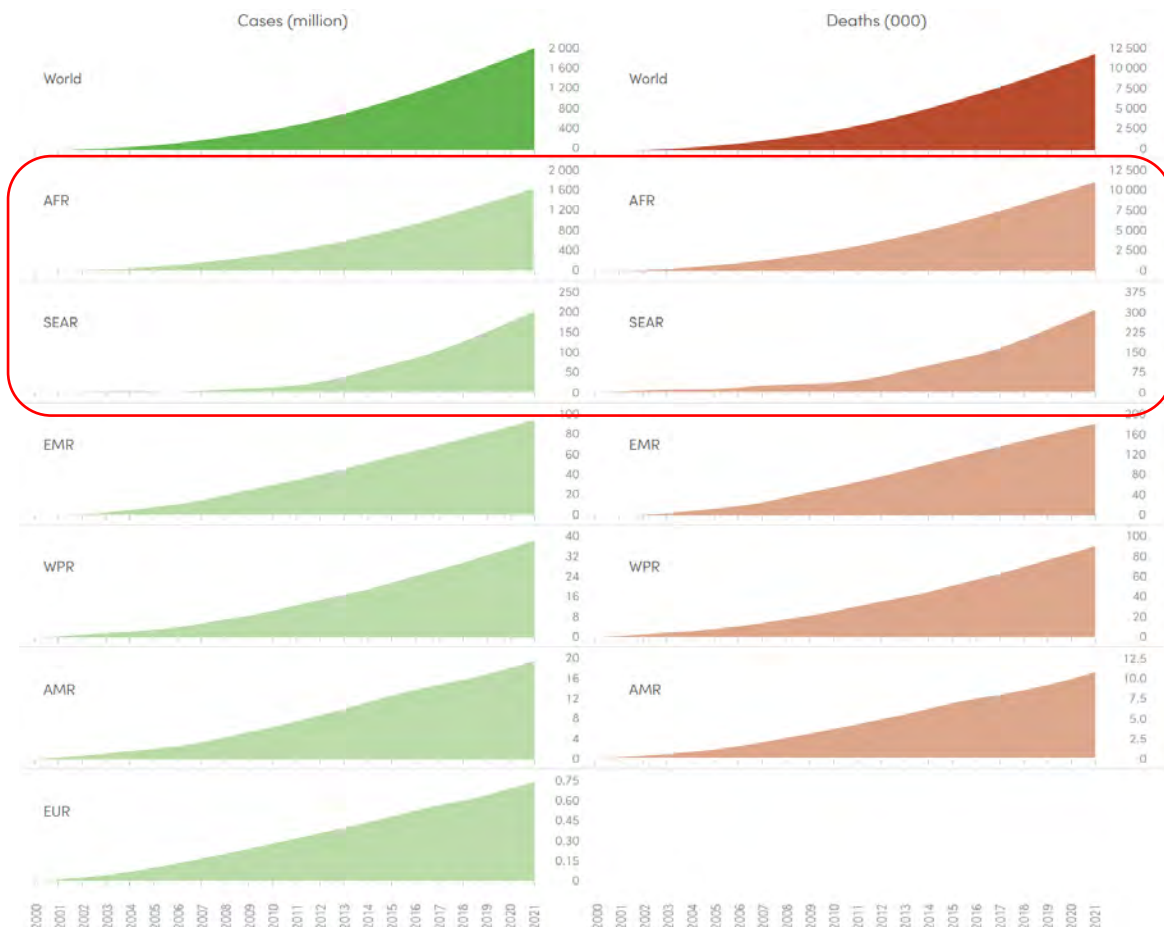
Figure 1.7. Cumulative number of malaria cases and deaths caused during 2000-2021 globally. AFR: Africa; AMR: America; EMR: Eastern Mediterranean Region; EUR: European Region; SEAR: South-East Asia Region; WPR: Western Pacific Region[18]

Due to the emergence of multi-drug-resistant (MDR) strains of *Plasmodium* against the currently available antimalarial agents, malaria remains one of the major health concerns despite the availability of a significant number of treatment options.[19,20] According to the most recent World malaria report published in December 2022, an estimated 6,19,000 persons died from malaria in 2021, and there were approximately 247 million malaria cases worldwide, compared to 245 million in 2020 (**Figure 1.7**).[18]

According to the WHO, Africa continues to endure the maximum burden of malaria with approximately 95% of all cases and at least 96% of all deaths worldwide.[18] During the period

between 2020 and 2021, India and the neighbouring regions of Bangladesh, Indonesia, Myanmar, and the Democratic People's Republic of Korea experienced an estimated increase of 4,000,000 cases.[21]

During its lifecycle in the host, the parasite consumes a substantial quantity of the host's haemoglobin to either maintain its amino acid supply or create space for itself within the red blood cell (RBC).[22] The parasite consumes haemoglobin within its digestive vacuole (DV), where it is degraded by multiple proteases, resulting in the formation of heme. The accumulation of heme within the parasite is detrimental to its survival; consequently, free heme is converted into hemozoin (Hz), which is non-toxic.[22]

Prior to the emergence of resistant plasmodium strains in the 1960s, chloroquine was the drug of choice in the WHO Global Eradication Programme for at least two decades.[18] *Plasmodium* uses host haemoglobin for growth and replication, and during this process, haemoglobin is degraded into heme. It has been hypothesized that chloroquine inhibits Hz formation and heme polymerase, resulting in the accumulation of toxic levels of heme, which disrupts the parasite's constitutive functions and causes its mortality.[23,24] Therefore, heme is detoxicated via various mechanisms to produce Hz, the non-toxic by-product of haemoglobin lysis.[25]

In chloroquine-resistant *Plasmodium*, accumulation of chloroquine within the cell is decreased due to an increase in the pH of the DV (causing decreased chloroquine influx), decreased affinity of chloroquine to heme, and *P. falciparum* chloroquine resistance transporter (*Pf*CRT) mutation (causing enhanced chloroquine efflux). Therefore, heme buildup decreases within the parasite's DV, resulting in diminished therapeutic efficacy of chloroquine.[26,27]

As recommended by WHO, ACT that is, artemisinin in combination with other antimalarial pharmaceuticals, is the only effective treatment for a variety of malarial strains.[20,28] In the past decade, this strategy has effectively reduced the number of malaria cases and associated

mortality.[18] However, recent reports from various regions indicate a decline in the malaria parasite's sensitivity to artemisinin due to emergence of resistance (**Figure 1.4**).[28,29]

Therefore, antimalarial therapy has advanced towards the new concept, epidrugs which act by modulating *Plasmodium's* epigenetic mechanisms.[30] Epigenetics is the study of modulations affecting the gene activity and its expression without affecting the deoxyribonucleic acid (DNA) sequence.[31] One of the widely studied epigenetic pathway includes post-translational modifications (PTM) at the histone protein. The enzymes histone deacetylase (HDAC) and histone lysine methyl transferases (HKMT) involved in PTM have been potential target attractions for various diseases. For example, the role of HDAC has been found to be important in cancer progression as well as malaria.[32] Moreover, the discovery of G9a, a mammalian enzyme that is an HKMT put forth the idea of HKMTs possible role in *Plasmodium*.

1.3 INTRODUCTION TO TB

TB is an ancient communicable disease that predominantly affects the respiratory system by infecting the lungs but can also spread to other organs. *Mycobacterium tuberculosis (Mtb)*, the causative agent of TB, is transmitted through the respiratory system when infected individuals wheeze, sneeze, or spit.[33] According to reports, *Mtb* evolved approximately 3 million years ago in East Africa from an early progenitor. During the 1800s, TB affected majorly the European and North American populations causing between 800 and 1,000 fatalities per one million people per year. In the 1800s, Koch created tuberculin, an extract of glycerine containing purified *Mtb* cultures that was used as a diagnostic to detect latent TB infections. Today, pure *Mtb* cultures in tuberculin have been supplanted by purified protein derivative (PPD), which is a sterile precipitate of *Mtb* culture filtrate.[34] The most prevalent symptoms of TB are a persistent cough that may progress and produce blood, chest pain, unexplained weight loss, weakness, fever, night chills, and fatigue.[34–36] Although TB primarily affects the respiratory

system and the symptoms listed above are the most common, the disease can also affect the kidneys, brain, epidermis, and spine. Consequently, the symptoms may vary among patients.

Nearly one-fourth of the global population is asymptomatically infected with TB, whereas approximately 10 million cases of active TB are reported annually. [33,36] TB is the 13th leading cause of death and the second deadliest infectious disease in the globe, claiming 4000 lives per day.[36] According to the most recent WHO data, approximately 10.6 million persons contracted TB, including 6 million men, 3.4 million women, and 1.2 million children. Globally, a fall in the absolute number of TB deaths was observed until 2019; however, a sudden rise in 2020 was evident in four of the six WHO regions (**Figure 1.8**).
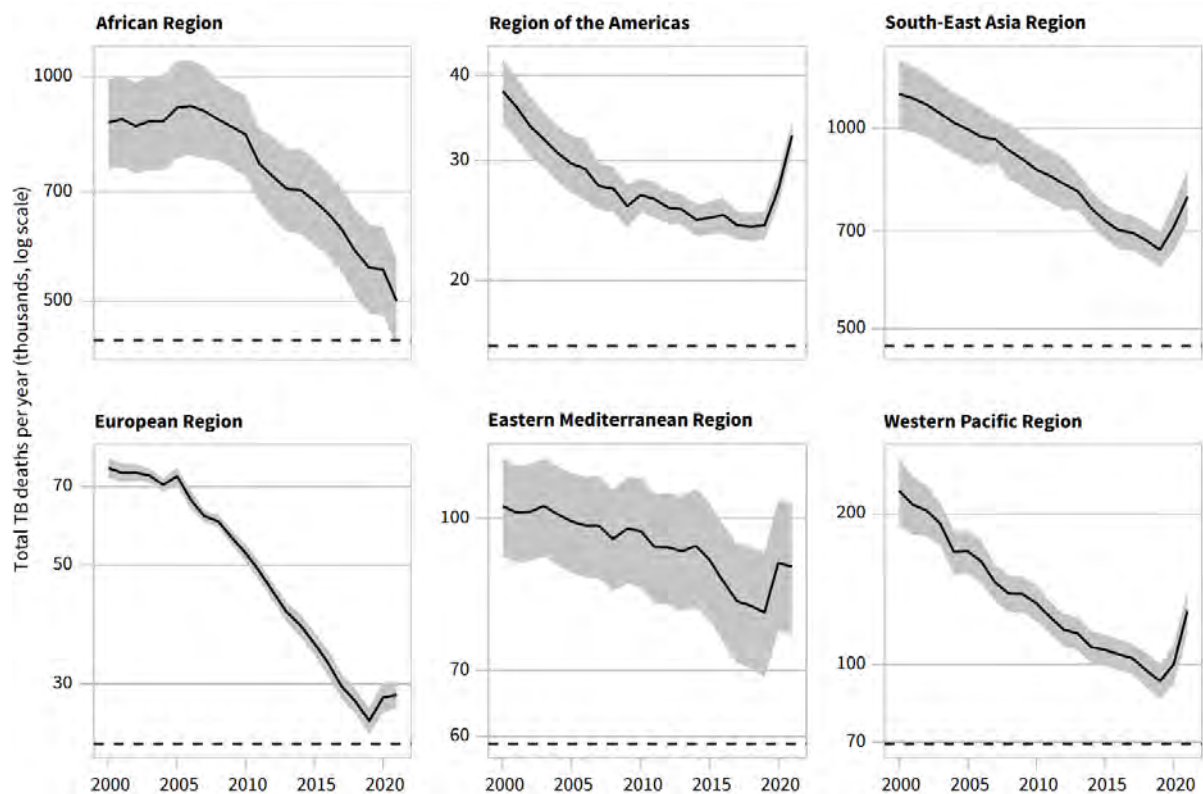
Figure 1.8. Total number of TB deaths per year from 2000-2020 in different regions[33]

In 2021, the Indian subcontinent was estimated to record the maximum, around 20,00,000 incident cases of TB (**Figure 1.9**) and it claimed the lives of 1.6 million individuals in 2021.[36]

9
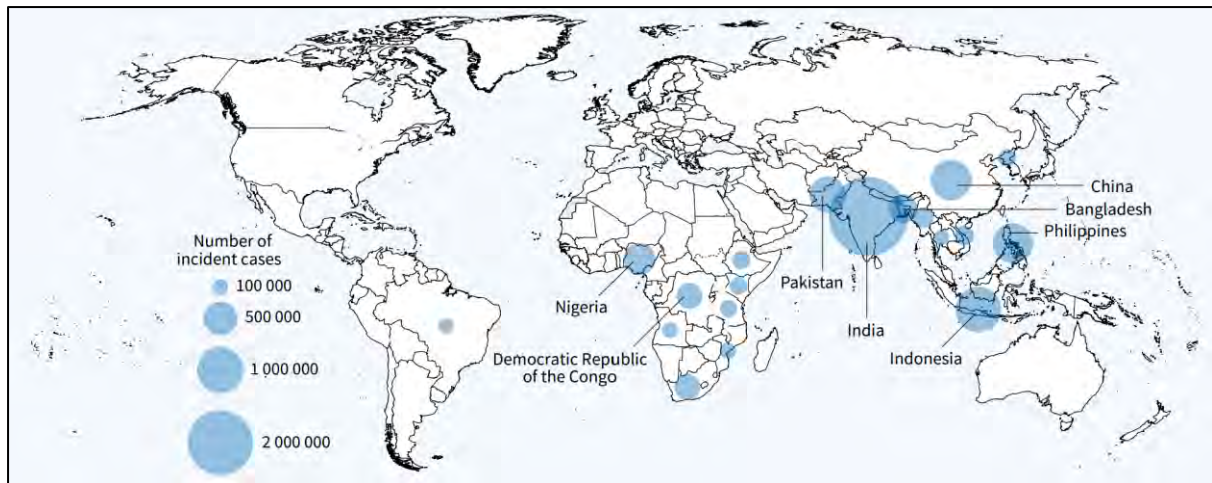
Figure 1.9. Estimated incidence of TB in 2021 for countries with at least 100 000 incident cases. The countries ranking from first to eighth in terms of the number of cases, and that resulted in around two-thirds of global cases in 2021 are labelled.[33]

The TB infection begins with the inhalation of tubercle bacilli loaded on aerosol droplets expectorated by a person actively carrying the disease. A single droplet may contain anywhere from 1-400 bacilli, and between 1-200 bacilli are considered a significantly infectious dose.[34,37] Once inhaled, the bacilli migrate to the alveoli, where the alveolar macrophages quickly phagocytose them. Broadly, the virulence potential of TB is attributed to proteins and the cell wall components of the bacteria. The toll-like receptors (TLRs) and pattern recognition receptors (PPRs) ligate to these macrophages and stimulate them to initiate the production of proinflammatory cytokines and chemokines, leading to the engagement of more leukocytes. The incoming bacteria are engulfed through phagocytosis by neutrophils and monocytes, and this initiates the production of granuloma. Similarly, dendritic cells phagocytose the bacteria and alert the lymphocytes in the regional lymph nodes by presenting the mycobacterial antigens to them. Ultimately, a granuloma develops, which eventually undergoes changes to become necrotic. Slowly, the granuloma begins to appear caseous due to the high lipid and protein content of the dead macrophages in it. *Mtb* dysregulates the host's lipid metabolism and leads to accumulation of lipids in the granuloma. The environment inside the granuloma is hypoxic which is important for metabolic process of *Mtb* and thus may be of importance for efficacy of antibiotic therapy. Before the formation of these granulomas, the bacilli may even spread to the

regional lymph nodes via lymphatic system. As the disease progresses, the granuloma advances to massive necrosis and cavity formation.[34] Communication with the airways breaks down, thus facilitating the growth of bacilli and its intrapulmonary spread.[34]

Therefore, the pathogenicity of *Mtb* is based on three factors: its capability to reprogram the macrophages of the host after initial infection to prevent self-clearance; granuloma formation, which serves as pathogen's survival camp in equilibrium with the defence system of the host; and going in the dormant state by reducing metabolic activity and replication. In this state, *Mtb* becomes resistant to the host defence system and therapy.[35]

MDR-TB and extensively drug-resistant tuberculosis (XDR-TB) strains pose an ever-rising risk, despite the availability of the standard TB treatment protocol.[35] Rifampicin, isoniazid, pyrazinamide, and ethambutol (RHZE regimen) are the traditional first-line treatment for TB. MDR-TB is TB induced by *Mtb* that is resistant to the two most effective antituberculars, isoniazid and rifampin. MDR-TB is reportedly treatable with second-line antituberculous drugs.[36] Cycloserine, ethionamide, para-amino salicylic acid, injectables such as streptomycin, amikacin/kanamycin, capreomycin, and fluoroquinolones (moxifloxacin and levofloxacin) are the second-line anti-TB medicines.[38] In comparison to first-line drugs, however, these regimens are costly and contain drugs with known adverse effects such as drug-induced liver injury (DILI), lifelong disability, anticipated therapy failure, and intolerance.[36,38] In 2021, only one-third of those infected with the MDR strain of TB had access to treatment.[36] Consequently, the recent emergence of drug-resistant strains has also posed a significant challenge to anti-TB therapy.[39,40]

Due to the impenetrable, lipid rich, hydrophobic, viscous nature of the *Mtb* cell wall, the development of new anti-TB drugs is exceedingly difficult.[41] Arabinogalactan, mycolic acid, and peptidoglycans make up the latter.[41] In addition, *Mtb* possesses transporter systems that

facilitate the efflux of numerous substances from the cell, rendering them ineffective. The approval of Bedaquiline, Pretomanid, and Delamanid for the treatment of MDR-TB has resulted in a newer clinical regimen. To obtain the desired therapeutic effect, the BPaL regimen (bedaquiline, pretomanid, linezolid) is modified by adding or removing other anti-tubercular drugs.[42–44] According to new WHO guidelines issued in 2022, a 6-month BPaLM (BPaL regime plus moxifloxacin)/BPaL regimen has been recommended as the treatment of choice for eligible patients.[36] However, the newly discovered anti-TB therapies are ineffective against totally drug-resistant TB (TDR-TB).[45] Despite this, the potential for resistance to the new pharmaceuticals necessitates ongoing efforts to identify novel anti-TB molecules and targets.[46]

Proteolysis is an essential process in *Mtb* that ensures the optimal level and quality of cellular proteins for the pathogen's optimal growth and virulence.[47] Recent research has identified the proteolytic complex formed by the caseinolytic protease (Clp) chaperone-protease system as one of the potential anti-TB targets.[48] This protease system is a bacterial oligomeric multi-subunit complex containing the barrel-shaped heterotetradecameric proteolytic component (ClpP1 and ClpP2) and regulatory adenosine triphosphatase (ATPase) component. The hexameric ring-like ATPase subunit contains the unfoldases ClpX, ClpA, ClpC1, and 19S proteasome.[49] The ATPases identify the target protein, unfold it, and translocate it to the proteolytic subunit of the complex in order to carry out proteolysis. This multi-subunit system is responsible for the degradation of cellular proteins in order to maintain homeostasis and check the proteins specifically implicated in regulatory processes. Using clustered regularly interspaced short palindromic repeats interference (CRISPRi)-mediated gene silencing, it was determined that ClpC1 is essential for the extracellular proliferation of *Mtb* and its survival in macrophages.[49]

By inhibiting ClpC1, the naturally occurring cyclic peptides cyclomarin A (CymA), lassomycin, ecumicin, and rufomycin have demonstrated potent activity against *Mtb*.[50–54]

However, these molecules are too complicated for chemical synthesis[55,56] and optimization based on medicinal chemistry. Thus, there is a need to develop ClpC1 inhibitors that are amenable to synthesis.

1.4 DRUG DISCOVERY USING HYBRID APPROACH AND CHEMINFORMATICS

These concerns pertaining to resistance against antimalarial and anti-TB drugs led to the initiation of high throughput screening (HTS) campaigns, yielding a vast quantity of information for rational learning and future forecasting. Some of these initiatives for antimalarial drugs predominately rely on phenotypic assays targeting either asexual or sexual stages of *Plasmodium*, and these have generated novel lead molecules and potential clinical candidates.[57–59] In the past twenty years, tafenoquine and arterolane are the only antimalarial drugs approved by Food and Drug Administration (FDA). Similarly, bedaquiline is the only new antitubercular developed in the past decade. Consequently, the design and synthesis of novel hybrid compounds and the development of new strategies to combat resistance are urgently required. Therefore, Meunier and colleagues proposed hybrid moieties, or multi-targeted drug ligands (MTDLs) (**Figure 1.10**), as a solution to the problem of drug resistance.
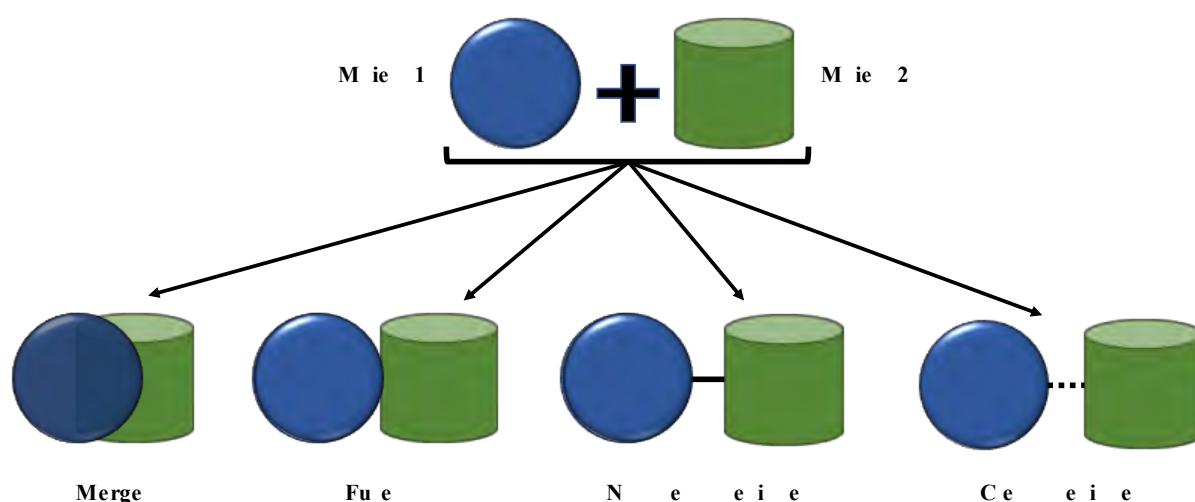
Figure 1.10. Different strategies used for MTDL designing

However, different studies have estimated that bringing a new drug to market will cost between $2.8 and $9.8 billion.[60,61] Nonetheless, the rate of failure in clinical trials remains high, which

is attributable, among other things, to inadequate bioavailability and safety.[62] Understanding the factors influencing "druglikeness" or "druglike properties" in a chemical space must therefore be pursued with diligence due to the high stakes involved in drug discovery. Chemical space may be explained as a collection of all molecules, which is believed to be around 10^{63}, with possible potential of importance in drug discovery.[63] To understand the enormity of the chemical space, it has been compared to 10^{24} stars in space.[64] However, till date there are only 2000 FDA-approved drugs (**Figure 1.11**). Virtually screening the chemical space reflects the vast number of molecules with physical properties similar to those of existing small-molecule therapeutics.[63] Further, advancing the prospect of small drug-like molecules to synthesis, and testing leads to discover new drug molecules.[64]

10^{63} Drug-like molecules in chemical space

10^{24} stars in the Universe

2000 FDA approved drugs
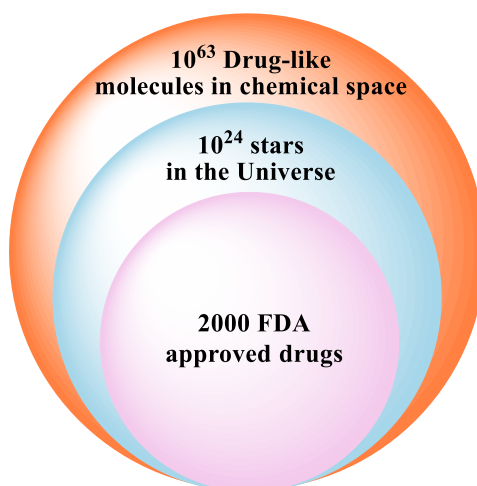
Figure 1.11. Depiction of the vastness of chemical space

Although the precise definition of "druglikeness" is debatable,[65] broadly speaking, it is comparable to oral bioavailability. In vivo interactions between a molecule and multiple biomolecules and biomembranes determine its absorption, permeation, metabolic stability, and transporter-mediated efflux. Thus, drug-likeness of a molecule is determined by its physicochemical properties and chemical structure, just as drug action is. Consequently, on average, orally available medications combine the optimal physicochemical properties necessary for a favourable interaction with the human physiology.

The introduction of the rule of five (Ro5) by Lipinski et al. represents one of the initial endeavours to comprehend the impact of molecular properties on drug-likeness.[66] To evaluate druglike properties, Lipinski's Ro5 proposes a cutoff for four molecular properties: molecular weight (MW ≤ 500 Da), calculated partition coefficient (clogP ≤ 5), hydrogen bond acceptor (HBA ≤ 10) and hydrogen bond donor (HBD ≤ 5). Molecules within the prescribed limits for at least two of these four descriptors are anticipated to have good permeation and absorption, resulting in good oral bioavailability. Despite a number of limitations and criticisms[65,67] the Ro5 appears to be a useful criterion for eliminating non-ideal molecules in the early stages of drug discovery.[68,69] Since Lipinski's seminal work, other structural descriptors such as aromatic rings (#Ar),[70–72] the fraction of sp3 carbon (Fsp3),[73] topological polar surface area (TPSA),[74,75] distribution coefficient (log D),[76–78] and the number of rotatable bonds (#RB)[75] have been acknowledged as influencing the "developability" of a molecule. Several authors have proposed using score-based and other quantitative druglikeness metrics in lieu of rules with strict cutoffs.[77,79] In addition, mapping of compound optimization trajectories primarily relying on ligand lipophilic efficiency and ligand efficiency has been suggested for effective drug searching.[80–82]

The nature of a drug's intended biological target also regulates its overall properties. For instance, Zhao et al. formulated eNTRy rules that may assist in screening compounds which would accumulate inside gram-negative bacteria.[83,84] Similarly, Wager et al. analyzed different properties to identify CNS drug space.[85] On similar lines, other research groups have also identified chemical space for SARS-CoV-2,[86] kinases,[87] proteases, decaprenylphosphoryl-β-d-ribose 2'-epimerase (DprE1),[88] etc. Thus, a target- or organ-specific chemical space exists within the expansive oral drug space. Consequently, conducting a systematic analysis of antimalarial property space would be intriguing.

1.5 REFERENCES

1.   Bracing for Superbugs: Strengthening environmental action in the One Health response to antimicrobial resistance. UNEP - UN Environment Programme. Accessed June 6, 2023. https://www.unep.org/resources/superbugs/environmental-action

2.   Liu Y, Liu W, Yang X, et al. Microplastics are a hotspot for antibiotic resistance genes: Progress and perspective. *Sci Total Environ*. 2021;773. doi:10.1016/J.SCITOTENV.2021.145643

3.   Bartkova S, Kahru A, Heinlaan M, et al. Techniques Used for Analyzing Microplastics, Antimicrobial Resistance and Microbial Community Composition: A Mini-Review. *Front Microbiol*. 2021;12. doi:10.3389/FMICB.2021.603967

4.   Kaur K, Reddy S, Barathe P, et al. Microplastic-associated pathogens and antimicrobial resistance in environment. *Chemosphere*. 2022;291:133005. doi:10.1016/J.CHEMOSPHERE.2021.133005

5.   Zhang Y, Gu AZ, He M, et al. Subinhibitory Concentrations of Disinfectants Promote the Horizontal Transfer of Multidrug Resistance Genes within and across Genera. *Environ Sci Technol*. 2017;51(1):570-580. doi:10.1021/ACS.EST.6B03132/SUPPL_FILE/ES6B03132_SI_001.PDF

6.   Anwar M, Iqbal Q, Saleem F. Improper disposal of unused antibiotics: an often overlooked driver of antimicrobial resistance. *Expert Rev Anti Infect Ther*. 2020;18(8):697-699. doi:10.1080/14787210.2020.1754797

7.   Kümmerer K, Henninger A. Promoting resistance by the emission of antibiotics from hospitals and households into effluent. *Clinical Microbiology and Infection*. 2003;9(12):1203-1214. doi:10.1111/J.1469-0691.2003.00739.X

8.   Giguère S. Front Matter. *Antimicrobial Therapy in Veterinary Medicine*. Published online September 20, 2013:i-xvii. doi:10.1002/9781118675014.FMATTER

9.   Lerman LS, Tolmach LJ. Genetic transformation. I. Cellular incorporation of DNA accompanying transformation in Pneumococcus. *Biochim Biophys Acta*. 1957;26(1):68-82. doi:10.1016/0006-3002(57)90055-0

10.   Kim JS, Kim JW, Kathariou S. Differential effects of temperature on natural transformation to erythromycin and nalidixic acid resistance in Campylobacter coli. *Appl Environ Microbiol*. 2008;74(19):6121-6125. doi:10.1128/AEM.01075-08

11.   Vegge CS, Brøndsted L, Ligowska-Marzeta M, et al. Natural Transformation of Campylobacter jejuni Occurs Beyond Limits of Growth. *PLoS One*. 2012;7(9):e45467. doi:10.1371/JOURNAL.PONE.0045467

12.   O'Neill J. Tackling drug-resistant infections globally: final report and recommendations. Published online 2016.

13.   Murray CJ, Ikuta KS, Sharara F, et al. Global burden of bacterial antimicrobial resistance in 2019: a systematic analysis. *Lancet*. 2022;399(10325):629-655. doi:10.1016/S0140-6736(21)02724-0

14. Antimicrobial resistance : tackling a crisis for the health and wealth of nations / the Review on Antimicrobial Resistance chaired by Jim O'Neill. Wellcome Collection. Accessed May 28, 2023. https://wellcomecollection.org/works/rdpck35v

15. Antimicrobial resistance. Accessed June 1, 2023. https://www.who.int/news-room/fact-sheets/detail/antimicrobial-resistance

16. Global Tuberculosis Cases, Deaths Rise During COVID Pandemic. Accessed May 31, 2023. https://www.webmd.com/lung/news/20221028/global-tb-cases-deaths-rise-covid-pandemic

17. Garcia LS. Malaria. *Clin Lab Med*. 2010;30(1):93-129. doi:10.1016/J.CLL.2009.10.001

18. World malaria report 2022. Accessed April 19, 2023. https://www.who.int/publications/i/item/9789240064898

19. White A, Hughes JM. Critical Importance of a One Health Approach to Antimicrobial Resistance. *Ecohealth*. 2019;16(3):404-409. doi:10.1007/S10393-019-01415-5

20. Oliveira R, Miranda D, Magalhães J, et al. From hybrid compounds to targeted drug delivery in antimalarial therapy. *Bioorg Med Chem*. 2015;23(16):5120-5130. doi:10.1016/j.bmc.2015.04.017

21. Regional data and trends briefing kit. Published online 2022.

22. Deshpande S, Kuppast B. 4-aminoquinolines: An Overview of Antimalarial Chemotherapy. *Med Chem (Los Angeles)*. 2016;06(01). doi:10.4172/2161-0444.1000315

23. Sunduru N, Sharma M, Srivastava K, et al. Synthesis of oxalamide and triazine derivatives as a novel class of hybrid 4-aminoquinoline with potent antiplasmodial activity. *Bioorg Med Chem*. 2009;17(17):6451-6462. doi:10.1016/J.BMC.2009.05.075

24. Pussard E, Verdier F. Antimalarial 4-aminoquinolines: mode of action and pharmacokinetics. *Fundam Clin Pharmacol*. 1994;8(1):1-17. doi:10.1111/J.1472-8206.1994.TB00774.X

25. Ribbiso KA, Heller LE, Taye A, et al. Artemisinin-based drugs target the plasmodium falciparum heme detoxification pathway. *Antimicrob Agents Chemother*. 2021;65(4). doi:10.1128/AAC.02137-20/FORMAT/EPUB

26. Nqoro X, Tobeka N, Aderibigbe B. Quinoline-Based Hybrid Compounds with Antimalarial Activity. *Molecules*. 2017;22(12):2268. doi:10.3390/molecules22122268

27. Agarwal D, Gupta RD, Awasthi SK. Are Antimalarial Hybrid Molecules a Close Reality or a Distant Dream? *Antimicrob Agents Chemother*. 2017;61(5). doi:10.1128/AAC.00249-17

28. Sundriyal S, Malmquist NA, Caron J, et al. Development of diaminoquinazoline histone lysine methyltransferase inhibitors as potent blood-stage antimalarial compounds. *ChemMedChem*. 2014;9(10):2360-2373. doi:10.1002/CMDC.201402098

29. Noedl H, Se Y, Sriwichai S, et al. Artemisinin resistance in Cambodia: a clinical trial designed to address an emerging problem in Southeast Asia. *Clin Infect Dis*. 2010;51(11). doi:10.1086/657120

30. Malmquist NA, Moss TA, Mecheri S, et al. Small-molecule histone methyltransferase inhibitors display rapid antimalarial activity against all blood stage forms in Plasmodium falciparum. *Proc Natl Acad Sci U S A*. 2012;109(41):16708-16713. doi:10.1073/PNAS.1205414109/SUPPL_FILE/PNAS.201205414SI.PDF

31. Chookajorn T, Dzikowski R, Frank M, et al. Epigenetic memory at malaria virulence genes. *Proc Natl Acad Sci U S A*. 2007;104(3):899-902. doi:10.1073/PNAS.0609084103

32. Dokmanovic M, Clarke C, Marks PA. Histone deacetylase inhibitors: overview and perspectives. *Mol Cancer Res*. 2007;5(10):981-989. doi:10.1158/1541-7786.MCR-07-0324

33. Geneva: World Health Organization. Licence: CC BY-NC-SA 3.0 IGO. *Global Tuberculosis Report 2021*; 2021.

34. Sakamoto K. The pathology of Mycobacterium tuberculosis infection. *Vet Pathol*. 2012;49(3):423-439. doi:10.1177/0300985811429313

35. Miggiano R, Rizzi M, Ferraris DM. Mycobacterium tuberculosis Pathogenesis, Infection Prevention and Treatment. *Pathogens*. 2020;9(5). doi:10.3390/PATHOGENS9050385

36. WHO. Tuberculosis. Published October 14, 2021. Accessed June 10, 2022. https://www.who.int/news-room/fact-sheets/detail/tuberculosis

37. Balasubramanian V, Wiegeshaus EH, Taylor BT, et al. Pathogenesis of tuberculosis: pathway to apical localization. *Tuber Lung Dis*. 1994;75(3):168-178. doi:10.1016/0962-8479(94)90002-7

38. Nahid P, Dorman SE, Alipanah N, et al. Executive Summary: Official American Thoracic Society/Centers for Disease Control and Prevention/Infectious Diseases Society of America Clinical Practice Guidelines: Treatment of Drug-Susceptible Tuberculosis. *Clinical Infectious Diseases*. 2016;63(7):853-867. doi:10.1093/cid/ciw566

39. Hameed HMA, Islam MM, Chhotaray C, et al. Molecular Targets Related Drug Resistance Mechanisms in MDR-, XDR-, and TDR- Mycobacterium tuberculosis Strains. *Front Cell Infect Microbiol*. 2018;8(APR). doi:10.3389/FCIMB.2018.00114

40. Dookie N, Rambaran S, Padayatchi N, et al. Evolution of drug resistance in Mycobacterium tuberculosis: a review on the molecular determinants of resistance and implications for personalized care. *J Antimicrob Chemother*. 2018;73(5):1138-1151. doi:10.1093/JAC/DKX506

41. Kalscheuer R, Palacios A, Anso I, et al. The Mycobacterium tuberculosis capsule: a cell structure with key implications in pathogenesis. *Biochem J*. 2019;476(14):1995. doi:10.1042/BCJ20190324

42. Märtson AG, Burch G, Ghimire S, Alffenaar JWC, et al. Therapeutic drug monitoring in patients with tuberculosis and concurrent medical problems. *Expert Opin Drug Metab Toxicol*. 2021;17(1). doi:10.1080/17425255.2021.1836158

43. Black TA, Buchwald UK. The pipeline of new molecules and regimens against drug-resistant tuberculosis. *J Clin Tuberc Other Mycobact Dis*. 2021;25:100285. doi:10.1016/J.JCTUBE.2021.100285

44. Peloquin CA, Davies GR. The Treatment of Tuberculosis. *Clin Pharmacol Ther*. 2021;110(6):1455-1466. doi:10.1002/CPT.2261

45. Maeurer M, Schito M, Zumla A. Totally-drug-resistant tuberculosis: hype versus hope. *Lancet Respir Med*. 2014;2(4):256-257. doi:10.1016/S2213-2600(14)70020-7

46. Huszár S, Chibale K, Singh V. The quest for the holy grail: new antitubercular chemical entities, targets and strategies. *Drug Discov Today*. 2020;25(4):772-780. doi:10.1016/J.DRUDIS.2020.02.003

47. Santra M, Farrell DW, Dill KA. Bacterial proteostasis balances energy and chaperone utilization efficiently. *Proceedings of the National Academy of Sciences*. 2017;114(13):E2654-E2661. doi:10.1073/pnas.1620646114

48. Leodolter J, Warweg J, Weber-Ban E. The Mycobacterium tuberculosis ClpP1P2 Protease Interacts Asymmetrically with Its ATPase Partners ClpX and ClpC1. Zeth K, ed. *PLoS One*. 2015;10(5):e0125345. doi:10.1371/journal.pone.0125345

49. Lunge A, Gupta R, Choudhary E, et al. The unfoldase ClpC1 of Mycobacterium tuberculosis regulates the expression of a distinct subset of proteins having intrinsically disordered termini. *Journal of Biological Chemistry*. 2020;295(28):9455-9473. doi:10.1074/jbc.RA120.013456

50. Vasudevan D, Rao SPS, Noble CG. Structural basis of mycobacterial inhibition by Cyclomarin A. *Journal of Biological Chemistry*. 2013;288(43):30883-30891. doi:10.1074/jbc.M113.493767

51. Schmitt EK, Riwanto M, Sambandamurthy V, et al. The natural product cyclomarin kills mycobacterium tuberculosis by targeting the ClpC1 subunit of the caseinolytic protease. *Angewandte Chemie - International Edition*. 2011;50(26):5889-5891. doi:10.1002/anie.201101740

52. Gavrish E, Sit CS, Cao S, et al. Lassomycin, a ribosomally synthesized cyclic peptide, kills mycobacterium tuberculosis by targeting the ATP-dependent protease ClpC1P1P2. *Chem Biol*. 2014;21(4):509-518. doi:10.1016/j.chembiol.2014.01.014

53. Gao W, Kim JY, Anderson JR, et al. The cyclic peptide ecumicin targeting CLpC1 is active against Mycobacterium tuberculosis in vivo. *Antimicrob Agents Chemother*. 2015;59(2):880-889. doi:10.1128/AAC.04054-14

54. Wolf NM, Lee H, Choules MP, et al. High-Resolution Structure of ClpC1-Rufomycin and Ligand Binding Studies Provide a Framework to Design and Optimize Anti-Tuberculosis Leads. *ACS Infect Dis*. 2019;5(6):829-840. doi:10.1021/acsinfecdis.8b00276

55. Barbie P, Kazmaier U. Total Synthesis of Cyclomarin A, a Marine Cycloheptapeptide with Anti-Tuberculosis and Anti-Malaria Activity. *Org Lett*. 2016;18(2):204-207. doi:10.1021/ACS.ORGLETT.5B03292

56. Lear S, Munshi T, Hudson AS, et al. Total chemical synthesis of lassomycin and lassomycin-amide. *Org Biomol Chem*. 2016;14(19):4534-4541. doi:10.1039/C6OB00631K

57. Ashley EA, Phyo AP. Drugs in Development for Malaria. *Drugs*. 2018;78(9):861-879. doi:10.1007/S40265-018-0911-9

58. Tse EG, Korsik M, Todd MH. The past, present and future of antimalarial medicines. *Malar J*. 2019;18(1):1-21. doi:10.1186/s12936-019-2724-z

59. Okombo J, Chibale K. Recent updates in the discovery and development of novel antimalarial drug candidates. *Medchemcomm*. 2018;9(3):437-453. doi:10.1039/C7MD00637C

60. Wouters OJ, McKee M, Luyten J. Estimated Research and Development Investment Needed to Bring a New Medicine to Market, 2009-2018. *JAMA*. 2020;323(9):844-853. doi:10.1001/JAMA.2020.1166

61. DiMasi JA, Grabowski HG, Hansen RW. Innovation in the pharmaceutical industry: New estimates of R&D costs. *J Health Econ*. 2016;47:20-33. doi:10.1016/J.JHEALECO.2016.01.012

62. Dowden H, Munro J. Trends in clinical success rates and therapeutic focus. *Nat Rev Drug Discov*. 2019;18(7):495-496. doi:10.1038/D41573-019-00074-Z

63. Coley CW. Defining and Exploring Chemical Spaces. *Trends Chem*. 2021;3(2):133-145. doi:10.1016/J.TRECHM.2020.11.004

64. Reymond JL, Van Deursen R, Blum LC, et al. Chemical space as a source for new drugs. *Medchemcomm*. 2010;1(1):30-38. doi:10.1039/C0MD00020E

65. Shultz MD. Two Decades under the Influence of the Rule of Five and the Changing Properties of Approved Oral Drugs. *J Med Chem*. 2019;62(4):1701-1714. doi:10.1021/ACS.JMEDCHEM.8B00686

66. Lipinski CA, Lombardo F, Dominy BW, et al. Experimental and computational approaches to estimate solubility and permeability in drug discovery and development settings. *Adv Drug Deliv Rev*. 1997;23(1-3):3-25. doi:10.1016/S0169-409X(96)00423-1

67. Abad-Zapatero C. A sorcerer's apprentice and The Rule of Five: from rule-of-thumb to commandment and beyond. *Drug Discov Today*. 2007;12(23-24):995-997. doi:10.1016/J.DRUDIS.2007.10.022

68. Tinworth CP, Young RJ. Facts, Patterns, and Principles in Drug Discovery: Appraising the Rule of 5 with Measured Physicochemical Data. *J Med Chem*. 2020;63(18):10091-10108. doi:10.1021/ACS.JMEDCHEM.9B01596

69. Leeson PD. Molecular inflation, attrition and the rule of five. *Adv Drug Deliv Rev*. 2016;101:22-33. doi:10.1016/J.ADDR.2016.01.018

70. Ritchie TJ, Macdonald SJF. The impact of aromatic ring count on compound developability--are too many aromatic rings a liability in drug design? *Drug Discov Today*. 2009;14(21-22):1011-1020. doi:10.1016/J.DRUDIS.2009.07.014

71. Ritchie TJ, MacDonald SJF, Peace S, et al. The developability of heteroaromatic and heteroaliphatic rings – do some have a better pedigree as potential drug molecules than others? *Medchemcomm*. 2012;3(9):1062-1069. doi:10.1039/C2MD20111A

72. Ritchie TJ, MacDonald SJF, Young RJ, et al. The impact of aromatic ring count on compound developability: further insights by examining carbo- and hetero-aromatic and -aliphatic ring types. *Drug Discov Today*. 2011;16(3-4):164-171. doi:10.1016/J.DRUDIS.2010.11.014

73. Lovering F, Bikker J, Humblet C. Escape from flatland: increasing saturation as an approach to improving clinical success. *J Med Chem*. 2009;52(21):6752-6756. doi:10.1021/JM901241E

74. Whitty A, Zhong M, Viarengo L, et al. Quantifying the chameleonic properties of macrocycles and other high-molecular-weight drugs. *Drug Discov Today*. 2016;21(5):712-717. doi:10.1016/J.DRUDIS.2016.02.005

75. Veber DF, Johnson SR, Cheng HY, et al. Molecular properties that influence the oral bioavailability of drug candidates. *J Med Chem*. 2002;45(12):2615-2623. doi:10.1021/JM020017N

76. Young RJ, Green DVS, Luscombe CN, et al. Getting physical in drug discovery II: the impact of chromatographic hydrophobicity measurements and aromaticity. *Drug Discov Today*. 2011;16(17-18):822-830. doi:10.1016/J.DRUDIS.2011.06.001

77. Degoey DA, Chen HJ, Cox PB, et al. Beyond the Rule of 5: Lessons Learned from AbbVie's Drugs and Compound Collection. *J Med Chem*. 2018;61(7):2636-2651. doi:10.1021/ACS.JMEDCHEM.7B00717

78. Fullam E, Young RJ. Physicochemical properties and Mycobacterium tuberculosis transporters: keys to efficacious antitubercular drugs? *RSC Med Chem*. 2021;12(1):43-56. doi:10.1039/D0MD00265H

79. Bickerton GR, Paolini G V., Besnard J, et al. Quantifying the chemical beauty of drugs. *Nat Chem*. 2012;4(2):90-98. doi:10.1038/NCHEM.1243

80. Young RJ, Leeson PD. Mapping the Efficiency and Physicochemical Trajectories of Successful Optimizations. *J Med Chem*. 2018;61(15):6421-6467. doi:10.1021/ACS.JMEDCHEM.8B00180

81. Leeson PD, Springthorpe B. The influence of drug-like concepts on decision-making in medicinal chemistry. *Nat Rev Drug Discov*. 2007;6(11):881-890. doi:10.1038/NRD2445

82. Hopkins AL, Groom CR, Alex A. Ligand efficiency: A useful metric for lead selection. *Drug Discov Today*. 2004;9(10):430-431. doi:10.1016/S1359-6446(04)03069-7

83. Zhao S, Adamiak JW, Bonifay V, et al. Defining new chemical space for drug penetration into Gram-negative bacteria. *Nature Chemical Biology 2020 16:12*. 2020;16(12):1293-1302. doi:10.1038/s41589-020-00674-6

84. Richter MF, Drown BS, Riley AP, et al. Predictive compound accumulation rules yield a broad-spectrum antibiotic. *Nature 2017 545:7654*. 2017;545(7654):299-304. doi:10.1038/nature22308

85. Wager TT, Chandrasekaran RY, Hou X, et al. Defining desirable central nervous system drug space through the alignment of molecular properties, in vitro ADME, and safety attributes. *ACS Chem Neurosci*. 2010;1(6):420-434. doi:10.1021/CN100007X

86. Kumar A, Loharch S, Kumar S, et al. Exploiting cheminformatic and machine learning to navigate the available chemical space of potential small molecule inhibitors of SARS-CoV-2. *Comput Struct Biotechnol J.* 2021;19:424-438. doi:10.1016/J.CSBJ.2020.12.028

87. Adrian G, Marcel V, Robert B, et al. A comparison of physicochemical property profiles of marketed oral drugs and orally bioavailable anti-cancer protein kinase inhibitors in clinical development. *Curr Top Med Chem*. 2007;7(14):1408-1422. doi:10.2174/156802607781696819

88. Chhabra S, Kumar S, Parkesh R. Chemical Space Exploration of DprE1 Inhibitors Using Chemoinformatics and Artificial Intelligence. *ACS Omega*. 2021;6(22):14430-14441. doi:10.1021/ACSOMEGA.1C01314

Chapter 2

Physiochemical profiling and property space characterization of antimalarials

2.1 INTRODUCTION AND BACKGROUND

During the drug development process, the pharmaceutical industry loses several drug candidates due to poor safety profile or subtherapeutic pharmacokinetic properties. These failures in clinical studies lead to the wastage of valuable resources and time. Therefore, to overcome this problem studying the optimal drug properties in an identified chemical space is important.[1] Several authors have utilized target/organ chemical space to identify hits with desired properties (**Figure 2.1**).
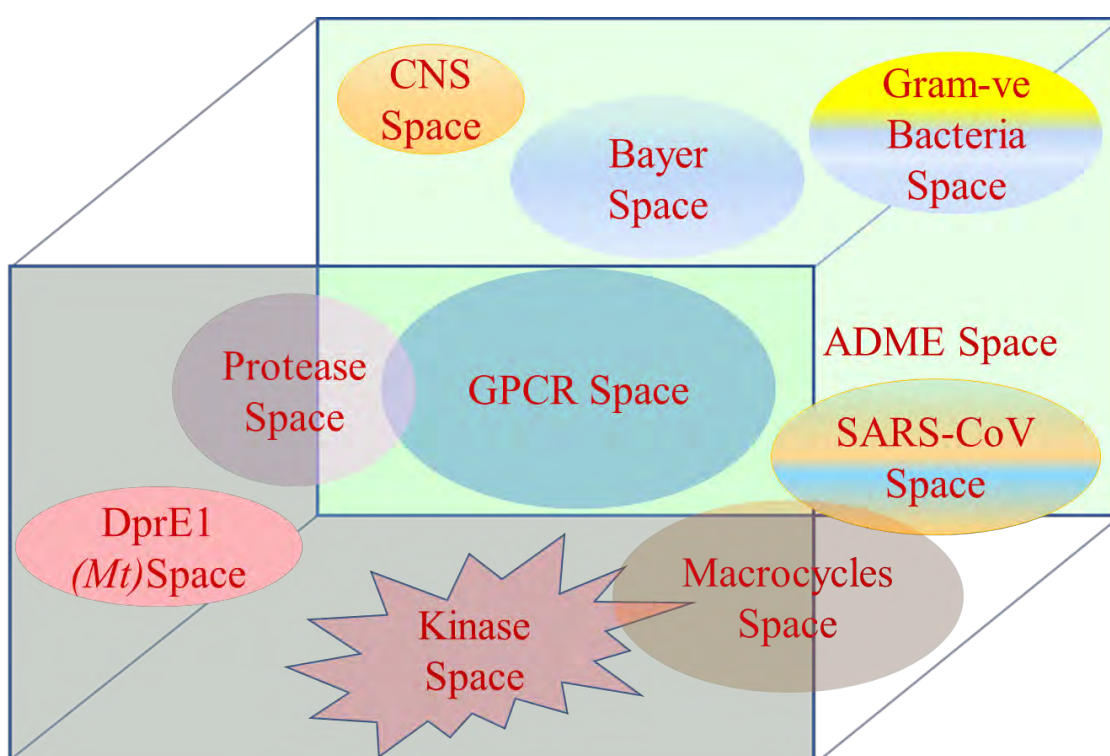
Figure 2.1. Depiction of target or organ-specific drug space within the vast drug-like chemical space

Overall properties of drugs ought to be governed by the nature of their target. Indeed, drugs targeting different protein classes (such as kinases, nuclear hormone receptors, and proteases) possess variable properties.[2,3] This is because of these targets' distinct binding pockets requiring unique molecular size ranges, lipophilicity, ionization, or H-bonding capacity. For instance, Wager et al. collated a dataset of 227 compounds, 119 marketed drugs and 108 clinical candidates from Pfizer acting on the CNS. The study was focused on evaluating the relationship between ADME (absorption, distribution, metabolism, and elimination), primary

pharmacology binding efficiencies, in vitro safety, and physiochemical properties to determine the CNS drug space. In general, CNS drugs are smaller, lipophilic, and unionized, as there is a need for these molecules to overcome the BBB.[4,5] **Figure 2.2** represents the optimum values for CNS drug space.
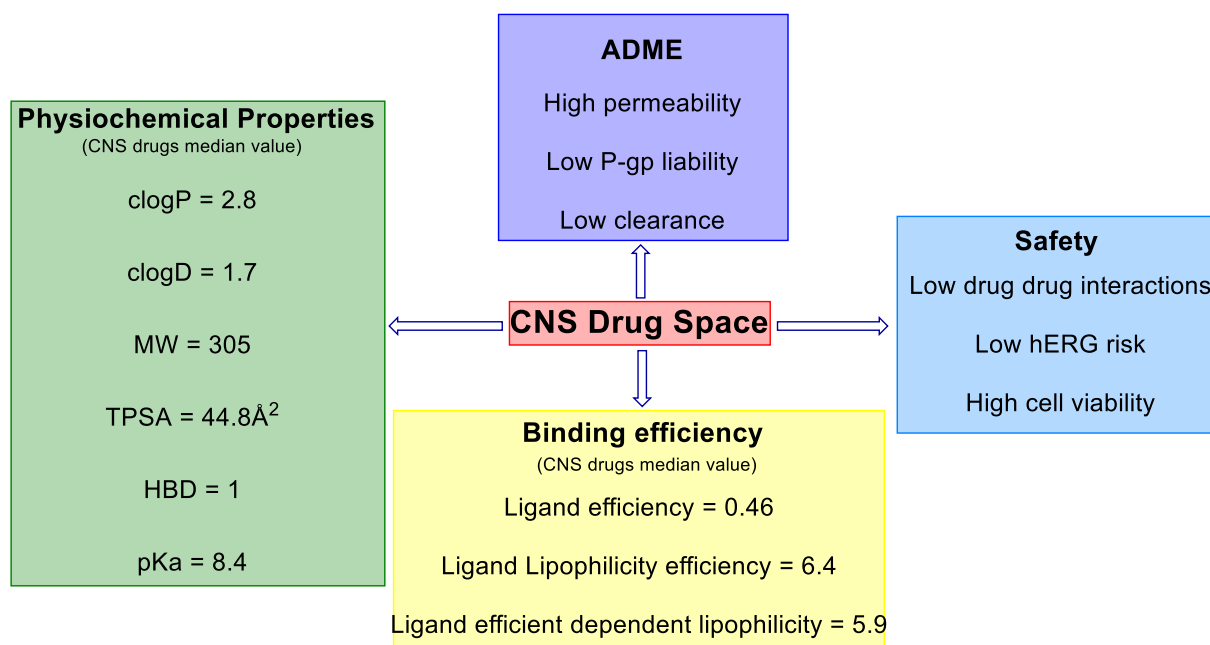
Figure 2.2. Properties governing CNS drug space

Similarly, Kumar et al. utilized machine learning and cheminformatic approaches to expand severe acute respiratory syndrome coronavirus-2 (SARS-CoV-2) small molecules chemical space using anti-corona dataset (433 compounds) and drug-like anti-viral dataset (20963 compounds). A machine learning study on coronavirus main protease inhibitors was performed to generate a model which revealed structural features essential for high pIC_{50}. This model was used to screen FDA-approved drugs and found 6 drugs (**Figure 2.3**) that showed high predicted pIC_{50}; therefore, these drugs may be repurposed for the treatment of COVID-19. Fragment-based analysis revealed indole and pyrrolidine scaffolds to be the most potent and may be used to design novel SARS-CoV-2 inhibitors.[6]

Intensive screening of chemical space relevant to antibacterial drug discovery by several researchers led to the formation of a set of eNTRy rules which may be helpful in identifying

drugs that would accumulate inside the gram-negative bacteria (**Figure 2.4**).[7,8] In another study, Chhabra et al. utilized cheminformatic analysis to identify DprE1 chemical space and found drugs targeting DprE1 to be more hydrophobic in comparison to anti-TB drugs.[9]
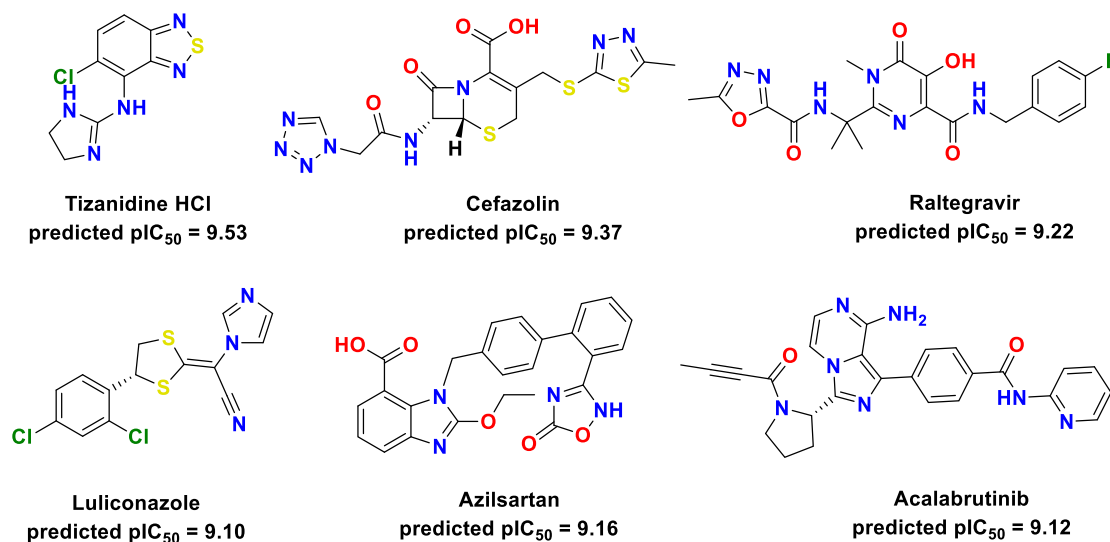
Figure 2.3. Novel SARS-CoV-2 inhibitors identified using small molecules chemical space

On similar lines, it was identified that compared to marketed oral drugs, orally available anticancer protein kinase inhibitors are larger, more lipophilic, and more complex.[10] Orally used anti-infective drugs have higher MW, low lipophilicity, and greater HBA/HBD and ring counts.[11–13] Specific properties may also be required to access a particular tissue/organ/organelle where a biological target might be residing, exemplified by the drugs acting on the CNS.
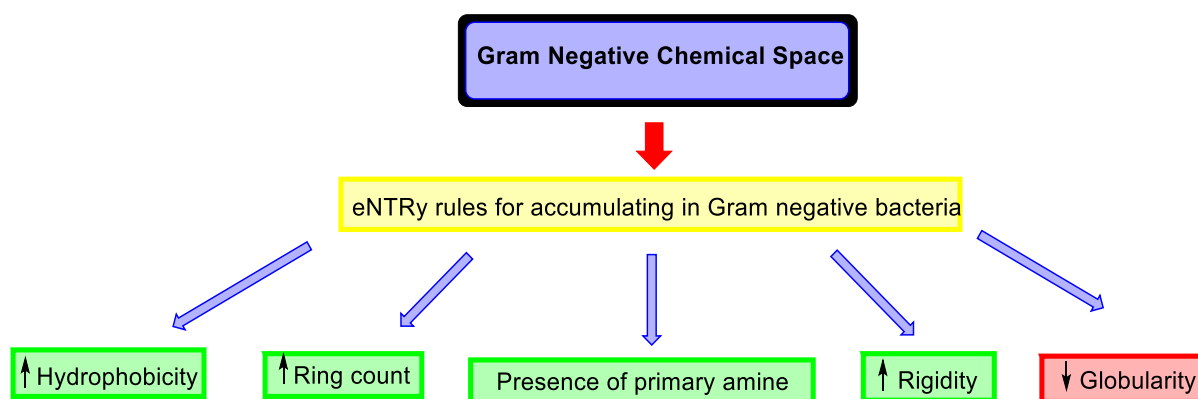
Figure 2.4. eNTRy rules for discovery of potent drugs in gram-negative bacteria space

Thus, a target- or organ-specific chemical space exists within a broad oral drug space. Optimal properties required by a molecule to interact with its biological target (for in vitro potency) may or may not be orthogonal to those required for desirable oral bioavailability. Understanding oral drug space in a particular biological target context may provide useful insights that guide the drug design for the target/biological endpoint. Therefore, on the basis of the above-mentioned studies, exploration of antimalarial chemical space was undertaken as the objective of this study.

Malaria is an infectious disease caused by the *Plasmodium* species belonging to the Apicomplexan phylum, spread by mosquito bite. Malaria mostly affects tropical and sub-tropical populations, with children and pregnant women being the most vulnerable groups.[14] ACT has been the gold standard for the treatment of malaria; however, resistance is spreading against artemisinin at alarming levels and may lead to devastating outcomes.[15–20] These concerns have prompted large-scale HTS campaigns against *P. falciparum*, resulting in a large amount of data for retrospective learning and prospective predictions. These efforts are mostly based on phenotypic whole-cell assays against asexual or sexual stages of the parasite and have produced novel leads and clinical candidates.[21–23] Despite the tremendous efforts in the past decade,[24] only two small antimalarial molecules, tafenoquine and arterolane, have been approved in the past 20 years.

The antiplasmodial molecules act through different targets residing in different organelles, such as parasite cell membranes, mitochondria, apicoplasts, food vacuoles, and the cytoplasm. Since the parasite inhabits host RBCs, the molecules active in antiplasmodial phenotypic assays must cross at least three membrane barriers. The latter consists of the host RBC membrane, parasitophorous vacuolar membrane (PVM), and parasite plasma membrane.[25,26] Such a permeability barrier may impose specific properties on the active set of molecules compared to the inactive ones in these assays. For instance, large-scale phenotypic HTS by

GlaxoSmithKline (GSK) found hit molecules to be larger and more lipophilic compared to the average source compound collection.[27]

2.2 GAPS IN EXISTING RESEARCH AND OBJECTIVES

1. It would be interesting to perform a systematic analysis of the property space of research antiplasmodial (RAP) molecules with differential potencies. Such comparison may reveal the key chemical descriptors important for allowing permeation across host/parasite lipoidal membranes or target engagement. However, cellular permeation alone is not enough to achieve optimum oral bioavailability properties.

2. Research molecules are known to differ from clinical candidates and drugs in terms of physicochemical properties.[28–30] A comparison is required between RAP and the advanced-stage antimalarial (ASAM) molecules with the proven in vivo oral bioavailability and efficacy. Such a comparison among RAP and ASAM would help map the trajectory as the initial antimalarial hit advances from the discovery stage to the lead stage.[2]

3. To further characterize the antimalarial property space, a comparison with other oral drugs is also required. Therefore, we will collate and study the average properties of the datasets. Furthermore, we will characterize an antimalarial property space that may facilitate the identification of new antimalarial molecules.

2.3 RESULTS AND DISCUSSION

2.3.1 Data collection and data analysis

We used readily available open-source tools and resources for the data collection and analysis. The set of RAP molecules was collated from the ChEMBL database, one of the largest collections of biologically active compounds reported in the medicinal chemistry literature.[31,32] Additionally, the results of several phenotypic HTS campaigns against *P. falciparum* have also been deposited in ChEMBL by pharmaceutical companies like

GSK.[27] While compounds disclosed from such large screens may not be ideal for further development,[33] such data may be used for the physicochemical profiling of antimalarials. Nevertheless, to ensure the quality of activity data, we have included compounds tested at multiple concentrations against the parasite with known IC_{50}/EC_{50} values. Although several of these molecules are tested in different labs under different assay conditions, such heterogeneous data are acceptable for the qualitative comparison of bioactivities.[34] These molecules were classified into different potency classes: highly active (HA), moderately active (MA), and inactive (IN) to observe the effect of various properties on the in vitro potency. The HA dataset is the largest one since mostly successful results are reported in the literature. Due to the same reason, the IN class was found to have comparatively few molecules, and hence, the latter was topped up with the inactive molecules reported by GSK-Tres Cantos Antimalarial Set (TCAMS) screening.[27]

In addition to the marketed antimalarials, the ASAM set consists of antimalarials currently undergoing clinical trials and molecules considered "leads" with promising efficacy and oral bioavailability in animal studies.[15,21] Thus, the difference between the RAP and ASAM molecular properties may indicate the influence these properties have on the "developability" of antimalarials.

For this study, the "oral drug" is defined as a small molecule (MW < 900 Da) currently approved by a regulatory body for oral administration to treat or prevent any disease in humans. The set of oral drugs was obtained from the DrugCentral[35] database, which consists of drugs approved not only by the US FDA but also by the regulatory agencies in Europe, Japan, and other countries. The library was further updated with the recently approved drugs by the US FDA (till July 2020). Consequently, our library of oral drugs is extended (total 1954) in comparison to the recently compiled set of 750 oral drugs used for property profiling.[36,37] The latter is limited to oral drugs approved till 2017 by the US FDA.

While Lipinski suggested the cutoff of 500 Da for the MW, some authors have suggested that the actual limit for the MW may be higher for the orally absorbed drugs,[13,38,39] prompting us to use a cutoff of 900 Da for the collation of all datasets. Using these criteria, the final datasets of IN, MA, HA, ASAM, and oral drugs consist of 7365, 6620, 10,557, 66, and 1954 molecules, respectively. Some of the molecules are present in more than one category. For example, several oral drugs are also part of the IN dataset. Similarly, currently marketed antimalarials are part of both ASAM as well as oral drug datasets.
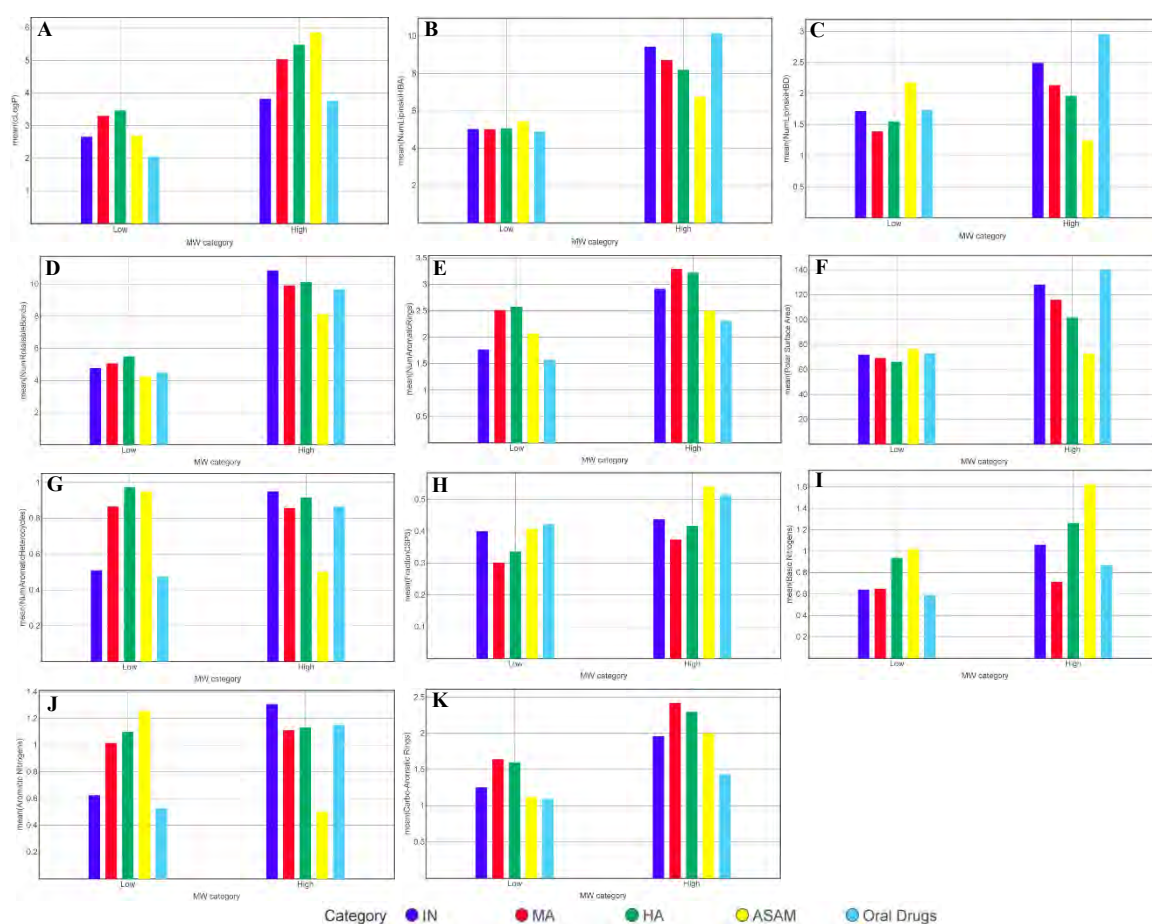
Figure 2.5. Distribution of mean of A) clogP, B) HBA, C) HBD, D) #RB, E) #Ar, F) TPSA, G) #HetAr, H) Fsp3, I) #BaN, J) #ArN and K) #CarboAr among low (MW < 500) and high (MW > 500 Da) molecular weight compounds within the IN, MA, HA, ASAM, and oral drugs categories

The open-source program RDKit was used to calculate the MW, HBA, HBD, Fsp^3, #RB, #Ar, and heteroaromatic ring count (#HetAr), while DataWarrior was used for the computation of the clog P, TPSA, carboaromatic ring count (#CarboAr), aromatic nitrogen count (#ArN), and

basic nitrogen count (#BaN). Comparison among the different categories of molecules was performed using various statistical parameters and hypothesis tests employed earlier in similar studies.[36,40–42] Given the skewness and kurtosis in the data, the Kruskal–Wallis test was employed for hypothesis testing, in addition to the t-test.[36] Certain properties like clog P, HBA, HBD, and TPSA are known to be correlated with the MW.[42] Hence, property trends were monitored for both large (MW > 500 Da) and small (MW < 500 Da) molecules within the given category (**Figure 2.5A-K**). Expectedly, most of the molecules (~80%) in our complete dataset belong to the latter class (**Table 2.1**). The large molecules in the ASAM class possess only eight molecules, and hence, the results for this category should be interpreted with caution.

Table 2.1. Distribution of low (MW<500 Da) and high (MW>500 Da) molecular weight compounds in each category

Category	Low (MW<500 Da)	Percentage Low	High (MW>500Da)
IN	6037	~82%	1328
MA	5432	~82%	1188
HA	8036	~76%	2521
ASAM	58	~88%	8
Oral drugs	1730	~88%	224
Total	**21293**	**~80%**	**5269**

2.3.2 Comparison of the Globally Approved Oral Drugs with the FDA-Approved Drugs

Since our library consists of globally approved oral drugs, we compared it with the recently reported set of FDA-approved oral drugs. Most of the physicochemical properties can be computed unambiguously except for log P, which displays variable results based on the algorithm and computational programs used.[36] For this study, we used the open-source Actelion clog P algorithm implemented in the DataWarrior program,[43] which recognizes 368 atom types contributing toward the final value. This algorithm has been shown to outperform many other programs when tested on a dataset of 96,000 compounds.[44] Moreover, a satisfactory correlation was observed for Actelion clog P versus the experimental log P (0.882) and Actelion clog P versus StarDrop clog P (0.935) (**Figures 2.6A** and **2.6B**) for the set of 452 drugs compiled by Shultz.[36]
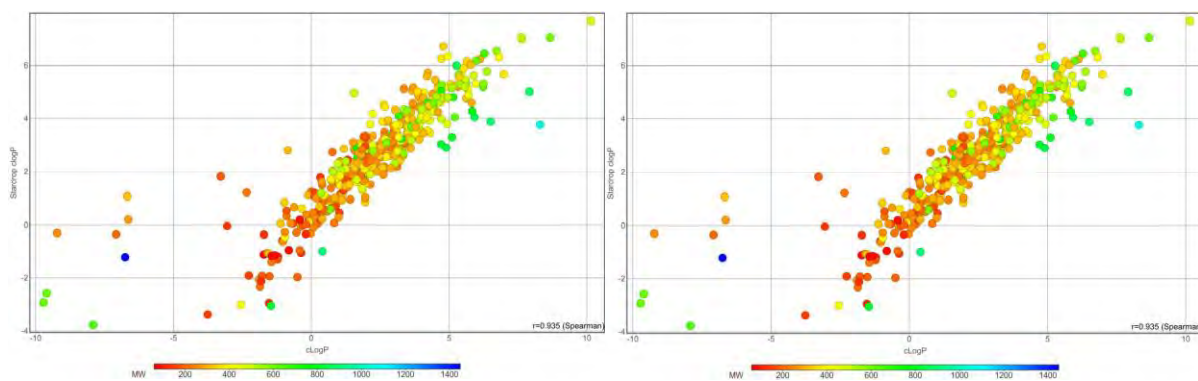
Figure 2.6. A) Correlation between Actelion clog*P* (X-axis) vs the experimental log*P* for a set of 452 drugs reported in the supporting information of reference 37; and B) Correlation between Actelion clog*P* (X-axis) vs the Stardrop clog*P* for a set of 452 drugs reported in the supporting information of reference 37

Despite the different compilation criteria and clog *P* algorithms, our extended set and the FDA-approved oral drugs show comparable 90th and 10th percentile values for important physicochemical properties (**Table 2.2**). The 90th percentiles for all properties, except for MW, are within Lipinski's cutoffs for both the libraries. Consequently, 786 out of 1954 drugs (~91%) in our library pass the Ro5. The drop in the 90th percentile of MW in our dataset (519.0 Da) in comparison to that of the FDA drugs (552.2 Da) may be due to the applied MW cutoff of 900 Da in the former case. Moreover, 90th percentiles of the TPSA and #RB of both libraries are also close to the limits proposed by Veber et al. for optimum bioavailability.[42] The 90th and 10th percentiles for #Ar and Fsp[3] descriptors are also identical for both libraries. The comparison of FDA-approved oral drugs before 1997[36] with the combined oral drugs demonstrates slight inflation in MW, clog *P*, and TPSA descriptors, in line with the earlier reports.[11,28,36]

However, our analysis is limited to clog *P* and other key properties as we do not have access to any commercial software for log *D* calculation. Also, to our knowledge, no open-source program is available to compute log *D* for an extensive database such as the one used in this study. Overall, our oral drug library is updated with the most recent approvals and conforms to the property space of drug-like compounds reported by other authors.

Table 2.2: Comparison of 90th and 10th Percentiles of Various Molecular Properties[a].

Molecular Property	Oral Drugs (N = 1954)	ASAM (N = 66)	HA (N = 10,557)	MA (N = 6620)	IN (N = 7365)
MW	519.0 (204.2),[b] 552.2 (197.0),[c] 470.3 (171.2)	500.9 (253.6)	588.8 (296.6)	568.7 (277.8)	567.1 (242.4)
clog P[d]	4.85 (−0.87),[b] 4.80 (−0.36),[c] 4.65 (−0.64)	5.54 (0.34)	6.43 (1.50)	5.78 (1.50)	5.64 (0.20)
HBA	9 (2),[b] 10 (2),[c] 10 (2)	8 (3)	9 (3)	9 (3)	10 (3)
HBD	4 (0),[b] 4 (0),[c] 4 (0)	4 (0)	4 (0)	3 (0)	4 (0)
TPSA	145.1 (27.4),[b] 143.3 (29.0),[c] 139.8 (21.3)	118.3 (43.2)	125.0 (33.1)	129.1 (33.5)	142.3 (34.9)
#Ar	3 (0),[b] 3 (0),[c] 3 (0)	4 (0)	4 (1)	4 (1)	4 (0)
#RB	10 (1),[b] 11 (1),[c] 10 (1)	9 (1)	12 (2)	11 (2)	12 (1)
Fsp^3	0.78 (0.13),[b] 0.78 (0.13),[c] 0.83 (0.08)	0.94 (0.12)	0.71 (0.09)	0.59 (0.07)	0.87 (0.07)

[a]The values in brackets represent 10th percentiles.
[b]The 90th percentile values of all oral drugs (N=750) approved by the US FDA for the period 1900-2017. Taken from the supporting information of reference (37).
[c]The 90th percentile values for oral drugs (N=341) approved before the proposal of the Ro5, that is, for the period 1900-1997. Taken from the supporting information of reference (37).
[d]clog$P$ values were calculated using the DataWarrior program for our dataset, while the StarDrop program was used in reference (37).

2.3.3 MW and clog P

MW has been shown to affect oral absorption, especially of hydrophilic drugs. The latter are mostly absorbed through paracellular spaces or cell junctions, which have a restricted size of 3–6 Å in humans. This is supported by the distinctive absorption kinetics of polar drugs observed in different species of animals and is attributable to the variation in the paracellular pore size.[45] Nevertheless, Lipinski's cutoff of MW may also arise from the limited number of large molecules pursued in drug discovery due to the challenges associated with their synthesis[36,46] or due to the limit imposed by other descriptors correlated to MW.[42,47] Lipophilicity affects the cellular uptake and oral absorption by influencing dissolution and partitioning of a drug into the lipid bilayer.

Table 2.3. Comparison of mean/median of molecular properties among the different categories of molecules

Molecular Property	Oral Drugs (*N* = 1954) mean (median)	ASAM (*N* = 66) mean (median)	HA (*N* = 10,557) mean (median)	MA (*N* = 6620) mean (median)	IN (*N* = 7365) mean (median)
MW	357.2 (339.5)	389.9 (391.4)	432.2 (418.4)	408.8 (393.5)	384.0 (361.4)
clog *P*	2.23 (2.43)	3.07 (3.13)	3.94 (3.40)	3.60 (3.60)	2.90 (3.00)
HBA	5.48 (5)	5.60 (5.5)	5.80 (6)	5.68 (5)	5.82 (5)
HBD	1.90 (2)	2.10 (2)	1.70 (1)	1.52 (1)	1.85 (1)
TPSA	80.38 (72.34)	75.90 (73.11)	74.68 (69.30)	77.44 (71.44)	82.00 (73.12)
#Ar	1.70 (2)	2.12 (2)	2.73 (3)	2.65 (3)	1.97 (2)
#CarboAr	1.13 (1)	1.23 (1)	1.76 (2)	1.78 (2)	1.38 (1)
#HetAr	0.52 (0)	0.89 (1)	0.96 (1)	0.86 (1)	0.59 (0)
#RB	5.09 (4)	4.72 (4)	6.59 (6)	5.94 (5)	5.86 (5)
Fsp^3	0.432 (0.4)	0.423 (0.375)	0.355 (0.310)	0.314 (0.285)	0.407 (0.363)
#BaN	0.62 (1)	1.09 (1)	1.01 (1)	0.66 (0)	0.71 (0)
#ArN	0.60 (0)	1.16 (1)	1.10 (1)	1.03 (0)	0.75 (0)

In RAP molecules, the mean (and median) MW increases with increasing antiplasmodial activity (**Table 2.3**, **Figure 2.7**). The HA and MA categories display significantly higher MW than the IN class. This trend is also visible in the 90th and 10th percentile values for MW for these classes. The average MW of the ASAM group is lower (389.9 Da) compared to that of the HA class (432.1 Da) but higher than that of the oral drugs (357.2 Da), results statistically significant according to the *t*-test but not the Kruskal–Wallis test. The 90th percentile for the MW of the ASAM molecules (500.9 Da) is almost identical to the threshold of 500 Da suggested by Lipinski.

Like MW, mean, and 90th percentile values for clog *P* also show a steady increase from IN to MA to HA categories (**Figure 2.7**), suggesting a positive correlation between lipophilicity and antiplasmodial activity in phenotypic assays. However, like MW, the clog *P* of ASAM molecules also converges back to lower values while maintaining a statistically higher average than that of the oral drugs, as per the *t*-test. The trend is maintained for both low and high MW categories of RAP molecules, with average clog *P* showing an increase with increasing potency (**Figure 2.8**).
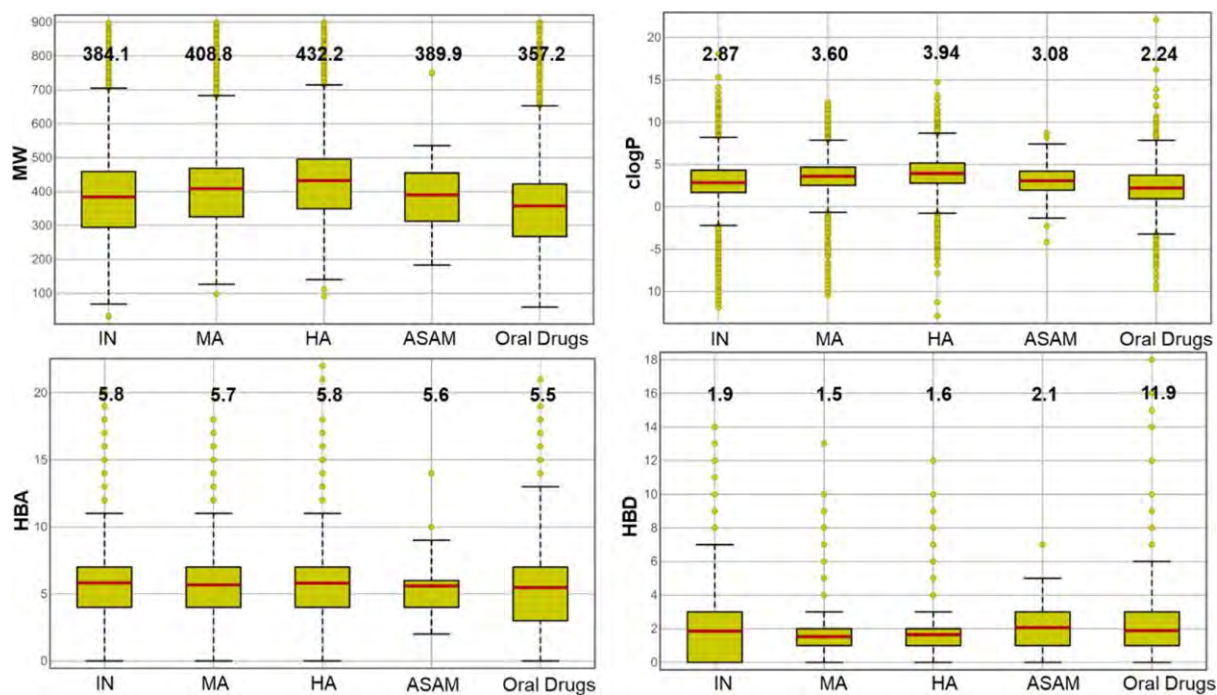
Figure 2.7. Boxplots for the MW, clog*P*, HBA, and HBD properties for different sets of molecules. The mean values are given in bold above each boxplot and represented by the red line within the boxes. The yellow dots represent outliers.

Figure 2.8. Distribution of mean of clog*P* among low (MW < 500) and high (MW > 500 Da) molecular weight compounds within the IN, MA, HA, ASAM, and oral drugs categories.

In summary, bulkier and lipophilic molecules tend to show potent in vitro antiplasmodial activity, which agrees with GSK-TCAMS screening results.[27] This means that in the currently

used antiplasmodial phenotypic assays, membrane permeability of molecules is not adversely affected by their large size or high lipophilicity. Nevertheless, to advance these molecules in the antimalarial pipeline, MW and clog P must be optimized toward Lipinski's thresholds.

RAP molecules' high permeability, despite their bulky and lipophilic nature, may result from their facilitated transport via parasite-induced new permeation pathways. The latter allows the entry of diverse molecules within the infected RBC.[48] For instance, the plasmodial surface anion channel linked to the *clag* gene family[46] induced on the infected RBC membrane can carry large lipophilic molecules.[49] Once inside the infected RBCs, these molecules may further cross the PVM, which itself contains several non-selective channels to carry bulky molecules.[50–52] The high lipophilicity may also allow molecules to partition within the lipid portion of the biological membrane, thus enabling passive diffusion.[53] However, such "obese"[54] molecules are likely to exhibit low solubility, extensive metabolism, and P-glycoproteins-mediated efflux, preventing their progression to the ASAM category, which explains the relatively lower MW and clog P averages of the latter class.

2.3.4 HBA and HBD

The HBA (sum of O and N atoms) and HBD (sum of NH and OH groups) are important parameters that determine the overall polarity and H-bonding capacity of a molecule. These two descriptors also affect the aqueous solubility,[55,56] a prerequisite for oral absorption.

The HA and MA molecules show a significantly higher average HBA but lower HBD compared to the oral drugs (**Table 2.3**, **Figure 2.7**). The ASAM molecules display averages for HBA and HBD that do not differ statistically from those of oral drugs. However, the 90th percentile for both descriptors complies with Lipinski's thresholds for all the categories of molecules. The larger antimalarial molecules (MW > 500 Da) consistently display lower HBA and HBD than the oral drugs, and the averages decrease with increasing in vitro potency.

Overall, for small molecules (MW < 500), the HBA and HBD do not seem to have a noticeable influence on the antimalarial activity, but lower values for these descriptors are preferred for larger molecules.

2.3.5 TPSA and #RB

Veber and co-workers demonstrated TPSA and #RB descriptors to be better predictors of oral bioavailability in comparison to the Ro5 with their undisclosed dataset ($N = 1100$).[42] The molecules with a TPSA ≤ 140 Å^2 and #RB ≤ 10 were found to have good oral bioavailability in rat models. In DataWarrior, TPSA is calculated using the original approach of Ertl et al., which was also adopted by Veber and co-workers.[57] Our dataset of oral drugs ($N = 1954$) displays comparable results with the 90th percentiles of 144.7 Å^2 and 10 for the TPSA and #RB, respectively (**Table 2.2**).
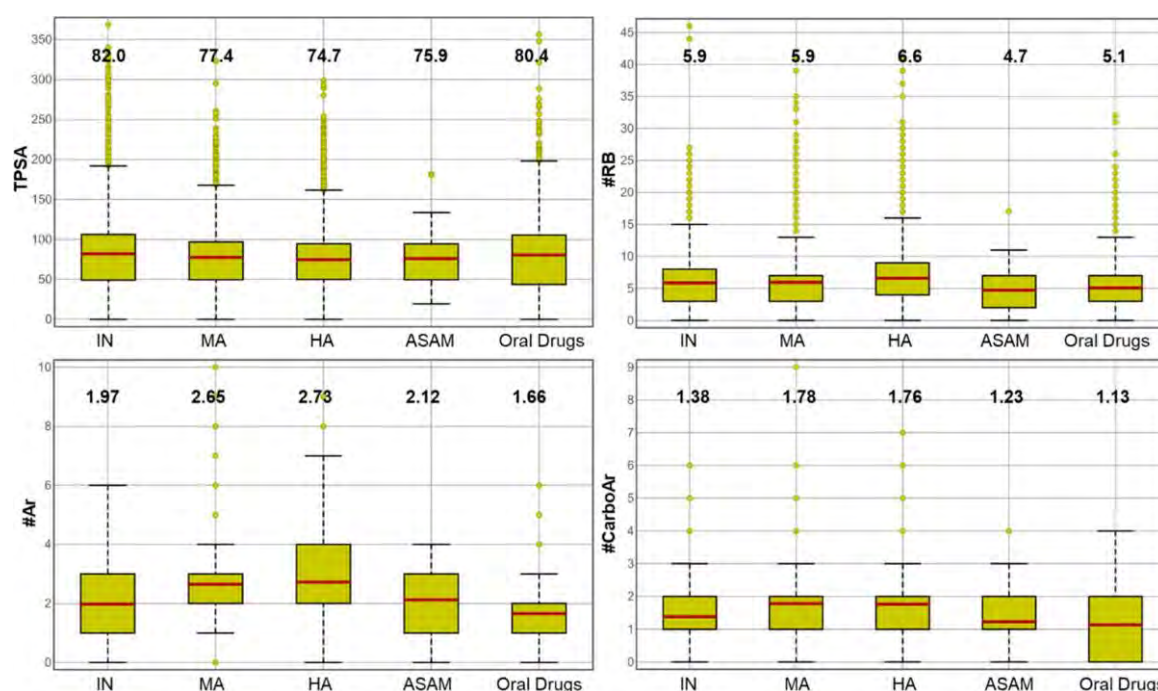
Figure 2.9. Boxplots for the TPSA, #RB, #Ar, and #CarboAr properties for different sets of molecules. The mean values are given in bold above each boxplot and represented by the red line within the boxes. The yellow dots represent outliers

In RAP molecules, mean TPSA decreases (**Figure 2.9**) with an increase in potency (IN = 81.99 Å^2, MA = 77.44 Å^2, and HA = 74.68 Å^2), with 90th percentiles also showing the same trend

(**Table 2.2**). While the HA and MA molecule averages are significantly lower than that of the oral drugs (as per the *t*-test but not the Kruskal–Wallis test), statistical difference is not observed either between the HA/MA versus ASAM (75.9 Å^2) or ASAM versus oral drugs (80.4 Å^2). Interestingly, ASAM molecules display the lowest 90th percentile (mean = 118.3 Å^2) among all categories. This trend of TPSA variation is exhibited by small and large molecules, albeit differences are more dramatic in the latter case (**Figure 2.10**). Inclusively, these results suggest that a lower TPSA is advantageous for both in vitro and in vivo antimalarial activity, especially for the larger molecules. Presumably, higher polarity negatively affects permeability across the multiple membranes that an antimalarial molecule must cross.[25]
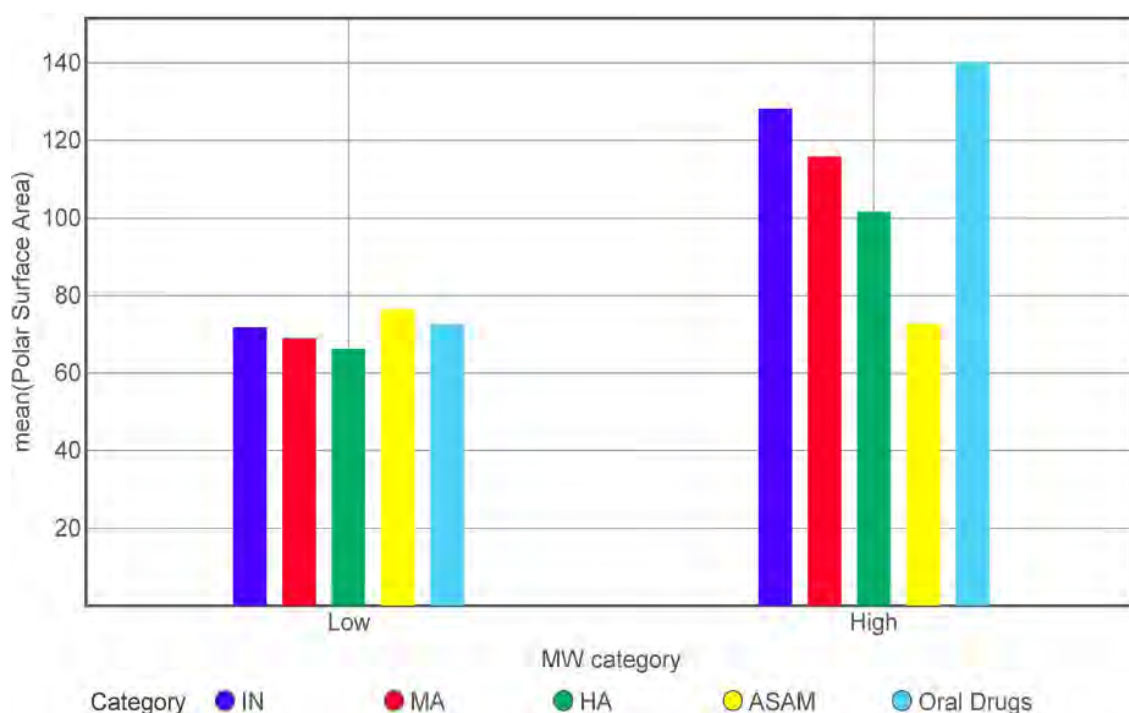
Figure 2.10. Distribution of mean of TPSA among low (MW < 500) and high (MW > 500 Da) molecular weight compounds within the IN, MA, HA, ASAM, and oral drugs categories.

The average for the #RB descriptor increases (**Figure 2.9**) significantly with increasing antiplasmodial potency, especially for the smaller molecules (**Figure 2.11**), with the HA class displaying the highest mean of 6.6. In contrast, the ASAM molecules are relatively rigid, with fewer #RB (mean = 4.7) comparable to that of the oral drugs (mean = 5.09). This suggests that

high flexibility or a greater RB count is not detrimental to the in vitro antiplasmodial activity. Nevertheless, lower #RB averages of ASAMs and oral drugs as compared to that of the HA molecules confirms the importance of lower flexibility for overall oral bioavailability and agrees with the observation of Veber et al. [42]
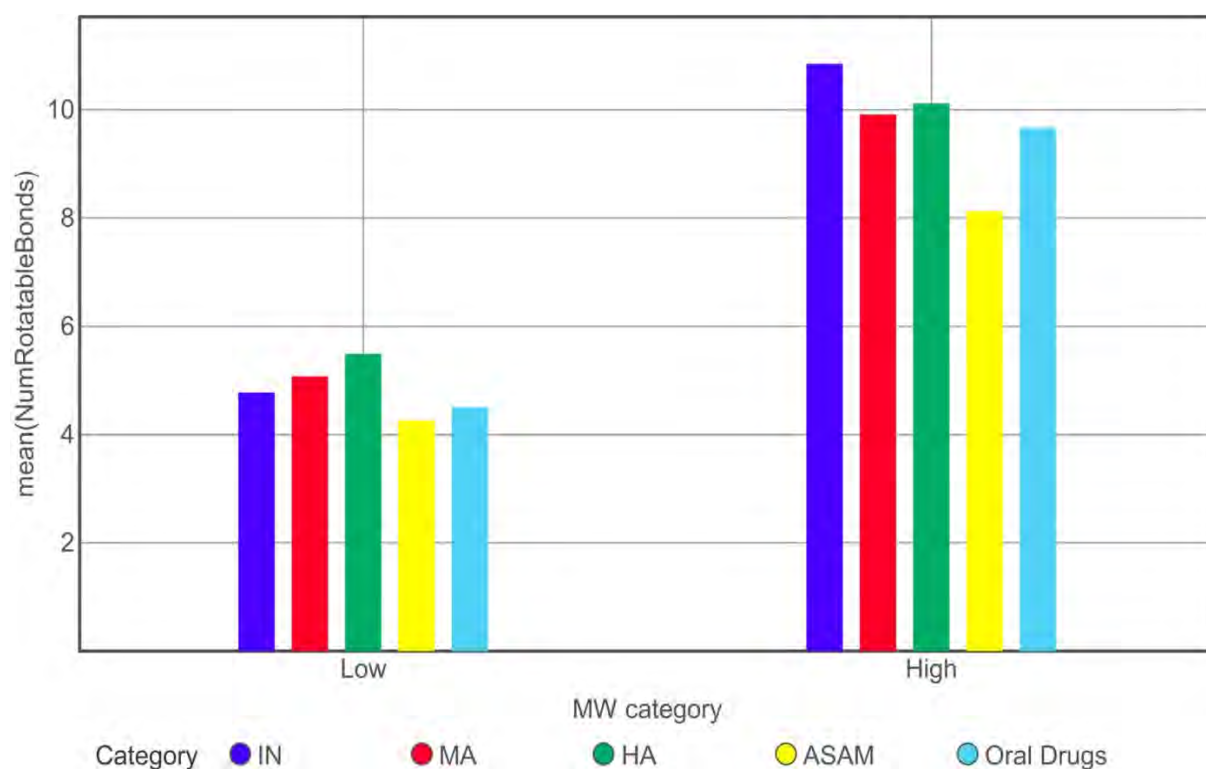
Figure 2.11. Distribution of mean of #RB among low (MW < 500) and high (MW > 500 Da) molecular weight compounds within the IN, MA, HA, ASAM, and oral drugs categories

2.3.6 #Ar and Type of Rings

The number and nature of rings in a molecule can influence its physicochemical properties, ultimately influencing its clinical success.[41,58,59] The high attrition rate of molecules with a higher #Ar may be due to the low water solubility, high protein binding, and non-specific binding with other proteins leading to undesired effects. One crucial implication of the high content of aromatic carbons is the inhibition of human ether-à-go-go-related gene (hERG) channels that may lead to cardiotoxicity.[41]

On average, the HA molecule possesses more aromatic rings (mean = 2.73) than the MA (mean = 2.65) and IN (mean = 1.97) categories (**Figure 2.9**). However, the mean #Ar falls significantly in ASAM molecules (mean = 2.12) compared to that of HA but is still greater than that of oral drugs (mean = 1.66). These results are statistically significant, as indicated by both the *t*-test and the Kruskal–Wallis test. The 90th percentile for #Ar in ASAM and RAP molecules is 4, a unit higher than that of the oral drugs. This trend for #Ar also seems to be equally important for the large and small molecules (**Figure 2.12**), suggesting aromaticity to be a key determinant for both in vitro and in vivo antimalarial activity.
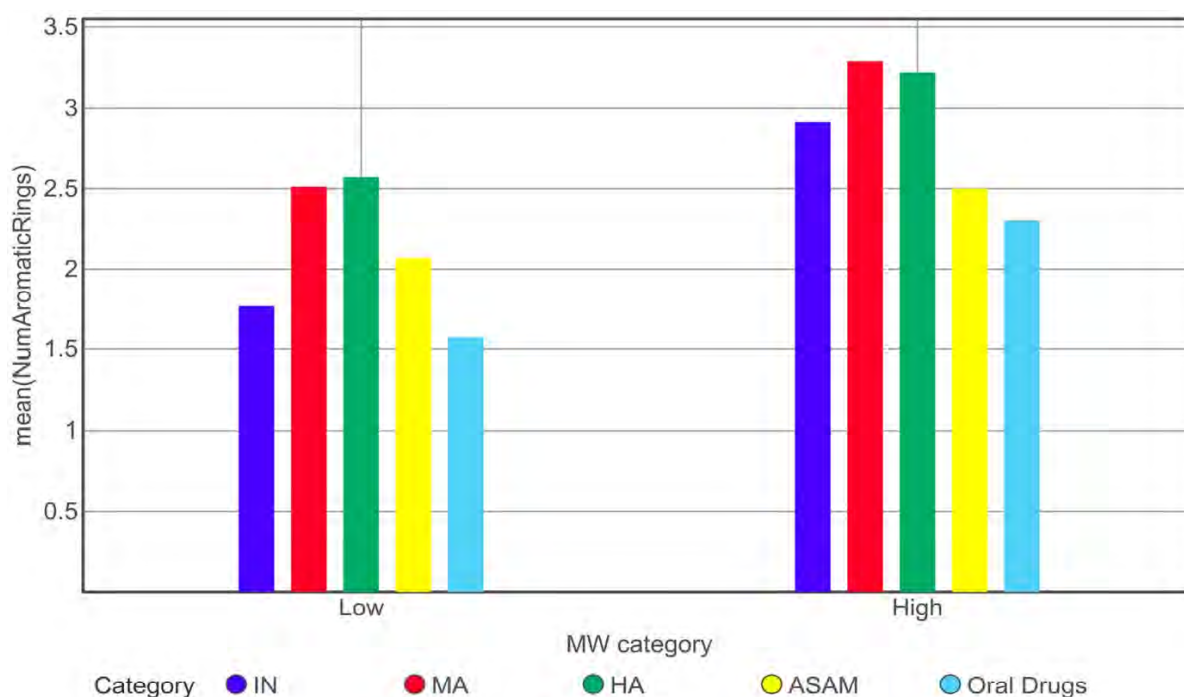
Figure 2.12. Distribution of mean of #Ar among low (MW < 500) and high (MW > 500 Da) molecular weight compounds within the IN, MA, HA, ASAM, and oral drugs categories.

The structurally related carboaromatic and heteroaromatic rings (*e.g.*, phenyl *vs* pyridine) display distinct values of lipophilicity, polarity, conformation preference, and H-bond capability.[60] Consequently, #CarboAr and #HetAr descriptors have varying influences on a molecule's pharmacokinetics and pharmacodynamic profile.[58]

While the mean #CarboAr of the ASAM category (1.23) is not different from that of the oral drugs (1.13), the #HetAr mean of bioavailable ASAMs (0.89) is significantly higher as

compared to the mean of oral drugs (0.52). Additionally, for active molecules (HA and MA), both #CarboAr and #HetAr are significantly higher than those of the IN class. A similar trend is observed in both the high and low MW class of compounds (**Figure 2.13A** and **2.13B**). These observations suggest that while aromaticity is vital for both in vitro and in vivo antimalarial activity, there is a need to limit the #CarboAr to advance the antimalarial molecules toward clinical application. These observations agree with an earlier study, which suggests that a higher #CarboAr has a more substantial detrimental effect on a compound's developability than a higher #HetAr.[58]

Given the importance of nitrogen-containing heterocycles in drug discovery,[61] in general and for antimalarial drug discovery,[62–64] in particular, we analyzed the aromatic nitrogen count (#ArN) in all compounds.

The #ArN is positively correlated with in vitro potency, as apparent from the mean #ArN for HA (1.11), MA (1.03), and IN (0.75) categories (**Figure 2.14**). The ASAM molecules display a mean value of 1.17 for the #ArN, which is significantly higher than that of the oral drugs (0.60) but not that of the HA class. However, the #ArN seems to be more critical for low MW compounds than for the bulkier molecules (**Figure 2.15**). All antimalarial categories also display the 90th percentile of 3 for the #ArN, one unit higher than that of the oral drugs. The proportion of molecules possessing at least one N-heteroaromatic ring also increases with an increase in vitro antiplasmodial activity (HA > MA > IN) and attains the highest value of ~62% for ASAM molecules (**Table 2.1**), much higher than that of the oral drugs (~30%). In contrast, no noticeable trend was observed for the aliphatic N-heterocycle, with all molecules showing similar percentages (**Table 2.1**). Amongst all aromatic N-heterocycles, the quinoline ring appears most frequently in antimalarial molecules, followed by pyridine and pyrimidine (**Table 2.4**). The latter two rings are also prevalent in oral drugs, an observation in line with the earlier reports.[59,65]
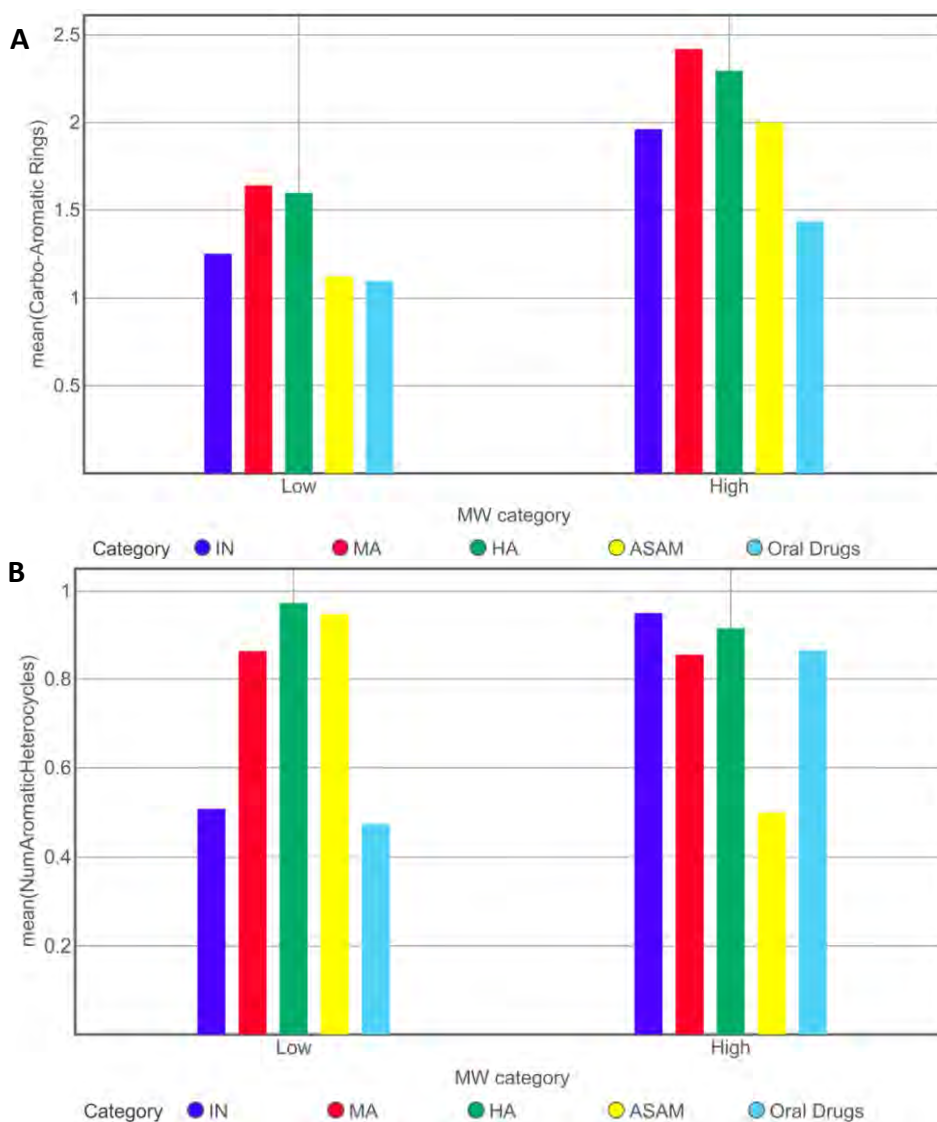
Figure 2.13. A) Distribution of mean of #CarboAr among low (MW < 500) and high (MW > 500 Da) molecular weight compounds within the IN, MA, HA, ASAM, and oral drugs categories. B) Distribution of mean of #HetAr among low (MW < 500) and high (MW > 500 Da) molecular weight compounds within the IN, MA, HA, ASAM, and oral drugs categories.

Table 2.4. Distribution of aromatic and aliphatic N-heterocycles in each category

Category	Total molecules	Molecules having at least 1 aromatic N-heterocycle	%age	Molecules having at least 1 aliphatic N-heterocycle	%age
IN	7365	2636	36	2543	35
MA	6620	3211	49	2836	43
HA	10557	5978	57	4771	45
ASAM	66	41	62	25	38
Oral Drugs	1954	591	30	899	46

Together, these observations suggest that higher content of the #ArN is favourable for the in vitro and in vivo antimalarial activity, and N-heterocyclics have a high probability of advancing in the antimalarial discovery pipeline.
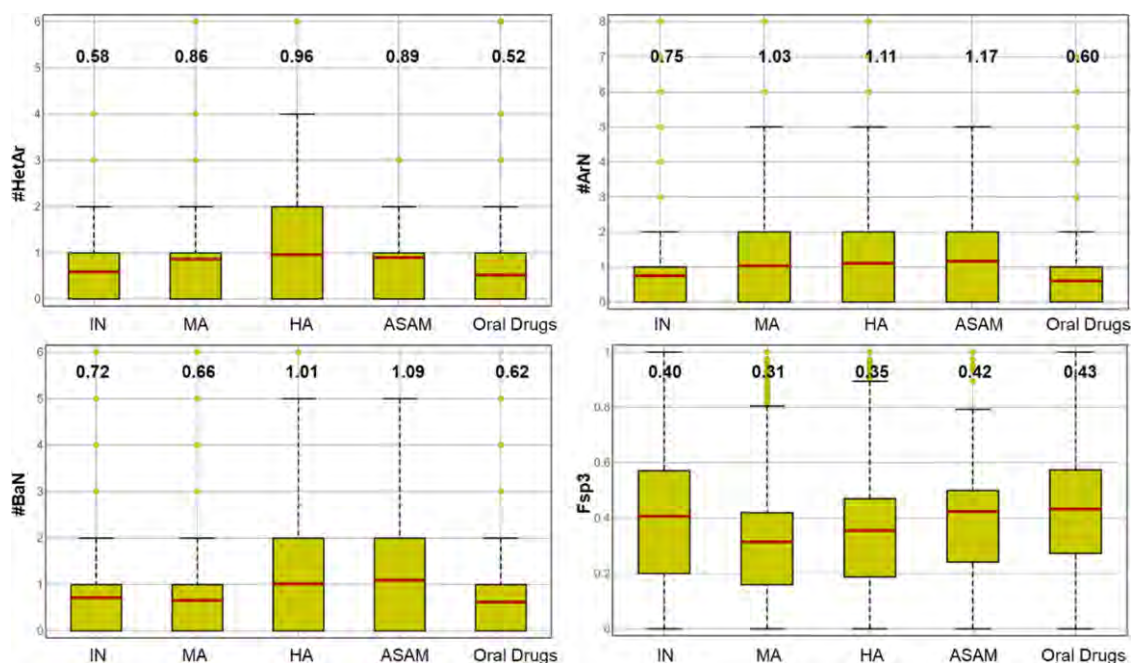
Figure 2.14. Boxplots for the #HetAr, #ArN, #BaN, and Fsp^3 properties for different sets of molecules. The mean values are given in bold above each boxplot and represented by the red line within the boxes. The yellow dots represent outliers.
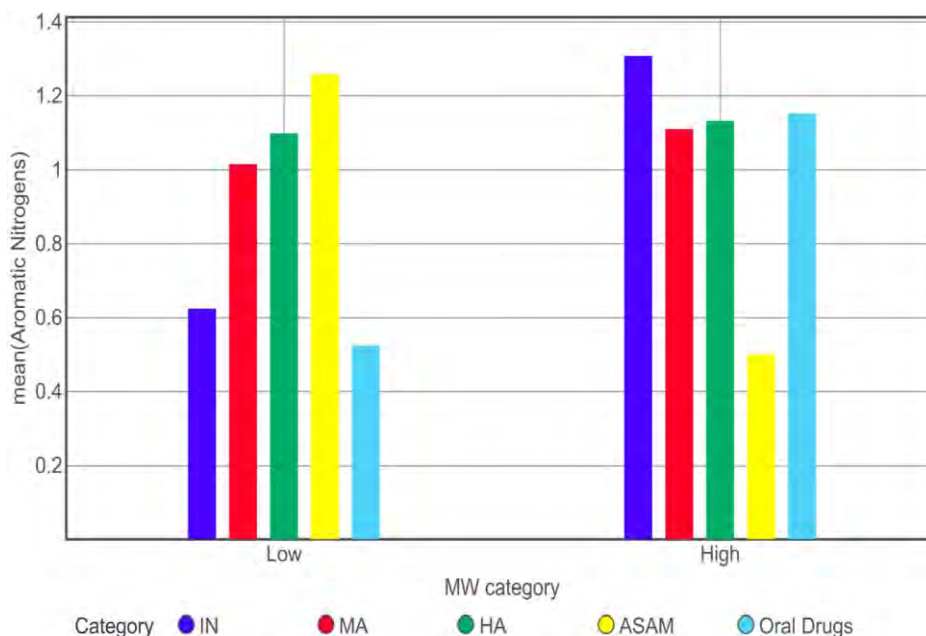
Figure 2.15. Distribution of mean of #ArN among low (MW<500) and high (MW>500 Da) molecular weight compounds within the IN, MA, HA, ASAM, and oral drug categories.

High content of the #CarboAr and #HetAr in antimalarials may be attributed to the historical success of quinoline-based antimalarials. The quinoline ring consists of two aromatic rings, one CarboAr and one HetAr. After several years, quinoline derivatives are still being pursued as antimalarials due to the synthetic tractability, cost-effectiveness, and ability of quinoline-based molecules to retain activity against chloroquine-resistant *Plasmodium* strains.[66] Consequently, the antimalarial literature is replete with quinoline and related heterocyclic molecules.[62] Additionally, several hybrid molecules[67,68] and bisquinoline molecules[69–72] are reported to possess potent antiplasmodial activity. The former consists of 4-aminoquinoline pharmacophore in conjunction with other heterocycles, while the latter contains two quinoline rings (total four #Ar) attached with a variable linker. Such bulky molecules are represented more in the RAP molecules, resulting in a higher #Ar and a high MW in these sets of molecules (*vide supra*).

Most of the quinoline and related N-heterocycle-based antimalarials target the hemozoin formation inside the parasite food vacuole. The latter is an essential process carried by the parasite to detoxify heme resulting from the hemoglobin degradation.[73–76] The quinoline and related cyclic scaffolds foster π-stacking interactions with the porphyrin's pyrrole rings, thereby inhibiting the nucleation and growth of the hemozoin crystals.[75,77–80]

In the context of target engagement, aromatic nitrogen can also act as an HBA and may dramatically improve potency, as observed for *Plasmodium* L-lactate transporter, *P. falciparium* formate-nitrite transporter (*Pf*FNT) inhibitors.[81] Another reason for the prevalence of N-heteroaromatics in the antimalarial design might be the emergence of *Plasmodium* kinases as drug targets.[82–84] The majority of kinase inhibitors target the ATP-binding pocket of the kinases, and several N-heterocycles mimic the adenosine ring of ATP. Another speculation may be that flatness might be favourable for transporting these molecules across the RBC or parasite membranes mediated by hitherto undiscovered transporters.

2.3.7 Fsp^3

The fraction of sp^3 hybridized or tetrahedral carbons, calculated as the ratio of sp^3 carbons to total carbons, is another critical physicochemical descriptor.[85] The oral drugs are known to attain a higher Fsp^3 in comparison to the clinical candidates. The higher Fsp^3 correlates well with improved solubility and lower melting points, factors likely to improve oral bioavailability.[85–87] This observation is confirmed with our compiled library of oral drugs and ASAM molecules, both of which possess higher 90th percentile values and averages for Fsp^3 than that of RAP molecules (**Table 2.2** and **2.3**). The Fsp^3 and #Ar descriptors show an overall negative correlation ($r = -0.632$ for all molecules), yet the ASAM molecules possessing a higher 90th percentile for the #Ar also display a higher 90th percentile for the Fsp^3, in comparison to that of the oral drugs. Among RAP molecules, MA and HA categories possess a significantly lower Fsp^3 (**Figure 2.14**) than the ASAM/oral drugs categories; a trend was also observed in both small and bulkier molecules (**Figure 2.16**). Together with the #Ar (*vide supra*), the results of Fsp^3 analysis reemphasize that the flat structure of antimalarials may have a positive influence on the in vitro potency. Nonetheless, as suggested for other orally available drugs,[85] a higher Fsp^3 is advantageous to advance antimalarials in the drug discovery pipeline.
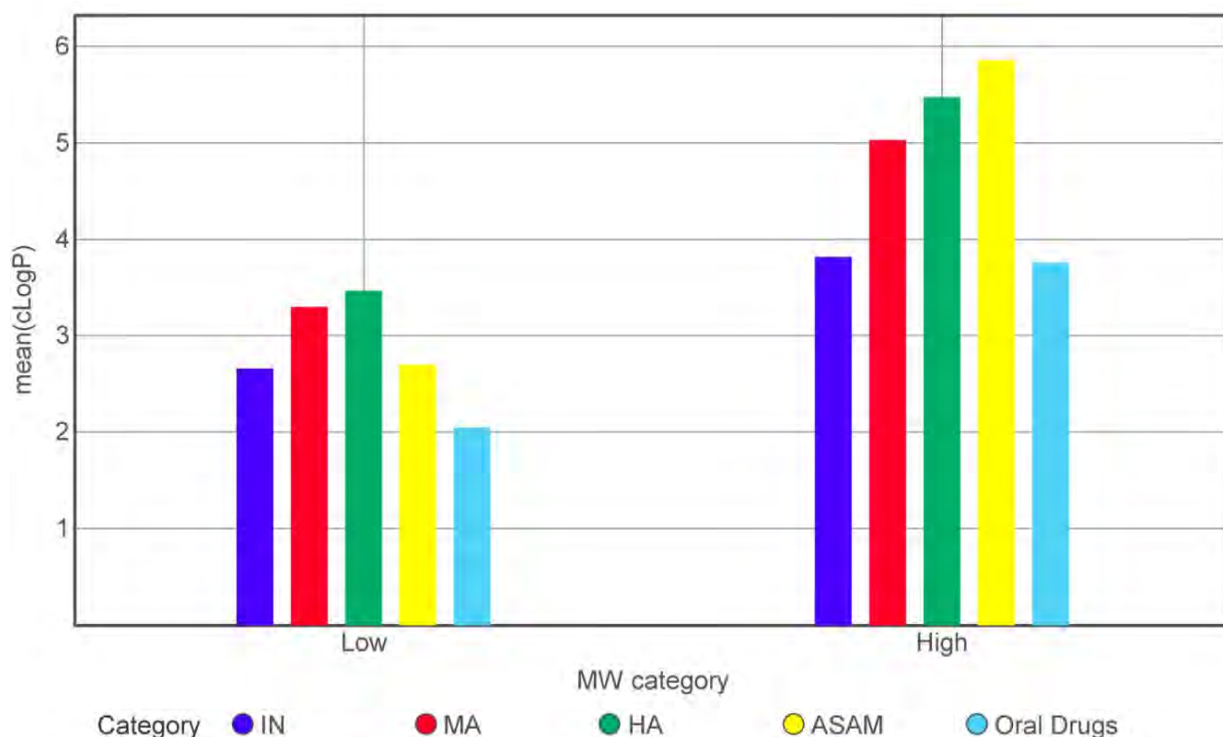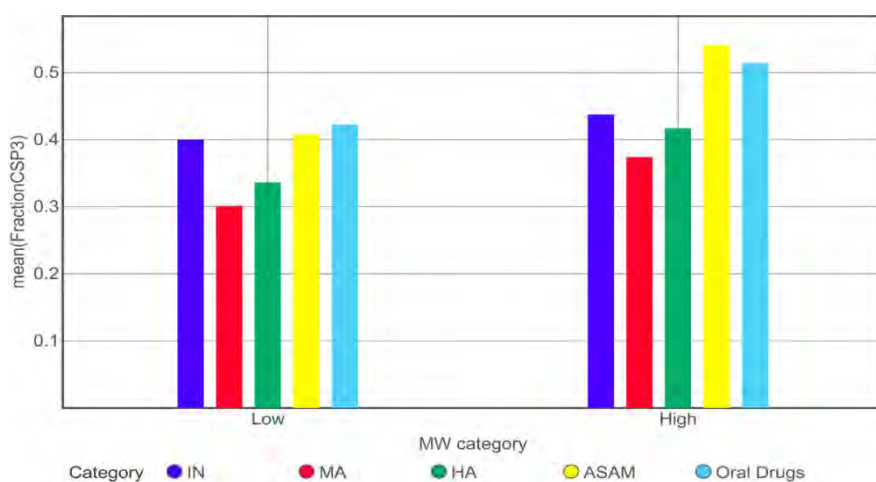

Figure 2.16. Distribution of mean of Fsp3 among low (MW < 500) and high (MW > 500 Da) molecular weight compounds within the IN, MA, HA, ASAM, and oral drugs categories.

2.3.8 Basicity

In DataWarrior, the basic nitrogen count (#BaN) can be used to estimate the molecule's basicity. The #BaN descriptor is based on a set of empirical rules rather than the computation of pK_a values. In addition to the amine groups, nitrogen atoms in certain heterocycles, such as quinoline, pyridine, and imidazole, are counted as BaN depending on the other ring substituents. However, only a weak correlation (0.328) is observed between the #BaN and #ArN in the dataset, suggesting the two descriptors to be orthogonal.

On average, all categories of antimalarial molecules possess a higher #BaN (**Figure 2.14**); however, statistical significance is displayed only in the case of oral drugs versus ASAM and oral drugs versus HA categories. Among RAP molecules, HA molecules possess a significantly higher #BaN than MA and IN molecules. These trends are also found to apply to small and large molecules (**Figure 2.17**). Also, #BaN 90th percentiles are consistently higher for all antimalarials than that of oral drugs. This observation confirms the importance of basic character for antimalarial molecules for in vitro and in vivo activity.
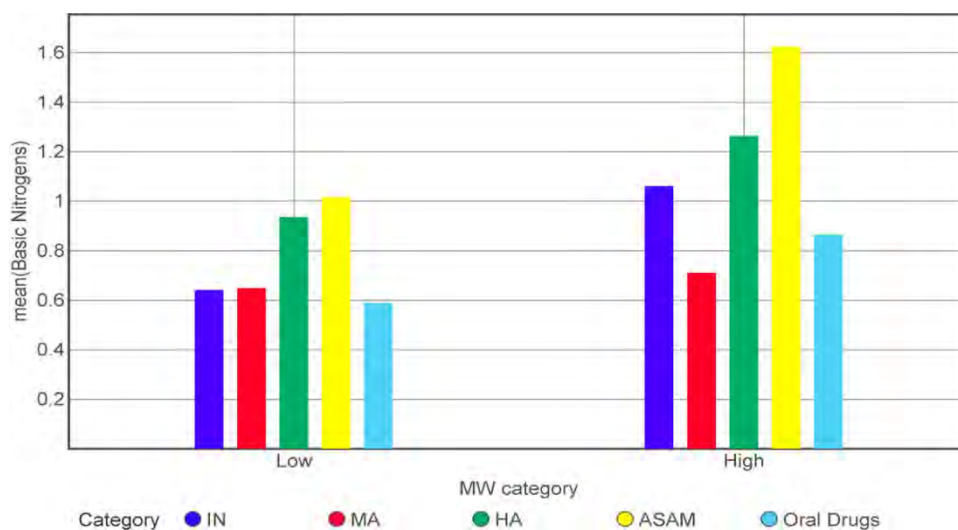
Figure 2.17. Distribution of mean of #BaN among low (MW < 500) and high (MW > 500 Da) molecular weight compounds within the IN, MA, HA, ASAM, and oral drugs categories.

The presence of basic centers in the form of amines or ArN (as in aminoquinolines) is known to improve the in vitro antiplasmodial potency of molecules acting through diverse

mechanisms.[88–94] This is especially true for the antimalarials that target hemozoin formation within the parasite DV.[75,95–97] The basic molecules ionize inside the acidic contents of the parasite's DV[98] leading to their entrapment and high intravacuolar concentration.[96,98] The basic side chain and ring nitrogen of quinoline antimalarials are also proposed to make crucial interaction with the heme.[75,90,94,99] In fact, the initial ionic interaction between the protonated nitrogen of the chloroquine side chain and heme carboxylate may be required to bring these together for further binding.[99] The slightly lower cytoplasmic pH of the parasite might also be the driving force for the internalization of the basic molecules.[97] In summary, the basicity of antimalarials may be necessary for both target binding and distribution within the parasite and its acidic DV. Also, the basic nitrogen centers are often added during lead optimization to improve solubility and metabolism, resulting in improved bioavailability.[60,92] This justifies the highest proportion of the #BaN and #ArN in ASAM molecules compared to RAP molecules. One notable exception is the artemisinin class of antimalarials,[100] which lack ArN or BaN in their structure and yet possess high in vitro and in vivo potency.

2.3.9 Antimalarial Property Space

One of this study's objectives was to probe if an antimalarial space may be defined within the broad oral drug space. According to the widely cited Lipinski's and Veber's rules, the majority of the compounds in all categories conform to the drug-like space (**Table 2.5**). Expectedly, oral drugs and ASAM molecules show higher compliance with both rules. However, the combination of various fundamental properties used in these rules (MW, clog P, HBA, HBD, TPSA, and #RB) did not reveal a property space typical of antimalarial molecules. Given the importance of the #BaN and #ArN in antimalarials (*vide supra*), we hypothesized that these structural features might be used as a scaling factor to differentiate antimalarials from other molecules. Thus, a new descriptor, the sum of #BaN and #ArN (SBAN), was defined and used

to scale various Lipinski's and Veber's properties by taking the latter's ratio to the factor of 1 + SBAN.

Table 2.5. Number of Molecules Compliant with the Specified Guidelines

Guidelines	Oral drugs (N = 1954)	ASAM (N = 66)	HA (N = 10,557)	MA (N = 6620)	IN (N = 7365)
Lipinski's Ro5	1786 (91%)	59 (89%)	8713 (83%)	5777 (87%)	6451 (88%)
Veber's rule	1647 (84%)	61 (92%)	8693 (82%)	5609 (85%)	5933 (81%)
Guideline-1 s-TPSA 5 to 65; s-RB ≤ 6; s-HBA ≤ 5; s-HBD ≤ 2	1338 (68%)	60 (91%)	8234 (78%)	4823 (73%)	4924 (67%)
Guideline-2 s-TPSA 5 to 65; s-RB ≤ 6; s-HBA ≤ 5; s-HBD ≤ 2; MW ≥ 235	1114 (57%)	60 (91%)	8090 (77%)	4639 (70%)	4418 (60%)

Interestingly, the property space described by the resulting scaled descriptors (s-MW, s-clog P, s-HBA, s-HBD, s-TPSA, and s-RB) revealed the confinement of the ASAM molecule to a narrow region within the broad drug-like space. Two typical examples of azithromycin and albitiazolium are represented in **Figure 2.18**. Azithromycin is overtly bulky (MW 749 Da) and highly polar (TPSA 180 Å^2) due to several HBAs. However, the SBAN value of 2 in azithromycin results in lowered s-HBA and s-TPSA, pushing it to the antimalarial space with other ASAM molecules (**Figure 2.18A** *vs* **2.18B**). Similarly, highly flexible albitiazolium (#RB = 17) also relocates to the antimalarial space upon using scaled descriptors (**Figure 2.18C** *vs* **2.18D**).

These results encouraged us to propose guidelines or thresholds based on the scaled descriptors to characterize an antimalarial property space, particularly for the ASAM class. Based on the importance of individual properties and various plots between different scaled descriptors, we focused on s-TPSA, s-RB, s-HBA, and s-HBD. We found guideline-1 based on s-TPSA (5–65 Å^2), s-RB (≤6), s-HBA (≤5), and s-HBD (≤2) to be more selective for antimalarial molecules (ASAM, HA, and MA) than for other oral drugs and IN molecules. 91% of ASAM, 78% of HA, and 73% of MA molecules comply with guideline-1, while only 68% of oral drugs and 67% of IN class are included in the same region (**Table 2.5**; **Figure 2.19**).
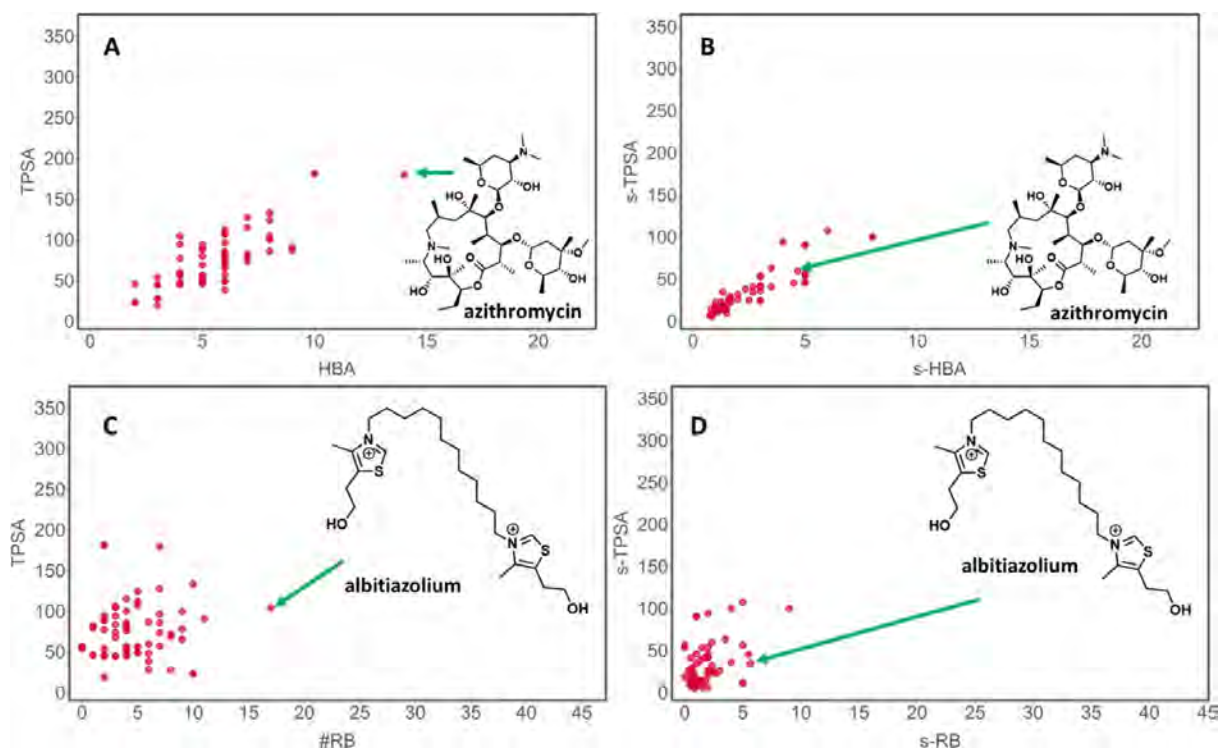
Figure 2.18 Plots showing ASAM molecules (red circles) in the property space. The bulky and polar azithromycin (A) converges to the antimalarial space defined by guideline-2 (B) when the corresponding scaled descriptors, s-TPSA and s-HBA, are used. Similarly, highly flexible and polar albitiazolium (C) also moves to the antimalarial space (D) following the application of the scaled descriptors, s-TPSA and s-RB.

Adding a threshold of MW $\geq$ 235 Da (guideline-2) further resulted in improved selectivity for the ASAM compared to that of the oral drugs and IN category. These results highlight the importance of the SBAN-scaled descriptors in defining the antimalarial drug space. Interestingly, all six ASAM molecules not complying with guideline-2 have high TPSA with no (or only one) SBAN count, resulting in their exclusion with the application of only the s-TPSA threshold (60–65 Å^2). Five of these are natural products (or natural product analogue) displaying high polarity owing to the presence of carboxylic (artesunate and CDRI 9778), phosphonic (fosmidomycin), or phenolic/enolic (tetracycline and doxycycline) acidic moieties (**Figure 2.20**). Dapsone, on the other hand, possesses two aromatic amines that are not considered "basic" by the DataWarrior program.

Several oral drugs and their close analogues have been shown to have potent activity against *P. falciparum* in several repurposing studies.[101–105] As a result, out of the 1114 oral drugs picked by guideline-2, 186 are already part of either RAP or ASAM libraries. Interestingly, of the

remaining 928 oral drugs, 516 (~56%) show the SkelSpheres[43] descriptors-based similarity of 0.7 or more to at least one HA or MA class of molecules. These observations further raise confidence in the use of guideline-2 for defining the antimalarial property space and offer a testable hypothesis. For example, it would be interesting to systematically evaluate these drugs, some of which are recently approved, against the parasite.
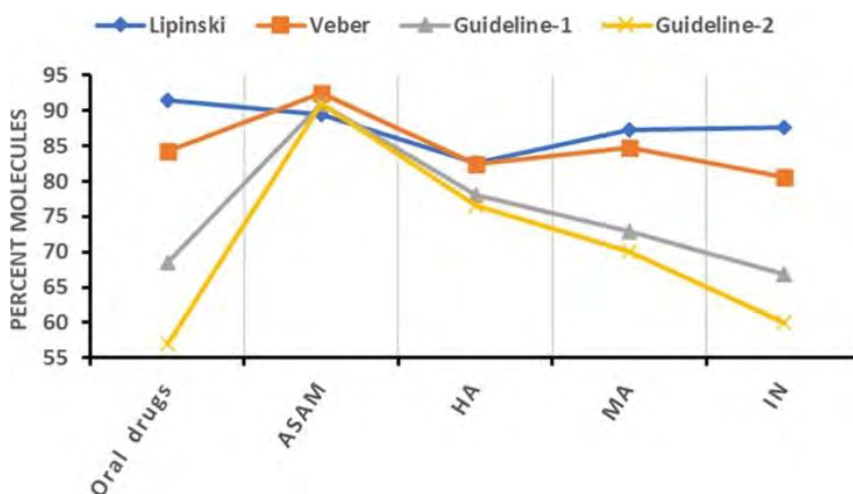
Figure 2.19. Plot portraying the percentage of molecules in compliance with specific guidelines. While most of the molecules in each category pass Lipinski's and Veber's rules, the thresholds based on the scaled descriptors (guideline-1 and guideline-2) are more selective for antimalarials.
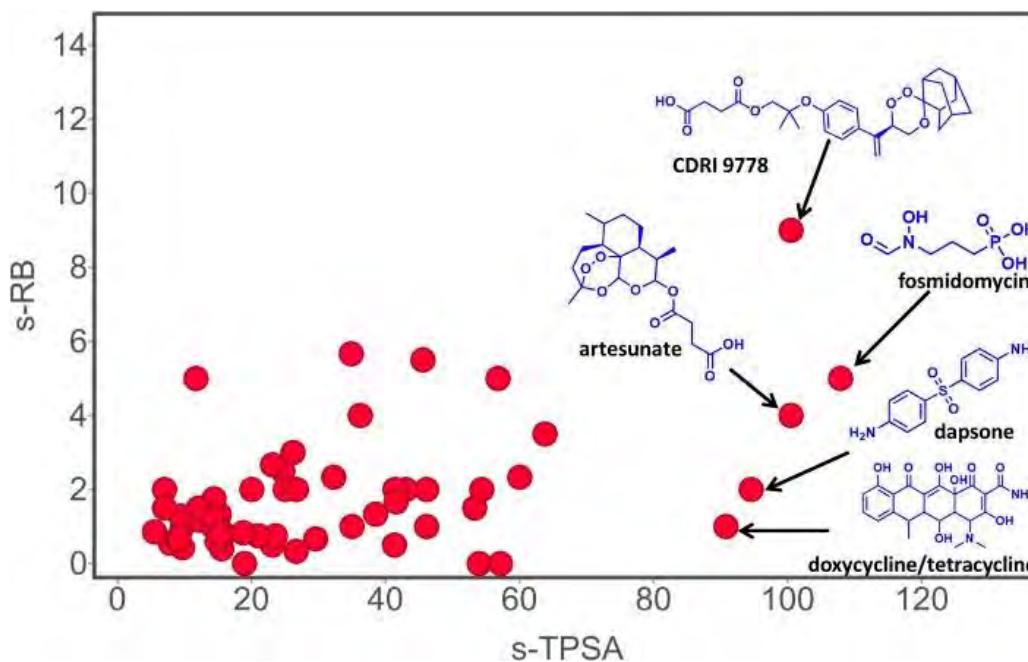
Figure 2.20. Plot of s-RB vs s-TPSA descriptors displaying ASAM molecules with high polarity not complying to Guideline-2.

2.4 CONCLUSION

In summary, this work provides insights into the average property space of RAP and ASAM molecules, vis-à-vis oral drugs using readily available open-source cheminformatics tools. The RAP molecules are significantly "obese" [54,106] and belong to "flatland".[85] These research molecules display a positive correlation between their MW, #Ar, and clog P descriptors and in vitro potency (IN < MA < HA). However, for ASAM molecules, these properties converge close to Lipinski's Ro5 thresholds while still maintaining higher averages than those of oral drugs. This suggests that overtly higher MW, lipophilicity, and a flat molecular shape may be helpful for the permeability across the RBC/parasite membranes, but lower values are preferred to obtain clinical or lead antimalarials. These observations also highlight the inability of the whole-cell antiplasmodial assays to filter out non-ideal molecules, which is an often-cited advantage of phenotypic assays.

Although a higher #Ar seems to contribute to in vitro potency, drug-likeness is maintained only by increasing the #HetAr rather than the #CarboAr.[58,59] Similarly, the higher average and 90th percentile of the Fsp^3 descriptor in the ASAM and oral drugs than that of RAP molecules reconfirm its influence on clinical success.[85] The HBA/HBD descriptors appear significant only for the bulky (MW > 500 Da) molecules with lower values favouring antimalarial activity. The lower TPSA and #RB also improve the likelihood of obtaining antimalarials with oral bioavailability, an observation in line with that of Veber et al.[42]

We also recognized that the #ArN and #BaN, the lesser-studied descriptors, are essential elements present in structurally diverse antimalarials, including historically successful aminoquinolines. Both the #ArN and #BaN might be assisting in target engagement and/or distribution within the parasite's acidic DV. We found a positive correlation between antimalarial activity and the #ArN and #BaN, while oral drugs were revealed to have lower values for these two descriptors. The high #ArN is primarily due to the expansive explorations

of quinoline, pyridine, and pyrimidine rings, while amine groups contribute to the high #BaN. Judging by its high frequency in all categories of antimalarial molecules, the quinoline ring is still relevant to the antimalarial drug design.

We also propose using properties scaled by the SBAN count to define a region in the property space where the probability of finding drug-like antimalarials (ASAMs) seems to be high. Two guidelines specifying the thresholds of scaled descriptors are suggested, albeit natural product-like molecules with acidic functionalities do not appear to conform to this space. In a physiological context, it seems that the SBAN count and other favourable properties assist antimalarials in crossing multiple membrane barriers to reach the intracellular targets of the parasite.[25] There is a clear indication that the *Plasmodium*'s highly evolved transportome[25,107–109] interacts with several marketed or advanced-stage antimalarials either as an antimalarial target or as part of a resistance mechanism.[107,109] Thus, a family of transporters in the parasitized RBC or PVM may be responsible for transporting antimalarials within the property space identified in this study. This is in line with Kell's hypothesis, implying that the carrier-mediated cellular uptake of molecules is more common than the diffusion across the phospholipid bilayer.[110–113] This is supported by the fact that the majority of drugs display high similarity to natural human metabolites.[114] It must be noted, however, that the characterization of *Plasmodium*'s transporters and their substrate specificities is challenging owing to its complex biology.

Overall, these results may have important implications in future explorations of antimalarial molecules. In general, relatively bulky, lipophilic, and flat molecules consisting of nitrogen scaffolds decorated with amine groups are preferable candidates for antimalarial drug design. The libraries conforming to the proposed antimalarial property space may provide higher hit rates in experimental or virtual HTS studies.

Specific properties, such as MW, may change over time, apparently due to the exploration of newer targets and technologies.[11,28,36] This change may also be reflected upon antimalarial leads and drugs.[115] Hence, property-based studies such as this should be reassessed as more data emerge in the future.

2.5 EXPERIMENTAL

2.5.1 Data curation

The ChEMBL-26 database[116] was searched within the DataWarrior program (version 5.2.1) to obtain the RAP set of molecules.[43] The molecules screened in a whole-cell phenotypic assay against *P. falciparum* were imported within DataWarrior, where macromolecules (MW > 900 Da) and organometallic compounds were removed. The compounds annotated with definite IC_{50} or EC_{50} values (with the qualifier "=", "~"; and not "<", ">") in nM or μM units were retained, and salt forms were neutralized. The canonical codes were generated using the DataWarrior program, and duplicate molecules were merged. In the case of multiple IC_{50}/EC_{50} values for the same compounds, the geometric average was calculated. The molecules with a large difference (>10 folds) in their multiple IC_{50}/EC_{50} values were discarded. The average IC_{50}/EC_{50} values were used for the classification of RAP molecules into HA ($IC_{50}/EC_{50} \leq 1000$ nM), MA IC_{50}/EC_{50} 1001−9999 nM), and IN ($IC_{50}/EC_{50} \geq 10,000$ nM) classes. The molecules found inactive in the HTS study conducted by GSK using the TCAMS[27] were also added to the IN set to expand the latter. The data for the TCAMS screening was downloaded from ChEMBL-neglected tropical disease webpage.[117] Only small (MW < 900 Da) and non-redundant molecules found to be inactive against both DD2 and 3D7 strains (for which no percentage inhibition data is reported) were retained (total 4351). The ASAM set of molecules was gathered from various literature reports and consisted of 33 marketed antimalarials, 19 clinical candidates, and 14 lead molecules. The structure of oral drugs was downloaded from

DrugCentral[35] database and updated with the new chemical entities approved by the US FDA till July 2020.

2.5.2 Physicochemical property analysis

The physicochemical properties were calculated either using the DataWarrior program or RDKit[118] nodes implemented in KNIME platform 4.1.2.[119] GraphPad Prism was used for the computation of various statistical parameters (such as mean, median, $90^{th}/10^{th}$ percentiles, and confidence intervals) and hypothesis testing using the non-parametric one-way analysis of variance (Kruskal−Wallis method). The p-values were calculated at a 95% confidence level. DataWarrior was used to compute boxplots and associated p-values using the t-test and for calculating Spearman correlation coefficients. The frequency of rings for all categories of molecules was carried out by counting the "plain ring systems" using DataWarrior.

2.5.3 Data and software availability

The structures and related data of RAP molecules can be freely obtained from ChEMBL database (https://www.ebi.ac.uk/chembl/). The ASAM set of molecules was manually curated from the recent literature. The set of oral drugs was obtained from DrugCentral database, downloadable from https://drugcentral.org/download. The KNIME platform (v 4.1.2) is freely available at https://www.knime.com/downloads. The RDKit nodes for KNIME are available to download within the KNIME platform. The DataWarrior program (v 5.2.1) is an open-source cheminformatic software downloadable from https://openmolecules.org/datawarrior/.

2.6 REFERENCES

1. Kola I, Landis J. Can the pharmaceutical industry reduce attrition rates? *Nat Rev Drug Discov*. 2004;3(8):711-715. doi:10.1038/NRD1470

2. Young RJ, Leeson PD. Mapping the Efficiency and Physicochemical Trajectories of Successful Optimizations. *J Med Chem*. 2018;61(15):6421-6467. doi:10.1021/ACS.JMEDCHEM.8B00180

3. Vieth M, Sutherland JJ. Dependence of molecular properties on proteomic family for marketed oral drugs. *J Med Chem*. 2006;49(12):3451-3453. doi:10.1021/JM0603825

4. Wager TT, Chandrasekaran RY, Hou X, et al. Defining desirable central nervous system drug space through the alignment of molecular properties, in vitro ADME, and safety attributes. *ACS Chem Neurosci*. 2010;1(6):420-434. doi:10.1021/CN100007X

5. Mahar Doan KM, Humphreys JE, Webster LO, et al. Passive permeability and P-glycoprotein-mediated efflux differentiate central nervous system (CNS) and non-CNS marketed drugs. *J Pharmacol Exp Ther*. 2002;303(3):1029-1037. doi:10.1124/JPET.102.039255

6. Kumar A, Loharch S, Kumar S, et al. Exploiting cheminformatic and machine learning to navigate the available chemical space of potential small molecule inhibitors of SARS-CoV-2. *Comput Struct Biotechnol J*. 2021;19:424-438. doi:10.1016/J.CSBJ.2020.12.028

7. Zhao S, Adamiak JW, Bonifay V, et al. Defining new chemical space for drug penetration into Gram-negative bacteria. *Nature Chemical Biology 2020 16:12*. 2020;16(12):1293-1302. doi:10.1038/s41589-020-00674-6

8. Richter MF, Drown BS, Riley AP, et al. Predictive compound accumulation rules yield a broad-spectrum antibiotic. *Nature 2017 545:7654*. 2017;545(7654):299-304. doi:10.1038/nature22308

9. Chhabra S, Kumar S, Parkesh R. Chemical Space Exploration of DprE1 Inhibitors Using Chemoinformatics and Artificial Intelligence. *ACS Omega*. 2021;6(22):14430-14441. doi:10.1021/ACSOMEGA.1C01314

10. Adrian G, Marcel V, Robert B, et al. A comparison of physicochemical property profiles of marketed oral drugs and orally bioavailable anti-cancer protein kinase inhibitors in clinical development. *Curr Top Med Chem*. 2007;7(14):1408-1422. doi:10.2174/156802607781696819

11. Leeson PD, Davis AM. Time-related differences in the physical property profiles of oral drugs. *J Med Chem*. 2004;47(25):6338-6348. doi:10.1021/JM049717D

12. Gualtieri M, Baneres-Roquet F, Villain-Guillot P, et al. The antibiotics in the chemical space. *Curr Med Chem*. 2009;16(3):390-393. doi:10.2174/092986709787002628

13. Macielag MJ. Chemical properties of antimicrobials and their uniqueness. *Antibiotic Discovery and Development*. 2012;9781461414001:793-820. doi:10.1007/978-1-4614-1400-1_24/COVER

14. World malaria report 2019. Accessed April 29, 2023. https://www.who.int/publications/i/item/9789241565721

15. Conrad MD, Rosenthal PJ. Antimalarial drug resistance in Africa: the calm before the storm? *Lancet Infect Dis*. 2019;19(10):e338-e351. doi:10.1016/S1473-3099(19)30261-0

16. Woodrow CJ, White NJ. The clinical impact of artemisinin resistance in Southeast Asia and the potential for future spread. *FEMS Microbiol Rev*. 2017;41(1):34-48. doi:10.1093/FEMSRE/FUW037

17. Müller O, Lu GY, Von Seidlein L. Geographic expansion of artemisinin resistance. *J Travel Med*. 2019;26(4). doi:10.1093/JTM/TAZ030

18. Imwong M, Suwannasin K, Kunasol C, et al. The spread of artemisinin-resistant Plasmodium falciparum in the Greater Mekong subregion: a molecular epidemiology observational study. *Lancet Infect Dis*. 2017;17(5):491-497. doi:10.1016/S1473-3099(17)30048-8

19. Hassett MR, Roepe PD. Origin and Spread of Evolving Artemisinin-Resistant Plasmodium falciparum Malarial Parasites in Southeast Asia. *Am J Trop Med Hyg*. 2019;101(6):1204-1211. doi:10.4269/AJTMH.19-0379

20. Ashley EA, Dhorda M, Fairhurst RM, et al. Spread of artemisinin resistance in Plasmodium falciparum malaria. *N Engl J Med*. 2014;371(5):411-423. doi:10.1056/NEJMOA1314981

21. Ashley EA, Phyo AP. Drugs in Development for Malaria. *Drugs*. 2018;78(9):861-879. doi:10.1007/S40265-018-0911-9

22. Tse EG, Korsik M, Todd MH. The past, present and future of anti-malarial medicines. *Malar J*. 2019;18(1):1-21. doi:10.1186/s12936-019-2724-z

23. Okombo J, Chibale K. Recent updates in the discovery and development of novel antimalarial drug candidates. *Medchemcomm*. 2018;9(3):437-453. doi:10.1039/C7MD00637C

24. Burrows JN, Duparc S, Gutteridge WE, et al. New developments in anti-malarial target candidate and product profiles. *Malar J*. 2017;16(1). doi:10.1186/S12936-016-1675-X

25. Basore K, Cheng Y, Kushwaha AK, et al. How do antimalarial drugs reach their intracellular targets? *Front Pharmacol*. 2015;6(MAY). doi:10.3389/FPHAR.2015.00091

26. Goldberg DE, Zimmerberg J. Hardly Vacuous: The Parasitophorous Vacuolar Membrane of Malaria Parasites. *Trends Parasitol*. 2020;36(2):138-146. doi:10.1016/J.PT.2019.11.006

27. Gamo FJ, Sanz LM, Vidal J, et al. Thousands of chemical starting points for antimalarial lead identification. *Nature*. 2010;465(7296):305-310. doi:10.1038/NATURE09107

28. Leeson PD, Springthorpe B. The influence of drug-like concepts on decision-making in medicinal chemistry. *Nat Rev Drug Discov*. 2007;6(11):881-890. doi:10.1038/NRD2445

29. Wenlock MC, Austin RP, Barton P, et al. A comparison of physiochemical property profiles of development and marketed oral drugs. *J Med Chem*. 2003;46(7):1250-1256. doi:10.1021/JM021053P

30. Tyrchan C, Blomberg N, Engkvist O, et al. Physicochemical property profiles of marketed drugs, clinical candidates and bioactive compounds. *Bioorg Med Chem Lett*. 2009;19(24):6943-6947. doi:10.1016/J.BMCL.2009.10.068

31. Bento AP, Gaulton A, Hersey A, et al. The ChEMBL bioactivity database: an update. *Nucleic Acids Res*. 2014;42(D1):D1083-D1090. doi:10.1093/NAR/GKT1031

32. Gaulton A, Bellis LJ, Bento AP, et al. ChEMBL: A large-scale bioactivity database for drug discovery. *Nucleic Acids Res*. 2012;40(D1). doi:10.1093/NAR/GKR777

33. Ekins S, Williams AJ. When pharmaceutical companies publish large datasets: an abundance of riches or fool's gold? *Drug Discov Today*. 2010;15(19-20):812-815. doi:10.1016/J.DRUDIS.2010.08.010

34. Dimova D, Stumpfe D, Bajorath J. Systematic assessment of coordinated activity cliffs formed by kinase inhibitors and detailed characterization of activity cliff clusters and associated SAR information. *Eur J Med Chem*. 2015;90:414-427. doi:10.1016/J.EJMECH.2014.11.058

35. Ursu O, Holmes J, Bologa CG, et al. DrugCentral 2018: an update. *Nucleic Acids Res*. 2019;47(D1):D963-D970. doi:10.1093/NAR/GKY963

36. Shultz MD. Two Decades under the Influence of the Rule of Five and the Changing Properties of Approved Oral Drugs. *J Med Chem*. 2019;62(4):1701-1714. doi:10.1021/ACS.JMEDCHEM.8B00686

37. Tinworth CP, Young RJ. Facts, Patterns, and Principles in Drug Discovery: Appraising the Rule of 5 with Measured Physicochemical Data. *J Med Chem*. 2020;63(18):10091-10108. doi:10.1021/ACS.JMEDCHEM.9B01596

38. Pye CR, Hewitt WM, Schwochert J, et al. Nonclassical Size Dependence of Permeation Defines Bounds for Passive Adsorption of Large Drug Molecules. *J Med Chem*. 2017;60(5):1665-1672. doi:10.1021/ACS.JMEDCHEM.6B01483/SUPPL_FILE/JM6B01483_SI_002.CSV

39. Doak BC, Over B, Giordanetto F, et al. Oral druggable space beyond the rule of 5: insights from drugs and clinical candidates. *Chem Biol*. 2014;21(9):1115-1142. doi:10.1016/J.CHEMBIOL.2014.08.013

40. Lipinski CA, Lombardo F, Dominy BW, et al. Experimental and computational approaches to estimate solubility and permeability in drug discovery and development settings. *Adv Drug Deliv Rev*. 1997;23(1-3):3-25. doi:10.1016/S0169-409X(96)00423-1

41. Ritchie TJ, Macdonald SJF. The impact of aromatic ring count on compound developability--are too many aromatic rings a liability in drug design? *Drug Discov Today*. 2009;14(21-22):1011-1020. doi:10.1016/J.DRUDIS.2009.07.014

42. Veber DF, Johnson SR, Cheng HY, et al. Molecular properties that influence the oral bioavailability of drug candidates. *J Med Chem*. 2002;45(12):2615-2623. doi:10.1021/JM020017N

43. Sander T, Freyss J, Von Korff M, et al. DataWarrior: an open-source program for chemistry aware data visualization and analysis. *J Chem Inf Model*. 2015;55(2):460-473. doi:10.1021/CI500588J

44. Mannhold R, Poda GI, Ostermann C, et al. Calculation of molecular lipophilicity: State-of-the-art and comparison of log P methods on more than 96,000 compounds. *J Pharm Sci*. 2009;98(3):861-893. doi:10.1002/JPS.21494

45. Van de Waterbeemd H, Smith DA, Beaumont K, et al. Property-based design: optimization of drug absorption and pharmacokinetics. *J Med Chem*. 2001;44(9):1313-1333. doi:10.1021/JM000407E

46. Nguitragool W, Bokhari AAB, Pillai AD, et al. Malaria parasite clag3 genes determine channel-mediated nutrient uptake by infected red blood cells. *Cell*. 2011;145(5):665-677. doi:10.1016/J.CELL.2011.05.002

47. Egan WJ, Merz KM, Baldwin JJ. Prediction of drug absorption using multivariate statistics. *J Med Chem*. 2000;43(21):3867-3877. doi:10.1021/JM000292E

48. Desai SA. Why do malaria parasites increase host erythrocyte permeability? *Trends Parasitol*. 2014;30(3):151-159. doi:10.1016/J.PT.2014.01.003

49. Cohn JV, Alkhalil A, Wagner MA, et al. Extracellular lysines on the plasmodial surface anion channel involved in Na+ exclusion. *Mol Biochem Parasitol*. 2003;132(1):27-34. doi:10.1016/J.MOLBIOPARA.2003.08.001

50. Desai SA, Rosenberg RL. Pore size of the malaria parasite's nutrient channel. *Proc Natl Acad Sci U S A*. 1997;94(5):2045-2049. doi:10.1073/PNAS.94.5.2045

51. Nyalwidhe J, Baumeister S, Hibbs AR, et al. A Nonpermeant Biotin Derivative Gains Access to the Parasitophorous Vacuole in Plasmodium falciparum-infected Erythrocytes Permeabilized with Streptolysin O. *J Biol Chem*. 2002;277(42):40005-40011. doi:10.1074/JBC.M207077200

52. Desai SA, Krogstad DJ, McCleskey EW. A nutrient-permeable channel on the intraerythrocytic malaria parasite. *Nature*. 1993;362(6421):643-646. doi:10.1038/362643A0

53. Refsgaard HHF, Jensen BF, Brockhoff PB, et al. In Silico Prediction of Membrane Permeability from Calculated Molecular Parameters. *J Med Chem*. 2005;48(3):805-811. Accessed April 29, 2023. https://orbit.dtu.dk/en/publications/in-silico-prediction-of-membrane-permeability-from-calculated-mol

54. Hann MM. Molecular obesity, potency and other addictions in drug discovery. *Medchemcomm*. 2011;2(5):349-355. doi:10.1039/C1MD00017A

55. Schultes S, De Graaf C, Berger H, et al. A medicinal chemistry perspective on melting point: matched molecular pair analysis of the effects of simple descriptors on the melting point of drug-like compounds. *Medchemcomm*. 2012;3(5):584-591. doi:10.1039/C2MD00313A

56. Withnall M, Chen H, Tetko IV. Matched Molecular Pair Analysis on Large Melting Point Datasets: A Big Data Perspective. *ChemMedChem*. 2017;13(6):599-606. doi:10.1002/CMDC.201700303

57. Ertl P, Rohde B, Selzer P. Fast calculation of molecular polar surface area as a sum of fragment-based contributions and its application to the prediction of drug transport properties. *J Med Chem*. 2000;43(20):3714-3717. doi:10.1021/JM000942E

58. Ritchie TJ, MacDonald SJF, Young RJ, et al. The impact of aromatic ring count on compound developability: further insights by examining carbo- and hetero-aromatic and -aliphatic ring types. *Drug Discov Today*. 2011;16(3-4):164-171. doi:10.1016/J.DRUDIS.2010.11.014

59. Ritchie TJ, MacDonald SJF, Peace S, et al. The developability of heteroaromatic and heteroaliphatic rings – do some have a better pedigree as potential drug molecules than others? *Medchemcomm*. 2012;3(9):1062-1069. doi:10.1039/C2MD20111A

60. Pennington LD, Moustakas DT. The Necessary Nitrogen Atom: A Versatile High-Impact Design Element for Multiparameter Optimization. *J Med Chem*. 2017;60(9):3552-3579. doi:10.1021/ACS.JMEDCHEM.6B01807

61. Vitaku E, Smith DT, Njardarson JT. Analysis of the structural diversity, substitution patterns, and frequency of nitrogen heterocycles among U.S. FDA approved pharmaceuticals. *J Med Chem*. 2014;57(24):10257-10274. doi:10.1021/JM501100B

62. Kalaria PN, Karad SC, Raval DK. A review on diverse heterocyclic compounds as the privileged scaffolds in antimalarial drug discovery. *Eur J Med Chem*. 2018;158:917-936. doi:10.1016/J.EJMECH.2018.08.040

63. Kaur K, Jain M, Reddy RP, et al. Quinolines and structurally related heterocycles as antimalarials. *Eur J Med Chem*. 2010;45(8):3245-3264. doi:10.1016/J.EJMECH.2010.04.011

64. Chugh A, Kumar A, Verma A, et al. A review of antimalarial activity of two or three nitrogen atoms containing heterocyclic compounds. *Medicinal Chemistry Research*. 2020;29(10):1723-1750. doi:10.1007/S00044-020-02604-6

65. Ertl P, Jelfs S, Mühlbacher J, et al. Quest for the rings. In silico exploration of ring universe to identify novel bioactive heteroaromatic scaffolds. *J Med Chem*. 2006;49(15):4568-4573. doi:10.1021/JM060217P

66. Parhizgar A, Tahghighi A. Introducing New Antimalarial Analogues of Chloroquine and Amodiaquine: A Narrative Review. *Iran J Med Sci*. Published online 2017.

67. Feng LS, Xu Z, Chang L, et al. Hybrid molecules with potential in vitro antiplasmodial and in vivo antimalarial activity against drug-resistant Plasmodium falciparum. *Med Res Rev*. 2020;40(3):931-971. doi:10.1002/MED.21643

68. Nqoro X, Tobeka N, Aderibigbe B. Quinoline-Based Hybrid Compounds with Antimalarial Activity. *Molecules*. 2017;22(12):2268. doi:10.3390/molecules22122268

69. Vennerstrom JL, Ellis WY, Ager AL, et al. Bisquinolines. 1. N,N-Bis(7-chloroquinolin-4-yl)alkanediamines with Potential against Chloroquine-Resistant Malaria. *J Med Chem.* 1992;35(11):2129-2134. doi:10.1021/JM00089A025/ASSET/JM00089A025.FP.PNG_V03

70. Liebman KM, Burgess SJ, Gunsaru B, et al. Unsymmetrical Bisquinolines with High Potency against P. falciparum Malaria. *Molecules 2020, Vol 25, Page 2251.* 2020;25(9):2251. doi:10.3390/MOLECULES25092251

71. Kondaparla S, Agarwal P, Srivastava K, et al. Design, synthesis and in vitro antiplasmodial activity of some bisquinolines against chloroquine-resistant strain. *Chem Biol Drug Des.* 2017;89(6):901-906. doi:10.1111/CBDD.12914

72. Vennerstrom JL, Ager AL, Dorn A, et al. Bisquinolines. 2. Antimalarial N,N-bis(7-chloroquinolin-4-yl)heteroalkanediamines. *J Med Chem.* 1998;41(22):4360-4364. doi:10.1021/JM9803828

73. Egan TJ. Haemozoin formation. *Mol Biochem Parasitol.* 2008;157(2):127-136. doi:10.1016/J.MOLBIOPARA.2007.11.005

74. Fong KY, Wright DW. Hemozoin and antimalarial drug discovery. *Future Med Chem.* 2013;5(12):1437-1450. doi:10.4155/FMC.13.113

75. Weissbuch I, Leiserowitz L. Interplay between malaria, crystalline hemozoin formation, and antimalarial drug action and design. *Chem Rev.* 2008;108(11):4899-4914. doi:10.1021/CR078274T/ASSET/CR078274T.FP.PNG_V03

76. Combrinck JM, Mabotha TE, Ncokazi KK, et al. Insights into the role of heme in the mechanism of action of antimalarials. *ACS Chem Biol.* 2013;8(1):133-137. doi:10.1021/CB300454T

77. Olafson KN, Nguyen TQ, Rimer JD, et al. Antimalarials inhibit hematin crystallization by unique drug-surface site interactions. *Proc Natl Acad Sci U S A.* 2017;114(29):7531-7536. doi:10.1073/PNAS.1700125114

78. Sullivan DJ. Quinolines block every step of malaria heme crystal growth. *Proc Natl Acad Sci USA.* 2017;114(29):7483-7485. doi:10.1073/PNAS.1708153114/ASSET/502F9E85-2591-4860-86B5-A896E7730425/ASSETS/GRAPHIC/PNAS.1708153114FIG01.JPEG

79. Buller R, Peterson ML, Almarsson Ö, et al. Quinoline Binding Site on Malaria Pigment Crystal: A Rational Pathway for Antimalaria Drug Design. *Cryst Growth Des.* 2002;2(6):553-562. doi:10.1021/CG025550I/ASSET/IMAGES/MEDIUM/CG025550IN00001.GIF

80. Solomonov I, Osipova M, Feldman Y, et al. Crystal nucleation, growth, and morphology of the synthetic malaria pigment beta-hematin and the effect thereon by quinoline additives: The malaria pigment as a target of various antimalarial drugs. *J Am Chem Soc.* 2007;129(9):2615-2627. doi:10.1021/JA0674183

81. Walloch P, Henke B, Häuer S, et al. Introduction of Scaffold Nitrogen Atoms Renders Inhibitors of the Malarial l-Lactate Transporter, PfFNT, Effective against the Gly107Ser

Resistance Mutation. *J Med Chem*. 2020;63(17):9731-9741. doi:10.1021/ACS.JMEDCHEM.0C00852

82. Kappes B, Doerig CD, Graeser R. An overview of Plasmodium protein kinases. *Parasitol Today*. 1999;15(11):449-454. doi:10.1016/S0169-4758(99)01527-6

83. Doerig C, Billker O, Haystead T, et al. Protein kinases of malaria parasites: an update. *Trends Parasitol*. 2008;24(12):570-577. doi:10.1016/J.PT.2008.08.007

84. Cabrera DG, Horatscheck A, Wilson CR, et al. Plasmodial Kinase Inhibitors: License to Cure? *J Med Chem*. 2018;61(18):8061-8077. doi:10.1021/ACS.JMEDCHEM.8B00329

85. Lovering F, Bikker J, Humblet C. Escape from flatland: increasing saturation as an approach to improving clinical success. *J Med Chem*. 2009;52(21):6752-6756. doi:10.1021/JM901241E

86. Ward SE, Beswick P. What does the aromatic ring number mean for drug design? *Expert Opin Drug Discov*. 2014;9(9):995-1003. doi:10.1517/17460441.2014.932346

87. Thomas VH, Bhattachar S, Hitchingham L, et al. The road map to oral bioavailability: an industrial perspective. *Expert Opin Drug Metab Toxicol*. 2006;2(4):591-608. doi:10.1517/17425255.2.4.591

88. Large JM, Birchall K, Bouloc NS, et al. Potent inhibitors of malarial P. Falciparum protein kinase G: Improving the cell activity of a series of imidazopyridines. *Bioorg Med Chem Lett*. 2019;29(3):509-514. doi:10.1016/J.BMCL.2018.11.039

89. Tsagris DJ, Birchall K, Bouloc N, et al. Trisubstituted thiazoles as potent and selective inhibitors of Plasmodium falciparum protein kinase G (PfPKG). *Bioorg Med Chem Lett*. 2018;28(19):3168-3173. doi:10.1016/J.BMCL.2018.08.028

90. Natarajan JK, Alumasa JN, Yearick K, et al. 4-N-, 4-S-, and 4-O-chloroquine analogues: influence of side chain length and quinolyl nitrogen pKa on activity vs chloroquine resistant malaria. *J Med Chem*. 2008;51(12):3466-3479. doi:10.1021/JM701478A

91. Hameed P. S, Solapure S, Patil V, et al. Triaminopyrimidine is a fast-killing and long-acting antimalarial clinical candidate. *Nat Commun*. 2015;6. doi:10.1038/NCOMMS7715

92. Masch A, Nasereddin A, Alder A, et al. Structure–activity relationships in a series of antiplasmodial thieno[2,3-b]pyridines. *Malar J*. 2019;18(1). doi:10.1186/S12936-019-2725-Y

93. Lavrado J, Cabal GG, Prudêncio M, et al. Incorporation of basic side chains into cryptolepine scaffold: Structure-antimalarial activity relationships and mechanistic studies. *J Med Chem*. 2011;54(3):734-750. doi:10.1021/JM101383F

94. Egan TJ, Hunter R, Kaschula CH, et al. Structure-function relationships in aminoquinolines: effect of amino and chloro groups on quinoline-hematin complex formation, inhibition of beta-hematin formation, and antiplasmodial activity. *J Med Chem*. 2000;43(2):283-291. doi:10.1021/JM990437L

95.   Tam DNH, Tawfik GM, El-Qushayri AE, et al. Correlation between anti-malarial and anti-haemozoin activities of anti-malarial compounds. *Malar J.* 2020;19(1). doi:10.1186/S12936-020-03370-X

96.   Kaschula CH, Egan TJ, Hunter R, et al. Structure-activity relationships in 4-aminoquinoline antiplasmodials. The role of the group at the 7-position. *J Med Chem.* 2002;45(16):3531-3539. doi:10.1021/JM020858U

97.   Yayon A, Cabantchik ZI, Ginsburg H. Identification of the acidic compartment of Plasmodium falciparum-infected human erythrocytes as the target of the antimalarial drug chloroquine. *EMBO J.* 1984;3(11):2695-2700. doi:10.1002/J.1460-2075.1984.TB02195.X

98.   Kuhn Y, Rohrbach P, Lanzer M. Quantitative pH measurements in Plasmodium falciparum-infected erythrocytes using pHluorin. *Cell Microbiol.* 2007;9(4):1004-1013. doi:10.1111/J.1462-5822.2006.00847.X

99.   Bachhawat K, Thomas CJ, Surolia N, et al. Interaction of chloroquine and its analogues with heme: An isothermal titration calorimetric study. *Biochem Biophys Res Commun.* 2000;276(3):1075-1079. doi:10.1006/BBRC.2000.3592

100.   O'Neill PM, Posner GH. A medicinal chemistry perspective on artemisinin and related endoperoxides. *J Med Chem.* 2004;47(12):2945-2964. doi:10.1021/JM030571C

101.   Teixeira C, Vale N, Pérez B, et al. "Recycling" classical drugs for malaria. *Chem Rev.* 2014;114(22):11164-11220. doi:10.1021/CR500123G/ASSET/IMAGES/CR500123G.SOCIAL.JPEG_V03

102.   Chong CR, Chen X, Shi L, et al. A clinical drug library screen identifies astemizole as an antimalarial agent. *Nature Chemical Biology 2006 2:8.* 2006;2(8):415-416. doi:10.1038/nchembio806

103.   Da Cruz FP, Martin C, Buchholz K, et al. Drug screen targeted at plasmodium liver stages identifies a potent multistage antimalarial drug. *Journal of Infectious Diseases.* 2012;205(8):1278-1286. doi:10.1093/infdis/jis184

104.   Pazhayam NM, Chhibber-Goel J, Sharma A. New leads for drug repurposing against malaria. *Drug Discov Today.* 2019;24(1):263-271. doi:10.1016/J.DRUDIS.2018.08.006

105.   Kaiser M, Mäser P, Tadoori LP, et al. Antiprotozoal activity profiling of approved drugs: A starting point toward drug repositioning. *PLoS One.* 2015;10(8):e0135556. doi:10.1371/JOURNAL.PONE.0135556

106.   Gleeson MP, Hersey A, Montanari D, et al Probing the links between in vitro potency, ADMET and physicochemical parameters. *Nat Rev Drug Discov.* 2011;10(3):197-208. doi:10.1038/NRD3367

107.   Martin RE. The transportome of the malaria parasite. *Biol Rev Camb Philos Soc.* 2020;95(2):305-332. doi:10.1111/BRV.12565

108. Cowell AN, Istvan ES, Lukens AK, et al. Mapping the malaria parasite druggable genome by using in vitro evolution and chemogenomics. *Science*. 2018;359(6372):191-199. doi:10.1126/SCIENCE.AAN4472

109. Meier A, Erler H, Beitz E. Targeting Channels and Transporters in Protozoan Parasite Infections. *Front Chem*. 2018;6(MAR). doi:10.3389/FCHEM.2018.00088

110. Dobson PD, Kell DB. Carrier-mediated cellular uptake of pharmaceutical drugs: an exception or the rule? *Nature Reviews Drug Discovery 2008 7:3*. 2008;7(3):205-220. doi:10.1038/nrd2438

111. Kell DB. What would be the observable consequences if phospholipid bilayer diffusion of drugs into cells is negligible? *Trends Pharmacol Sci*. 2015;36(1):15-21. doi:10.1016/J.TIPS.2014.10.005

112. Kell DB, Oliver SG. How drugs get into cells: tested and testable predictions to help discriminate between transporter-mediated uptake and lipoidal bilayer diffusion. *Front Pharmacol*. 2014;5. doi:10.3389/FPHAR.2014.00231

113. Kell DB, Dobson PD, Oliver SG. Pharmaceutical drug transport: the issues and the implications that it is essentially carrier-mediated only. *Drug Discov Today*. 2011;16(15-16):704-714. doi:10.1016/J.DRUDIS.2011.05.010

114. O'Hagan S, Swainston N, Handl J, et al. A 'rule of 0.5' for the metabolite-likeness of approved pharmaceutical drugs. *Metabolomics*. 2015;11(2):323. doi:10.1007/S11306-014-0733-Z

115. Charman SA, Andreu A, Barker H, et al. An in vitro toolbox to accelerate anti-malarial drug discovery and development. *Malar J*. 2020;19(1). doi:10.1186/S12936-019-3075-5

116. ChEMBL Database. Accessed April 29, 2023. https://www.ebi.ac.uk/chembl/

117. https://chembl.gitbook.io/chembl-   ntd/downloads/deposited-set-1-gsk-tcams-dataset-20th-may-2010 (accessed Oct 3 2020). GSK-TCAMS Dataset.

118. Landrum G. RDKit: Open-source cheminformatics. Release 2014.03.1. Published online 2014. doi:10.5281/ZENODO.10398

119. Berthold MR, Cebron N, Dill F, et al. KNIME: The Konstanz Information Miner. *Studies in Classification, Data Analysis, and Knowledge Organization*. Published online 2007:319-326. doi:10.1007/978-3-540-78246-9_38

Chapter 3

Synthesis and evaluation of bisquinazolines and quinazoline based hybrids as potential antimalarials

3.1 INTRODUCTION AND BACKGROUND

Malaria is a life-threatening epidemic disease caused by *Plasmodium* and transmitted to humans by female *anopheles* mosquito.[1] Malaria has affected around 2.4 billion people worldwide, with Africa and South East Asia being the most affected regions (**Figure 1.7**).[1]

3.1.1 Life cycle of *Plasmodium*

The life cycle of malarial parasite involves two hosts: *anopheles* mosquito and human. *Plasmodium* life cycle beings with injection of *Plasmodium* sporozoites into the host's blood stream with the bite of a female *anopheles* mosquito. Sporozoites migrate to the liver via blood, begin their replication in the hepatocytes and are released back into the blood stream as merozoites. This stage is known as the pre-erythrocytic stage. When *Plasmodium* remains in a dormant state in the liver, it is known as hypnozoite. Hypnozoites may cause malaria relapse within a week or even after a year. Further, merozoites enter the red blood cells (RBCs) and go through the ring stage and trophozoite stage to form schizonts which give rise to multiple invasive daughter merozoites (**Figure 3.1**).[2,3] During the erythrocytic stage, the malarial parasite multiplies inside the RBC of the host and destroys the cells in the process.[2]
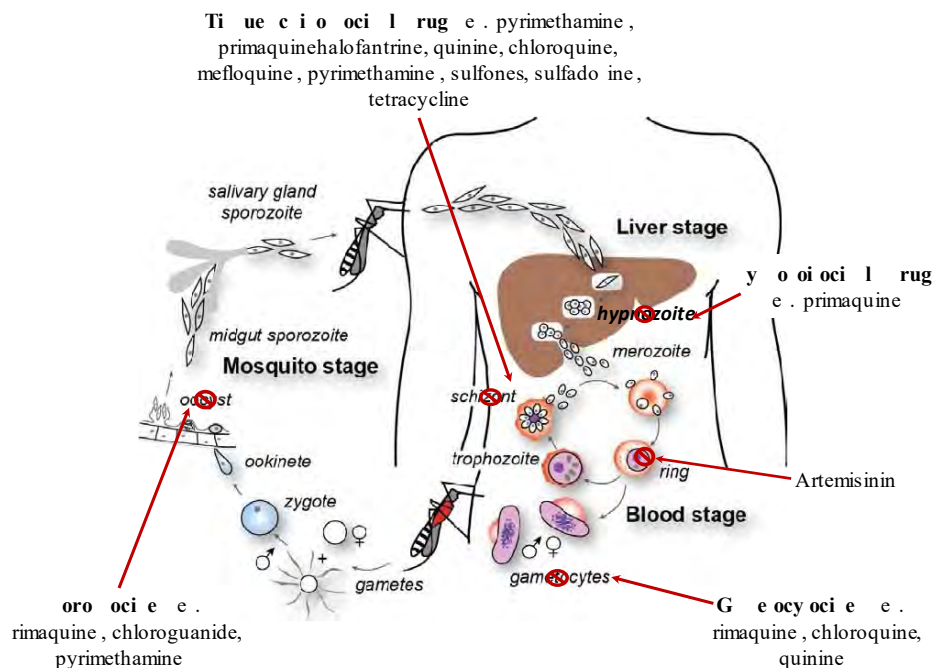
Figure 3.1. Different stages of the Life cycle of *Plasmodium* and cognate antimalarial drugs[4]

A large amount of host's haemoglobin is consumed by the parasite for either maintaining the amino acid supply or creating space for itself inside the RBC.[5] The parasite ingests haemoglobin inside its digestive vacuole (DV), where it undergoes degradation by the action of several proteases, resulting in the formation of free heme. Accumulation of heme inside the parasite is lethal for its e ist ence; therefore, free heme is converted into Hz, which is a non-to i c form.[5]

3.1.2 Role of   i *Plasmodium* life cycle

The formation of Hz begins from the intraerythrocytic stage of *Plasmodium*. During this stage, the parasite feeds on hemoglobin from the host erythrocytes through its cytostome via a process known as pinocytosis. Inside the parasite, the cytostome releases several small haemoglobin-containing vesicles which fuse to the acidic food vacuole.[6] Due to the acidic environment inside the food vacuole, haemoglobin undergoes o idation to produce methemoglobin and further hydrolysis via aspartic proteases (including plasmepsin I, II, IV and histo-aspartic protease) to convert methemoglobin into free heme (Fe^{+3}) and denatured globin protein. Under the influence of cysteine proteases (falcipain) and zinc-containing metallopeptidase (falcilysin), this denatured globin is further hydrolyzed into small peptides.[7,8] These proteases show optimal activity at pH 5, which appropriately coincides with the digestive vacuole environment. While cysteine proteases are responsible for around 20-40%, aspartic proteases account for 60-80% of globin-degradation activity.[9] Initial attack is initiated between α33 he and 34 Leu residues of haemoglobin by   lasmepsin I, followed by incisions at other locations. Nicks at these specific locations result in the uncoiling of haemoglobin, which in turn e pose s the sites for degradation by cysteine and aspartic proteases.[10] The peptides formed are then transported from the food vacuole to the cytoplasm of the parasite with the aid of a peptide transporter present in the food vacuole membrane.[11,12] Cytosolic e o peptidase acts on the peptides to hydrolyze them into amino acids, used for synthesizing parasite proteins and free heme.[13] Along

with amino acid formation by peptidases, free heme (Fe^{+3}) is also generated. When the free heme is not neutralized, it accumulates to a high concentration (300-500 mM) inside the parasite DV. This accumulation of free heme causes parasite death via the production of reactive oygen species leading to oidative stress.[14–17] Furthermore, due to its lipophilic properties, free heme intercalates in the parasite's membrane and results in the alteration of permeability and lipid organization of the membrane leading to lipid peroidation of the membrane culminating in death of the parasite.[18,19] In addition, free heme has a negative impact on the degradation of hemoglobin by cysteine protease (falcipain), which is e tre mely sensitive to free heme.[20] Hence, it is crucial for the survival of the parasite to get rid of free heme molecules.

3.1.3 e e e oxific io ec i i   r i e

Heme deto i fication is a vital process for the survival of the parasite. The parasite protects itself from the to i city induced by free heme through different heme deto i fication mechanisms, which are classified into two types:

a. Via Hz formation[21]
b. Systems situated mainly in the cytosol[22]

- Deto i fication by GSH[23]
- Heme binding proteins[23]
- Degradation by hydrogen pero ide [15]

3.1.3.1 Detoxification via Hz formation (primary mechanisms)

Free heme is converted to inactive form Hz through the polymerization of hematin, leading to the survival of the parasite.[9] This process is considered the primary mechanism of deto i fication of to i c heme into non-to i c Hz.[13] Several theories regarding Hz formation mechanism have been around in the literature, which are as follows:

3.1.3.1.1   Spontaneous formation of Hz:

The e act mechanisms for the formation of Hz in *Plasmodium* are not e pli citly understood to date despite the fact that deto i fication of heme is highly important for parasite survival.[24] However, it is stated that *Plasmodium* deto i fies free heme (Fe^{3+}) into an insoluble Hz crystal, often called malaria pigment, via a process known as biocrystallization. In the Hz crystal, the iron of one heme molecule is coordinated to the propionate carbo y late group of the ne t heme. The pigment is identified as dark black or brown crystalline spots in the RBC of patients infected with the parasite.[25] Hz is chemically and structurally similar to its synthetic analogue known as β-hematin, a cyclic dimer of ferritoprotoporphyrin IX. β-hematin may be synthesized artificially under in vitro conditions for assay purposes via several methods discussed later in the section. A study conducted in 1996 showed during the screening of ring-stage complementary DNA (cDNA) of *P. falciparum* to Hz, the clones contained sequence for HR II. Further, immunoblotting and immunofluorescence identified the presence of HR II in the purified digestive vacuoles.[25] Moreover, the involvement of HR II was confirmed by the intense HR II staining of the erythrocyte cytoplasm and trophozoite. Therefore, most of the parasites' HR II is in the digestive vacuole.[25] The HR II sequence was studied, and it was found that it contains 51 His-His-Ala tripeptide repeats, which is similar to the heme-binding site in the human histidine-rich glycoprotein (HRG).[26] Therefore, HR II in the digestive vacuole could bind the free heme and play an important role in its conversion to Hz.[25] In vitro, HR II binds with multiple heme molecules via bis-histidyl coordination and converts them into Hz.[27]

3.1.3.1.2 Hz formation via lipids:

The endogenous lipids of the *Plasmodium* play a crucial role in the formation of Hz. It was observed that the lipid e tracts of the *Plasmodium* induced spontaneous formation of Hz over several days under in vitro conditions with no preformed Hz present initially.[28] Addition of

acetonitrile e tr act of malarial trophozoites (containing methyl esters of oleic, palmitic and steric acids) hastened the process of Hz formation. Moreover, phospholipids (phosphatidylcholine, phosphatidylinositol, phosphatidylserine and sphingomyelin) also accelerate the process of β-hematin formation.[29] It has been hypothesized that since parasite's DV is rich in linoleic acid, it could be the primary lipid that acts as catalysis in the formation of Hz in vivo.[28]

3.1.3.1.3 Biomineralization or biocrystallization process induced Hz formation:

Several studies stated that biomineralization (a process of inorganic salts genesis under closely regulated conditions)[30] or biocrystallization (a biologically controlled process for nucleation and crystal growth dominated by the organism)[31,32] are the alternative pathways involved during Hz formation in plasmodium.[33]

Biocrystallization follows two steps initiation or nucleation of Hz (an inert biocrystal); and growth of the crystal.[34] The proposed mechanism of Hz formation by biocrystallization suggests the free heme (insoluble protein) in the transport vesicle (TV) of *Plasmodium* comple e s with soluble protein, and therefore, heme is carried to the TV's inner membrane. Diffusion of heme through the inner membrane is very slow owing to its insolubility. Therefore, it cumulates in the inner membrane at high concentration. Hence, the ideal hydrophobic environment of the membrane favours iron-carbo ylate bond formation of β-hematin dimer leading to nucleation of Hz. The membrane has also been known to act as a template for Hz growth.[32] Hempelmann et al. performed electron microscopy to observe this mechanism of Hz nucleation in the inner membrane of TV (mature Hz crystals associated with TV membrane fragments).[32] During the process of Hz nucleation, to keep other membranes of *Plasmodium* intact, the TV membrane breaks down, which appears as fragments in electron microscopy. Therefore, this mechanism came to be known as 'the membrane sacrifice' mechanism.[8,32]

3.1.3.2 Heme detoxification via systems situated mainly in the cytosol (secondary mechanisms)

The free heme remaining after deto i fication via primary mechanisms reaches the cytoplasm of *Plasmodium*, which is further processed for deto ific ation by the following mechanisms.

3.1.3.2.1 By reduced glutathione (GSH):

GSH is the endogenous cellular enzyme associated with various biological processes like maintaining protein-SH moieties in redo state via its antio idant effect, decreased accumulation of hydrogen and lipid pero ide s, and e puls ion of heme. During the uptake of haemoglobin, *Plasmodium* also ingests a small amount of GSH from the host erythrocyte into its food vacuole. Here, this GSH binds with free heme and deto i fies.[35,36] In the presence of GSH, heme competes with GSH for binding with the cytoskeletal membrane proteins and membrane lipid core. Therefore, membrane injury and, thus, the hemolytic effect of heme on red cells is prevented.[35,37]

3.1.3.2.2 By heme binding proteins:

Some of the proteins isolated from *Plasmodium* known to bind with heme and prevent o idative stress induced by heme include glutathione-S-transferase, glyceraldehyde-3-phosphate dehydrogenase (*Pf*GA DH), *P. falciparum* glutathione reductase (*Pf*GR) and *P. falciparum* protein disulfide isomerase.[38] The cytosolic protein, 1-Cys pero ir edo in (r) (*Pf*1-Cys- r), is e pre ssed during the later stages of heme degradation. It acts as an antio idant to neutralize the o idative burden created by free heme. Moreover, it prevents the formation of reactive o y gen species derived from iron generated during heme formation. Also, the membrane-associated heme formation is arrested, thus protecting the parasite.[35,39]

3.1.3.2.3 By hydrogen peroxide (H₂O₂):

Deto i fication of heme is also possible by pero ida tion, which targets the porphyrin ring of heme and leads to its rapid decomposition. The pH of 5.2 of the food vacuoles is considered the appropriate pH for pero ida tion to occur. This pH inside the food vacuole is maintained via AT ase pump-activated AT gradient. Ferryl [Fe(IV)] intermediate is formed on the reaction of heme molecules with H_2O_2. Further, the transfer of electrons within ferryl intermediates destroys heme's porphyrin ring.[35,39]

3.1.4 Curre re e of l ri

The treatment of malaria is based on the severity of the disease along with its progression stage, molecular targets, etc. Currently, available antimalarial drugs are listed in **Figure 3.2, 3.3** and **T b le 3.1** and belong to various chemotypes such as 4-aminoquinolines, 8-aminoquinolines, hydronaphthoquinones, sesquiterpene-lactones, artemisinin and sulfonamides. These drugs can also be classified based on the stage of the *Plasmodium* life cycle they act on (**Figure 3.1** and **T b le 3.1**).

Artesun®
Guilin Pharmaceutical
Artesunate

SPAQ-CQ™
Guilin Pharmaceutical
Pyrimethamine/Sulfadoxine-Amodiaquine

ASMQ
Cipla
Artesunate-Mefloquine

Krintafel
GSK
Tafenoquine

Eurartesim®
Alfasigma/pierre fabre
Dihydroartemisinin-Piperaquine

Pyramax® (granules)
Shin Poong
Pyronaridine-Artesunate

ASAQ Winthrop®
Sanofi
Artesunate-Amodiaquine

Coartem® Dispersible
Novartis
Artemether-Lumefantrine

Malarone
GSK
Atovaquone/Proguanil

Figure 3.2. New FDA approved combination medicines and formulations

T ble 3.1. Antimalarial drugs, based on structure and the stage of *Plasmodium* life cycle they act on

Class	Example/s of drugs	Chemical structure	Stage of *Plasmodium* life cycle they act on	Reference
4-Aminoquinoline	Chloroquine Amodiaquine	**1** **2**	- On blood schizonts - On gametocytes	40
8-Aminoquinoline	Primaquine Tafenoquine	**3** **4**	- Erythrocytic stage - On hypnozoites - On gametocytes - Hinder development of oocyst and multiplication of parasite in gut	3 41
4-Quinolinemethanols	Mefloquine	**5**	- On blood schizonts	2
Quinoline containing Cinchona alkaloids	Quinine Quinidine	**6** **7**	- On blood schizonts - On gametocytes	3
Hydronaphthoquinones	Atovaquone	**8**	- Inhibits mitochondrial electron transport chain	40
Diaminopyrimidines	Pyrimethamine	**9**	- Erythrocytic stage - On blood schizonts	2
Sesquiterpene lactones	Artemisinin	**10**	- Free radical - Parasite protein	40
Sulfonamides	Sulfalene Sulfadoxine Dapsone	**11** **12** **13**	- On blood schizonts	3
Biguanides	Proguanil Chlorproguanil Cycloguanil	**14** **15** **16**	Hinder development of oocyst and multiplication of parasites in the gut	41
Antibiotics	Tetracycline Azithromycin Doxycycline	**17** **18** **19**	- On blood schizonts	2
Phenanthrene-methanols	Lumefantrine	**20**	- Blood schizont	40
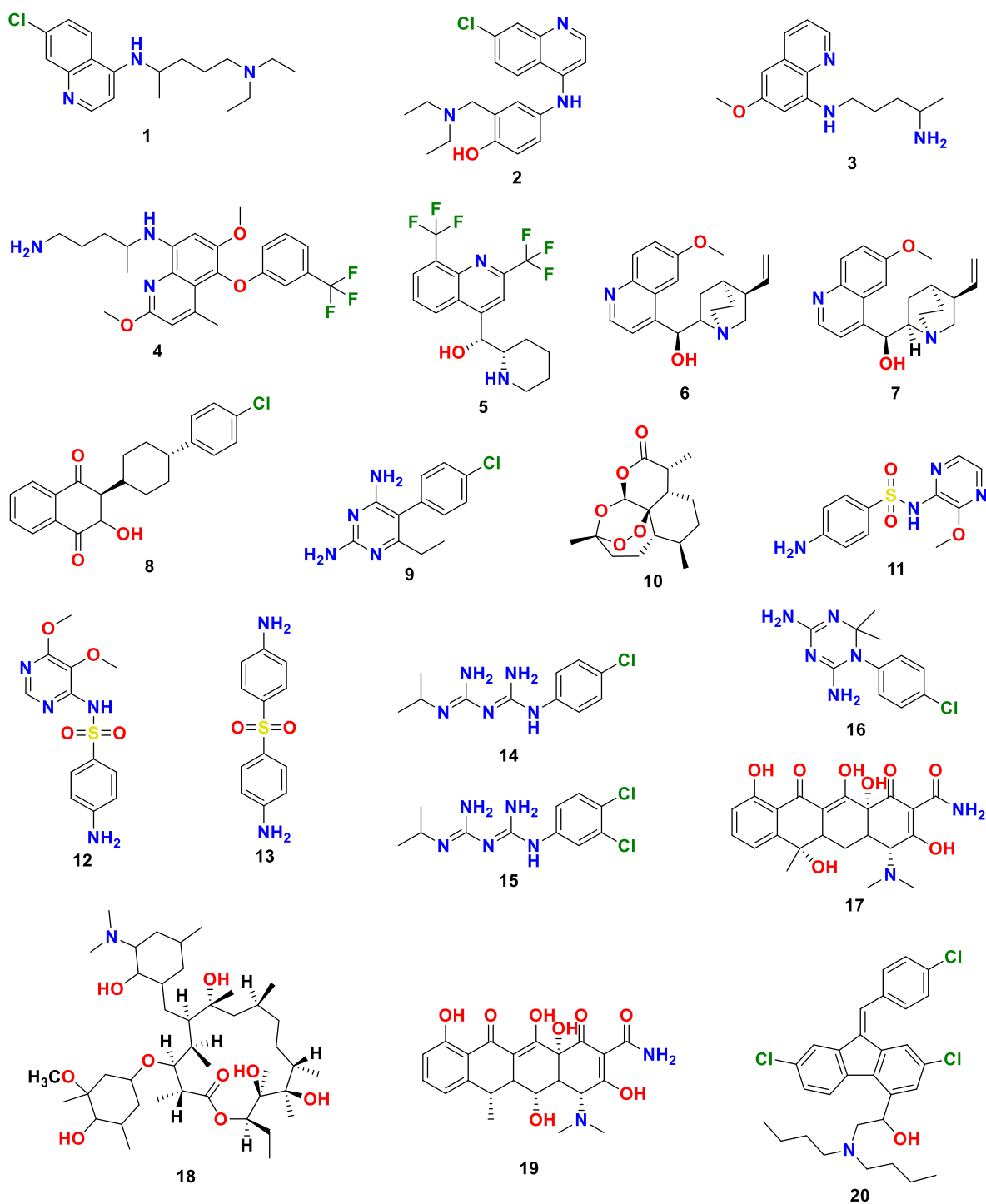
Figure 3.3. Current antiplasmodial drugs corresponding Table 3.1

3.1.5 Drug in clinical trial

Several new antimalarials acting on novel targets have been developed by different research groups, which are in different phases of clinical trials (**Figure 3.4** and **Table 3.2**). These include *Pf*ATP4 inhibitors such as cipargamin, GSK3191607, SJ733; *Pf*DHODH inhibitors

like DSM265 and 218; and KAF156 and ZY19489 whose mechanism of action is still unknown.[42–48]

T ble 3.2. Antimalarial drugs in clinical trials

Compound	Target	Structure	Phase clinical trials/ in market	References
DM1157	Interferes with parasite's metabolism and reversed chloroquine inhibits its ability to efflux drug	**21**	Phase I	49
Cipargamin (NITD609)	P-type cation-transporter ATPase4 (*Pf*ATP4) inhibitor	**22**	Phase II	42
AQ-13	Chloroquine like mechanism, interference with heme detoxification, but efflux of drug spared	**23**	Phase II	50
KAF156 (Ganaplacide)	Belongs to imidazolopiperazines, unknown mechanism of action	**24**	Phase II	47
SJ733	*Pf*ATP4 inhibitor	**25**	Phase I	44
DSM 265	*Plasmodium* dihydroorotate dehydrogenase inhibitor	**26**	Phase II	45
OZ 439	Cleavage of the endoperoxide bond by Fe^{2+} and heme released during haemoglobin digestion could generate free radicals that alkylate key parasitic proteins	**27**	Phase II	51
ZY 19489	The actual mode of action yet to be discovered. Rapid parasites-killing activity across all intra-erythrocytic malaria stages	**28**	Phase I	52
P218	*Plasmodium* dihydroorotate dehydrogenase inhibitor	**29**	Phase I	46
PA21A092	Disruption of Na^+ regulation in blood-stage *P. falciparum* parasites	**30**	Phase I	53
GSK 3191607	*Pf*ATP4 inhibitor	**29**	Phase I	54
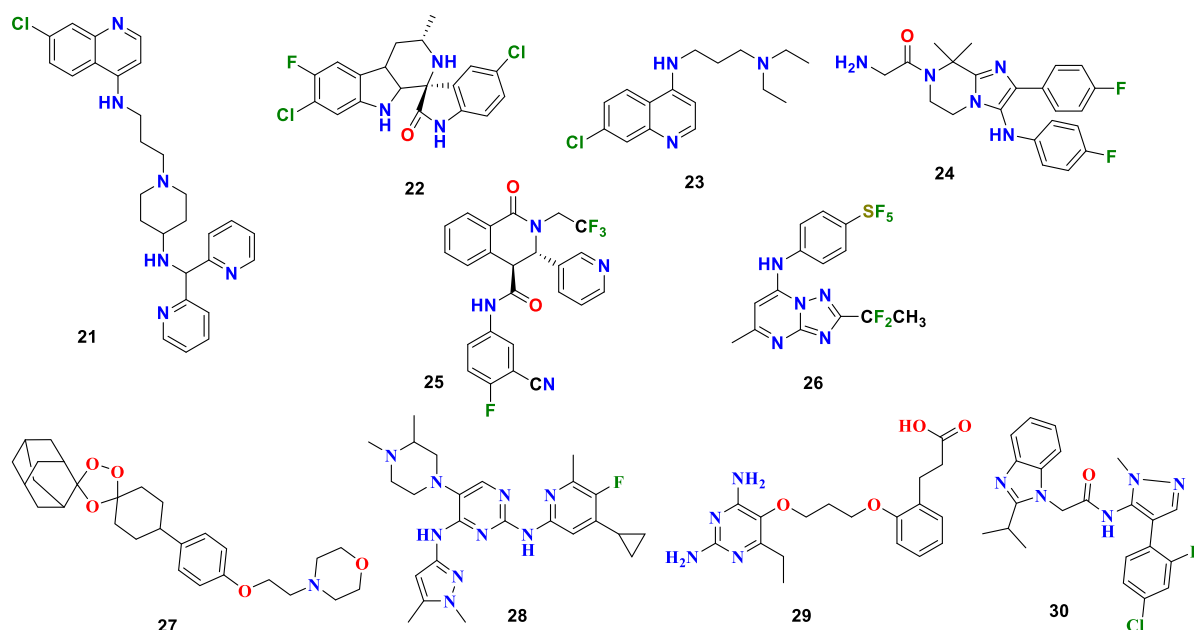
Figure 3.4. Antimalarial compounds in clinical trials

3.1.6 Re i ce o exi i g i l ri l

Chloroquine held the position of being the drug of choice in the World Health Organization (WHO) Global Eradication rogram for at least 2 decades until the emergence of resistant *Plasmodium* strains in the 1960s. *Plasmodium* utilizes host haemoglobin for its growth and replication, and during this process, haemoglobin is broken down to form heme. It has been proposed that chloroquine inhibits Hz formation and heme polymerase resulting in the accumulation of heme to to i c levels, leading to the disruption of constitutive functions of the parasite culminating in death of the parasite.[55,56] Therefore, via different mechanisms, heme is deto i fied to form Hz, the non-to i c product of haemoglobin lysis.[57]

Several studies have reported that resistance associated with chloroquine is due to an increase in the pH of the digestive vacuole (causing decreased chloroquine influ), decreased affinity of chloroquine to heme, or *P. falciparum* chloroquine resistance transporter (*Pf*CRT) mutation (causing enhanced chloroquine efflu) . Accumulation of chloroquine inside the cell is reduced, resulting in decreased heme (to ic for the *Plasmodium*) buildup inside the parasite, leading to loss of therapeutic potential of chloroquine (**Figure 3.5**).[2,3]
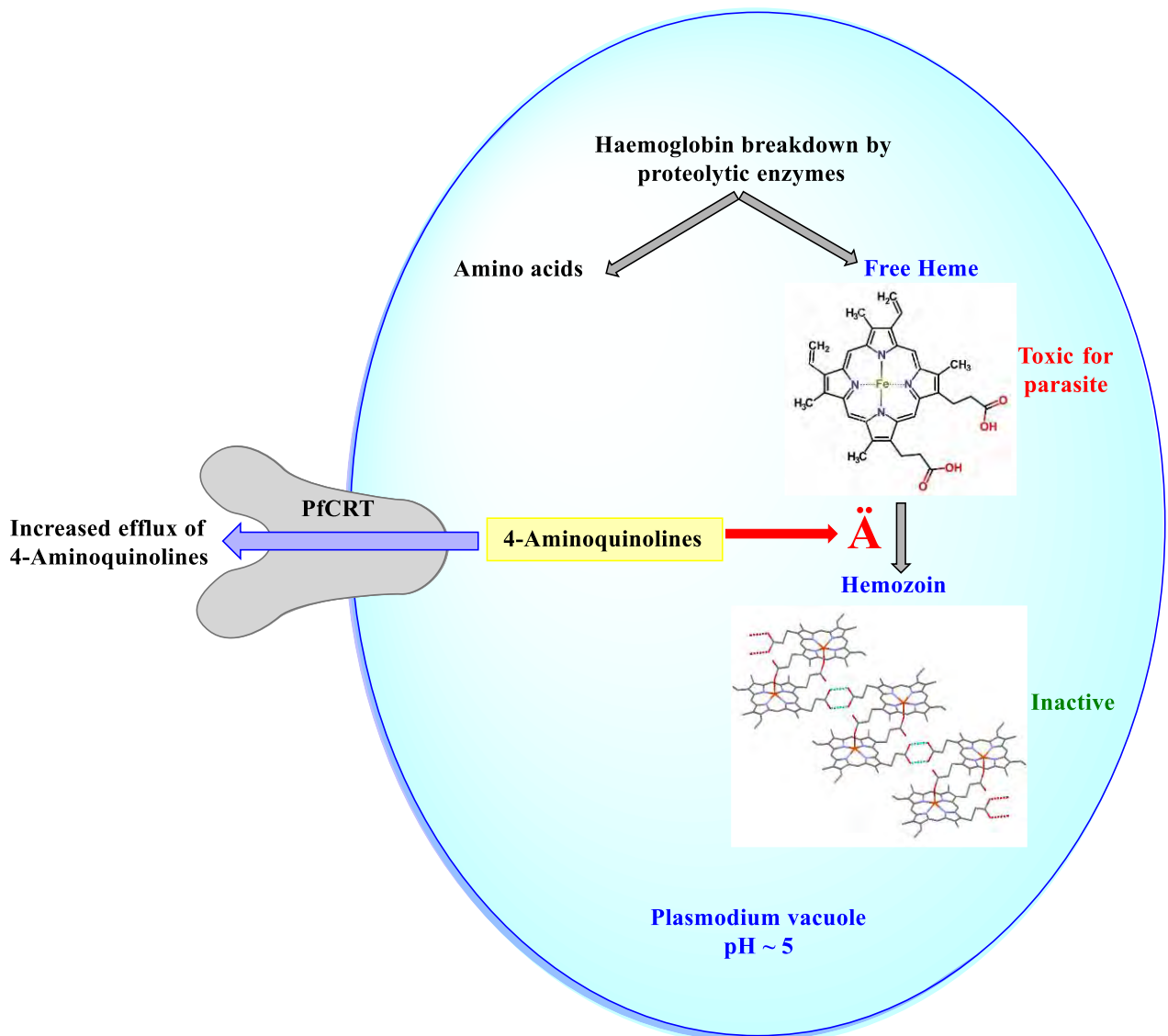
Figure 3.5. Mechanism of chloroquine resistance in *Plasmodium*

Currently, ACT, that is, artemisinin in combination with other antimalarial drugs has been recommended by WHO and is the only efficient way for the treatment of a variety of malarial strains.[58,59] This strategy has effectively reduced the number of malarial cases and associated mortality over the last decade.[1] However, recent reports from different areas have declared decreased sensitivity of the malaria parasite to artemisinin due to mutations in the *Plasmodium falciparum* Kelch 13 (*Pf*K13) protein.[59,60] Resistance has also developed against other classes of antimalarials due to mutations in different target proteins (**Figure 3.6**).[58] Therefore, the development of new strategies is required to overcome resistance. Therefore, the design and

synthesis of novel hybrid compounds and development of new strategies to overcome the resistance is the need of the hour.
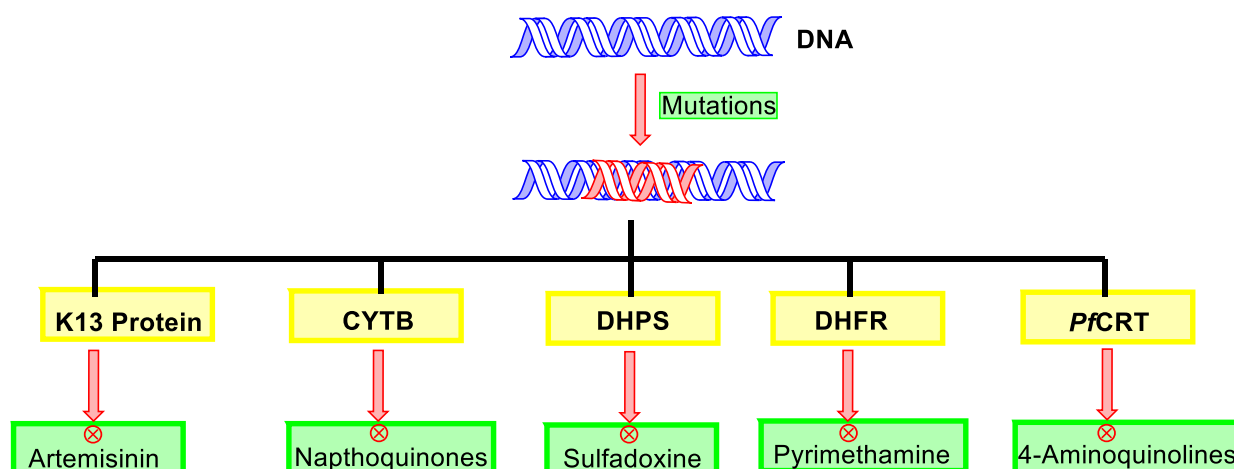
Figure 3.6. Mutations leading to resistance in e isting drugs. K13: Kelch 13; CYTB: Cytochrome B; DH S : dihydropteroate synthase; DHFR: dihydrofolate reductase; *Pf*CRT: *P. falciparum* CQ-resistance transporter

3.1.7 yb ri olecule i rug evelo e

Meunier and co-workers put forth the concept of hybrid moieties to overcome the problem of drug resistance against antimalarial drugs.[61] Hybrid molecules are chemical compounds which contain two or more pharmacological moieties with different biological functions covalently linked together, resulting in a single molecule.[2] Hence, these molecules are also known by the term Multitarget-directed ligands (MTDLs).[62] There are four commonly used strategies for MTDL designing, including merged-pharmacophore, fused-pharmacophore, non-cleavable linked-pharmacophore and cleavable linked-pharmacophore (**Figure 3.7**). Based on the requirement, either of these techniques may be used for designing a novel molecule.[62] Design of hybrid molecules against various therapeutic targets is emerging as a useful medicinal chemistry strategy due to various advantages. Individual pharmacophores used to form the hybrid mutually protect each other from the risk of development of drug resistance, for e a mple, sulfado in e/pyrimethamine. One pharmacophore of the hybrid may help enhance the bioavailability of the other pharmacophore. Moreover, the structural property of the linker employed may positively modulate the solubility of the hybrid; for e a mple, linker containing

two ethylene o ide units used to synthesize the chloroquine-pyrimethamine hybrid forms H-bonding with water molecules resulting in good solubility of the hybrid in both acidic as well as neutral media. Different pharmacophores in a hybrid molecule may show better therapeutic effects than the parent molecules alone, for e ample, artemisinin and quinine hybrid.
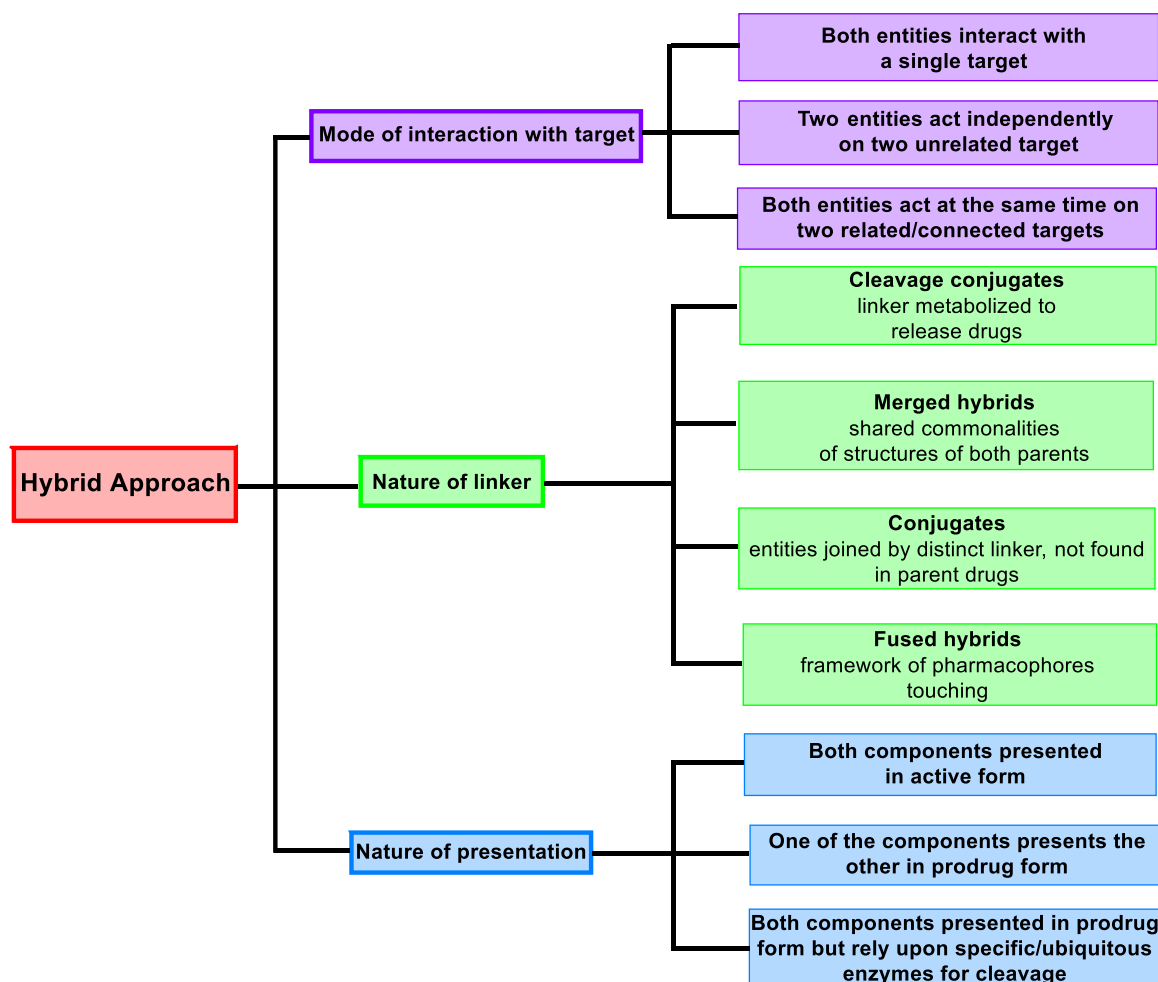
Figure 3.7. Classification of hybrid compounds

Similarly, trio a ne and chloroquine hybrid (trio aquine) showed better activity (IC$_{50}$ = 5-74 nM).[49] Moreover, artemisinin and primaquine phosphate and stilbene and chalcone hybrids all showed synergistically improved antimalarial activity.[42] A drug molecule that may be to i c on the whole may become non-to i c by combining it with another pharmacophore; for e a mple, Bosquesi et al. combined thalidomide with glutarimide subunit using hybridization to form derivatives free of teratogenic effects.[50] Similarly, Vangapandu et al. synthesized primaquine phosphate compounds free of hemolysis-inducing property.[47]

T ble 3.3. Some e a mples of antimalarial hybrid compounds

Property	First Pharmacophore (IC$_{50}$)		Second pharmacophore (IC$_{50}$)		Structure of the hybrid	IC$_{50}$ value of hybrid		Reference
	CQS	CQR	CQS	CQR		CQS	CQR	
Overcoming drug resistance	Chloroquine		Imipramine		31	2.9 nM	5.3 nM	44
	6.5 nM	102 nM	-	-				
	Artesunate		Indoloquinoline		32	0.45 nM	0.42 nM	45
	4.3 nM	2.8 nM	9.4 nM	209.5 nM				
	Dihydroartemisinin		Quinoline		33	8.7 nM	5.31 nM	63
	5.11 ± 0.64 nM	2.09 ± 0.33 nM	21.54 ± 6.73 nM	157.90 ± 52.70 nM				
	Artemisinin		Quinine		34	10.4 nM	10.2 nM	64
	45.5 nM	55 nM	73.5 nM	75.3 nM				
Increase solubility	Chloroquine		Pyrimethamine		35	0.070 M	0.157 M	65
	0.040 M	0.417 M	0.070 M	-				
Synergism	Trioxane		Chloroquine		36	4 nM	5 nM	49
	6 nM	5 nM	25 nM	115 nM				
	Artemisinin		Primaquine		37	-	9.1 nM	42
	-	8.2 ± 0.9 nM	-	3300 ± 55 nM				
Provide stability	9-aminoacridine		Artemisinin		38	2.6 nM	-	66
	-	-	<5.2 nM	15.1 ± 0.5 nM				

Likewise, the formation of hybrids resulted in improved stability in comparison with that of individual drugs, for e a mple, the 9-aminoacridine-artemisinin hybrid, wherein the former, due to the presence of acridine ring imparts stability to otherwise unstable artemisinin.[2] Antimalarial hybrid compounds have been found useful in overcoming drug resistance against individual pharmacophores. For e ample, artesunate-indoloquinoline hybrid (IC$_{50}$ = 0.42 nM against CQR) (**Figure 3.8**, **32**). Deshpande et al. combined calcium channel blockers, such as imipramine and verapamil, with chloroquine to restore chloroquine's efficacy against *Plasmodium*. Calcium channel blockers linked with aminoquinoline prevent the efflu of the drug from the digestive vacuole.[5] The first hybrid to block the chloroquine efflu involved

linking an aminoquinoline to a reversal agent using an alkyl linker.[44] Similarly, certain reversal agents linked with aminoquinoline moiety directly inhibit the *Pf*CRT to prevent the drug's efflu . These hybrids are known as 'reversed chloroquine' (**T b le 3.3**).[2,42,45,63,64]
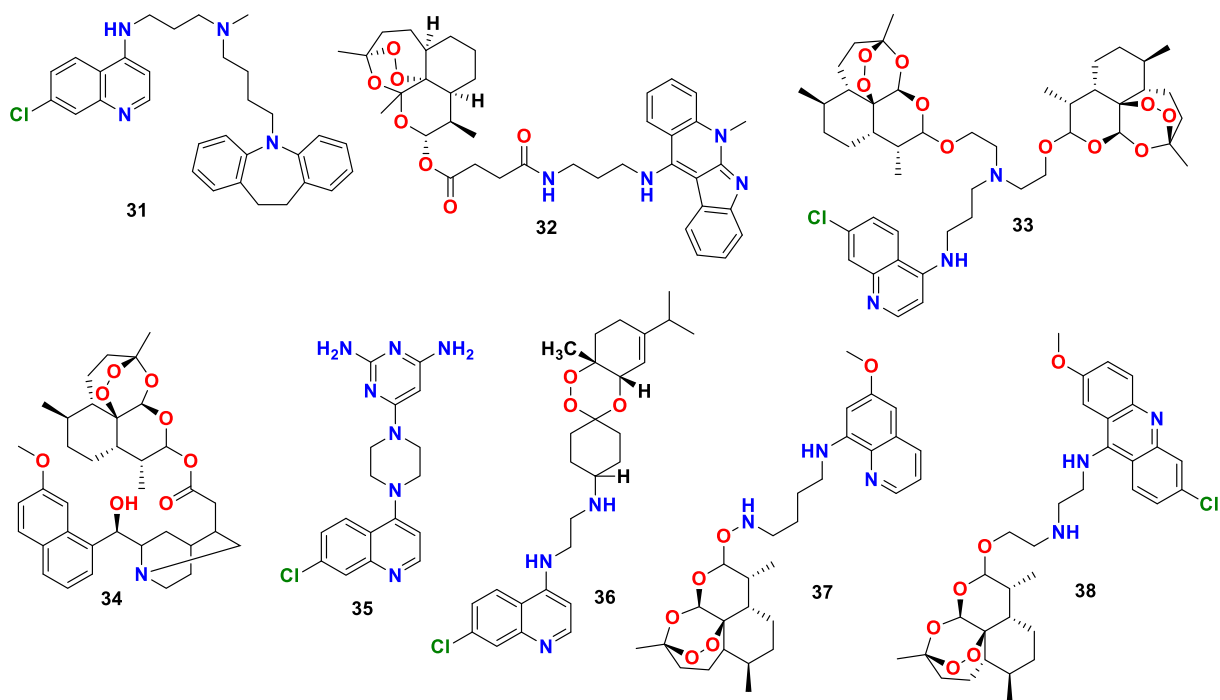
Figure 3.8. Structures of hybrid compounds

In several studies, quinoline-artemisinin hybrids have been reported to show enhanced antimalarial activity in comparison to the individual compounds (**T b le 3.3**).[42,45,63,64] Recently, Çapcı et al. synthesized novel artesunic acid hybrids with quinoline and isoquinoline (**Figure 3.9**). These hybrids showed superior activity compared to precursors against drug-sensitive (3D7) and MDR strains (Dd2 and K1). Moreover, it was reported that the artesunic acid hybrids with quinoline showed comparatively better antiplasmodial activity than isoquinoline hybrids.[67]

In a similar approach, the bisquinolines have also been developed during the search for quinoline compounds which could help overcome the resistance of the *Plasmodium*. Bisquinolines consist of two quinoline moieties combined via a linker, which may be aliphatic or aromatic.[68]
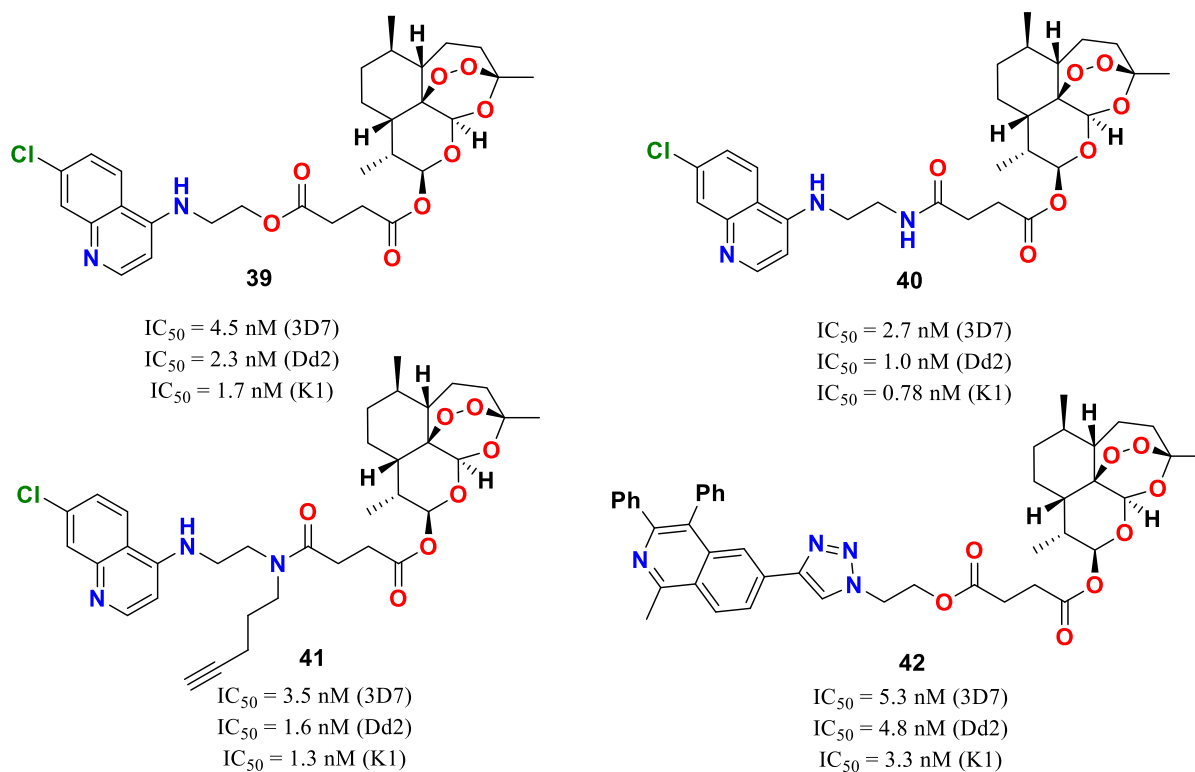
Figure 3.9. Artesunic acid hybrids with quinoline and isoquinoline

Some of the e a mples of the bisquinolines synthesized in the past include piperaquine (**43**), hydro ypiper aquine (**43b**), dichloroquinazine (**44**).[68] These compounds showed better antiplasmodial activity in comparison to chloroquine in addition to a longer duration of action and lesser to ic ity at the therapeutic dose, unlike chloroquine.
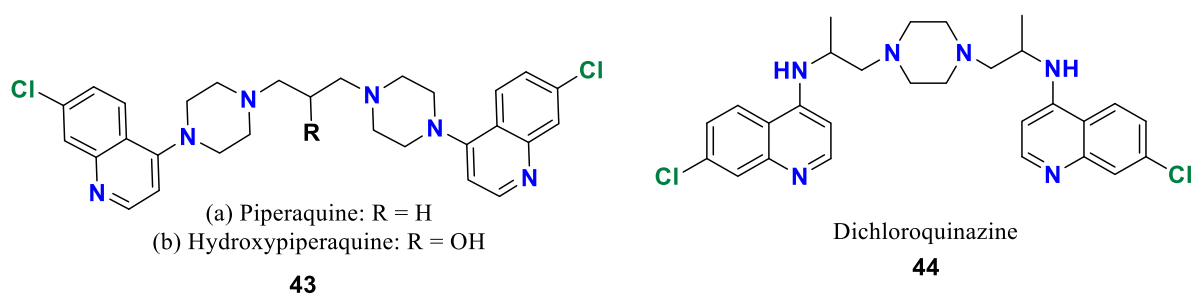
Figure 3.10. E a mples of bisquinolines

rimaquine, an 8-amino quinoline, was introduced in 1950 with the aim to prevent malarial relapse and sterilize infectious plasmodia in their se ua lly active phase. It has been known to significantly reduce plasmodial transmission by decreasing the number of gametocytes. rimaquine monotherapy at the dose of 15 mg daily for 14 days has been effectively

recommended against blood-stage *P. vivax*. Moreover, primaquine treatment at the 15 mg dose for five days post-treatment with pyrimethamine has been used as anti-relapse therapy.[69] Even after 70 years, primaquine remains on the WHOs list of essential medicines. However, severe to i city has been observed in patients with glucose-6-phosphate dehydrogenase (G6 D) deficiency on long-term use of primaquine. Methemoglobinemia (increase in the level of methaemoglobin, a haemoglobin o idation by-product) is another one of the disconcerting adverse effects of primaquine.[70,71]

In the past few years, cases of primaquine therapy failure have been reported indicating the development of resistance to primaquine as well. atients on previously successful anti-relapse therapy against *P. vivax* at 15 mg/day doses for five days after chloroquine treatment and 15mg/day for the fourteen days showed treatment failure. rimaquine was the only anti-relapse drug effective for the latent stage of *P. vivax* and *P. ovale* until the introduction of tafenoquine in 2018. Tafenoquine was recently tested in clinical settings as a replacement for primaquine, and it has been reported to be comparatively more efficacious than primaquine. However, it is not safe to be prescribed to G6 D deficiency patients and pregnant women.[72]

In 2018, hybrid compounds SAHAquines were synthesized by hybridization of suberoylanilidehydro a mic acid (SAHA) and primaquine. SAHA is an anticancer agent with potential but relatively weak antiplasmodial activity due to its HDAC inhibitory action. Therefore, SAHA and primaquine hybrids were synthesized to enhance the antiplasmodial activity of SAHA and overcome resistance to primaquine. Moreover, many studies have indicated some relationship between anticancer and antimalarials as far as diagnostics, drug research, treatment, prevention and epidemiology are concerned.[73–76] The SAHAquines (**Figure 3.11**, structure **45** and **46**) were found to be most effective against *P. falciparum* and *P. berghei*.[76]
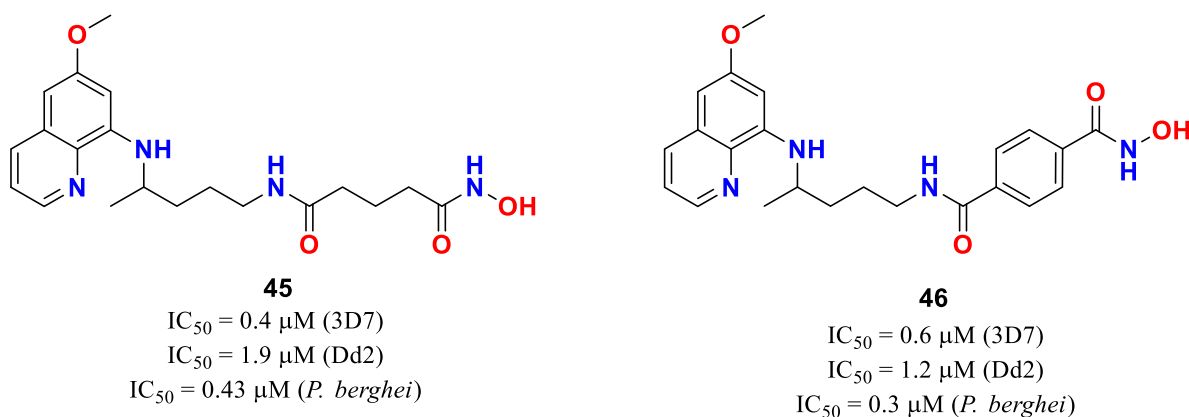
Figure 3.11. E a mples of SAHAquines

In 2021, Sauza ereira et al. synthesized chloroquine-primaquine hybrid linked via gold(I). These compounds showed multi-stage activity in vitro in *P. falciparum* blood and *P. berghei* liver stages. The combination also showed significant activity against *P. berghei* in the in vivo assay. Gold(I) compounds are known to inhibit thioredo in reductase (Tr R) system present in parasites (**47**).[77]

Similarly, chloroquine and primaquine were hybridized with phenylacetic acid and gem-difluoro derivatives by Boechat et al. The hybrid of chloroquine and phenylacetic acid (**48**) was reported to be the most potent of all synthesized compounds. However, primaquine-phenylacetic acid hybrids (**50**) were found to be less potent. Moreover, the geminal-difluoro hybrids of chloroquine (**49**) and primaquine (**51**) showed significantly reduced antiplasmodial activity.[78]

Along similar lines, da Silva Neto et al. synthesized quinoline scaffold hybridized with pharmacophores with anti-inflammatory properties such as glycine, lauric acid, tryptophan and ibuprofen. The hybrids were evaluated for anti-plasmodium activity against 3D7 and Dd2 strains of *Plasmodium*. Quinoline-ibuprofen hybrid (**52**) showed promising activity against both strains.[79] Though the primary goal of antimalarials is to kill the parasite, combating the

inflammatory mediators (cytokines and chemokines) may be helpful against cerebral malaria, the most severe manifestation of this disease which is caused due to inflammation.[78]
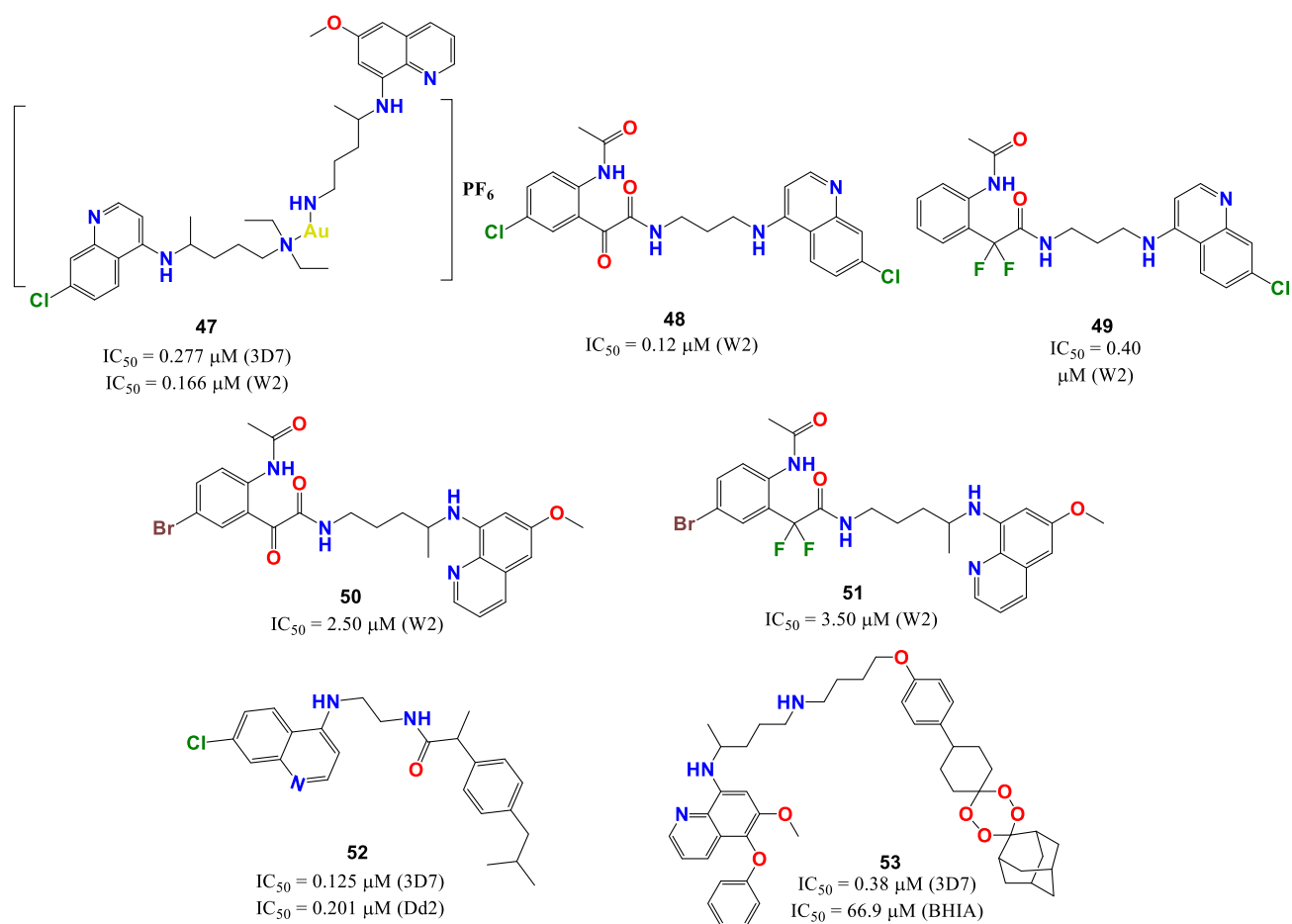
Figure 3.12. Structures of hybrids

Further, in 2021, Jansongsaeng et al. synthesized primaquine-5-pheno y -tetrao a ne hybrids. In comparison to primaquine, these hybrids showed remarkably improved antimalarial activity with almost 30-fold improvement (IC$_{50}$ = 0.38 µM). The 5-pheno y primaquine analogues e hibi ted significant inhibition of heme polymerization process, similar to chloroquine (**53**).[80]

3.1.8 Role of qui oli e i l ri

Quinazoline scaffold have recently gained increased interest for the design and synthesis of potent antimalarial agents. Quinazoline is a heterocyclic compound and belongs to the benzodiazine family.[81] Research on quinazolines began after the discovery of febrifugine, a

'quinazolinone alkaloid' (**Figure 3.13**, structure **54**). It was isolated from a Chinese plant, 'Aseru' for the first time, which potentially cured malaria. Thereafter, it was synthesized in 1903 by Gabrial.[82] Quinazolines are e tensive ly used in medicine for the wide range of pharmacological effects produced by this heterocyclic compound besides the well-reported antimalarial effect.[81,83,84] Some of the noteworthy uses of quinazolines and their derivatives include anti-tobacco mosaic virus (anti-TMV), anti-HIV, anti-cancer, antimicrobial, antifungal,[85,86] anti-tuberculosis,[87] analgesic, anti-inflammatory,[88] diuretic, anti-hypertensive,[81] hypoglycemic,[86] sedative and anti-convulsant.[89] Some of the several quinazoline-based drugs which are in the market include prazosin hydrochloride, do a zosin mesylate and do azosin hydrochloride as α-1 blockers used as an antihypertensive and the recently discovered gefitinib an endothelial growth factor receptor (EGFR) inhibitor and erlotinib an anti-cancer agent.[87,89,90]

The impressive wide-spread activities of quinazolines considerably depend on the presence of a fused benzene ring which significantly affects the properties of the pyrimidine ring.[81,91] Quinazolines have also been successfully evaluated as an antimalarial.[92] Fröhlich et al. synthesized novel artemisinin-quinazoline hybrids to counter the developing resistance against artemisinin and enhance the already well-known pharmacological properties of quinazolines.[93] Out of the synthesized hybrids, one of the compounds showed an EC_{50} value of 1.4 nM, comparable to the EC_{50} values of the individual parent compounds (**Figure 3.13**, structure **55**).[93] Moreover, the activity of the synthesized hybrid was reported to be higher than the clinically used antimalarial dihydroartemisinin. This increased antimalarial activity of the hybrid has been attributed to the free secondary amine of the 4-anilinoquinazoline.[93] Moreover, quinazolines may also be employed successfully as a reversal agent owing to their potent T-type calcium channel blocking property, like most other reversal agents. Therefore, hybridization of quinazoline with other antimalarial drugs, which have become inefficient due

to the development of resistance, may help overcome the problem of resistance and additionally provide improved activity.[94]
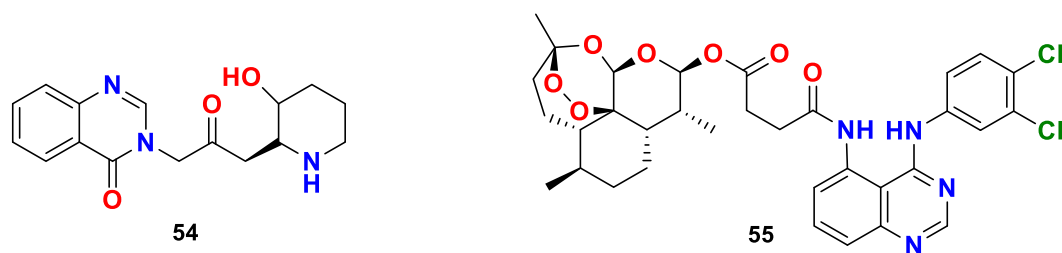
Figure 3.13. Febrifugine and an e ample of a quinazoline hybrid

Antimalarial therapy has also advanced towards the relatively new concept of epi-drugs which modulate epigenetic mechanisms.[95] Epigenetics refers to the study of changes which affect gene activity and its e pr ession without any effect on the DNA sequence.[96] ost-translational modifications (TM) at the histone protein are one of the widely studied epigenetic pathways.[59] These TMs involve acetylation and methylation at the N-terminal histone tails of histone 3 and 4. Acetylation at the lysine residues of histone is catalyzed by the enzyme histone acetyltransferase (HAT), which transfers the acetyl group from acetyl coenzyme A to the lysine residue. Additionally, the histone deacetylase (HDAC) enzyme is involved in the removal of acetyl group from lysine of histone. The changes at the histone tails lead to modification of gene e pre ssion. The role of HDAC has been observed in cancer progression and malaria, and its inhibition has been proven beneficial.[97]

Methylation at lysine residues of histone protein (H3 and H4) is regulated by the histone lysine methyl transferases (HKMTs). The methylation process at the lysine 9 of histone H3 in mammalian cells is catalyzed by G9a, an HKMT. This leads to the silencing of the respective gene sequence to induce associated alterations.[98] The discovery of G9a in mammalian cells and the development of its inhibitors, such as UNC0224 (**Figure 3.14,** structure **56**), encouraged researchers to e plor e the diaminoquinazoline (DAQ) scaffold. This led to the development of

BIX01249 and TM2-115 (**Figure 3.14,** structure **57** and **58**), which put forth the idea of HKMT's role in *Plasmodium*.[95,99]

In *P. falciparum,* methylation at lysine 4 of histone H3 by *Pf*HKMTs has been proposed to result in silencing of the *var* gene.[96] This enables the *Plasmodium* to evade the immune system of the host. Inhibition of the enzyme *Pf*HKMT may therefore result in the prevention of methylation at the H3K4Me, leading to loss of *var* gene silencing.[96,100] This makes the *Plasmodium* susceptible to attack by the immune system of the host.[100] DAQ derivatives have been recognized as epi-drugs which may show HKMT inhibition. However, the HKMT inhibitors are required to be selective for *Pf*HKMT. Hence, human G9a activity should be inhibited while preserving the activity against *Plasmodium*.[59,99]

Based on the above observations, Sundriyal et al. synthesized several compounds which showed significant selectivity towards *Plasmodium* (**Figure 3.14**, structures **59** and **61**).[99] The SAR elucidation of these DAQ suggested an increase in the *Pf*3D7 inhibitory activity by keeping the free NH functionality at position 4 intact, preventing any change in the N-benzyl position, not inducing any changes in the size of the piperidine ring, presence of dimetho y groups and substitution of various secondary amines at the position 2 of DAQ. Therefore, based on these findings, it was concluded that the free NH group is essential for the formation of hydrogen bonding, the spatial changes in the structure lead to a decrease in the activity, and that position 2 of the moiety may be utilized to improvise the physiochemical properties of the antiplasmodial.[59,99] Appro im ately 11-53% of sequence homology has been reported previously in humans and *Plasmodium*. On this basis, the authors evaluated the HKMT inhibitory effect of their synthesized compounds using the homology model of *Pf*HKMT.[99]

Combining quinazoline scaffold with other antimalarial pharmacophores such as quinolines could also yield potent antiplasmodial agents active against resistant *Plasmodium* strains.

Quinoline-quinazoline bi-substrate inhibitors of human DNMT3a and DNMT1 have been identified (**Figure 3.14**, structures **63** and **64**). Upon e ploring an in-house generated chemical library, Nardella et al. identified compounds containing a quinoline scaffold at one end and an amino-quinazoline scaffold at the other with cyclic piperidine methanol containing linker. These hybrids showed significant inhibition of *P. falciparum* in the ase ua l blood stage.[101,102]

Several studies have shown that under various conditions, chloroquine and similar antimalarials act by inhibiting β-hematin formation, which suggests that the historical antimalarials chloroquine and other 4-aminoquinolines might be acting via β-hematin inhibition.[21,25,103–106] Sullivan et al. incubated cultured *Plasmodium* parasite with chloroquine and quinidine and observed via electron microscope autoradiography and subcellular fractionation that these compounds were associated with Hz in vivo.[25] Under in vitro settings, quinoline inhibitors increase the accumulation of heme inside the *Plasmodium* DV and disrupt the further heme sequestration. Electron microscope autoradiography showed strong Hz signals in the infected erythrocytes compared to the non-infected erythrocytes. The Hz signal was also reduced in the parasite lysates incubated with chloroquine, indicating Hz formation inhibition as the possible mechanism of action of chloroquine.[25] Later, Egan et al. tested the β-hematin inhibitory activity of 4-aminoquinolines and quinolines. They reported that the quinolines act by slowly blocking the formation of β-hematin. Five equivalents of chloroquine completely inhibited the formation of β-hematin.[103]

In 2022 Olivier et al. recently tested eight compounds for their β-hematin inhibiting potential. They identified a primary binding site on (001) face of β-hematin at which the inhibitors interacted via π-π interactions. They established a good correlation between adsorption energies and β-hematin inhibition. Based on these results, 5 new amino-pheno a zine compounds were tested for their β-hematin inhibitory potential.
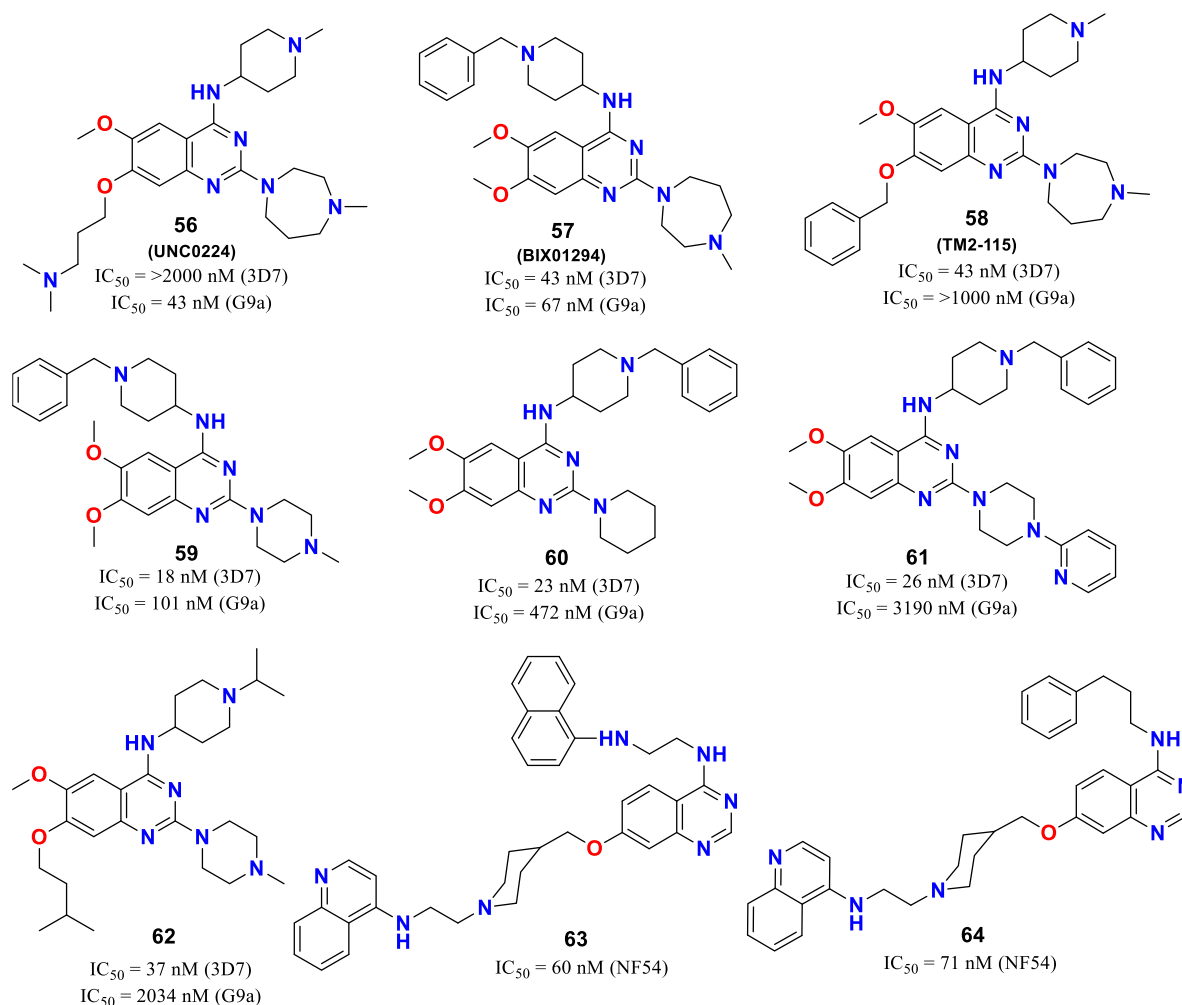
Figure 3.14. Structures of molecules acting on epigenetic targets

3.1.9 β-hematin inhibition assay (BHIA)

For very long, various groups have proposed different methods for the formation of β-hematin and therefore study its inhibition to identify novel antimalarials and study the mechanism of action of already existing antimalarials.[104,106–110] The assay methods differed based on reaction conditions such as pH, temperature and duration, on the basis of end product identification methods such as differential solubility or infrared and lastly, based on quantification of the products by spectrophotometric or radioisotopic methods. Spontaneous formation of β-hematin has been observed if monomeric hematin is incubated over several days at physiological temperature (37 °C) at pH 4.8 without the requirement of any other reagents. β-hematin thus formed is confirmed using FTIR (peaks at 1664 and 1210 cm^{-1}) after washing any residual

monomeric hematin with $NaHCO_3$. However, the addition of trophozoite-acetonitrile e tr act to hematin promoted heme polymerisation more rapidly, though acetonitrile alone cannot enhance the rate of polymerisation. Therefore, mainly lipids are responsible for promoting hematin polymerisation.[111] The role of lipids in polymerisation was further studied and proven by Dorn and the group.[106]

Recently, lipid-mediated Hz formation has gained much importance. *P. falciparum* infected RBCs at the trophozoite stage, when viewed under transmission electron microscopy, showed Hz crystals enveloped in nanosphere lipid droplets. These lipids comprise fatty acyl glycerides, including monostearic, monopalmitic, dipalmitic, dioleic and dilinoleic glycerols (the lipid blend). These glycerides, when added individually or together to hemin, promoted the formation of β-hematin. This indicated the fact that hydrophobic environment favours β-hematin crystallisation.[112]. The use of surfactants such as sodium dodecyl sulfate (SDS), Tween 80 and Tween 20 in vitro also resulted in significant β-hematin crystallization. However, a comparison of concentration-response curves of chloroquine gave IC_{50} values appro imately 10 times higher with Tween 20 compared with neutral lipid blend. This suggested that some other surfactant was required to closely mimic the lipid blend.[112–114] Carter et al. performed the lipophilic-mediated assay under optimized conditions with si different detergents (lipophilic mediators).[115] Of these detergents, zwitterionic CHA S, nonionic Triton X-100 and anionic SDS did not show significant β-hematin crystallisation. However, the non-ionic surfactants, including Tween 20, Tween 80 and N -40 (**Figure 3.15**), showed promising results with a β-hematin yield of more than 69%. This result may be attributed to the ability of non-ionic surfactants to create a neutral lipid environment similar to that of the neutral lipid blend. Consequently, this environment led to the localisation of heme at high concentrations leading to enhanced dimer formation and further polymerisation. Further, to narrow down to the best ine pe nsive surfactant for the assay, the antimalarials already known to inhibit the

crystallization process were tested under the final optimized conditions. Tween 20 and 80 showed at least 10 times higher IC_{50} values than that observed with the neutral lipid blend. On the other hand, N -40 yielded an IC_{50} value very similar to that of the neutral lipid blend.[115]
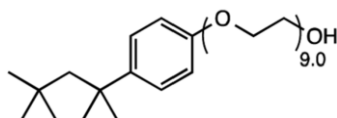
Figure 3.15. Structure of N -40

Sandlin et al. utilized N -40 as the lipophilic mediator for the assay and tested around 530 β-hematin inhibitors. Out of these inhibitors, around 171 antimalarial compounds (32%) were identified.[116] In other previous reports, with different assay conditions, only 17 out of 644 inhibitors were identified (3%).[117] This difference in the efficiency of assays may be attributed to the use of a particular detergent for crystal formation. One of many models of Hz formation shows that Hz crystals arrange themselves on the 100 and 00$\bar{1}$ faces allowing e posure of polar head groups and for the heme's free propionic acid groups to form hydrogen bonds. Further, the crystal grows near the lipid/water interface of the neutral lipid droplets (NLDs).[118]

Other than synthetic neutral lipid droplets (SNLDs), other synthetic routes, which included the use of alcohols, phospholipids and lipophilic detergents, have been reported for the formation of β-hematin. The effect of these mediators on β-hematin formation has been studied on the basis of their amphipathic structures, charges on them and their polarity. The use of alcohol showed an increase in the rate of β-hematin formation because alcohols decrease the surface tension at the aqueous interface resulting in a reduction in the energy barrier of crystal initiation.[119] hospholipids, especially unsaturated phosphatidylethanolamine and phosphatidylcholine, rapidly form β-hematin crystals very similar to Hz formed in vivo.[120]

Detergents are amphiphilic in nature and show very peculiar behaviour in an aqueous environment. Detergents are capable of e ist ing in any form ranging from monomers to aggregates; however, this depends on the conditions such as pH, temperature, concentration

and ions. It has been observed that the nanostructures formed by the detergents are very much similar to the SNLDs and, therefore, prove to be beneficial for the formation of β-hematin.

Of the several detergents tested, N -40 at a concentration between 5-50 μM yielded the highest, around 76-88% β-hematin. This yield is comparable to that obtained with phospholipids and SNLDs. Moreover, upon spectrophotometric analysis and observing the e ter nal morphology of the crystals formed, it was confirmed that β-hematin formed with N -40 was significantly similar to well-formed crystals of Hz.

Another important aspect of polymerisation assay is optimum pH. The reactions initiated individually with both Hz and trophozoite-acetonitrile e tra ct were studied at different pH. For both, the optimum pH was found to be between 4-5. However, the range of pH was found to be broader when the reaction was begun with Hz in comparison with trophozoite-acetonitrile e tra ct-initiated polymerisation. With Hz as the starting material, 50% of the polymerisation occur at pH 6.5 and almost no activity is reported at pH 7.0. On the other hand, with trophozoite-acetonitrile e tra ct, at pH 5.5, the activity is 50%, and no activity is observed above pH 6.0 (**Figure 3.16**).[106] The buffers used in these assays included: 500 mM sodium acetate buffer for assays up to the pH of 5 and 250 mM phosphate buffer for assays above pH 5.

Based on various assays performed by various groups, four possible equations have been proposed (**T b le 3.4**). The irreversible equation 1 in **T b le 3.4** is dependent on temperature and pH and, therefore, depicts the rate of the process. The product of this equation is β-hematin crystals made up of ferritoprotoporphyrin IX (Fe^{3+} IX) dimers linked together via iron-carbo y late bonds to the propionic side chain of porphyrin.[121] Equation 2 depicts two aspects which are the formation and inhibition of β-hematin. The result of this equation shows the formation of π-π adducts, and it has been reported that π-π adduct formation is important for the antimalarials to inhibit polymerisation. Therefore, it was found that pH affects the

physicochemical properties of the molecules involved in the reaction, which consequently affects the π-π adduct formation.[122]
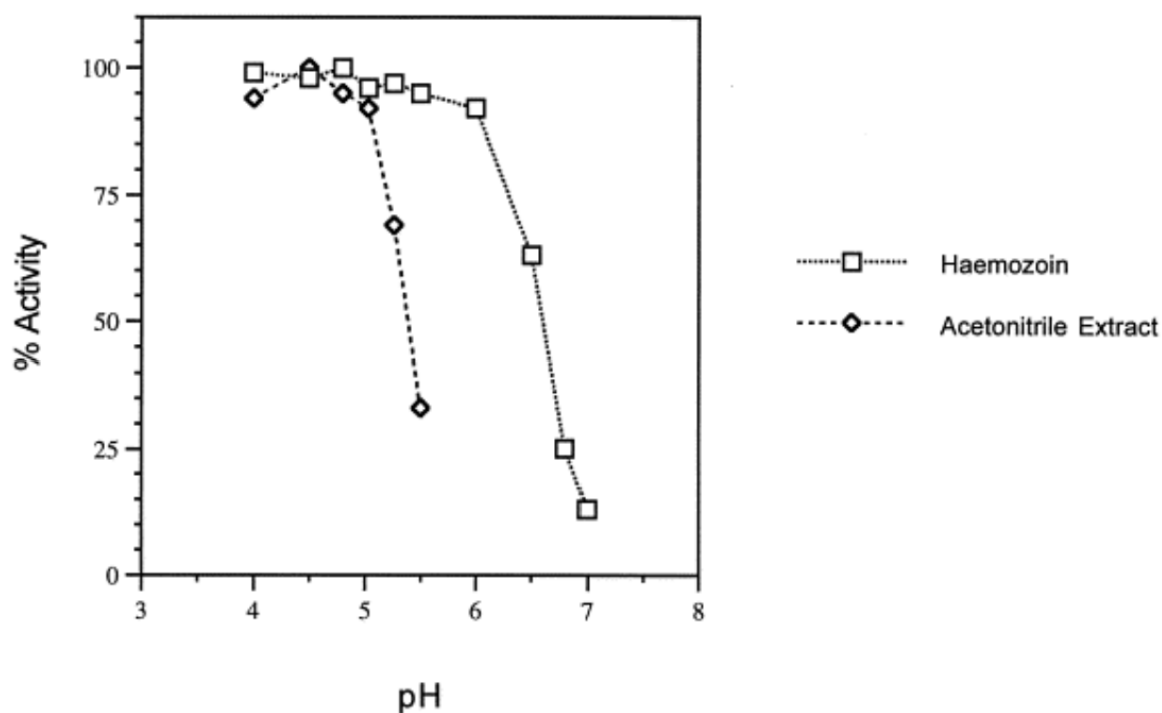
Figure 3.16. Influence of pH on the activity of Hz and acetonitrile e tract of hematin[106]

Further, equations 3 and 4 are also pH-dependent reactions for the formation of μ-o o dimers of hematin linked via an o yge n atom in the a ial posi tion.[123,124] In all these equations, pH has played an important role. Hence, arapini et al. suggested that variation in pH affects the yield of β-hematin as well inhibition via different antimalarials. At pH above 6, the μ-o o bridged aggregates are pre-dominant and at pH lower than 6, aggregation of hematin is reduced, and the e ist ence of monomers becomes more prominent. For β-hematin to form, it is important for the monomers to e ist because when the μ-o o dimers form, the o yge n atom creates a bridge between the iron atoms of two porphyrins, leading to the unavailability of the propionate side chain of the adjoining porphyrin for coordination.[29,125] It could be safely concluded from here that the properties of the reagent used, the solvent involved, and the pH used for the reaction play a very important role.

Table 3.4. Proposed equations for in vitro β-hematin formation. Fe^{3+} IX, ferriprotoporphyrin IX; aL, axial ligand; πL, π ligand.

Equation number	Equation	Resulted in	Reference
1	$Fe^{3+}PPIX + Fe^{3+}PPIX \rightarrow [Fe^{3+}PPIX]2(s)$	Formation of β-hematin	121
2	Fe^{3+} IX $+ πL \rightleftarrows Fe^{3+}PPIX\text{-}πL$	Formation of π- π complex with ligands such as chloroquine	122
3	$Fe^{3+}PPIX + aL \rightleftarrows Fe^{3+}PPIX\text{-}aL$	Formation of complex with axial ligand	123
4	$Fe^{3+}PPIX + Fe^{3+}PPIX \rightleftarrows Fe^{3+}PPIX\text{-}O\text{-}Fe^{3+}PPIX$	Formation of oxo-bridge complex	124

The BHIA is significantly improved when the starting material hematin is replaced by hemin, DMSO is employed as the solvent, and the optimum pH used is 5. Amodiaquine (AQ) and chloroquine (CQ) show significant inhibitory results; however, only primaquine (PQ) has been shown to be ineffective, as has been observed in several studies. In comparison with the old method, BHIA is considerably advantageous as there is significantly increased recovery of β-hematin and improved quality of reagents owing to hemin being chemically more stable and homogenous in comparison with hematin. Moreover, when the compounds are in the salt form, the interference of salts has been reported in the hematin heme polymerisation inhibition activity assay. However, in BHIA, this interference is overcome owing to the use of DMSO at high concentrations resulting in the displacement of salts over a wide range of pH.[126]

It is well established that ART-based drugs do not show inhibition in the traditionally used oxidized β-hematin inhibition assay (O-BHIA).[57,127] However, various mechanisms have been proposed confirming the role of ART-based drugs acting on heme. In the reductive scission model, the ferrous (Fe2+) ions from heme can cause cleavage of the peroxide bridge leading to the formation of highly reactive free radicals.[128,129] Another model proposes that iron may act as a lewis acid, irreversibly modifying protein residues by direct oxidation resulting in parasite death.[130–132] Therefore, Ribbiso et al. developed a new method to detect the β-hematin inhibition properties of ART-based drugs using reduced conditions (R-BHIA). In this method,

the authors preincubated F IX with GSH to convert F IX to obtain Fe(II) IX. Using this method, the author reported clear inhibition of Hz formation by ART-based drugs.[57]

3.2 GAP IN EXI TING RE EARC AND OBJECTIVE

1. The failure of anti-plasmodium therapy in the management of malaria due to severe drug resistance is a major health concern. Therefore, there is an unmet need to find new antiplasmodials. The concept of making hybrid compounds is in the early stages and may not only lead to the discovery of new pharmacophores but can also be used to revive drugs that have already developed resistance and for repurposing e ist ing drugs. Therefore, chloroquine and primaquine-based hybrids shall be synthesized. The chloroquine scaffold will be employed owing to its promising history against *Plasmodium*. rimaquine is effective in the liver stage of the *Plasmodium* life cycle, so its hybrid with antiplasmodial acting on the blood stage might possess dual action.

2. DAQ scaffold has shown potency against the *Plasmodium* by acting on an epigenetic target, possibly *Pf*HKMT and thus has a distinct mechanism of action compared to other clinically available drugs. Moreover, it has shown activity against MDR strains of *Plasmodium*, including Artemisinin-resistant strains. Therefore, the hybrids of DAQ with other pharmacophores may serve as promising agents against *Plasmodium*. Also, since quinazoline pharmacophore target T-type calcium channels, it may also act as a reversal agent and may be effective against the resistant strains.

3. In this conte t , we planned to synthesize aminoquinoline-quinazoline hybrids hypothesized to act on epigenetic and Hz inhibition mechanisms of the malarial parasite resulting in activity against resistant strains.

4. Similar to bisquinolines that show superior antimalarial activity, increased bioavailability and lower to i city, we also envisaged the synthesis of bisquinazolines as potential antimalarial agents.

5. β-hematin inhibition activity of DAQ has not been reported in previous studies; therefore, we also set an objective to perform BHIA of our synthesized hybrids to check for possible inhibition of the hemozoin pathway.

3.3 RE ULT AND DI CU ION

3.3.1 C e i r y

The target molecules were synthesized employing the well-known chemical reactions with slight modifications as depicted in **c e e 3.1, 3.2, 3.3** and **3.4**. Initially, we synthesized the reported HKMT inhibitors (**65** and **66**) with known antimalarial activity as standards using **c e e 3.1**. Thus, the commercially available 2,4-dichloro-6,7-dimetho y quinazoline was reacted with 4-amino-1-benzylpiperidine at room temperature, intermediate formed was reacted with a secondary amine under microwave conditions to get the desired products.
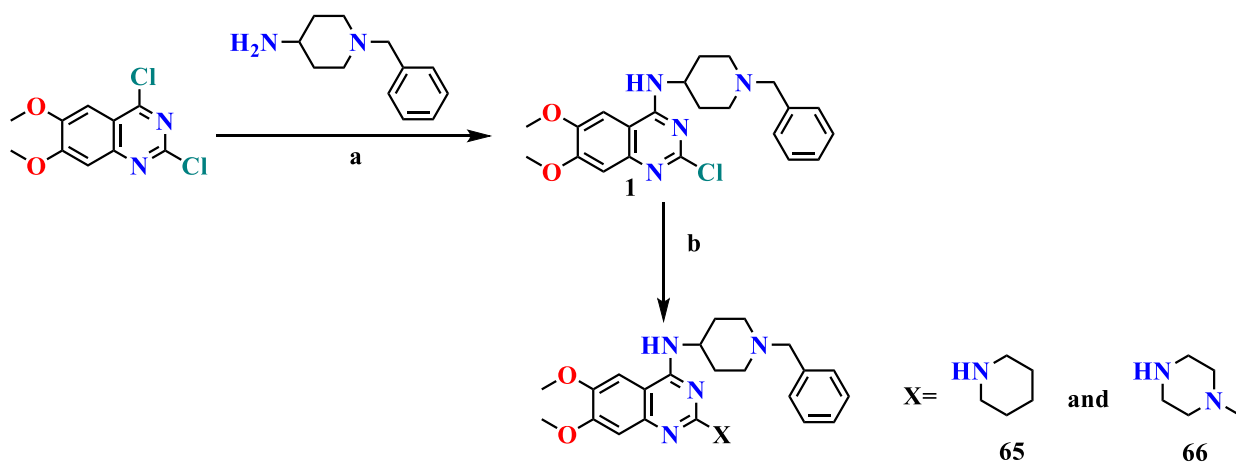
c e e 3.1. Synthesis of known HKMT inhibitors. *Reaction conditions: (a) THF, DIEA, rt, 18 h; (b) Secondary amine (X), Toluene, Microwave, 160°C, 2 h*

In **c e e 3.2**, 4,7-dichloroquinoline was heated with different bis-amine linkers under microwave irradiation. The intermediate was reacted with commercially available quinazolines at room temperature to obtain the quinoline-quinazoline intermediate, which was further reacted with a secondary amine under microwave conditions to get the final product. **c e e 3.3** was used for the synthesis of bisquinazoline derivatives by reacting the quinazoline with

different bis amine linkers at 60° for 24 hours. In **c e e 3.4**, primaquine was reacted with 2,4-dichloro-6,7-dimetho y quinazoline at room temperature and the intermediate was reacted with a secondary amine under microwave conditions to obtain the final product.
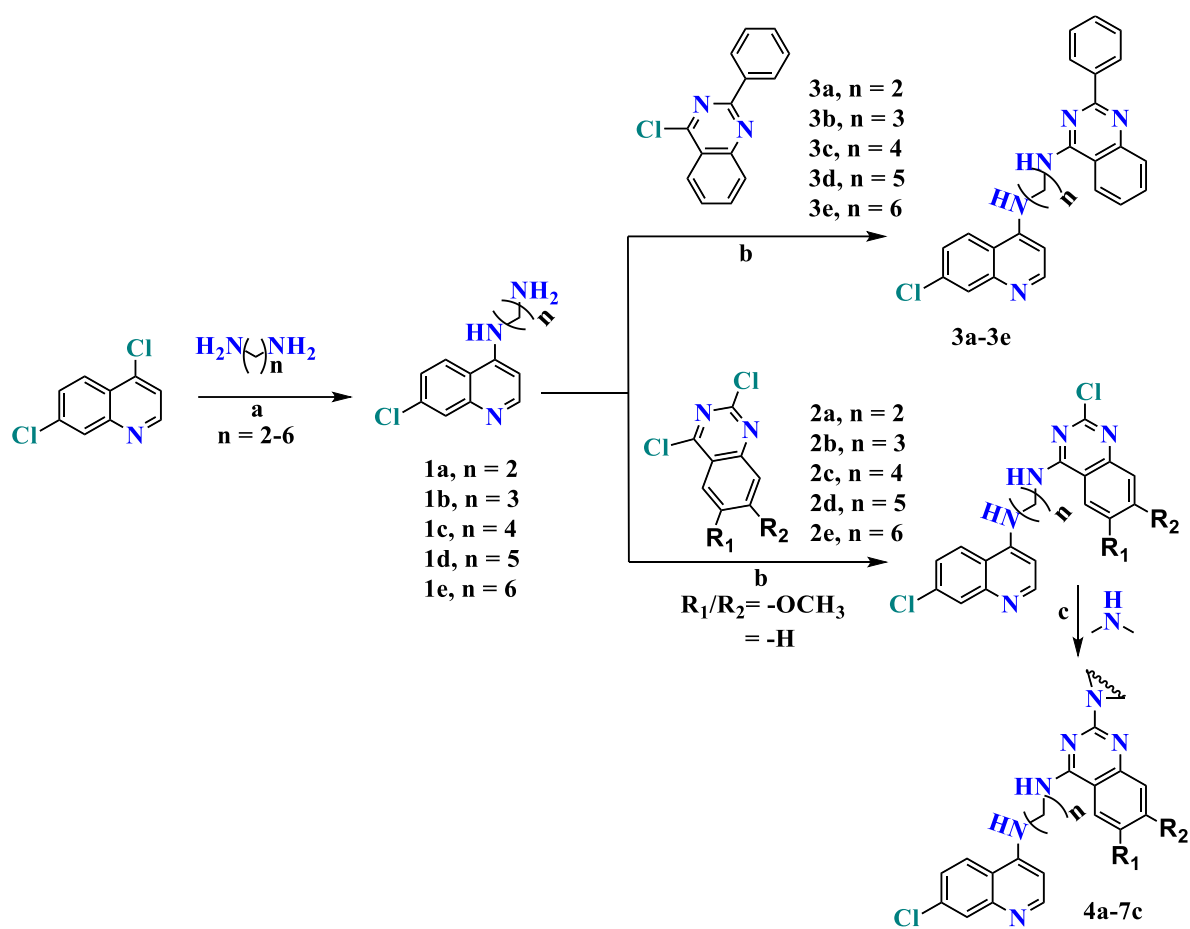
c e e 3.2. Synthesis of 4-aminoquinoline-quinazoline hybrid molecules. *Reaction conditions: a) 1h, neat, 110°C, MW; b) DIEA, DCM, 24h, Rt; c) 15min, 160°C, MW, 4M HCl Dioxane, IPA*
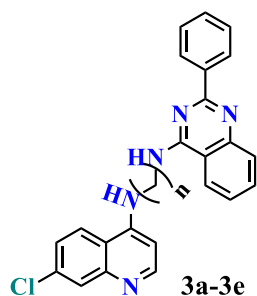
T ble 3.5. Compounds 3 -3e

S.No	Code	n
1	3a	2
2	3b	3
3	3c	4
4	3d	5
5	3e	6

4a-7c
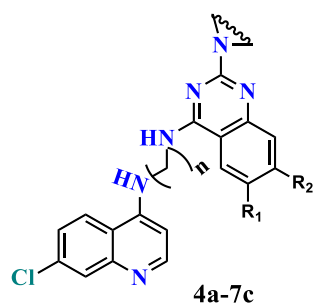
T ble 3.6. Compounds **4** -**7c**

S.No	Code	n	R$_1$/ R$_2$	Secondary amine
1	**4a**	2	-OCH$_3$	Piperidine
2	**4b**	3	-OCH$_3$	Piperidine
3	**4c**	4	-OCH$_3$	Piperidine
4	**4d**	5	-OCH$_3$	Piperidine
5	**4e**	6	-OCH$_3$	Piperidine
6	**5c**	4	-OCH$_3$	Pyrrolidine
7	**6c**	4	-H	Piperidine
8	**7c**	4	-H	Pyrrolidine

8a-8e
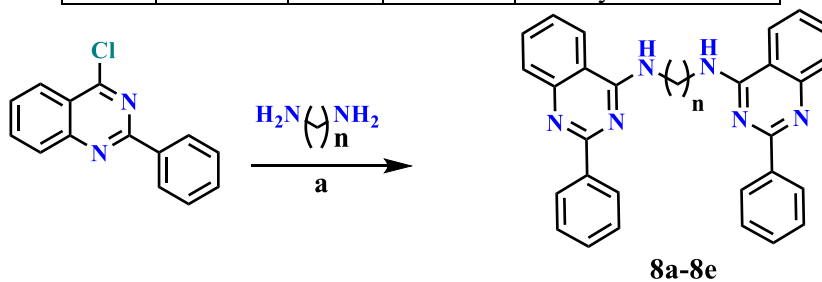
c e **e 3.3.** Synthesis of bisquinazolines. *Reaction conditions: a) DIEA, DCM, ACN, 60ºC, 24h*

8a-8e
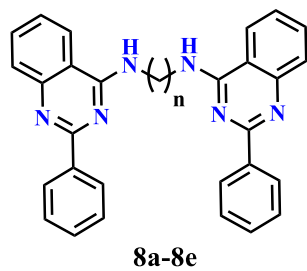
T ble 3.7. Compounds **8** -**8e**

S.No	Code	n
1	**8a**	2
2	**8b**	3
3	**8c**	4
4	**8d**	5
5	**8e**	6

96
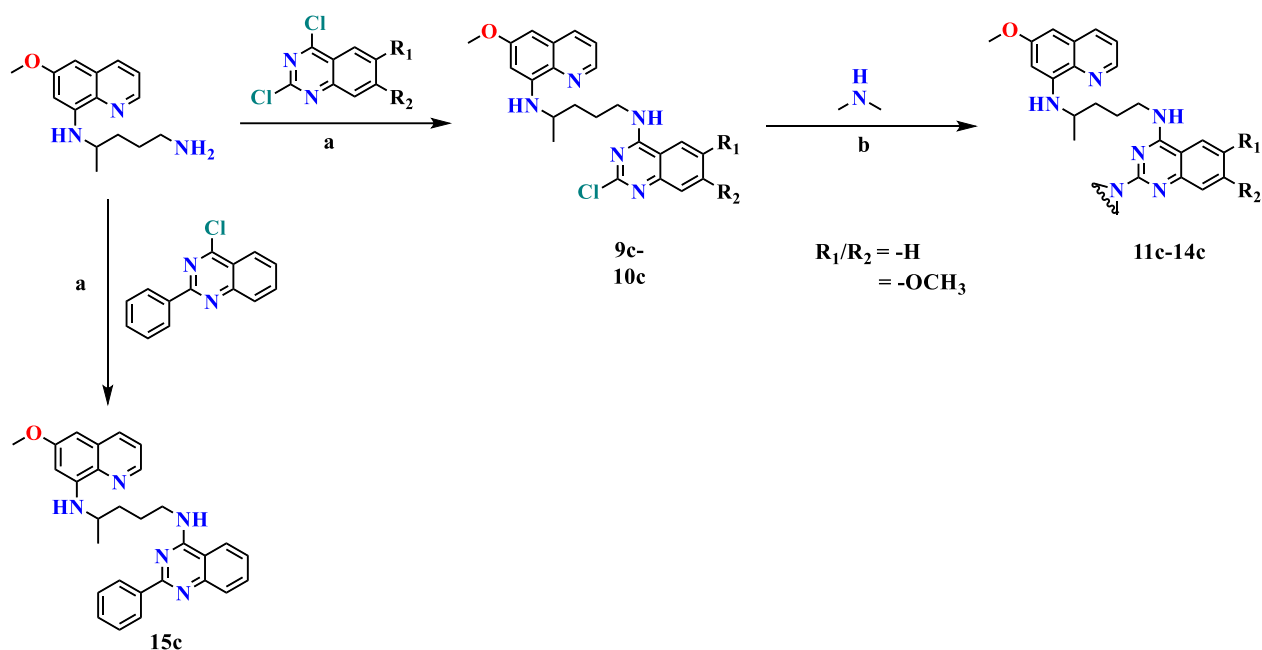
c e e **3.4.** Synthesis of 8-aminoquinoline-quinazoline hybrid molecules. *Reaction conditions: a) DIEA, DCM, ACN, Rt, 24h; b) TFA, IPA, MW, 160°C, 25min*

T ble **3.8.** Compounds **9c-15c**

S.No	Code	R$_1$/R$_2$	Secondary amine
1	**9c**	-H	-
2	**10c**	-OCH$_3$	-
3	**11c**	-H	Piperidine
4	**12c**	-H	Pyrrolidine
5	**13c**	-OCH$_3$	Piperidine
6	**14c**	-OCH$_3$	Pyrrolidine
7	**15c**	-H	-

3.3.2 PL C e o evelo e for y e i e co ou

As our synthesized compounds were highly polar, they did not show retention in the column and were rapidly eluted from the R column. The initial trials were done with equal amounts of organic and aqueous phase (50:50), and gradually the amount of organic solvent decreased; however no peaks were observed in the chromatogram. This problem was persistent even if the organic solvent was decreased to the lowest possible limit in the mobile phase (95:5 aqueous: organic). No improvement was observed even when the pH was modified, and the entire pH range was checked using various buffers. So, after a literature survey, it was found that ion-pair chromatography is suitable for such types of highly polar compounds.[133,134]

Ion pair (I) chromatography involves the use of a non-polar stationary phase (C18, C8, C5) and an ion pairing agent to separate polar compounds containing ionizable groups. The non-polar hydrocarbon chain of the I agent binds to the stationary phase of the column and modifies the stationary phase causing it to act as ion e c hange material, thereby increasing retention time (RT) for polar compounds.[133,135,136]
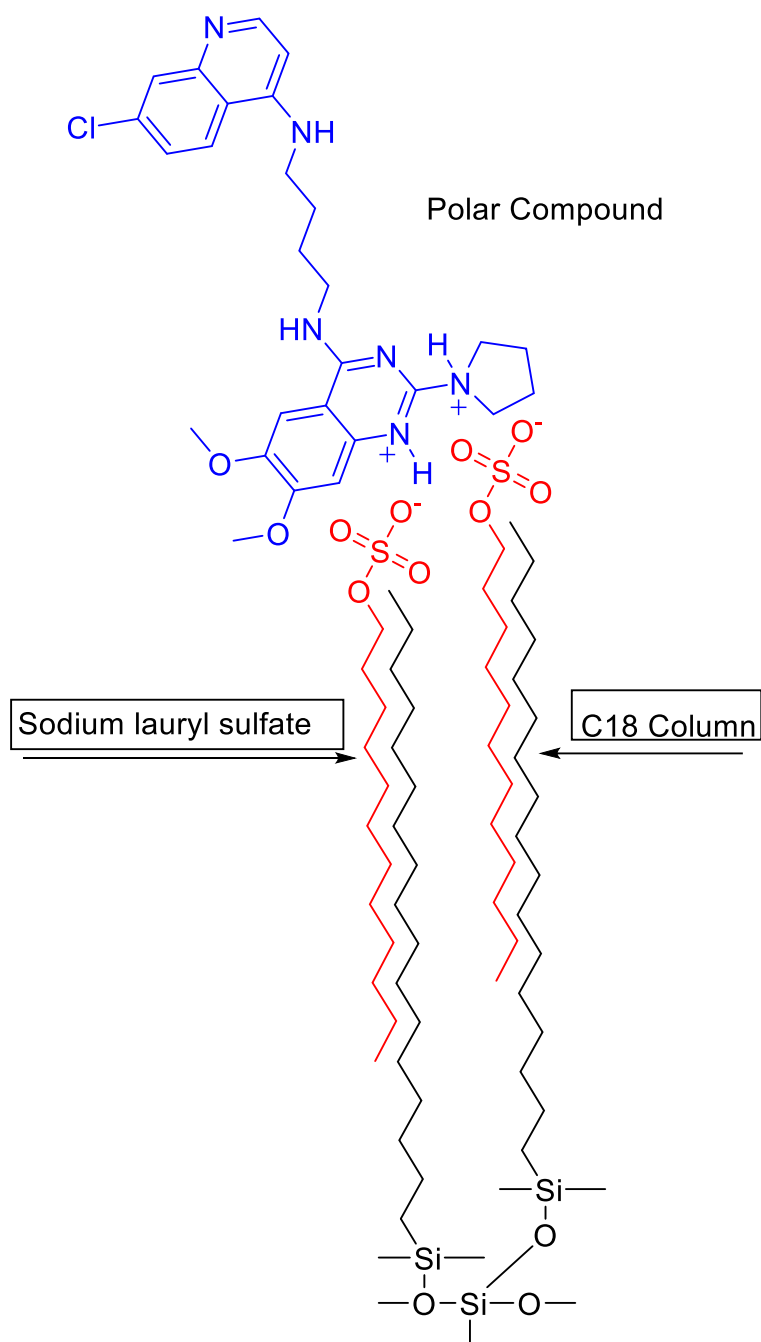
Figure 3.17. Interaction of synthesized compound with column

SLS was selected as the ion pairing agent, and initially, 1mM SLS formic acid buffer was used as the aqueous phase, and methanol was used as the organic phase; however, compound peaks at this concentration were observed close to the dead volume region due to insufficient interaction of I agent with stationary phase.[137–140] Therefore, 2.5 mM SLS formic acid buffer was used at a flow rate of 1mL/min, keeping methanol as the organic phase, which resulted in an improvement in retention time; however, broad peaks were observed. Finally, we replaced methanol with acetonitrile keeping the concentration of SLS formic acid buffer at 2.5mM, and this resulted in sharp peaks with good resolution (**Figure 3.17**).

3.3.2.1 Precautions while using Ion-Pair HPLC

Columns once used for ion-pair R H LC should be dedicated for this type of analysis and should not be used for R H LC as it is difficult to completely remove the ion-pairing agent from the column. At the start of the ion pair H LC, adequate time should be given for column equilibration and stabilization.

3.3.3. β-hematin crystal docking (BHCD)

The grid was generated so that the complete structure of β-hematin is enclosed inside the grid, and the drugs may interact with any of the preferred phases. It was found that most of the compounds showing the highest docking score interacted with the fastest-growing phase (001) (**Figure 3.18, Table 3.9**). The docked compounds showed H-bond, salt bridge, halogen bond and aromatic H-bond interactions. Some known drugs or previously synthesized compounds were tested using similar methods, but different software was also included in the docking studies to validate the method. The results obtained were in accordance with the previously reported literature.
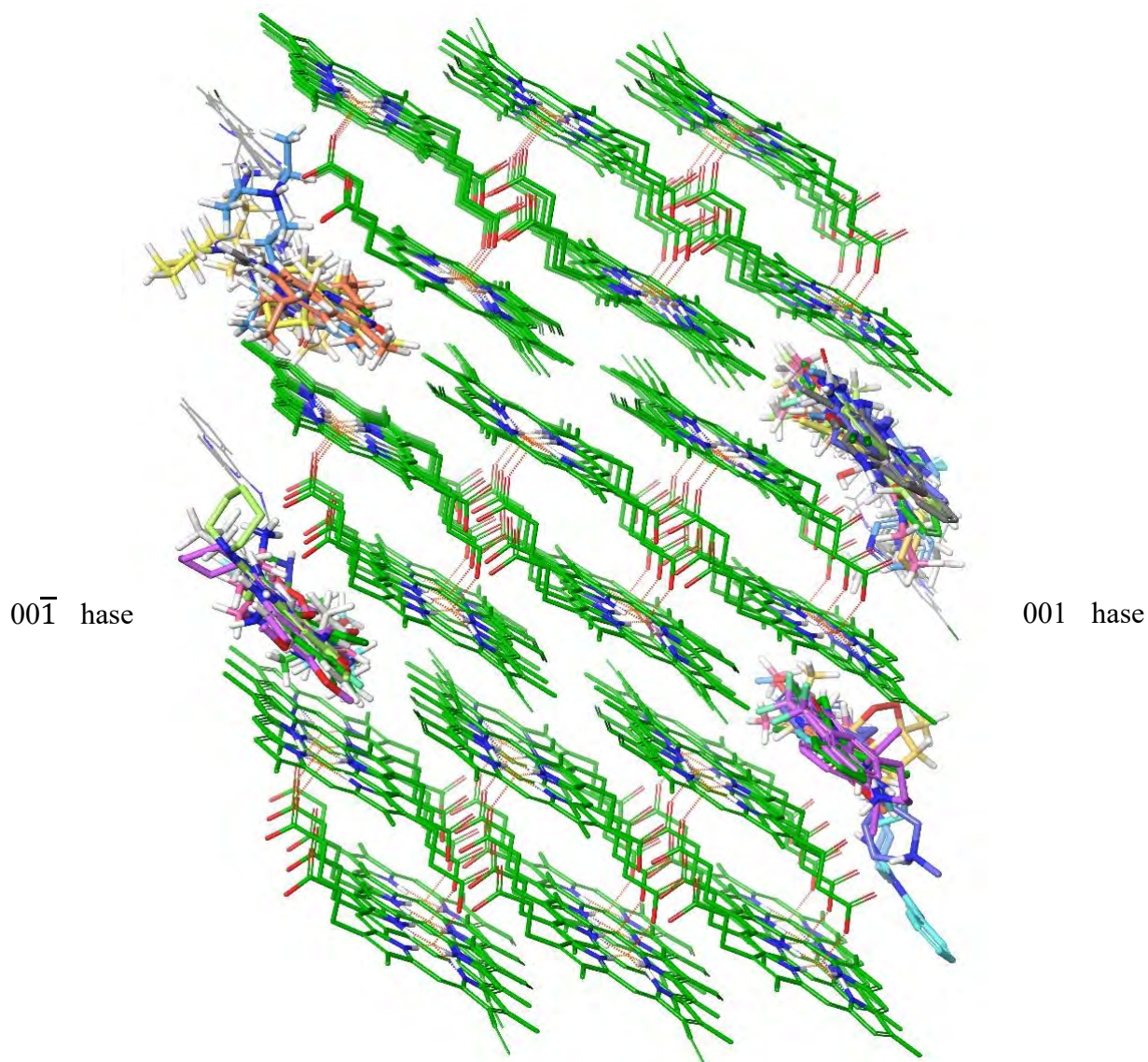
Figure 3.18. 3D structure of β-hematin crystal showing interaction with 001 and 00$\overline{1}$ phase.

Table 3.9. β-hematin crystal dock glide score of different compounds

.N o	CODE	β- e i cry l ock gli e g - c ore
Co ou i er c i g wi 00 1 e		
1	**9c**	-4.088
2	**8c**	-3.833
3	**10c**	-3.703
4	**15c**	-3.299
5	**13c**	-3.11
6	**3**	-2.998
7	**4b**	-2.931
8	**8e**	-2.924
9	**8**	-2.924

10	**14c**	-2.914
11	**7c**	-2.911
12	**12c**	-2.81
13	**3c**	-2.708
14	**5c**	-2.622
15	**4c**	-2.516
16	**3**	-2.483
17	**4**	-2.437
18	**3b**	-1.954
K ow rug		
19	**Ci c lce**	-3.7
20	**I i ib**	-3.399
21	**Ar e e er**	-2.347
22	**A el i e**	-2.034
23	**A o i qu i e**	-1.538
24	**Flib e ri**	-5.784
Co ou i er c i g wi -001 e		
28	**8**	-3.472
29	**8b**	-3.263
30	**1c**	-2.961
31	**11c**	-2.879
32	**4**	-2.488
33	**6c**	-2.287
34	**4e**	-2.285
35	**3e**	-1.916
36	**65**	-2.061
K ow rug		
38	**L i b**	-5.464
39	**C lor oqui e**	-1.604
40	**Pi er qu i e (re o r e B IA 15)**	-1.658
41	**Pri qu i e (re or e B IA i c ive)**	-0.626

3.3.4 β-hematin inhibition assay

While starting for the β-hematin inhibition assay, the first step was to ensure the conversion of

hemin chloride to β-hematin. Therefore, both the pure hemin chloride and β-hematin formed

after conversion was evaluated by UV (**Figure 3.19**) and IR spectroscopy (**Figure 3.20**). SEM image of β-hematin was also obtained (**Figure 3.21**).[141]
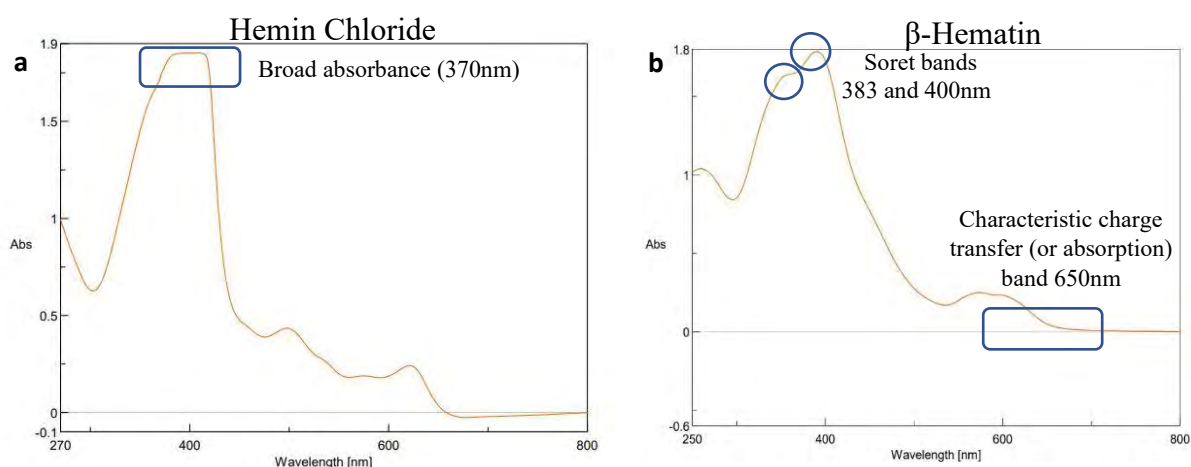
Figure 3.19. UV spectra of a) Hemin chloride and b) β-hematin

3.3.4.1 UV-Visible spectra

The UV-visible spectroscopy results of hemin chloride (the starting material for β-hematin) and the synthesized β-hematin are shown in **Figure 3.19**. The wavelength for maximum absorbance (λma) for the two molecules is different, confirming the successful conversion of the hemin chloride (**Figure 3.19**) to β-hematin (**Figure 3.19b**). Hemin chloride has a broad absorbance at around 370 nm, while the synthesized β-hematin has its characteristic charge transfer (or absorption) band at around 650 nm and two broad soret bands at 383 and 400 nm. The differences in the absorbance of the two materials signify successful synthesis of β-hematin, which can be used as a biomarker for the detection of malaria. The UV-visible result of β-hematin obtained in this study is in agreement with that reported by Fitch and Kanjananggulpan and Laure et al. for Hz or β-hematin.[142,143]

3.3.4.2 IR spectra

The infrared spectroscopy analysis further confirmed the successful synthesis of β-hematin with Hz characteristic peaks at 1211 and 1664 cm^{-1} (**Figure 3.20** and **b**) attributed to a dimeric ferriprotoporphyrin IX aggregate which is identical to *P. falciparum* Hz. The intense peak at

1664 cm^{-1} indicates the presence of C=O stretching, unidentate carboxylate coordination onto iron in the β-hematin. The peak at 1211 cm^{-1} indicates an axial carboxylate ligand (C–O stretching frequency) from O-methyl groups linked to various metalloporphyrins.[107]
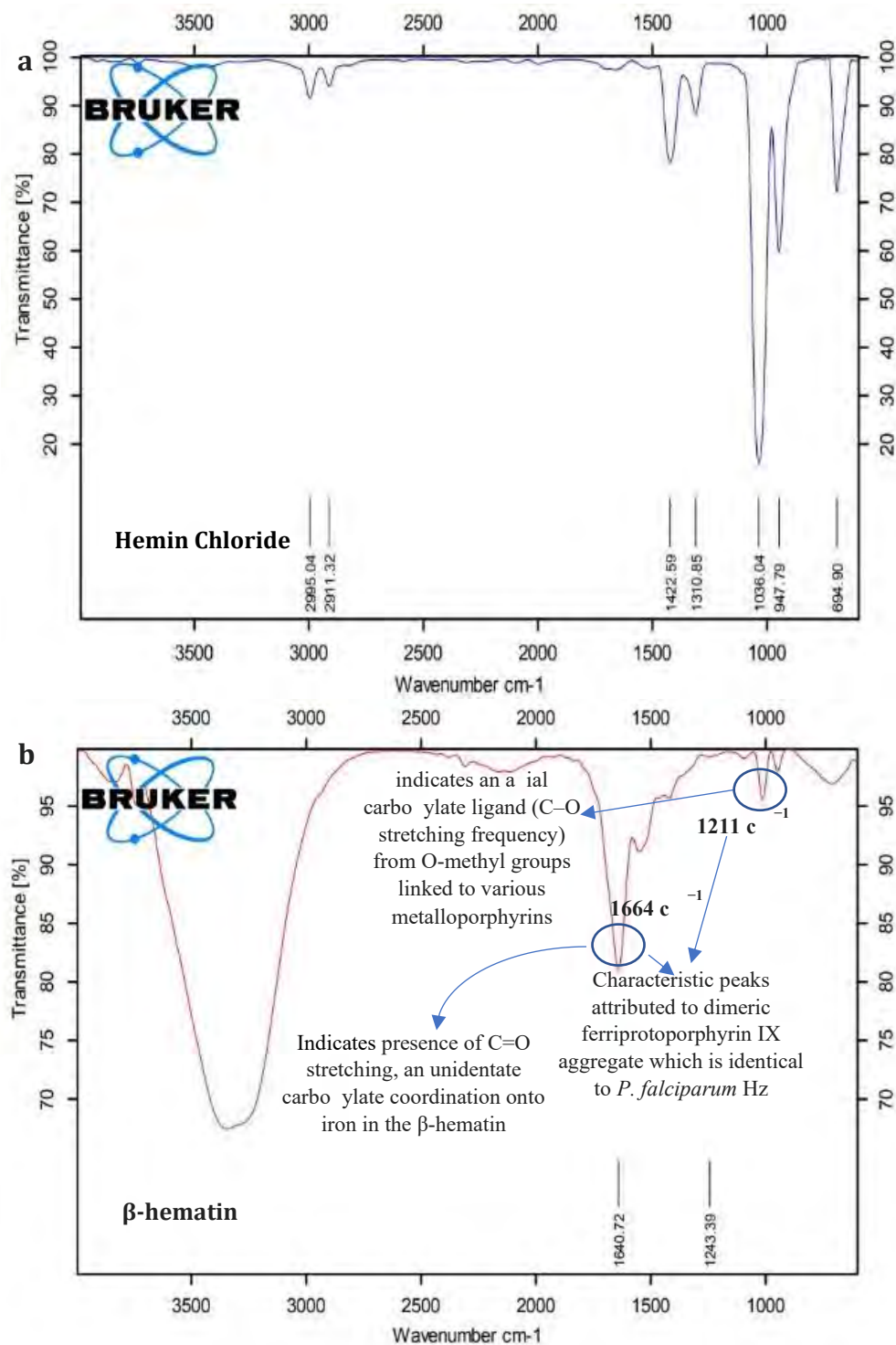
Figure 3.20. IR spectroscopy of a) hemin chloride and b) the synthesized β-hematin
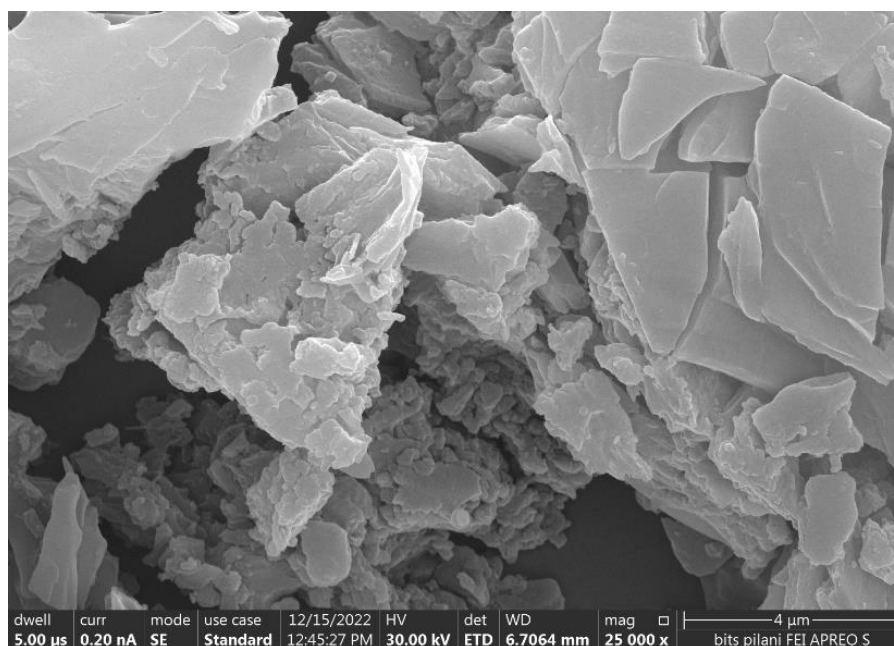
Figure 3.21. SEM image of hematin

After confirmation of the conversion of hemin to hematin, the BHIA assay protocol was followed for the known drugs (**Table 3.10**). The BHIA IC_{50} obtained for the known drugs was compared with previous literature. The results showed that the BHIA IC_{50} values obtained in our assay are similar to previously reported data, and hence the method can be used for further evaluation of novel antimalarial hybrids synthesized in our lab.
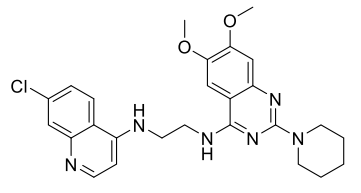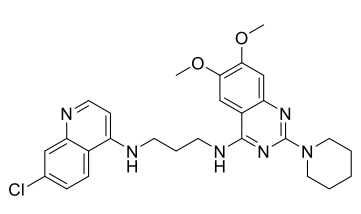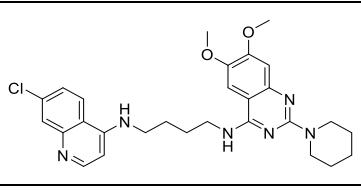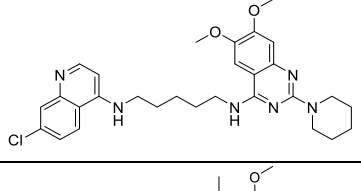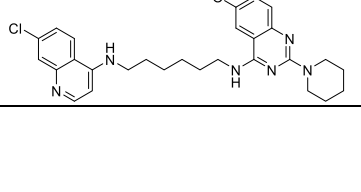
Table 3.10. BHIA method validation using docking score and BHIA values of known drugs

S.No	Compound	Calculated docking score	Found BHIA(µM)	Reported BHIA(µM)	Reference
1	Chloroquine	-1.604	35	19	144
2	Amodiaquine	-1.538	24	8.6	144
3	Piperaquine	-1.658	55	15	57
4	Primaquine	-0.626	>1000	>1000	126
5	Artemether	-2.347	>1000	>1000	57

Since the compounds with a chain length of four carbons were the most active in the in vitro assay, therefore from all the series, those compounds were selected which had a linker chain length of four carbons. The standard G9a inhibitor **65** was also checked. To our knowledge, this is the first study to check G9a inhibitors for their potential BHIA activity. The final compounds from series 2 compounds **4c, 5c** and **3c**, and the intermediates **2c** and **1c** were selected. From series 3, **8c** was selected. From series 4, **11c, 12c, 13c, 14c** and **15c** were

analyzed. All the selected compounds showed a BHIA IC_{50} value of >100 μM. This validated our hypothesis to synthesize the primaquine-quinazoline hybrids as primaquine showed BHIA IC_{50} of >1000 μM. Interestingly the compounds **15c, 3c, 2c, 1c** and **8c,** which are inactive in the in vitro assay, showed good IC_{50} values in the BHIA. This may be because the synthesized series of compounds are showing their activity through other mechanisms in addition to G9a inhibition, either through ABC transporters or through plasmepsins which cannot be studied by the used in vitro assays, and therefore these compounds are inactive in the in vitro assay.

T ble 3.11. Antimalarial compounds synthesized by Scheme 3.2

S.No	Code	Formula	IC_{50} for antimalarial activity at schizont stage (nM) (A)		β-hematin IC_{50} (μM)	Cytotoxicity HEK (% viability)
			Artemisinin sensitive (3D7)	Artemisinin resistant (C580Y)		
1	**4a**		28	16	NT	100
2	**4b**		RA	75	NT	69
3	**4c**		21	16	29	64
4	**4d**		43	67	NT	70
5	**4e**		RA	N.T	NT	100

#	Compound	Structure				
6	5c	(structure)	15	19	12	88
7	6c	(structure)	RA	NT	NT	NT
8	7c	(structure)	RA	NT	NT	NT
9	2c	(structure)	3195	N.T	21	NT
10	1c	(structure)	N.T	N.T	16	NT
11	3a	(structure)	N.T	N.T	N.T	48
12	3b	(structure)	N.T	N.T	N.T	66
13	3c	(structure)	N.A	N.T	31	86
14	3d	(structure)	N.A	N.T	N.T	33
15	3e	(structure)	N.T	N.T	N.T	90

CONTROLS AND STANDARDS					
Piperaquine		27	22	55	89
Chloroquine		16	41	35	N.T
65 (std)		2	4.3	58	69

RA = result awaited, NT= Not tested, NA= Not active at highest tested concentration (10μM)

T ble 3.12. Antimalarial compounds synthesized using Scheme 3.3

S.No	Code	Structure	IC_{50} for antimalarial activity at schizont stage (nM) (A)		β-hematin IC_{50} (μM)	Cytotoxicity HEK (% viability at 10 μM)
			Artemisinin sensitive (3D7)	Artemisinin resistant (C580Y)		
1	**8a**		N.T	N.T	N.T	88
2	**8b**		N.T	N.T	N.T	100
3	**8c**		N.A	N.T	74	69
4	**8d**		N.T	N.T	N.T	102

| 5 | **8e** | | N.A | N.T | N.T | 83 |

NT= Not tested, NA= Not active at highest tested concentration (10µM)

T ble 3.13. Antimalarial compounds synthesized using Scheme 3.4

S.No	Code	Structure	IC$_{50}$ for ring stage (*Pf* 3D7) (nM)	β-hematin IC$_{50}$ (µM)	Cytotoxicity HEK (% viability at 10 µM)
1	**9c**		NA	NA	NT
2	**10c**		NA	NT	NT
3	**11c**		NA	83	NT
4	**12c**		1804	100	NT
5	**13c**		140	75	98

108

6	**14c**		198	59	20
7	**15c**		NA	92	NT
Standard drugs					
Primaquine			9370	>1000	NT
65			66	58	69

RA = result awaited, NT= Not tested, NA= Not active at highest tested concentration (10 μM**)**

3.4 CONCLU IO N

3.4.1 4-A i oqui oli e-qui oli e ybri

We synthesized DMDAQ **65** and **66** with known antimalarial activity to use them as standard for further in vitro, docking and β-hematin inhibition studies. Chloroquine has been the drug of choice for malaria since long, but due to development of resistance it has lost its potency. Therefore, we planned to synthesize hybrids containing quinoline moiety (from chloroquine) and hybridize it with quinazoline scaffold (from DMDAQ) through a linker to obtain quinoline-quinazoline hybrids (fused pharmacophore). These hybrids were synthesized by using **c e e 3.2**. The quinoline part was kept constant and modifications were introduced either in the type of quinazoline used or the chain length of linker used to fuse the two pharmacophores. The synthesized compounds were tested in vitro against artemisinin sensitive (3D7) and resistant (C580Y) strains of *P. falciparum*.
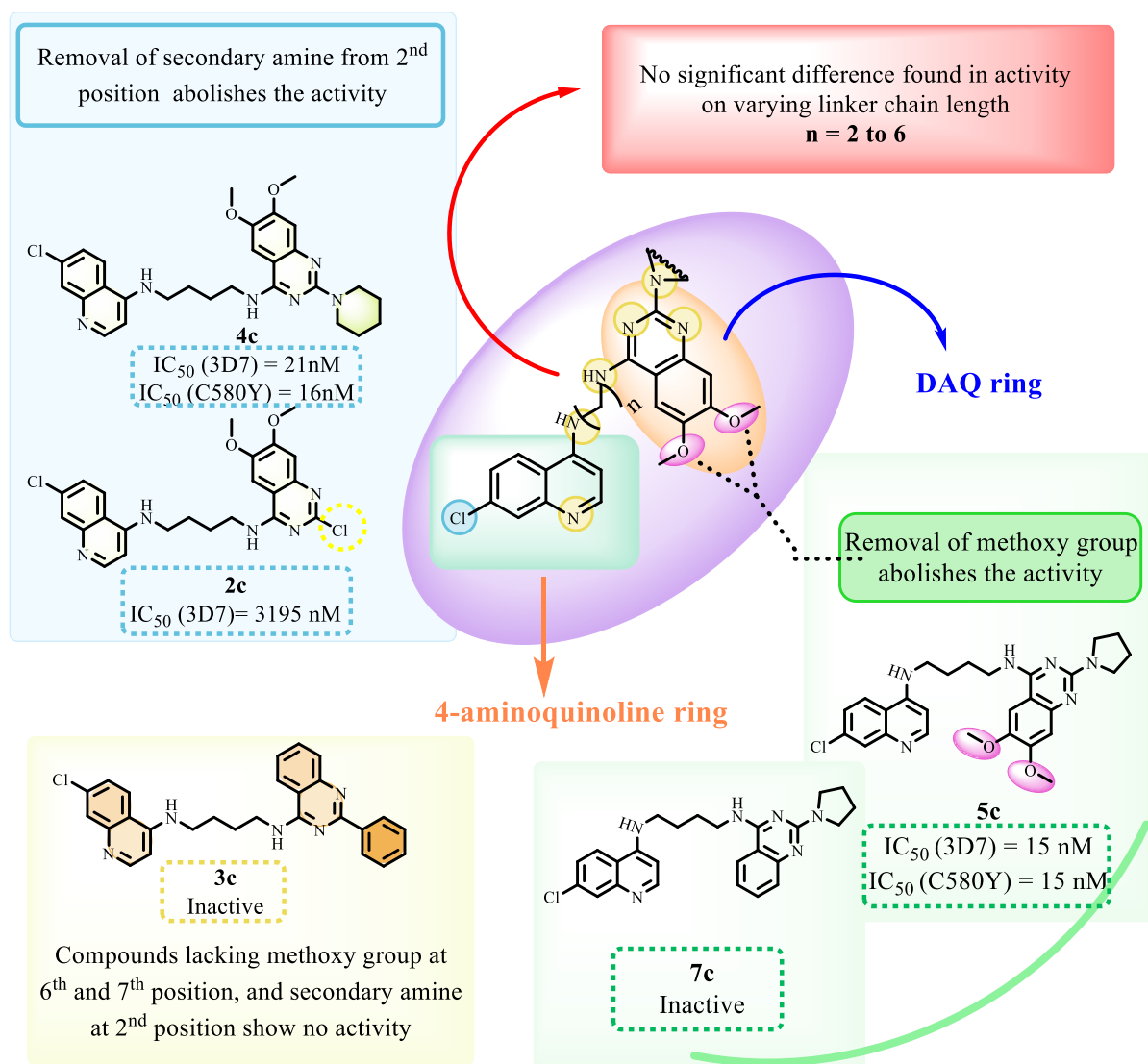
Figure 3.22. SAR of 4-aminoquinoline-quinazoline hybrids

The compounds **3c** and **3** were found to be inactive against 3D7 strain; therefore, rest of the compounds from the series were not tested. The most active compounds from the series were **5c** (IC$_{50}$ = 15 and 19 nM in 3D7 and C580Y, respectively) followed by **4c** (IC$_{50}$ = 21 and 16 nM in 3D7 and C580Y, respectively) and **4** (IC$_{50}$ = 28 and 16 Nm in 3D7 and C580Y, respectively). The common characteristic in all these compounds was the presence of di-metho y group at 6th and 7th position and secondary amine at 2nd position of the quinazoline ring. The size of the secondary amine had little to no effect on the antimalarial potency. If the metho y groups were removed (**6c** and **7c**) or the secondary amine was absent (**3c**), the compounds became inactive. So, it can be concluded that the presence of di-metho y gr oup at

the 6th and 7th position and a secondary amine at the 2nd position is most important for in vitro antimalarial activity of the compounds (**Figure 3.22**). To gain insight into the possible mechanism of action, the compounds were tested for their potential to act against the Hz pathway by performing docking studies and BHIA. β-hematin crystal docking (BHCD), an accurate procedure corresponding with the BHIA was employed. The hybrids were found to be more potent than CQ in BHIA**,** and we observed a direct correlation between antiplasmodial activity and inhibition of β-hematin formation.

3.4.2 8-A i oqui oli e-qui oli e ybri

The synthesized compounds and standard drugs were tested against 3D7 ring-stage parasites. The results showed that rimaquine was inactive (IC_{50} = 9370 nM) against the ring-stage parasite. In line with previously reported literature, **65** (IC_{50} = 66 nM) showed significant activity against 3D7 ring-stage parasites. Therefore, a fused pharmacophore strategy was used where free NH_2 of primaquine was reacted with various quinazolines to synthesize hybrid compounds containing the essential features of both pharmacophores. In the quinazoline scaffold presence of dimetho y groups at positions 6 and 7 and piperidine at position 2 is essential for activity. Therefore, compound **13c** (IC_{50} = 140 nM) was synthesized containing these essential features, and this proved to be the most potent molecule of the series. Replacing piperidine with pyrrolidine in **14c** (IC_{50} = 198 nM) led to a slight decrease in activity. Compounds containing chlorine at the 2nd position of quinazoline led to a twenty-fold decrease in activity (**9c** and **10c**) irrespective of the presence of metho y groups. Moreover, when chlorine was substituted with secondary amine while metho y groups were removed (**11c** and **12c**), there was a 10-fold decrease in activity compared to **13c**. This shows that the 2nd position of quinazoline ring is most important for antimalarial activity, and the presence of an amine group is essential for the activity (**Figure 3.23**).
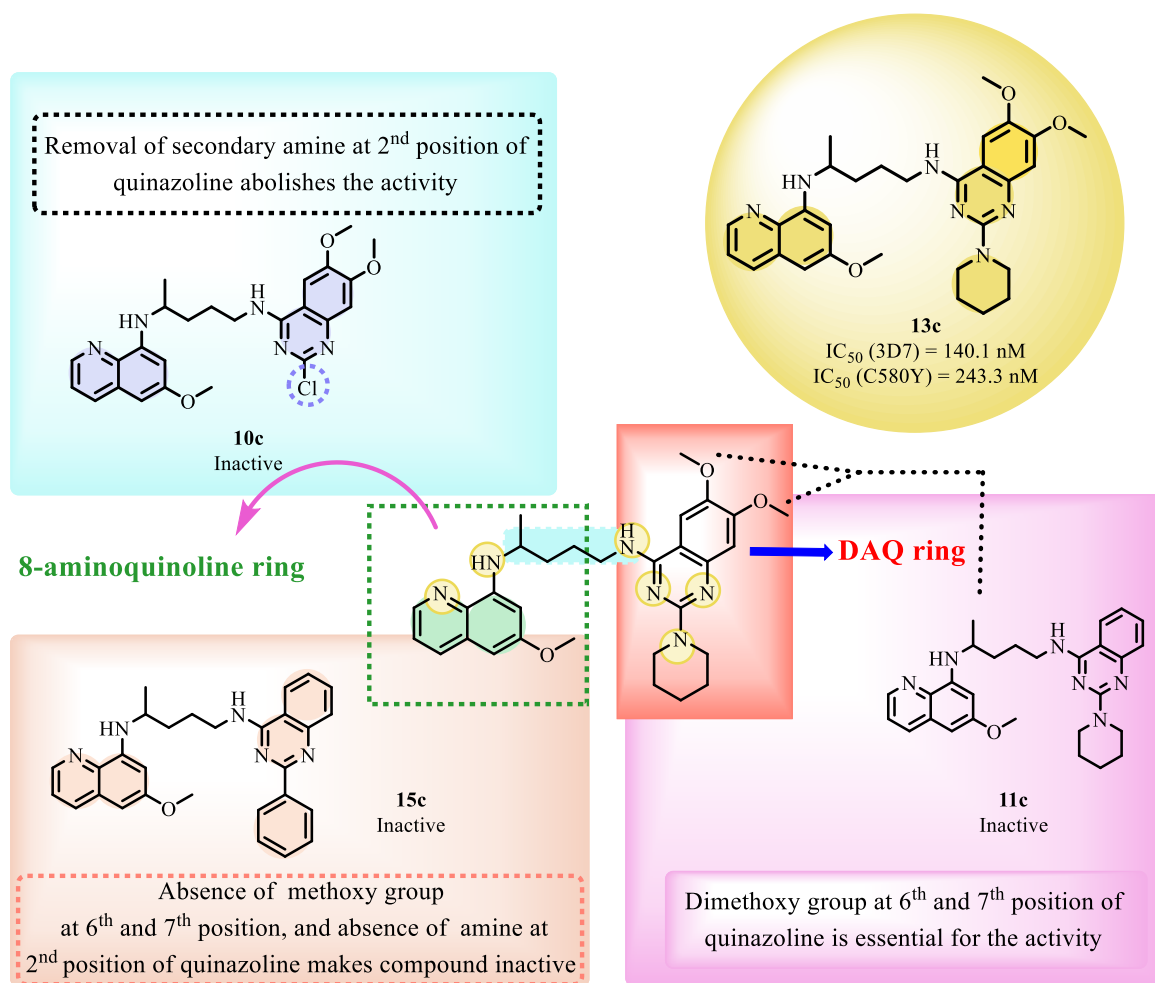
Figure 3.23. SAR of 8-aminoquinoline hybrids

3.4.3 Bisquinoline

Bisquinolines have been widely reported in the literature for their antimalarial activity; however, there are no reports for the bisquinazoline pharmacophore. Since quinoline and quinazoline are alternatively used in medicinal chemistry in place of each other, we planned to synthesize bisquinazolines linked together via a linker of variable chain length using **scheme 3.3**. Some of the compounds from this series (**8c** and **8e**) were tested against the artemisinin-sensitive strain (3D7); however, they did not show any activity, even at the highest tested concentration.

Finally, the synthesized compounds were evaluated for their ability to act on the Hz pathway by performing β-hematin crystal docking studies and β-hematin inhibition assay (BHIA). In the case of primaquine, BHCD gave a docking score of (-0.626). PQ is inactive for BHIA and

shows IC$_{50}$ of >1000 µM. The most active synthesized compounds showed interaction with the fastest-growing face and good docking score in the BHCD and were active in the BHIA.

3.5 EXPERIMENTAL

3.5.1 Ge er l roce ure c e e 3.1

To synthesize the compound **1** [N-(1-benzylpiperidin-4yl)-2-chloro-6,7-dimetho yquinaz olin-4-amine], 2,4-Dichloro-6,7-dimetho yqui nazoline (800 mg, 3.08 mmol) was stirred with 4-Amino-1-benzylpiperidine (1.254 mL, 6.18 mmol) in the presence of DIEA (1072 µL, 6.18 mmol) and THF for 18h at room temperature. Water workup was performed, and the reaction mi ture was removed from the aqueous layer with DCM. The DCM layer was concentrated and dried to obtain crude compound which was purified by column chromatography using silica as stationary phase solvent gradient of MeOH and CH$_2$Cl$_2$ (1-5% MeOH). Further, synthesized compound **1** (0.25 mmol) was reacted with secondary amine (1.025 mmol) and toluene under microwave irradiation at 160°C for 2 h to obtain compounds **2** and **3** which were further purified by column chromatography using silica as stationary phase and MeOH (7N NH$_3$) and CH$_2$Cl$_2$ as solvent (2-5% of MeOH).[145]

3.5.2 Ge er l roce ure c e e 3.2

4,7-dichloroquinoline was reacted with e c ess of diaminolinker under neat conditions using a microwave at 110°C for 1 hr to get diaminoquinolines (**1 -1e**). These were reacted with quinazolines at room temperature for 24h to obtain the quinoline-quinazoline hybrids (**2 -2e** and **3 -3e**). The quinoline-quinazoline hybrids (**2 -2e**) were further reacted with secondary amines under microwave conditions in the presence of I A and HCl in dio a ne at 160°C for 15 min to get the final product. The reaction mi ture was cooled to room temperature and poured carefully into water. The aqueous layer was e t racted with DCM (3 × 30 mL), the organic e tra cts were combined, washed with brine and dried over sodium sulphate. The solvent was

removed *in vacuo* and the resulting residue was purified by silica gel chromatography (DCM : MeOH = 90:10) to yield the desired product.

3.5.3 General procedure scheme 3.3

4-chloro-2-phenylquinazoline was reacted with various diamines at 60°C for 24 h in the presence of DIEA and THF to give the desired bisquinazolines. The reaction mixture was cooled to room temperature and poured carefully into water. The aqueous layer was extracted with DCM (3 × 30 mL), the organic extracts were combined, washed with brine and dried over sodium sulphate. The solvent was removed *in vacuo* and the resulting residue was purified by silica gel chromatography (DCM : MeOH = 90:10) to yield the desired product.

3.5.4 General procedure scheme 3.4

  primaquine was reacted with quinazoline at room temperature for 24 h to get the primaquine-quinazoline hybrid. These hybrids were further reacted with secondary amine in the presence of TFA and IPA at 160 °C for 25 min to get the final product. The reaction mixture was cooled to room temperature and poured carefully into water. The aqueous layer was extracted with DCM (3 × 30 mL), the organic extracts were combined, washed with brine and dried over sodium sulphate. The solvent was removed *in vacuo* and the resulting residue was purified by silica gel chromatography (DCM : MeOH = 90:10) to yield the desired product.

3.5.5 Compound characterization

3.5.5.1 Scheme 3.1 compounds

3.5.5.1.1 65 N-(1-benzylpiperidin-4-yl)-6,7-dimethoxy-2-(piperidin-1-yl)quinazolin-4-amine.

The yield of synthesized compound **65** was 75% (72 mg). ^{1}H NMR (400 MHz, DMSO-d_6) δ 7.40 (s, 1H), 7.34-7.30 (m, 4H), 7.27-7.22 (m, 1H), 6.71 (s, 1H), 4.02-3.93 (m, 1H), 3.79 (s, 3H), 3.78 (s, 3H), 3.67 (t, J = 5.4 Hz, 4H), 3.48 (s, 2H), 2.86 (d, J = 11.3 Hz, 2H), 2.06 (t, J = 11.4 Hz, 2H), 1.93 (d, J = 11.3 Hz, 2H), 1.67-1.55 (m, 4H), 1.49-1.43 (m, 4H). LCMS

(+ESI): *m/z* calculated for $C_{27}H_{35}N_5O_2$ 461.28 found 462.28 [M+H]⁺.   urity 100% [Mobile

 hase, ACN : Buffer (60:40) pH6.5; Rt 4.45 min].

3.5.5.1.2 **66** *N-(1-benzylpiperidin-4-yl)-6,7-dimethoxy-2-(4-methylpiperazin-1-yl)quinazolin-4-amine*

The yield of compound **66** was 88% (86 mg). ¹H NMR (400 MHz, DMSO-d_6) δ 7.42 (s, 1H),

7.34-7.28 (m, 4H), 7.26-7.21 (m, *J* = 6.0 Hz, 1H), 6.73 (s, 1H), 4.03-3.94 (m, *J* = 11.1 Hz, 1H),

3.79 (s, 3H), 3.78 (s, 3H), 3.71-3.65 (m, 4H), 3.46 (s, 2H), 2.83 (d, *J* = 11.3, Hz, 2H), 2.38-2.30

(m, 4H), 2.18 (s, 3H), 2.04 (t, *J* = 11.8 Hz, 2H), 1.95-1.88 (m, 2H), 1.68-1.55 (m, 2H). LCMS

(+ESI): *m/z* calculated for $C_{27}H_{36}N_6O_2$ 476.29 found 477.03 [M+H]⁺.   urity 100% [Mobile

 hase, ACN : Buffer (60:40) pH6.5; Rt 5.67 min].

3.5.5.2 Scheme 3.2 compounds

3.5.5.2.1 **4a** *(N1-(7-chloroquinolin-4-yl)-N2-(6,7-dimethoxy-2-(piperidin-1-yl)quinazolin-4-yl)ethane-1,2-diamine)*

Brown powder (yield 30 mg, 38%)**.** ¹H NMR (400 MHz, DMSO-d_6) δ 8.67 (t, *J* = 5.6 Hz, 1H),

8.47 (d, *J* = 5.5 Hz, 1H), 8.26 (d, *J* = 9.1 Hz, 1H), 7.84 (dd, *J* = 10.8, 3.7 Hz, 2H), 7.60 (s, 1H),

7.50 (dd, *J* = 8.9, 2.2 Hz, 1H), 7.10 (s, 1H), 6.98 (d, *J* = 5.6 Hz, 1H), 3.89 (d, *J* = 10.2 Hz, 6H),

3.75 – 3.61 (m, 4H), 1.30 – 1.16 (m, 6H). ¹³C NMR (101 MHz, DMSO) δ 160.69, 155.46,

154.98, 151.32, 151.24, 148.99, 148.34, 147.67, 134.40, 127.02, 124.93, 124.61, 117.73,

107.42, 107.02, 102.70, 99.50, 56.53, 56.35, 41.60, 40.60, 40.39, 40.19, 39.98, 39.77, 39.56,

39.35, 31.76, 29.48, 29.18, 22.57, 14.43. LCMS (+ESI): *m/z* calculated for $C_{26}H_{29}ClN_6O_2$

492.20 found 493. [M+H]⁺. HRMS (ESI/Q-TOF) m/z: [M + H]⁺ Calcd for $C_{26}H_{29}ClN_6O_2$

493.2113; Found 493.2122. Purity 100% [Mobile Phase, can : Buffer (60:40) ; Rt 3.65 min].

M.P. 210-216 ºC

3.5.5.2.2 **4b** *(N1-(7-chloroquinolin-4-yl)-N3-(6,7-dimethoxy-2-(piperidin-1-yl)quinazolin-4-*

yl)propane-1,3-diamine)

White powder (yield 42 mg, 53%)**.** ^{1}H NMR (400 MHz, DMSO-d_6) δ 8.36 (d, J = 5.4 Hz, 1H),

8.28 (d, J = 9.0 Hz, 1H), 7.78 (d, J = 2.2 Hz, 1H), 7.72 (bt, J = 5.5 Hz, 1H), 7.47-7.38 (m, 3H),

6.70 (s, 1H), 6.48 (d, J = 5.5 Hz, 1H), 3.80 (d, J = 11.4 Hz, 6H), 3.62 (dt, J = 16.9, 6.1 Hz, 6H),

2.04 (p, J = 7.0 Hz, 2H), 1.58-1.48 (m, 2H), 1.38 (tt, J = 8.2, 4.3 Hz, 4H). ^{13}C NMR (101 MHz,

DMSO) δ 159.44, 158.60, 154.18, 152.32, 150.49, 149.58, 149.02, 145.07, 133.79, 127.94,

124.54, 124.44, 117.98, 105.80, 103.45, 103.40, 99.09, 56.32, 55.79, 44.74, 40.60, 40.39,

40.18, 39.97, 39.77, 39.56, 39.35, 28.16, 25.84, 25.11. LCMS (+ESI): *m/z* calculated for

$C_{27}H_{31}ClN_6O_4$ 506.22 found 507.28 [M+H]$^+$. HRMS (ESI/Q-TOF) m/z: [M + H]$^+$ Calcd for

$C_{27}H_{31}ClN_6O_4$ 507.2270; Found 507.2282. Purity 100% [Mobile PhascanACN : Buffer (60:40)

; Rt 3.94 min]

3.5.5.2.3 **4c** *(N1-(7-chloroquinolin-4-yl)-N4-(6,7-dimethoxy-2-(piperidin-1-yl)quinazolin-4-*

yl)butane-1,4-diamine)

Cream powder (yield 77 mg, 58%)**.** ^{1}H NMR (400 MHz, Chloroform-*d*) δ 8.52 (d, J = 5.3 Hz,

1H), 7.97 (d, J = 2.2 Hz, 1H), 7.61 (d, J = 9.0 Hz, 1H), 7.34 (dd, J = 8.9, 2.2 Hz, 1H), 6.93 (s,

1H), 6.80 (s, 1H), 6.39 (d, J = 5.3 Hz, 1H), 5.54 (bs, 1H), 5.05 (bt, J = 5.3 Hz, 1H), 3.97 (s,

3H), 3.87 (s, 3H), 3.83 (t, J = 5.0 Hz, 4H), 3.72 (q, J = 6.4 Hz, 2H), 3.38 (q, J = 6.5, 5.9 Hz,

2H), 1.91 (h, J = 3.6 Hz, 4H), 1.59 (d, J = 9.8 Hz, 6H). ^{13}C NMR (101 MHz, Chloroform-*d*) δ

159.04 , 154.36 , 151.81 , 149.70 , 148.94 , 145.33 , 128.56 , 125.35 , 120.97 , 117.06 , 105.76

, 102.92 , 100.86 , 99.01 , 56.17 , 56.00 , 45.12 , 42.93 , 40.62 , 27.09 , 26.25 , 25.96 , 25.00 .

LCMS (+ESI): *m/z* calculated for $C_{28}H_{33}ClN_6O_2$ 520.24 found 521.03 [M+H]$^+$.HRMS (ESI/Q-

TOF) m/z: [M + H]$^+$ Calcd for C$_{28}$H$_{33}$ClN$_6$O$_2$ 521.2426; Found 521.2439. Purity 100% [Mobile

Pcane, ACN : Buffer (60:40) ; Rt 3.65 min]. M.P. 137-144 ºC

*3.5.5.2.4 **4d** (N1-(7-chloroquinolin-4-yl)-N5-(6,7-dimethoxy-2-(piperidin-1-yl)quinazolin-4-*

yl)pentane-1,5-diamine)

White powder (yield 50.5 mg, 58%). ^{1}H NMR (400 MHz, Chloroform-*d*) δ 8.54 (d, *J* = 5.3 Hz,

1H), 7.97 (d, *J* = 2.2 Hz, 1H), 7.57 (d, *J* = 9.0 Hz, 1H), 7.34 (dd, *J* = 8.9, 2.2 Hz, 1H), 6.93 (s,

1H), 6.76 (s, 1H), 6.41 (d, *J* = 5.4 Hz, 1H), 5.34 (bt, *J* = 5.6 Hz, 1H), 4.95 (bt, *J* = 5.1 Hz, 1H),

3.98 (s, 3H), 3.89 (s, 3H), 3.83 (t, *J* = 5.1 Hz, 4H), 3.69 (q, *J* = 6.6 Hz, 2H), 3.34 (td, *J* = 7.0,

5.1 Hz, 2H), 1.87 (dt, *J* = 15.3, 7.4 Hz, 4H), 1.67-1.56 (m, 8H). ^{13}C NMR (101 MHz, DMSO)

δ 159.42, 158.63, 154.14, 152.36, 150.54, 149.57, 149.02, 145.03, 133.78, 127.93, 124.58,

124.39, 117.92, 105.80, 103.47, 99.06, 56.34, 55.79, 44.80, 42.85, 40.60, 40.39, 40.19, 39.98,

39.77, 39.56, 39.35, 29.11, 28.12, 25.87, 25.12, 24.83. LCMS (+ESI): *m/z* calculated for

C$_{29}$H$_{35}$ClN$_6$O$_2$ 534.25 found 535.41 [M+H]$^+$. HRMS (ESI/Q-TOF) m/z: [M + H]$^+$ Calcd for

C$_{29}$H$_{35}$ClN$_6$O$_2$ 535.2583; Found 535.2592. Purity 100% [Mobilcanhase, ACN : Buffer (60:40)

; Rt 4.54 min]. M.P. 139-147 ºC

*3.5.5.2.5 **4e** (N1-(7-chloroquinolin-4-yl)-N6-(6,7-dimethoxy-2-(piperidin-1-yl)quinazolin-4-*

yl)hexane-1,6-diamine)

White powder (yield 45 mg, 51%). ^{1}H NMR (400 MHz, DMSO-*d$_6$*) δ 8.32 (d, *J* = 5.4 Hz, 1H),

8.20 (d, *J* = 9.0 Hz, 1H), 7.41 (dd, *J* = 9.0, 2.3 Hz, 1H), 7.33 (s, 1H), 6.71 (s, 1H), 6.43 (d, *J* =

5.6 Hz, 1H), 3.79 (s, 6H), 3.65 (t, *J* = 5.3 Hz, 4H), 3.43 (t, *J* = 7.1 Hz, 2H), 3.23 (t, *J* = 7.1 Hz,

2H), 1.64 (dt, *J* = 11.1, 5.4 Hz, 4H), 1.52-1.34 (m, 11H). ^{13}C NMR (101 MHz, DMSO-*d$_6$*) δ

159.40 , 158.62 , 154.13 , 152.37 , 150.54 , 149.56 , 149.00 , 145.03 , 133.79 , 127.93 , 124.57

, 124.41 , 105.80 , 103.46 , 103.43 , 99.03 , 56.33 , 55.79 , 44.80 , 42.82 , 40.78 , 29.26 , 28.25

, 26.98 , 26.95 , 25.88 , 25.11 . LCMS (+ESI): *m/z* calculated for C$_{30}$H$_{37}$ClN$_6$O$_2$ 548.27 found

549.41 [M+H]$^+$. HRMS (ESI/Q-TOF) m/z: [M + H]$^+$ Calcd for C$_{30}$H$_{37}$ClN$_6$O$_2$ 549.2739; Found 549.2750. Purity 100% [Mocane Phase, ACN : Buffer (60:40) ; Rt 6.28 min]

*3.5.5.2.6 **5c** (N1-(7-chloroquinolin-4-yl)-N4-(6,118yrrolidiney-2-(pyrrolidin-1-yl)quinazolin-4-yl)butane-1,4-diamine)*

White powder (yield 54 mg, 63%). ^{1}H NMR (400 MHz, DMSO-d_6) δ 9.34 (s, 1H), 8.69 (s, 1H), 8.50 (d, J = 9.1 Hz, 1H), 8.40 (d, J = 6.4 Hz, 1H), 7.90 (d, J = 2.2 Hz, 1H), 7.80 (s, 1H), 7.58 (dd, J = 9.0, 2.2 Hz, 1H), 7.31 (s, 1H), 6.68 (d, J = 6.5 Hz, 1H), 3.87 (d, J = 14.1 Hz, 6H), 3.62-3.48 (m, J = 25.2, 18.6, 5.8 Hz, 8H), 1.84 (s, 8H). ^{13}C NMR (101 MHz, DMSO-d_6) δ 159.14 , 154.36 , 151.97 , 150.70 , 149.20 , 145.25 , 133.93 , 127.62 , 124.68 , 124.47 , 117.84 , 103.99 , 103.13 , 99.07 , 56.47 , 55.94 , 46.75 , 42.62 , 26.77 , 25.77 , 25.40. LCMS (+ESI): *m/z* calculated for C$_{27}$H$_{31}$ClN$_6$O$_2$ 506.22 found 507.28 [M+H]$^+$. HRMS (ESI/Q-TOF) m/z: [M + H]$^+$ Calcd for C$_{27}$H$_{31}$ClN$_6$O$_2$ 507.2270; Found 507.2277. Purity 100% canbile Phase, ACN : Buffer (60:40) ; Rt 4.64 min]. M.P. 166-172 ºC

*3.5.5.2.7 **6c** (N1-(7-chloroquinolin-4-yl)-N4-(2-(piperidin-1-yl)quinazolin-4-yl)butane-1,4-diamine)*

White powder (yield 48 mg, 88%). ^{1}H NMR (400 MHz, Chloroform-d) δ 8.27 (s, 1H), 7.88 (d, J = 36.3 Hz, 2H), 7.60 (s, 1H), 7.47 (dd, J = 8.5, 7.1, 1.2 Hz, 1H), 7.35 (d, J = 8.2 Hz, 1H), 7.29 (dd, J = 8.9, 2.0 Hz, 1H), 7.03 (t, J = 7.6 Hz, 1H), 6.13 (d, J = 6.7 Hz, 1H), 3.59 (d, J = 5.6 Hz, 2H), 3.45 (d, J = 5.7 Hz, 2H), 2.02 (s, 4H), 1.66 (s, 9H). LCMS (+ESI): *m/z* calculated for C$_{26}$H$_{29}$ClN$_6$ 461.2215 found 461.2198 [M+H]$^+$. HRMS (ESI/Q-TOF) m/z: [M + H]$^+$ Calcd for C$_{26}$H$_{29}$ClN$_6$ 461.2215; Found 461.2198. urity 100% [Mobile hase, ACN : Buffer (60:40) ; Rt 3.09 min]

*3.5.5.2.8 **7c** (N1-(7-chloroquin119yrrolidine-N4-(2-(pyrrolidin-1-yl)quinazolin-4-yl)butane-1,4-diamine)*

White powder (yield 54 mg, 63%). ^{1}H NMR (400 MHz, DMSO-d_6) δ 8.35 (d, J = 5.4 Hz, 1H), 8.26 (d, J = 9.1 Hz, 1H), 7.94 (d, J = 8.3, 1.4 Hz, 1H), 7.90 (t, J = 5.5 Hz, 1H), 7.77 (d, J = 2.3 Hz, 1H), 7.51 – 7.40 (m, 2H), 7.32 (t, J = 5.4 Hz, 1H), 7.24 (dd, J = 8.4, 1.1 Hz, 1H), 6.99 (ddd, J = 8.1, 6.8, 1.3 Hz, 1H), 6.46 (d, J = 5.5 Hz, 1H), 3.56 (q, J = 6.3 Hz, 2H), 3.50 – 3.43 (m, 4H), 3.33 (d, J = 5.9 Hz, 2H), 1.86 – 1.70 (m, 8H). LCMS (+ESI): *m/z* calculated for $C_{26}H_{29}ClN_6O_2$ 447.2058 found 447.2046 [M+H]$^+$. HRMS (ESI/Q-TOF) m/z: [M + H]$^+$ Calcd for $C_{26}H_{29}ClN_6$ 447.2058; Found 447.2046.   urity 94.52% [Mobile   hase, ACN : Buffer (60:40) ; Rt 4.70 min]

*3.5.5.2.9 **3a** (N1-(7-chloroquinolin-4-yl)-N2-(2-phenylquinazolin-4-yl)ethane-1,2-diamine)*

White powder (yield 70 mg, 40%). ^{1}H NMR (400 MHz, DMSO-d_6) δ 8.59-8.45 (m, J = 24.1, 8.1, 3.8 Hz, 3H), 8.41 (s, J = 5.4 Hz, 1H), 8.23 (d, J = 8.3 Hz, 1H), 8.15 (d, J = 9.0 Hz, 1H), 7.83-7.76 (m, 3H), 7.67-7.61 (m, 1H), 7.51 (m, J = 4.4, 3.9 Hz, 4H), 7.37-7.30 (m, J = 7.7, 5.2, 2.2 Hz, 1H), 6.77-6.70 (m, J = 5.0 Hz, 1H), 4.05-3.98 (m, J = 6.3 Hz, 2H), 3.75-3.65 (m, J = 6.3 Hz, 2H). ^{13}C NMR (101 MHz, DMSO) δ 160.49, 159.85, 152.00, 150.78, 150.35, 149.19, 139.16, 134.00, 133.29, 130.55, 128.71, 128.40, 128.33, 127.69, 125.87, 124.58, 124.44, 123.12, 117.86, 114.33, 99.16, 42.24, 40.60, 40.39, 40.18, 39.98, 39.77, 39.56, 39.35, 39.23. HRMS (ESI/Q-TOF) m/z: [M + H]$^+$ Calcd for $C_{25}H_{20}ClN_5$ 426.1480; Found 426.1487. Purity 100% [Mobile Phase, ACN : Buffer (60:40) ; Rt 2.27 min]

*3.5.5.2.10 **3b** (N1-(7-chloroquinolin-4-yl)-N3-(2-phenylquinazolin-4-yl)propane-1,3-diamine)*

White powder (yield 39 mg, 18%). ^{1}H NMR (400 MHz, DMSO-d_6) δ 8.37-8.31 (d, 2H), 8.28-8.24 (m, 2H), 8.18 (d, J = 8.3, 1.0 Hz, 1H), 7.80-7.74 (m, 3H), 7.50-7.39 (m, 3H), 7.31 (t, J = 8.2, 7.0 Hz, 2H), 6.53 (d, J = 5.8 Hz, 1H), 3.82 (t, J = 6.9 Hz, 2H), 3.48 (t, J = 6.8 Hz, 2H),

2.14 (m, J = 6.8 Hz, 2H). HRMS (ESI/Q-TOF) m/z: [M + H]$^+$ Calcd for C$_{26}$H$_{22}$ClN$_5$ 440.1636; Found 440.1639. urity 100% [Mobile hase , ACN : Buffer (60:40) ; Rt 2.03 min]

3.5.5.2.11 **3c** *(N1-(7-chloroquinolin-4-yl)-N4-(2-phenylquinazolin-4-yl)butane-1,4-diamine)*

White powder (yield 56 mg, 30%). ^{1}H NMR (400 MHz, Methanol-d_4) δ 8.36 (d, 2H), 8.18 (d, J = 6.3 Hz, 1H), 8.06-8.01 (m, 2H), 7.81-7.73 (m, 2H), 7.70 (d, J = 2.1 Hz, 1H), 7.50-7.39 (m, 4H), 7.35 (dd, J = 9.0, 2.2 Hz, 1H), 6.59 (d, J = 6.3 Hz, 1H), 3.87 (t, J = 6.5 Hz, 2H), 3.56 (t, J = 6.7 Hz, 2H), 2.09-1.91 (m, 5H). ^{13}C NMR (101 MHz, CDCl$_3$) δ 165.11, 164.21, 155.41, 154.01, 151.25, 142.80, 139.47, 136.56, 133.94, 132.19, 132.04, 130.99, 129.87, 129.38, 129.10, 102.33, 81.71, 81.39, 81.07, 46.58, 44.35, 30.44, 29.48. HRMS (ESI/Q-TOF) m/z: [M + H]$^+$ Calcd for C$_{27}$H$_{24}$ClN$_5$ 454.1793; Found 454.1801. urity 100% [Mobile hase, ACN : Buffer (60:40) ; Rt 2.45 min]

3.5.5.2.12 **3d** *(N1-(7-chloroquinolin-4-yl)-N5-(2-phenylquinazolin-4-yl)pentane-1,5-diamine)*

White powder (yield 40 mg, 21%). ^{1}H NMR (400 MHz, Chloroform-d) δ 8.56 (d, 2H), 8.39 (d, J = 5.6 Hz, 1H), 7.94-7.89 (m, 2H), 7.80 (d, 1H), 7.75-7.67 (m, 2H), 7.51-7.44 (m, 3H), 7.39 (t, J = 8.2, 7.0, 1.2 Hz, 1H), 7.27 (d, J = 8.9, 2.2 Hz, 1H), 6.31 (d, J = 5.7 Hz, 1H), 6.17 (t, J = 5.7 Hz, 1H), 5.59 (bs, 1H), 3.90-3.82 (m, J = 6.6 Hz, 2H), 3.33-3.26 (m, J = 7.0, 5.0 Hz, 2H), 1.91-1.82 (m, J = 7.5 Hz, 4H), 1.66-1.57 (m, 2H). ^{13}C NMR (101 MHz, CDCl$_3$) δ 160.31, 159.90, 152.53, 149.99, 146.84, 138.78, 136.90, 132.48, 130.12, 128.35, 128.25, 128.20, 126.09, 125.34, 124.20, 123.54, 121.60, 116.40, 113.84, 98.27, 77.36, 77.04, 76.72, 53.56, 43.30, 41.92, 40.70, 28.59, 27.79, 24.27, 18.11, 12.34. HRMS (ESI/Q-TOF) m/z: [M + H]$^+$ Calcd for C$_{28}$H$_{26}$ClN$_5$ 468.1950; Found 468.1947. Purity 94.49% [Mobile Phase, ACN : Buffer (60:40) ; Rt 4.12 min]. M.P. 105-111 ºC

3.5.5.2.13 3e (N1-(7-chloroquinolin-4-yl)-N6-(2-phenylquinazolin-4-yl)hexane-1,6-diamine)

White powder (yield 63 mg, 32%). ^{1}H NMR (400 MHz, Chloroform-*d*) δ 8.56-8.53 (d, 2H), 8.37 (d, *J* = 5.6 Hz, 1H), 7.90-7.87 (m, 2H), 7.78-7.66 (m, 3H), 7.47-7.42 (m, 3H), 7.36 (t, *J* = 8.2, 6.9, 1.2 Hz, 1H), 7.24 (s, *J* = 2.2 Hz, 1H), 6.28 (d, *J* = 5.7 Hz, 1H), 6.14 (t, *J* = 5.6 Hz, 1H), 5.72 (t, *J* = 5.2 Hz, 1H), 3.82-3.74 (m, *J* = 6.6 Hz, 2H), 3.27-3.19 (m, *J* = 7.1, 5.0 Hz, 2H), 1.80-1.68 (m, *J* = 27.7, 7.1 Hz, 4H), 1.48-1.39 (m, 2H). HRMS (ESI/Q-TOF) m/z: [M + H]$^+$ Calcd for $C_{29}H_{28}ClN_5$ 482.2106; Found 482.2098. urity 99.37% [Mobile hase, ACN : Buffer (60:40) ; Rt 3.37 min

3.5.5.3 Scheme 3.3 compounds

3.5.5.3.1 8a (N1,N2-bis(2-phenylquinazolin-4-yl)ethane-1,2-diamine)

White powder (yield 90 mg, 47%). ^{1}H NMR (400 MHz, Chloroform-*d*) δ 8.58 (d, *J* = 6.6, 2.7 Hz, 4H), 7.85 (d, *J* = 8.4, 1.1 Hz, 2H), 7.59 (t, *J* = 8.4, 7.0, 1.3 Hz, 2H), 7.55-7.48 (m, 6H), 7.44 (bs, *J* = 8.3, 1.3 Hz, 2H), 7.00 (t, *J* = 8.3, 7.0, 1.2 Hz, 2H), 4.20-4.09 (m, 4H). HRMS (ESI/Q-TOF) m/z: [M + H]$^+$ Calcd for $C_{30}H_{24}N_6$ 469.2135; Found 469.2121. urity 100% [Mobile hase , ACN : Buffer (60:40) ; Rt 3.08 min]

3.5.5.3.2 8b (N1,N3-bis(2-phenylquinazolin-4-yl)propane-1,3-diamine)

White powder (yield 63 mg, 32%). ^{1}H NMR (400 MHz, Chloroform-*d*) δ 8.62-8.53 (m, 4H), 7.92 (d, *J* = 8.4, 1.1 Hz, 2H), 7.70 (t, *J* = 8.4, 7.0, 1.3 Hz, 2H), 7.56-7.46 (m, 8H), 7.24 (t, *J* = 8.2, 6.9, 1.2 Hz, 2H), 6.10 (t, *J* = 6.1 Hz, 2H), 4.08-4.00 (m, *J* = 6.1 Hz, 4H), 2.30-2.20 (m, 2H). HRMS (ESI/Q-TOF) m/z: [M + H]$^+$ Calcd for $C_{31}H_{26}N_6$ 483.2292; Found 483.2272. urity 99.46% [Mobile hase , ACN : Buffer (60:40) ; Rt 2.48 min]

3.5.5.3.3 8c (N1,N4-bis(2-phenylquinazolin-4-yl)butane-1,4-diamine)

White powder (yield 138 mg, 68%). ^{1}H NMR (400 MHz, Chloroform-*d*) δ 8.68-8.53 (d, 4H), 7.93 (d, *J* = 8.3 Hz, 2H), 7.72 (t, *J* = 8.4, 6.8, 2.8 Hz, 2H), 7.59-7.42 (m, 8H), 7.35 (t, 2H), 5.85 (t, *J* = 5.8 Hz, 2H), 3.97-3.86 (m, *J* = 6.7, 6.1 Hz, 4H), 2.03-1.90 (m, 4H). ^{13}C NMR (101 MHz, CDCl$_3$) δ 160.51, 159.65, 150.48, 139.08, 132.49, 130.11, 128.82, 128.33, 125.41, 120.42, 113.63, 77.36, 77.05, 76.73, 40.71, 26.73. HRMS (ESI/Q-TOF) m/z: [M + H]$^+$ Calcd for C$_{32}$H$_{28}$N$_6$ 497.2448; Found 497.2436. urity 99.83% [Mobile hase, ACN : Buffer (60:40) ; Rt 3.27 min]

3.5.5.3.4 *8d (N1,N5-bis(2-phenylquinazolin-4-yl)pentane-1,5-diamine)*

White powder (yield 114 mg, 54%). ^{1}H NMR (400 MHz, Chloroform-*d*) δ 8.59 (d, 4H), 7.93 (t, *J* = 6.9 Hz, 2H), 7.76-7.70 (m, *J* = 7.5 Hz, 2H), 7.63 (d, *J* = 8.2 Hz, 2H), 7.55-7.39 (m, 8H), 5.71 (t, *J* = 5.5 Hz, 2H), 4.03-3.84 (m, 4H), 2.03-1.88 (m, *J* = 15.8, 14.7, 8.5 Hz, 4H), 1.72-1.64 (m, 2H). HRMS (ESI/Q-TOF) m/z: [M + H]$^+$ Calcd for C$_{33}$H$_{30}$N$_6$ 511.2605; Found 511.2590. urity 100% [Mobile hase , ACN : Buffer (60:40) ; Rt 2.31 min]

3.5.5.3.5 *8e (N1,N6-bis(2-phenylquinazolin-4-yl)hexane-1,6-diamine)*

White powder (yield 84 mg, 39%). ^{1}H NMR (400 MHz, Chloroform-*d*) δ 8.64-8.58 (m, 4H), 7.94 (d, *J* = 8.4, 1.1 Hz, 2H), 7.73 (t, *J* = 8.4, 7.0, 1.3 Hz, 2H), 7.67 (d, *J* = 8.3, 1.3 Hz, 2H), 7.54-7.44 (m, 6H), 7.40 (t, *J* = 8.2, 6.9, 1.2 Hz, 2H), 5.74 (t, *J* = 5.6 Hz, 2H), 3.81 (td, *J* = 7.2, 5.7 Hz, 4H), 1.63-1.54 (m, 4H). HRMS (ESI/Q-TOF) m/z: [M + H]$^+$ Calcd for C$_{34}$H$_{32}$N$_6$ 525.2761; Found 525.2745. urity 86.71% [Mobile hase, ACN : Buffer (60:40) ; Rt 2.31 min]. M. . 210-216 ºC

3.5.5.4 Scheme 3.4 compounds

3.5.5.4.1 *9c (N1-(2-chloroquinazolin-4-yl)-N4-(6-methoxyquinolin-8-yl)pentane-1,4-diamine)*

Brown powder (yield 280mg, 76%). ^{1}H NMR (400 MHz, Chloroform-*d*) δ 8.56 (d, *J* = 4.2, 1.6 Hz, 1H), 7.96 (d, *J* = 8.3, 1.7 Hz, 1H), 7.75-7.66 (m, 2H), 7.50 (d, *J* = 7.8, 1.1 Hz, 1H), 7.39-

7.27 (m, 2H), 6.36 (d, 2H), 6.20 (t, *J* = 5.4 Hz, 1H), 6.05 (d, *J* = 8.7 Hz, 1H), 3.88 (s, 3H), 3.80-3.63 (m, 3H), 1.99-1.80 (m, 4H), 1.34 (d, *J* = 6.4 Hz, 3H).

3.5.5.4.2 *10c (N1-(2-chloro-6,7-dimethoxyquinazolin-4-yl)-N4-(6-methoxyquinolin-8-yl)pentane-1,4-diamine)*

Black powder (yield 155 mg, 25%). ^{1}H NMR (400 MHz, Chloroform-*d*) δ 8.53 (d, *J* = 4.2, 1.6 Hz, 1H), 7.92 (d, *J* = 8.3, 1.6 Hz, 1H), 7.34-7.28 (m, *J* = 8.3, 4.2 Hz, 1H), 7.10 (s, 1H), 6.86 (s, 1H), 6.30 (d, *J* = 19.8, 2.5 Hz, 2H), 6.01-5.95 (m, *J* = 5.5 Hz, 1H), 3.95 (s, 3H), 3.86 (s, 3H), 3.82 (s, 3H), 3.73-3.63 (m, *J* = 8.2, 7.0, 4.8 Hz, 3H), 1.92-1.83 (m, 2H), 1.80-1.72 (m, *J* = 5.4 Hz, 2H), 1.29 (d, *J* = 6.4 Hz, 3H).

3.5.5.4.3 *11c (N4-(6-methoxyquinolin-8-yl)-N1-(2-(piperidin-1-yl)quinazolin-4-yl)pentane-1,4-diamine)*

Brown semisolid (yield 39 mg, 56%). ^{1}H NMR (400 MHz, DMSO-*d*$_6$) δ 8.51 (d, *J* = 4.2, 1.7 Hz, 1H), 8.18 (s, 1H), 8.02 (dd, *J* = 38.6, 8.3, 1.5 Hz, 2H), 7.53-7.31 (m, 2H), 7.07 (t, *J* = 7.6 Hz, 1H), 6.46 (s, *J* = 2.5 Hz, 1H), 6.25 (s, *J* = 2.5 Hz, 1H), 6.14 (d, *J* = 8.7 Hz, 1H), 3.80 (s, 3H), 3.76-3.64 (m, *J* = 5.5 Hz, 5H), 3.51 (m, *J* = 6.4 Hz, 2H), 1.81-1.43 (m, 10H), 1.24-1.22 (d, 3H). LCMS (+ESI): *m/z* calculated for $C_{27}H_{26}N_6O$ 470.28 found 471.40 [M+H]$^+$. HRMS (ESI/Q-TOF) m/z: [M + H]$^+$ Calcd for $C_{27}H_{26}N_6O$ 471.2867; Found 471.2858.   urity 100% [Mobile hase , ACN:Buffer (60:40) pH4.2; Rt 1.37 min]

3.5.5.4.4 *12c (N4-(6-methoxyquinolin-8-yl)-N1-(2-(pyrrolidin-1-yl)quinazolin-4-yl)pentane-1,4-diamine)*

Black semisolid (yield 26 mg, 38%). ^{1}H NMR (400 MHz, Chloroform-*d*) δ 9.00 (bs, 1H), 8.48 (s, *J* = 4.2, 1.6 Hz, 1H), 7.95 (dd, *J* = 29.7, 8.3, 1.4 Hz, 2H), 7.78 (d, *J* = 8.3 Hz, 1H), 7.32-7.27 (m, 2H), 6.95 (t, 1H), 6.27 (dd, *J* = 17.9, 2.5 Hz, 2H), 5.99 (bs, 1H), 3.85 (s, 3H), 3.76-3.38 (m, 7H), 2.04-1.75 (m, 8H), 1.31 (s, 3H). LCMS (+ESI): *m/z* calculated for $C_{27}H_{32}N_6O$ 456.25

found 457.27 [M+H]$^+$. HRMS (ESI/Q-TOF) m/z: [M + H]$^+$ Calcd for C$_{27}$H$_{32}$N$_6$O 457.2710; Found 457.2689. urity 100% [Mobile hase , ACN:Buffer (60:40) pH4.2; Rt 3.7 min]

3.5.5.4.5 *13c (N1-(6,7-dimethoxy-2-(piperidin-1-yl)quinazolin-4-yl)-N4-(6-methoxyquinolin-8-yl)pentane-1,4-diamine)*

Brown semi-solid (yield 51 mg, 77%). ^{1}H NMR (400 MHz, Chloroform-*d*) δ 8.51 (s, *J* = 4.2, 1.7 Hz, 1H), 7.92 (d, *J* = 8.3, 1.7 Hz, 1H), 7.35-7.30 (m, 1H), 7.22 (s, 1H), 7.09 (s, 1H), 6.28 (d, *J* = 23.5, 2.5 Hz, 2H), 6.01 (bs, 1H), 3.92 (s, *J* = 4.0 Hz, 6H), 3.87 (s, 3H), 3.81-3.74 (m, 4H), 3.70-3.51 (m, 3H), 1.89-1.56 (m, 10H), 1.31 (d, *J* = 6.4 Hz, 3H). ^{13}C NMR (101 MHz, CDCl$_3$) δ 159.40, 158.54, 154.33, 146.17, 144.87, 144.25, 135.31, 134.77, 129.88, 121.84, 102.62, 96.79, 91.57, 77.34, 77.03, 76.71, 56.40, 56.20, 55.16, 47.84, 46.27, 41.51, 34.07, 25.65, 25.41, 24.48, 23.96, 20.54, 1.03. LCMS (+ESI): *m/z* calculated for C$_{30}$H$_{38}$N$_6$O$_3$ 530.30 found 531.41 [M+H]$^+$. HRMS (ESI/Q-TOF) m/z: [M + H]$^+$ Calcd for C$_{30}$H$_{38}$N$_6$O$_3$ 531.078; Found 531.3076. urity 99.4% [Mobile hase , ACN:Buffer (60:40) pH4.2; Rt 1.52 min]

3.5.5.4.6 *14c (N1-(6,7-dimethoxy-2-(pyrrolidin-1-yl)quinazolin-4-yl)-N4-(6-methoxyquinolin-8-yl)pentane-1,4-diamine)*

Black semi-solid (yield 29 mg, 56%). ^{1}H NMR (400 MHz, DMSO-*d$_6$*) δ 11.44 (bs, 1H), 9.07 (bs, 1H), 8.48 (s, *J* = 4.2, 1.6 Hz, 1H), 8.04 (d, *J* = 8.3, 1.7 Hz, 1H), 7.44-7.39 (m, *J* = 8.3, 4.2 Hz, 1H), 7.17 (s, 1H), 6.38 (s, *J* = 2.4 Hz, 1H), 6.20 (s, *J* = 2.5 Hz, 1H), 6.12 (d, *J* = 8.7 Hz, 1H), 3.89 (s, 3H), 3.83 (s, 3H), 3.77 (s, 3H), 3.74-3.67 (m, 1H), 3.62-3.54 (m, 2H), 3.52-3.43 (m, *J* = 6.5 Hz, 4H), 2.00-1.72 (m, 8H), 1.23 (d, *J* = 6.2 Hz, 3H). ^{13}C NMR (101 MHz, DMSO) δ 159.33, 158.62, 155.14, 146.80, 144.95, 144.58, 135.21, 134.94, 129.94, 122.49, 104.67, 102.37, 99.62, 96.71, 92.01, 56.56, 56.40, 55.35, 47.32, 41.62, 40.63, 40.43, 40.22, 40.01, 39.80, 39.59, 39.38, 33.46, 24.84, 20.79. LCMS (+ESI): *m/z* calculated for C$_{29}$H$_{36}$N$_6$O$_3$ 516.2

found 517.47 [M+H]$^+$. HRMS (ESI/Q-TOF) m/z: [M + H]$^+$ Calcd for $C_{29}H_{36}N_6O_3$ 517.2922; Found 517.2912.   urity 100% [Mobile hase , ACN:Buffer (60:40) pH4.2; Rt 6.55 min]

*3.5.5.4.7 **15c** (N4-(6-methoxyquinolin-8-yl)-N1-(2-phenylquinazolin-4-yl)pentane-1,4-diamine)*

Black semisolid (yield 50mg, 25%). ^{1}H NMR (400 MHz, Chloroform-*d*) δ 8.60-8.53 (m, 3H), 7.98-7.91 (, *J* = 12.5, 8.3, 1.4 Hz, 2H), 7.72 (t, *J* = 8.4, 6.3, 2.4 Hz, 1H), 7.61 (d, *J* = 8.3, 1.3 Hz, 1H), 7.53-7.46 (m, 3H), 7.38-7.30 (m, 2H), 6.40-6.33 (m, 2H), 3.85-3.74 (m, *J* = 17.0, 6.2 Hz, 2H), 2.40-2.32 (m, *J* = 7.6 Hz, 1H), 2.07-1.91 (m, 4H), 1.37 (d, *J* = 6.3 Hz, 3H). LCMS (+ESI): *m/z* calculated for $C_{29}H_{29}N_5O$ 463.24 found 464.28 [M+H]$^+$. HRMS (ESI/Q-TOF) m/z: [M + H]$^+$ Calcd for $C_{29}H_{29}N_5O$ 464.2445; Found 464.2423. Purity 100% [Mobile Phase, ACN : Buffer (60:40) pH4.2; Rt 3.45 min]

3.5.6 Puri y Profili g

Because the compounds were highly polar, ion pair reverse phase chromatography was used for purity profiling. A Shimadzu H LC system was used to analyze the purity of all synthesized compounds (LC-2010HT, Shimadzu Corporation, Japan). The chromatographic data acquisition and integration for the e pe riments were recorded using Lab solution software. The compounds were separated chromatographically at room temperature using an Ascentis® C18 stationary phase (50 mm 4.6 mm, i.d. 3.0 m) and an Acetonitrile and 2.5mM SLS buffer adjusted to pH 6.5 with formic acid as the mobile phase. The analysis was performed in isocratic mode at a flow rate of 1 mL/min.[146,147]

3.5.7 I   vi ro c ivi y g i   c i o   ge

This in vitro study was performed at NIMR by our collaborators to test the   c e   e **3.1** and   c e   e **3.2** compounds. *P. falciparum* parasites 3D7 strain was grown in vitro for antimalarial assay. The parasites were grown in fresh human erythrocytes {O+}, and suspended in a mi ture

of 10.4 g/L R MI 1640 (Gibco), 0.5% AlbuMAX II (Gibco), 0.2% sodium bicarbonate (Sigma), and the pH was maintained at 7.2) in a gaseous environment of 5% CO_2 and 37 °C as described in previous studies. For the antimalarial assay, 3D7 cultures were synchronized using 5% sorbitol, and parasitemia was assessed. These 3D7 cultures were synchronized with 5% sorbitol for antimalarial assay, and parasitemia was assessed. In vitro, synchronized ring- stages of erythrocyte cultures of *P. falciparum* parasites were taken in a mi ture of 5% hematocrit and 0.5% parasitemia in 96-well plates and were treated with the biogenic AgN s. The different concentrations of the e t racts were prepared, such as (50 ug/mL and 1 ug/mL), and incubated with the parasite culture in the treated wells at 37°C and 5% CO_2 for 24 hours.   arasite growth/inhibition was assessed by fi ing the thin blood smears in 100% methanol and stained for 20–30 min in 10% Giemsa stain solution. Chloroquine and DMSO served as the positive and negative controls for this assay and were grown for 4 days at 37°C under the gaseous 5% CO_2 environment in 96-well plates. Effective compounds were serially diluted and checked for IC_{50}.

3.5.8 I vi ro c ivi y g i   r i g ge

In this in vitro study,   c e e **3.4** compounds were tested by our collaborators at IBAB. *P. falciparum* 3D7 ring stage parasites at 1% parasitemia and either 1% or 2% hematocrit were treated for 48 h and 72 h with the various compounds. After the desired treatment time, the cultures were frozen at -80°C to lyse the cells and stained with SYBR Green I to assess relative parasite survival. 3 Biological Replicates (i.e., 3 different blood donors) were set up. Each replicate had three technical replicates. The compounds were tested at 1 μM and 10 μM. The compounds showing good results in the initial screening were tested for their IC_{50}. The following controls were used: untreated RBCs, 0.5% DMSO treatment, 3 conc WR99210 (1 nM, 10 nM and 50 nM), 3 conc of Chloroquine (1 nM, 10 nM and 50 nM).

3.5.9 Protocol for BCD

Ligands were prepared using the LigPrep module of Schrödinger to generate low-energy 3D structures and appropriate ionized forms.[148] The 27-unit cell crystal structure of β-hematin was prepared by using a heme dimer obtained from ccdc server (depositor number 162267), converted into crystal using VESTA and imported as a receptor in Maestro.[149] Grid (X=4.61, Y=7.16, Z=3.99) was generated by choosing the "centroid of selected residue" option around the β hematin crystal in order to cover all the faces, and the drugs may interact with any preferred face. The docking studies were performed using glide (version 2022–2).[150–152]

3.5.10 BHIA

Amodiaquine, chloroquine and piperaquine were taken as positive controls. Artemether and primaquine were taken as negative controls. 20mM stock solution for all the drugs was prepared in DMSO except for chloroquine and piperaquine, which were prepared in water. Appropriate dilutions were made for all drugs in NP40/water (61.1 mM). A hematin stock solution was prepared by sonicating hemin using DMSO and then suspending this stock in a 1 M acetate buffer. Both the drug (50μL) and hematin (48μL) were added to 96 well plates and incubated at ambient temp for 5h. A mixture containing 50% (v/v) pyridine, 30% (v/v) H_2O and 20% (v/v) acetone was prepared. The pH of the mixture was adjusted to pH 7.4 with 2 M 4-(2-hydroxy ethyl)-1-piperazineethanesulfonic acid (HEPES) buffer, and 32μL of this solution was added to each well. To further assist with hematin dispersion, acetone (60μL) was then added to each well. The UV−vis absorbance of the plates was recorded using an enzyme-linked immunosorbent assay (ELISA) plate reader at 405 nm (**Figure 3.24**). The IC_{50} value for each drug was calculated using GraphPad Prism v 8.0. The method validation was done by initially testing the known drugs (**Table 3.10**).
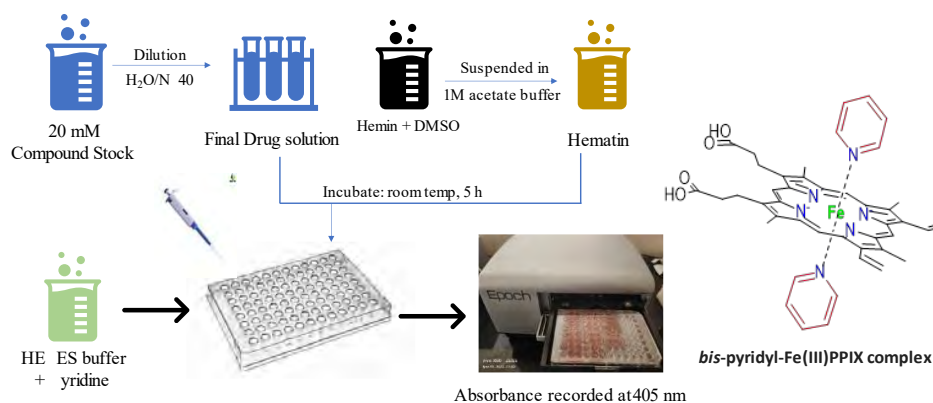
Figure 3.24. BHIA protocol

3.6 REFERENCES

1. World malaria report 2022. Accessed April 19, 2023. https://www.who.int/publications/i/item/9789240064898

2. Agarwal D, Gupta RD, Awasthi SK. Are Antimalarial Hybrid Molecules a Close Reality or a Distant Dream? *Antimicrob Agents Chemother*. 2017;61(5). doi:10.1128/AAC.00249-17

3. Nqoro X, Tobeka N, Aderibigbe B. Quinoline-Based Hybrid Compounds with Antimalarial Activity. *Molecules*. 2017;22(12):2268. doi:10.3390/molecules22122268

4. E pla in life cycle of la smodium with diagram. Accessed July 3, 2023. https://www.toppr.com/ask/question/e plain-life-cycle-of-plasmodium-with-diagram/

5. Deshpande S, Kuppast B. 4-aminoquinolines: An Overview of Antimalarial Chemotherapy. *Med Chem (Los Angeles)*. 2016;06(01). doi:10.4172/2161-0444.1000315

6. Yayon A, Timberg R, Friedman S, et al. Effects of chloroquine on the feeding mechanism of the intraerythrocytic human malarial parasite l asmodium falciparum. *J Protozool*. 1984;31(3):367-372. doi:10.1111/J.1550-7408.1984.TB02981.X

7. Eggleson KK, Duffin KL, Goldberg DE. Identification and Characterization of Falcilysin, a Metallopeptidase Involved in Hemoglobin Catabolism within the Malaria ar asite la smodium falciparum *. ublished online 1999. doi:10.1074/jbc.274.45.32411

8. Kumar S, Guha M, Choubey V, et al. Antimalarial drugs inhibiting hemozoin (β-hematin) formation: A mechanistic update. *Life Sci*. 2007;80(9):813-828. doi:10.1016/J.LFS.2006.11.008

9. Coronado LM, Nadovich CT, Spadafora C. Malarial hemozoin: From target to tool. *Biochimica et Biophysica Acta (BBA) - General Subjects*. 2014;1840(6):2032-2041. doi:10.1016/J.BBAGEN.2014.02.009

10. Herraiz T, Guillén H, González- eñ a D, et al. Antimalarial Quinoline Drugs Inhibit β-Hematin and Increase Free Hemin Catalyzing er o i dative Reactions and Inhibition of Cysteine rot eases. *Scientific Reports 2019 9:1*. 2019;9(1):1-16. doi:10.1038/s41598-019-51604-z

11. Rubio J , Cowman AF. The AT -binding cassette (ABC) gene family of la smodium falciparum. *Parasitology Today*. 1996;12(4):135-140. doi:10.1016/0169-4758(96)10003-X

12. Kolakovich KA, Gluzman IY, Duffin KL, et al. Generation of hemoglobin peptides in the acidic digestive vacuole of lasmodium falciparum implicates peptide transport in amino acid production. *Mol Biochem Parasitol*. 1997;87(2):123-135. doi:10.1016/S0166-6851(97)00062-5

13.   Sherman I. Malaria : parasite biology, pathogenesis, and protection. ub lished online 1998.

14.   Wright AD, Wang H, Gurrath M, et al. Inhibition of heme deto ification processes underlies the antimalarial activity of terpene isonitrile compounds from marine sponges. *J Med Chem*. 2001;44(6):873-885. doi:10.1021/JM0010724

15.   Kumar S, Bandyopadhyay U. Free heme to icity and its deto ification systems in human. *Toxicol Lett*. 2005;157(3):175-188. doi:10.1016/J.TOXLET.2005.03.004

16.   Vincent SH. O i dative effects of heme and porphyrins on proteins and lipids. *Semin Hematol*. 1989;26(2):105-113. Accessed March 13, 2023. https://europepmc.org/article/MED/2658086

17.   Schmitt TH, Frezzatti WA, Schreier S. Hemin-Induced Lipid Membrane Disorder and Increased er meability: A Molecular Model for the Mechanism of Cell Lysis. *Arch Biochem Biophys*. 1993;307(1):96-103. doi:10.1006/ABBI.1993.1566

18.   Ryter SW, Tyrrell RM. The heme synthesis and degradation pathways: role in o i dant sensitivity: Heme o y genase has both pro- and antio idant properties. *Free Radic Biol Med*. 2000;28(2):289-309. doi:10.1016/S0891-5849(99)00223-3

19.   Stojiljkovic I, Evavold BD, Kumar V. Antimicrobial properties of porphyrins. *http://dx.doi.org/101517/13543784102309*. 2005;10(2):309-320. doi:10.1517/13543784.10.2.309

20.   andey A V, Tekwani BL, Singh RL, et al. Artemisinin, an endopero ide antimalarial, disrupts the hemoglobin catabolism and heme deto i fication systems in malarial parasite. *Journal of Biological Chemistry*. 1999;274(27):19383-19388. doi:10.1074/jbc.274.27.19383

21.   Slater AFG, Cerami A. Inhibition by chloroquine of a novel haem polymerase enzyme activity in malaria trophozoites. *Nature*. 1992;355(6356):167-169. doi:10.1038/355167A0

22.   Ziegler J, Linck R, Wright DW. Heme aggregation inhibitors: Antimalarial drugs targeting an essential biomineralization process. *Studies in Natural Products Chemistry*. 2001;25:327-366. doi:10.1016/S1572-5995(01)80011-9

23.   Campanale N, Nickel C, Daubenberger CA, et al. Identification and characterization of heme-interacting proteins in the malaria parasite, l asmodium falciparum. *Journal of Biological Chemistry*. 2003;278(30):27354-27361. doi:10.1074/jbc.M303634200

24.   Chugh M, Sundararaman V, Kumar S, et al. ro tein comple directs hemoglobin-to-hemozoin formation in lasmodium falciparum. *Proc Natl Acad Sci U S A*. 2013;110(14):5392-5397. doi:10.1073/ N AS.1218412110/SU L_FILE/ N AS.201218412SI. D F

25.   Sullivan DJ, Gluzman IY, Goldberg DE. lasmodium Hemozoin Formation Mediated by Histidine-Rich roteins. *Science (1979)*. 1996;271(5246):219-222. doi:10.1126/SCIENCE.271.5246.219

26.   Wellems TE, Howard RJ. Homologous genes encode two distinct histidine-rich proteins in a cloned isolate of l asmodium falciparum. *Proc Natl Acad Sci U S A*. 1986;83(16):6065-6069. doi:10.1073/ N AS.83.16.6065

27.   Choi CYH, Schneider EL, Kim JM, et al. Interference with Heme Binding to Histidine-Rich rot ein-2 as an Antimalarial Strategy. *Chem Biol*. 2002;9(8):881-889. doi:10.1016/S1074-5521(02)00183-7

28.   Fitch CD. Ferriprotoporphyrin IX, phospholipids, and the antimalarial actions of quinoline drugs. *Life Sci*. 2004;74(16):1957-1972. doi:10.1016/J.LFS.2003.10.003

29. Dorn A, Vippagunta SR, Matile H, et al. An Assessment of Drug-Haematin Binding as a Mechanism for Inhibition of Haematin o lymerisation by Quinoline Antimalarials. *Biochem Pharmacol*. 1998;55(6):727-736. doi:10.1016/S0006-2952(97)00510-8

30. Egan T. Structure-function relationships in chloroquine and related 4-aminoquinoline antimalarials. *Mini Rev Med Chem*. 2001;1(1):113-123. doi:10.2174/1389557013407188

31. Hempelmann E, J. Egan T. ig ment biocrystallization in la smodium falciparum. *Trends Parasitol*. 2002;18(1):11. doi:10.1016/S1471-4922(01)02146-8

32. Hempelmann E, Motta C, Hughes R, et al. lasmodium falciparum: Sacrificing membrane to grow crystals? *Trends Parasitol*. 2003;19(1):23-26. doi:10.1016/S1471-4922(02)00011-9

33. Bohle DS, Kosar AD, Stephens W. has e homogeneity and crystal morphology of the malaria pigment β-hematin. *Acta Crystallogr D Biol Crystallogr*. 2002;58(10 II):1752-1756. doi:10.1107/S0907444902014294

34. Tekwani B, Walker L. Targeting the hemozoin synthesis pathway for new antimalarial drug discovery: technologies for in vitro beta-hematin formation assay. *Comb Chem High Throughput Screen*. 2005;8(1):63-79. doi:10.2174/1386207053328101

35. Egan TJ. Recent advances in understanding the mechanism of hemozoin (malaria pigment) formation. *J Inorg Biochem*. 2008;102(5-6):1288-1299. doi:10.1016/J.JINORGBIO.2007.12.004

36. Becker K, Tilley L, Vennerstrom JL, et al. O i dative stress in malaria parasite-infected erythrocytes: host–parasite interactions. *Int J Parasitol*. 2004;34(2):163-189. doi:10.1016/J.IJ ARA.2003.09.011

37. Shviro Y, Shaklai N. Glutathione as a scavenger of free hemin: A mechanism of preventing red cell membrane damage. *Biochem Pharmacol*. 1987;36(22):3801-3807. doi:10.1016/0006-2952(87)90441-2

38. Campanale N, Nickel C, Daubenberger CA, et al. Identification and characterization of heme-interacting proteins in the malaria parasite, l asmodium falciparum. *Journal of Biological Chemistry*. 2003;278(30):27354-27361. doi:10.1074/jbc.M303634200

39. Kawazu SI, Ikenoue N, Takemae H, et al. Roles of 1-Cys pero i redo i n in haem deto ification in the human malaria parasite lasmodium falciparum. *FEBS J*. 2005;272(7):1784-1791. doi:10.1111/J.1742-4658.2005.04611.X

40. Sevene E, González R, Menéndez C. Current knowledge and challenges of antimalarial drugs for treatment and prevention in pregnancy. *Expert Opin Pharmacother*. 2010;11(8):1277-1293. doi:10.1517/14656561003733599

41. Ashley EA, Ashley EA. Drugs in Development for Malaria. *Drugs*. 2018;78(9):861-879. doi:10.1007/s40265-018-0911-9

42. Capela R, Cabal GG, Rosenthal J, et al. Design and evaluation of primaquine-artemisinin hybrids as a multistage antimalarial strategy. *Antimicrob Agents Chemother*. 2011;55(10):4698-4706. doi:10.1128/AAC.05133-11

43. Okour M, Derimanov G, Barnett R, et al. A human microdose study of the antimalarial drug GSK3191607 in healthy volunteers. *Br J Clin Pharmacol*. 2018;84(3):482. doi:10.1111/BC .13476

44. Burgess SJ, Selzer A, Kelly JX, et al. A chloroquine-like molecule designed to reverse resistance in l asmodium falciparum. *J Med Chem*. 2006;49(18):5623-5625. doi:10.1021/jm060399n

45. Wang N, Wicht KJ, Shaban E, et al. Synthesis and evaluation of artesunate–indoloquinoline hybrids as antimalarial drug candidates. *Medchemcomm*. 2014;5(7):927-931. doi:10.1039/C4MD00091A

46. Chughlay MF, El Gaaloul M, Donini C, et al. Chemoprotective Antimalarial Activity of 2 18 against lasmodium falciparum: A Randomized, la cebo-Controlled Volunteer Infection Study. *Am J Trop Med Hyg*. 2021;104(4):1348-1358. doi:10.4269/AJTMH.20-1165

47. Vangapandu S, Sachdeva S, Jain M, et al. 8-Quinolinamines and Their pro prodrug conjugates as potent blood-Schizontocidal antimalarial agents. *Bioorg Med Chem*. 2003;11(21):4557-4568. doi:10.1016/J.BMC.2003.07.003

48. Barber BE, Fernandez M, atel HB, et al. Safety, pharmacokinetics, and antimalarial activity of the novel triaminopyrimidine ZY-19489: a first-in-human, randomised, placebo-controlled, double-blind, single ascending dose study, pilot food-effect study, and volunteer infection study. *Lancet Infect Dis*. 2022;22(6):879-890. doi:10.1016/S1473-3099(21)00679-4

49. Benoit-Vical F, Lelièvre J, Berry A, et al. Trio aq uines are new antimalarial agents active on all erythrocytic forms, including gametocytes. *Antimicrob Agents Chemother*. 2007;51(4):1463-1472. doi:10.1128/AAC.00967-06

50. Bosquesi L , Melo TRF, Vizioli EO, et al. Anti-Inflammatory Drug Design Using a Molecular Hybridization Approach. *Pharmaceuticals (Basel)*. 2011;4(11):1450-1474. doi:10.3390/ H 4111450

51. Mccarthy JS, Rückle T, Elliott SL, et al. A Single-Dose Combination Study with the E per imental Antimalarials Artefenomel and DSM265 To Determine Safety and Antimalarial Activity against Blood-Stage l asmodium Falciparum in Healthy Volunteers.; 2019. https://journals.asm.org/journal/aac

52. Barber BE, Fernandez M, atel HB, et al. Safety, pharmacokinetics, and antimalarial activity of the novel triaminopyrimidine ZY-19489: a first-in-human, randomised, placebo-controlled, double-blind, single ascending dose study, pilot food-effect study, and volunteer infection study. *Lancet Infect Dis*. 2022;22(6):879-890. doi:10.1016/S1473-3099(21)00679-4

53. Jiménez-Díaz MB, Ebert D, Salinas Y, et al. (+)-SJ733, a clinical candidate for malaria that acts through AT 4 to induce rapid host-mediated clearance of l asmodium. *Proc Natl Acad Sci U S A*. 2014;111(50):E5455-E5462. doi:10.1073/ N AS.1414221111

54. Okour M, Derimanov G, Barnett R, et al. A human microdose study of the antimalarial drug GSK3191607 in healthy volunteers. *Br J Clin Pharmacol*. 2018;84(3):482-489. doi:10.1111/bcp.13476

55. Sunduru N, Sharma M, Srivastava K, et al. Synthesis of o a lamide and triazine derivatives as a novel class of hybrid 4-aminoquinoline with potent antiplasmodial activity. *Bioorg Med Chem*. 2009;17(17):6451-6462. doi:10.1016/J.BMC.2009.05.075

56. ussa rd E, Verdier F. Antimalarial 4-aminoquinolines: mode of action and pharmacokinetics. *Fundam Clin Pharmacol*. 1994;8(1):1-17. doi:10.1111/J.1472-8206.1994.TB00774.X

57. Ribbiso KA, Heller LE, Taye A, et al. Artemisinin-based drugs target the plasmodium falciparum heme deto i fication pathway. *Antimicrob Agents Chemother*. 2021;65(4). doi:10.1128/AAC.02137-20/FORMAT/E U B

58. Oliveira R, Miranda D, Magalhães J, et al. From hybrid compounds to targeted drug delivery in antimalarial therapy. *Bioorg Med Chem*. 2015;23(16):5120-5130. doi:10.1016/j.bmc.2015.04.017

59. Sundriyal S, Malmquist NA, Caron J, et al. Development of diaminoquinazoline histone lysine methyltransferase inhibitors as potent blood-stage antimalarial compounds. *ChemMedChem*. 2014;9(10):2360-2373. doi:10.1002/CMDC.201402098

60. Noedl H, Se Y, Sriwichai S, et al. Artemisinin resistance in Cambodia: a clinical trial designed to address an emerging problem in Southeast Asia. *Clin Infect Dis*. 2010;51(11). doi:10.1086/657120

61. Dechy-Cabaret O, Benoit-Vical F, Robert A, et al. reparation and Antimalarial Activities of "Trio aq uines", New Modular Molecules with a Trio ane Skeleton Linked to a 4-Aminoquinoline. *ChemBioChem*. 2000;1(4):281-283. doi:10.1002/1439-7633(20001117)1:4<281::AID-CBIC281>3.0.CO;2-W

62. Li X, Li X, Liu F, et al. Rational Multitargeted Drug Design Strategy from the er spective of a Medicinal Chemist. *J Med Chem*. 2021;64(15):10581-10605. doi:10.1021/ACS.JMEDCHEM.1C00683

63. Lombard MC, N'Da DD, Breytenbach JC, et al. Antimalarial and anticancer activities of artemisinin–quinoline hybrid-dimers and pharmacokinetic properties in mice. *European Journal of Pharmaceutical Sciences*. 2012;47(5):834-841. doi:10.1016/J.EJ S.2 012.09.019

64. Walsh JJ, Coughlan D, Heneghan N, et al. A novel artemisinin-quinine hybrid with potent antimalarial activity. *Bioorg Med Chem Lett*. 2007;17(13):3599-3602. doi:10.1016/j.bmcl.2007.04.054

65. re torius SI, Breytenbach WJ, De Kock C, et al. Synthesis, characterization and antimalarial activity of quinoline–pyrimidine hybrids. *Bioorg Med Chem*. 2013;21(1):269-277. doi:10.1016/J.BMC.2012.10.019

66. Joubert J , Smit FJ, Du le ssis L, et al. Synthesis and in vitro biological evaluation of aminoacridines and artemisinin-acridine hybrids. *Eur J Pharm Sci*. 2014;56(1):16-27. doi:10.1016/J.EJ S.2014 .01.014

67. Çapcı A, Lorion MM, Wang H, et al. Artemisinin–(Iso)quinoline Hybrids by C−H Activation and Click Chemistry: Combating Multidrug-Resistant Malaria. *Angewandte Chemie - International Edition*. 2019;58(37):13066-13079. doi:10.1002/ANIE.201907224

68. Raynes K. Bisquinoline antimalarials: Their role in malaria chemotherapy. *Int J Parasitol*. 1999;29(3):367-379. doi:10.1016/S0020-7519(98)00217-3

69. Baird JK, Hoffman SL. *Primaquine Therapy for Malaria*. https://academic.oup.com/cid/article/39/9/1336/404549

70. Zorc B, e rković I, avić K, et al. r imaquine derivatives: Modifications of the terminal amino group. *Eur J Med Chem*. 2019;182. doi:10.1016/j.ejmech.2019.111640

71. Jansongsaeng S, Srimongkolpithak N, engon J, et al. 5-pheno y primaquine analogs and the tetrao ane hybrid as antimalarial agents. *Molecules*. 2021;26(13). doi:10.3390/molecules26133991

72. Thomas D, Tazerouni H, Sundararaj KGS, et al. Therapeutic failure of primaquine and need for new medicines in radical cure of la smodium viva . *Acta Trop*. 2016;160:35-38. doi:10.1016/j.actatropica.2016.04.009

73. Johnston WT, Mutalima N, Sun D, et al. Relationship between lasmodium falciparum malaria prevalence, genetic diversity and endemic Burkitt lymphoma in Malawi. *Sci Rep*. 2014;4. doi:10.1038/SRE 03741

74. Khan KH. DNA vaccines: roles against diseases. *Germs*. 2013;3(1):26-35. doi:10.11599/GERMS.2013.1034

75. Fedosov DA, Dao M, Karniadakis GE, et al. Computational Biorheology of Human Blood Flow in Health and Disease. *Ann Biomed Eng*. 2014;42(2):368. doi:10.1007/S10439-013-0922-3

76. Beus M, Rajić Z, Maysinger D, et al. SAHAquines, Novel Hybrids Based on SAHA and ri maquine Motifs, as ote ntial Cytostatic and Antiplasmodial Agents. *ChemistryOpen*. 2018;7(8):624. doi:10.1002/O E N.201800117

77. de Souza e reira C, Costa Quadros H, Magalhaes Moreira DR, et al. A Novel Hybrid of Chloroquine and rimaquine Linked by Gold(I): Multitarget and Multiphase Antiplasmodial Agent. *ChemMedChem*. 2021;16(4):662-678. doi:10.1002/CMDC.202000653

78. Boechat N, Carvalho RCC, Ferreira M de LG, et al. Antimalarial and anti-inflammatory activities of new chloroquine and primaquine hybrids: Targeting the blockade of malaria parasite transmission. *Bioorg Med Chem*. 2020;28(24). doi:10.1016/J.BMC.2020.115832

79. da Silva Neto GJ, Silva LR, de Omena RJM, et al. Dual quinoline-hybrid compounds with antimalarial activity against lasmodium falciparum parasites. *New Journal of Chemistry*. 2022;46(14):6502-6518. doi:10.1039/D1NJ05598D

80. Jansongsaeng S, Srimongkolpithak N, engon J, et al. 5- heno y r imaquine Analogs and the Tetrao ane Hybrid as Antimalarial Agents. *Molecules*. 2021;26(13). doi:10.3390/MOLECULES26133991

81. Ajani OO, Aderohunmu DV, Umeokoro EN, et al. Quinazoline pharmacophore in therapeutic medicine. *Bangladesh J Pharmacol*. 2016;11(3):716-733. doi:10.3329/BJ .V11I3.25731

82. Selvam T, a lanirajan VK. Quinazoline Marketed drugs - A Review. *undefined*. u blished online 2011.

83. Luo H, Yang S, Cai Y, et al. Synthesis and biological evaluation of novel 6-chloro-quinazolin derivatives as potential antitumor agents. *Eur J Med Chem*. 2014;84:746-752. doi:10.1016/J.EJMECH.2014.07.053

84. Werbel LM, Degnan MJ. Synthesis and antimalarial and antitumor effects of 2-amino-4-(hydrazino and hydro ya mino)-6-[(aryl)thio]quinazolines. *J Med Chem*. 1987;30(11):2151-2154. doi:10.1021/JM00394A038

85. at el NB, at el JC. Synthesis and antimicrobial activity of Schiff bases and 2-azetidinones derived from quinazolin-4(3H)-one. *Arabian Journal of Chemistry*. 2011;4(4):403-411. doi:10.1016/J.ARABJC.2010.07.005

86. Bb C, p B, Ak K, et al. Synthesis and evaluation of some new 4, 6- disubstituted quinazoline derivatives for antimicrobial and antifungal activities. *undefined*. ub lished online 2014. doi:10.15272/AJB S.V4I33.554

87.   Jafari E, Khajouei MR, Hassanzadeh F, et al. Quinazolinone and quinazoline derivatives: recent structures with potent antimicrobial and cytoto ic activities. *Res Pharm Sci*. 2016;11(1):1. Accessed August 30, 2022. /pmc/articles/ MC4794932/

88.   Kumar A, Sharma S, Archana, et al. Some new 2,3,6-trisubstituted quinazolinones as potent anti-inflammatory, analgesic and COX-II inhibitors. *Bioorg Med Chem*. 2003;11(23):5293-5299. doi:10.1016/S0968-0896(03)00501-7

89.   Aly MM, Mohamed YA, El-Bayouki KAM, et al. Synthesis of some new 4(3H)-quinazolinone-2-carbo aldehyde thiosemicarbazones and their metal comple e s and a study on their anticonvulsant, analgesic, cytoto ic and antimicrobial activities - part-1. *Eur J Med Chem*. 2010;45(8):3365-3373. doi:10.1016/J.EJMECH.2010.04.020

90.   ort ela-Cubillo F, Scott JS, Walton JC. Microwave-promoted syntheses of quinazolines and dihydroquinazolines from 2-aminoarylalkanone O-phenyl o i mes. *Journal of Organic Chemistry*. 2009;74(14):4934-4942. doi:10.1021/JO900629G/SU L_FILE/JO900629G_SI_001. D F

91.   Vijayakumar K, Ahamed AJ, Thiruneelakandan G. Synthesis, Antimicrobial, and Anti-HIV1 Activity of Quinazoline-4(3H)-one Derivatives. *Journal of Applied Chemistry*. 2013;2013:1-5. doi:10.1155/2013/387191

92.   Rojas-Aguirre Y, Hernández-Luis F, Mendoza-Martínez C, et al. Effects of an antimalarial quinazoline derivative on human erythrocytes and on cell membrane molecular models. *Biochimica et Biophysica Acta (BBA) - Biomembranes*. 2012;1818(3):738-746. doi:10.1016/J.BBAMEM.2011.11.026

93.   Fröhlich T, Reiter C, Ibrahim MM, et al. Synthesis of Novel Hybrids of Quinazoline and Artemisinin with High Activities against la smodium falciparum, Human Cytomegalovirus, and Leukemia Cells. *ACS Omega*. 2017;2(6):2422-2431. doi:10.1021/ACSOMEGA.7B00310/SU L_FILE/AO7B00310_SI_001. D F

94.   Yun JC, Han NS, Soo YJ, et al. Synthesis and SAR study of T-type calcium channel blockers. ar t II. *Arch Pharm (Weinheim)*. 2008;341(10):661-664. doi:10.1002/ARD .200800079

95.   Malmquist NA, Moss TA, Mecheri S, et al. Small-molecule histone methyltransferase inhibitors display rapid antimalarial activity against all blood stage forms in l asmodium falciparum. *Proc Natl Acad Sci U S A*. 2012;109(41):16708-16713. doi:10.1073/ N AS.1205414109/SU L_FILE/ N AS.201205414SI. D F

96.   Chookajorn T, Dzikowski R, Frank M, et al. Epigenetic memory at malaria virulence genes. *Proc Natl Acad Sci U S A*. 2007;104(3):899-902. doi:10.1073/ N AS.0609084103

97.   Dokmanovic M, Clarke C, Marks A. Histone deacetylase inhibitors: overview and perspectives. *Mol Cancer Res*. 2007;5(10):981-989. doi:10.1158/1541-7786.MCR-07-0324

98.   Greer EL, Shi Y. Histone methylation: a dynamic mark in health, disease and inheritance. *Nat Rev Genet*. 2012;13(5):343-357. doi:10.1038/nrg3173

99.   Sundriyal S, Chen B , Lubin AS, et al. Histone lysine methyltransferase structure activity relationships that allow for segregation of G9a inhibition and anti- la smodium activity. *Medchemcomm*. 2017;8(5):1069-1092. doi:10.1039/C7MD00052A

100.   David R. Immune evasion through silence. *Nature Reviews Microbiology 2013 11:8*. 2013;11(8):509-509. doi:10.1038/nrmicro3084

101. Nardella F, Halby L, Hammam E, et al. DNA Methylation Bisubstrate Inhibitors Are Fast-Acting Drugs Active against Artemisinin-Resistant l asmodium falciparum a rasites. *ACS Cent Sci*. 2020;6(1):16-21. doi:10.1021/ACSCENTSCI.9B00874

102. Koumpoura CL, Robert A, Athanassopoulos CM, et al. Antimalarial Inhibitors Targeting Epigenetics or Mitochondria in lasmodium falciparum: Recent Survey upon Synthesis and Biological Evaluation of ote ntial Drugs against Malaria. *Molecules*. 2021;26(18). doi:10.3390/MOLECULES26185711

103. Egan TJ, Ncokazi KK. Quinoline antimalarials decrease the rate of β-hematin formation. *J Inorg Biochem*. 2005;99(7):1532-1539. doi:10.1016/J.JINORGBIO.2005.04.013

104. Egan TJ, Ross DC, Adams A. Quinoline anti-malarial drugs inhibit spontaneous formation of β-haematin (malaria pigment). *FEBS Lett*. 1994;352(1):54-57. doi:10.1016/0014-5793(94)00921-X

105. Dorn A, Stoffel R, Matile H, et al. Malarial haemozoin/β-haematin supports haem polymerization in the absence of protein. *Nature 1995 374:6519*. 1995;374(6519):269-271. doi:10.1038/374269a0

106. Dorn A, Vippagunta SR, Matile H, et al. A Comparison and Analysis of Several Ways to ro mote Haematin (Haem) o lymerisation and an Assessment of Its Initiation In Vitro. *Biochem Pharmacol*. 1998;55(6):737-747. doi:10.1016/S0006-2952(97)00509-1

107. Slater AFG, Swiggard WJ, Orton BR, et al. An iron-carbo y late bond links the heme units of malaria pigment. *Proc Natl Acad Sci U S A*. 1991;88(2):325-329. doi:10.1073/ N AS.88.2.325

108. Basilico N, agani E, Monti D, et al. A microtitre-based method for measuring the haem polymerization inhibitory activity (H IA) of antimalarial drugs. *Journal of Antimicrobial Chemotherapy*. 1998;42(1):55-60. doi:10.1093/JAC/42.1.55

109. Bohle DS, Helms JB. Synthesis of β-Hematin by Dehydrohalogenation of Hemin. *Biochem Biophys Res Commun*. 1993;193(2):504-508. doi:10.1006/BBRC.1993.1652

110. Blauer G, Akkawi M. On the preparation of β-haematin. *Biochemical Journal*. 2000;346(2):249-250. doi:10.1042/0264-6021:3460249

111. Bendrat K, Berger BJ, Cerami A. Haem polymerization in malaria. *Nature 1995 378:6553*. 1995;378(6553):138-138. doi:10.1038/378138a0

112. is ciotta JM, Coppens I, Tripathi AK, et al. The role of neutral lipid nanospheres in la smodium falciparum haem crystallization. *Biochemical Journal*. 2007;402(1):197-204. doi:10.1042/BJ20060986

113. Huy NT, Uyen DT, Maeda A, et al. Simple colorimetric inhibition assay of heme crystallization for high-throughput screening of antimalarial compounds. *Antimicrob Agents Chemother*. 2006;51(1):350-353. doi:10.1128/AAC.00985-06

114. Fitch CD, Cai GZ, Chen YF, et al. Involvement of lipids in ferriprotoporphyrin IX polymerization in malaria. *Biochimica et Biophysica Acta (BBA) - Molecular Basis of Disease*. 1999;1454(1):31-37. doi:10.1016/S0925-4439(99)00017-4

115. Carter MD, he lan V V, Sandlin RD, et al. *Lipophilic Mediated Assays For-Hematin Inhibitors*. Vol 13.; 2010.

116. Sandlin RD, Fong KY, Wicht KJ, et al. Identification of β-hematin inhibitors in a high-throughput screening effort reveals scaffolds with in vitro antimalarial activity. *Int J Parasitol Drugs Drug Resist*. 2014;4(3):316-325. doi:10.1016/j.ijpddr.2014.08.002

117. Rush MA, Baniecki ML, Mazitschek R, et al. Colorimetric high-throughput screen for detection of heme crystallization inhibitors. *Antimicrob Agents Chemother*. 2009;53(6):2564-2568. doi:10.1128/AAC.01466-08

118. Kapishnikov S, Berthing T, Hviid L, et al. Aligned hemozoin crystals in curved clusters in malarial red blood cells revealed by nanoprobe X-ray Fe fluorescence and diffraction. *Proc Natl Acad Sci U S A*. 2012;109(28):11184-11187. doi:10.1073/ N AS.1118134109/-/DCSU LEMENTAL

119. Huy NT, Uyen DT, Maeda A, et al. Simple colorimetric inhibition assay of heme crystallization for high-throughput screening of antimalarial compounds. *Antimicrob Agents Chemother*. 2007;51(1):350-353. doi:10.1128/AAC.00985-06

120. Stiebler R, Majerowicz D, Knudsen J, et al. Unsaturated Glycerophospholipids Mediate Heme Crystallization: Biological Implications for Hemozoin Formation in the Kissing Bug Rhodnius proli u s. *PLoS One*. 2014;9(2):88976. doi:10.1371/journal.pone.0088976

121. agol a S, Stephens W, Bohle DS, Kosar AD, et al. The structure of malaria pigment β-haematin. *Nature*. 2000;404(6775):307-310. doi:10.1038/35005132

122. Constantinidis I, Satterlee JD. UV-Visible and Carbon NMR Studies of Chloroquine Binding to Urohemin I Chloride and Uroporphyrin I in Aqueous Solutions. *J Am Chem Soc*. 1988;110(13):4391-4395. doi:10.1021/JA00221A045/ASSET/JA00221A045.F . N G_V03

123. Buchler JW. SYNTHESIS AND R O E RTIES OF METALLO O R H YRINS. *ChemInform*. 1979;10(16). doi:10.1002/CHIN.197916394

124. The orp hyrins V5: h ysical Chemistry, art C - Google Books. Accessed April 15, 2023. https://books.google.co.in/books?hl=en&lr=&id=ZBOJ uB FsWIC&oi=fnd&pg= A205&dq= dio yg en+and+metalloporphyrins,+james&ots=3W_op8EE B &sig=Gzdg1kpCrK_rq1Lp0Oqi AcEGECs#v=onepage&q=dio yg en%20and%20metalloporphyrins%2C%20james&f=false

125. Egan TJ, Mavuso WW, Ross DC, et al. Thermodynamic factors controlling the interaction of quinoline antimalarial drugs with ferriprotoporphyrin IX. *J Inorg Biochem*. 1997;68(2):137-145. doi:10.1016/S0162-0134(97)00086-X

126. ar apini S, Basilico N, as ini E, et al. Standardization of the hys icochemical ar ameters to Assess in Vitro the β-Hematin Inhibitory Activity of Antimalarial Drugs. *Exp Parasitol*. 2000;96(4):249-256. doi:10.1006/EX R .2000.4583

127. Saritha M, Koringa K, Dave U, et al. A modified precise analytical method for anti-malarial screening: Heme polymerization assay. *Mol Biochem Parasitol*. 2015;201(2):112-115. doi:10.1016/J.MOLBIO ARA.2015.07.004

128. O'neill M, Barton VE, Ward SA. molecules The Molecular Mechanism of Action of Artemisinin-The Debate Continues. *Molecules*. 2008;15:1705-1721. doi:10.3390/molecules15031705

129. Ismail HM, Barton VE, an chana M, et al. A click chemistry-based proteomic approach reveals that 1,2,4-trio o lane and artemisinin antimalarials share a common protein alkylation profile. *Angewandte Chemie - International Edition*. 2016;55(22):6401-6405. doi:10.1002/ANIE.201512062

130.   osner GH, Wang D, Cumming JN, et al. Further Evidence Supporting the Importance of and the Restrictions on a Carbon-Centered Radical for High Antimalarial Activity of 1, 2, 4-Trio ane s Like Artemisinin. *J Med Chem*. 1995;38(13):2273-2275. doi:10.1021/JM00013A001/ASSET/JM00013A001.F . N G_V03

131.   Mercer AE, Maggs JL, Sun XM, et al. Evidence for the involvement of carbon-centered radicals in the induction of apoptotic cell death by artemisinin compounds. *Journal of Biological Chemistry*. 2007;282(13):9372-9382. doi:10.1074/JBC.M610375200

132.   Kumari A, Karnatak M, Singh D, et al. Current scenario of artemisinin and its analogues for antimalarial activity. *Eur J Med Chem*. 2019;163:804-829. doi:10.1016/J.EJMECH.2018.12.007

133.   Andraws G, Trefi S. Ionisable substances chromatography: A new approach for the determination of Ketoprofen, Etorico ib, and Diclofenac sodium in pharmaceuticals using ion – pair H L C. *Heliyon*. 2020;6(8):e04613. doi:10.1016/J.HELIYON.2020.E04613

134.   et ritis KN, Chaimbault , Elfakir C, et al. Ion-pair reversed-phase liquid chromatography for determination of polar underivatized amino acids using perfluorinated carbo yl ic acids as ion pairing agent. *J Chromatogr A*. 1999;833(2):147-155. doi:10.1016/S0021-9673(98)01060-7

135.   Yang ZY, Wang L, Tang X. Determination of azithromycin by ion-pair H L C with UV detection. *J Pharm Biomed Anal*. 2009;49(3):811-815. doi:10.1016/J.J B A.2008.12.018

136.   AbuRuz S, Millership J, McElnay J. Determination of metformin in plasma using a new ion pair solid phase e t raction technique and ion pair liquid chromatography. *Journal of Chromatography B*. 2003;798(2):203-209. doi:10.1016/J.JCHROMB.2003.09.043

137.   Zoest AR, Hung CT, Wanweviolruk S, et al. re diction of Retention in Reversed hase Ion- air Chromatography Using Sodium Dodecyl Sulphate as airing Ion. *https://doi.org/101080/10826079208017180*. 2006;15(3):395-410. doi:10.1080/10826079208017180

138.   Zheng J, Rustum AM. Rapid separation of desloratadine and related compounds in solid pharmaceutical formulation using gradient ion-pair chromatography. *J Pharm Biomed Anal*. 2010;51(1):146-152. doi:10.1016/J.J B A.2009.08.024

139.   Charlier B, i ngeon M, Dal ia z F, et al. Development of a novel ion-pairing H L C-FL method for the separation and quantification of hydro ych loroquine and its metabolites in whole blood. *Biomedical Chromatography*. 2018;32(8). doi:10.1002/BMC.4258

140.   Lu J, Wei YC, Markovich RJ, et al. THE RETENTION BEHAVIOR OF LORATADINE AND ITS RELATED COM O UNDS IN ION AIR REVERSED H ASE H L C. *http://dx.doi.org/101080/10826071003608389*. 2010;33(5):603-614. doi:10.1080/10826071003608389

141.   Obisesan OR, Adekunle AS, Oyekunle JAO, et al. Development of electrochemical nanosensor for the detection of malaria parasite in clinical samples. *Front Chem*. 2019;7(FEB):431872. doi:10.3389/FCHEM.2019.00089/BIBTEX

142.   Fitch CD, Kanjananggulpan . The state of ferriprotoporphyrin IX in malaria pigment. *Journal of Biological Chemistry*. 1987;262(32):15552-15555. doi:10.1016/s0021-9258(18)47761-7

143.   Johann L, Lanfranchi A, Davioud-Charvet E, et al. *A Physico-Biochemical Study on Potential Redox-Cyclers as Antimalarial and Antischistosomal Drugs*.

144. Lawong A, Gahalawat S, Okombo J, et al. Novel Antimalarial Tetrazoles and Amides Active against the Hemoglobin Degradation athway in la smodium falciparum. *J Med Chem*. 2021;64(5):2739-2761. doi:10.1021/acs.jmedchem.0c02022

145. Sundriyal S, Chen B , Lubin AS, et al. Histone lysine methyltransferase structure activity relationships that allow for segregation of G9a inhibition and anti- la smodium activity. *Medchemcomm*. 2017;8(5):1069-1092. doi:10.1039/C7MD00052A

146. Wright DH, Herman VK, Konstantinides FN, et al. Determination of quinolone antibiotics in growth media by reversed-phase high-performance liquid chromatography. *Journal of Chromatography B*. 1998;709:97-104.

147. Amin AS, Dessouki HA, Agwa IA, et al. Ion-pairing and reversed phase liquid chromatography for the determination of three different quinolones: Enroflo a cin, lomeflo ac in and oflo a cin. *Arabian Journal of Chemistry*. 2011;4:249-257. doi:10.1016/j.arabjc.2010.06.031

148. Lig r ep, Schrödinger, LLC, New York, NY, 2021.

149. Momma K, Izumi F. VESTA 3 for three-dimensional visualization of crystal, volumetric and morphology data. *urn:issn:0021-8898*. 2011;44(6):1272-1276. doi:10.1107/S0021889811038970

150. Amod L, Mohunlal R, Egan TJ, et al. Identifying inhibitors of β-haematin formation with activity against chloroquine-resistant la smodium falciparum malaria parasites via virtual screening approaches. ub lished online 2022. doi:10.21203/rs.3.rs-2329483/v1

151. Sousa ACC de de, Maepa K, Combrinck JM, et al. Lapatinib, Nilotinib and Lomitapide Inhibit Haemozoin Formation in Malaria ar asites. *Molecules*. ubl ished online 2020:1-15. doi:10.3390/molecules25071571

152. de Sousa ACC, Combrinck JM, Maepa K, et al. Virtual screening as a tool to discover new β-haematin inhibitors with activity against malaria parasites. *Sci Rep*. 2020;10(1):3374. doi:10.1038/s41598-020-60221-0

Chapter 4

Discovery of bisquinolines as Mycobacterium tuberculosis ClpC1 inhibitors: SAR studies and antimycobacterial evaluation

4.1 INTRODUCTION AND BACKGROUND

TB is a transmissible disease which infects the lungs and is caused by *Mtb*. The *Mtb* loaded droplets are inhaled by a healthy individual and the *Mtb* reaches the lungs and leads to one of the following possible outcomes:

a. Immediate clearance of *Mtb*

b. Primary disease: immediate onset of active disease

c. Latent TB infections

d. Reactivation disease: initiation of active disease after remaining latent for many years[1]

4.1.1 Primary disease

Among the individuals who contract TB, the active disease develops within 2-3 years of infection. When the host's immune system fails to eliminate the pathogen, it travels to the alveoli and proliferates inside the alveolar macrophages. These macrophages may travel away from the lungs towards other tissues. However, inside the lungs, the macrophages initiate the production of inflammatory mediators, cytokines and chemokines.[1] Further, they recruit other phagocytic cells, such as monocytes, more alveolar macrophages and neutrophils, which collectively initiate the formation of a nodular granulomatous structure known as a tubercle. In the absence of any treatment, the tubercle enlarges, and the bacteria enter the local lymph nodes. This results in lymphadenopathy, the predominant characteristic of primary TB.[1] Further tubercle expands into the lung parenchyma to produce the lesion known as Ghon focus, and additionally, lymph node enlarges and calcifies. Ghon focus and lymph node enlargement are together known as Ranke complex.[2] Moreover, in addition to the infection in the lungs, bacteraemia may also occur.

Generally, around 2-10 weeks after the initial infection, in more than 90% of the individuals exposed to the bacteria, an effective cell-mediated immune (CMI) response develops. However, if

a successful CMI is not achieved the failure to repair the tissue and curb the bacterial growth leads to progression of lung destruction. The host immune mechanisms such as release of tumor necrosis factor (TNF)-α, reactive oxygen and nitrogen species, and other mediators also collaterally damage the host cell and result in development of caseating necrosis (**Figure 4.1**).
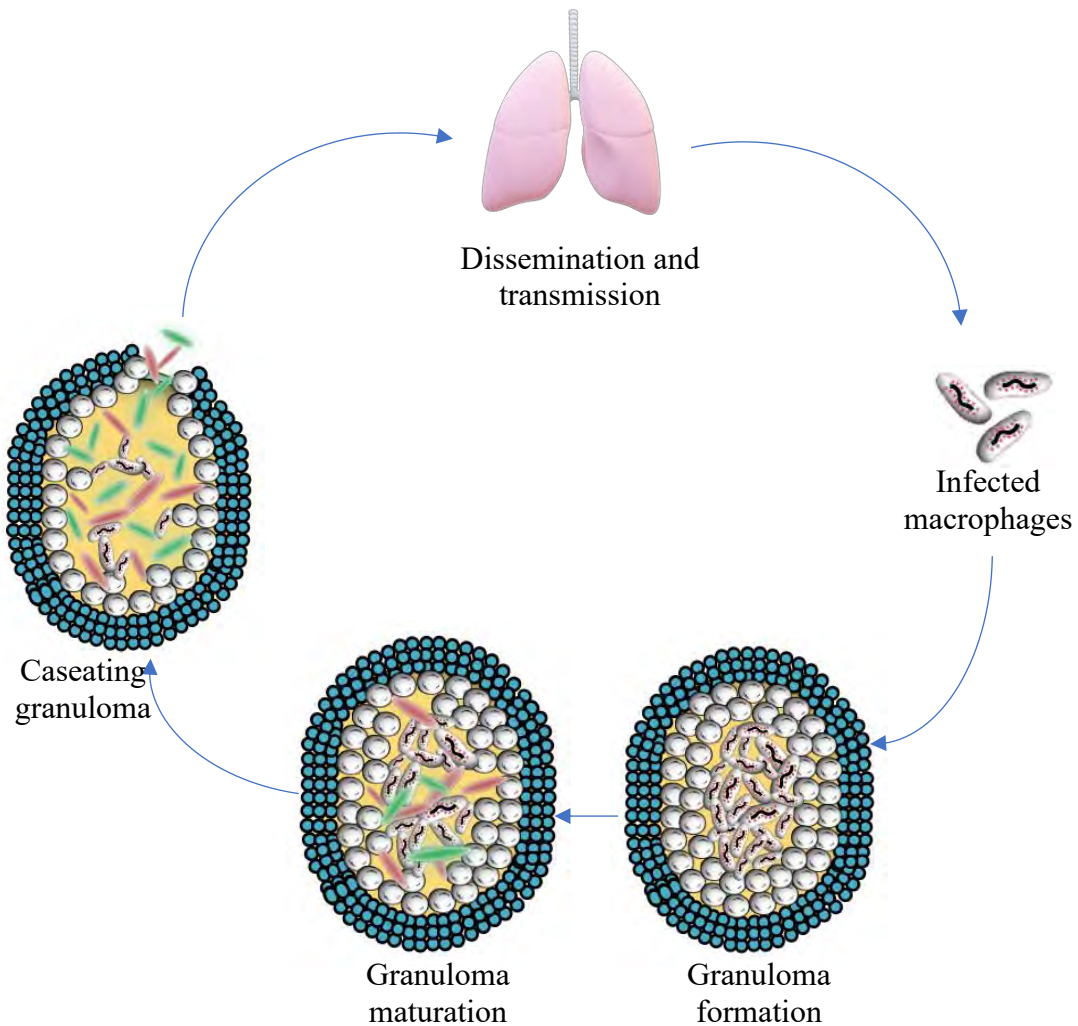
Figure 4.1. Pathogenesis of TB

The caseous lesions may erode to disseminate to other organs, known as miliary TB, and at this stage, the host becomes contagious to others. Approximately 80% of infected patients succumb to TB, while the remaining patients either recover or develop chronic disease.[1]

In the chronic form of disease, there is a cyclic healing of lesion by fibrotic changes around it and breakdown of the tissue.[1]

4.1.2 Reactivation TB

This form of TB occurs due to proliferation of a latent bacilli that hid in the lungs during primary infection. Reactivation occurs approximately in only 5-10% of cases[3] and the HIV patients and those with other underlying concomitant diseases such as chronic kidney disease, end-stage renal disease, diabetes, malignant lymphoma, cigarette smoking, etc are generally more susceptible to reactivation disease.[4–6] In reactivation TB, the lesion is present at the lung apices with the involvement of a very little regional lymph node, and the dissemination is very rare unless the host has severe immunosuppression.[1]

4.1.3 Virulence and Pathogenesis of TB

The following products of *Mtb* have been considered to produce virulence:

a. mycolic acid glycolipids and trehalose dimycolate, also known as cord factor: elicit the formation of granuloma in animal tissue

b. catalase-peroxidase: resists host cell oxidative response

c. sulfatides and trehalose dimycolate: triggers toxicity in animal models

d. lipoarabinomannan (LAM): induction of cytokines and resist host oxidative stress[1]

4.1.4 Treatment of TB

The development of the attenuated vaccine, Bacille Calmette-Guerin (BCG), by Calmette and Guerin was a major breakthrough in TB prevention efforts during the 19th century. Later, in 1944, 1952, 1957 and 1980, the discovery of today's well-known anti-TB regime, including streptomycin, isoniazid, rifamycins and pyrazinamide, respectively, brought another ray of hope in the fight against TB.[7]

Although a well-known regime for the treatment of TB is available, there is an ever-rising threat of multidrug-resistant TB (MDR-TB) and extensively drug-resistant (XDR) *Mtb* strains.[8] The traditional first-line treatment of TB includes rifampicin, isoniazid, pyrazinamide, and ethambutol (RHZE regimen). The MDR-TB is caused by the *Mtb,* which do not respond to isoniazid and rifampicin, the two most effective antituberculars. MDR-TB is said to be treatable using the second line antituberculars.[9] The second line anti-TB drugs are cycloserine, ethionamide, *para-aminosalicylic* acid, injectables such as streptomycin, amikacin/kanamycin, capreomycin, and fluoroquinolones (moxifloxacin and levofloxacin).[10] However, the number of MDR-TB cases showed a rise in the year 2020 (**Figure 4.2**). XDR-TB is a rare type of MDR-TB that is resistant to isoniazid and rifampicin, in addition to any fluoroquinolone and at least one of three injectable second line-drugs (i.e., amikacin, kanamycin or capreomycin). However, the second-line anti-TB regimen consists of very old drugs known to have serious adverse effects, including drug-induced liver injury (DILI), lifelong disability, expected therapy failure, and intolerance and are also expensive in comparison with first-line drugs.[9,10] In 2021, only 1 in 3 patients infected with the MDR strain of TB were able to access the treatment.[9] Therefore, lately, the emergence of drug-resistant strains has also posed a serious challenge against anti-TB therapy.[11,12]
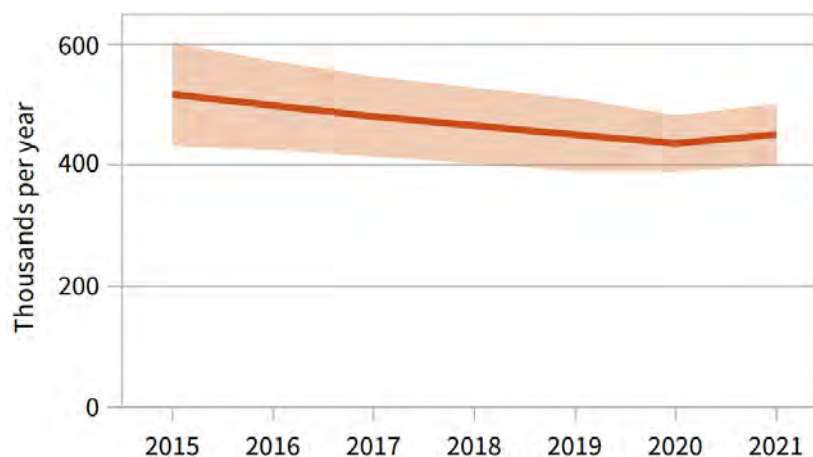
Figure 4.2. Estimated number of MDR-TB/RR-TB incident cases during 2015-2021

The discovery of new anti-TB drugs is exceptionally challenging due to the impervious and lipid-rich hydrophobic waxy nature of the *Mtb* cell wall.[13] The latter consists of peptidoglycans, mycolic acid, and arabinogalactan.[13] In addition, *Mtb* has transporter systems responsible for the efflux of many drugs out of the cell, rendering them ineffective. Bedaquiline, Pretomanid, and Delamanid have been approved for the treatment of MDR-TB, resulting in a newer regime for clinical use. The BPaL regimen (bedaquiline, pretomanid, linezolid) is tweaked by adding or removing other antitubercular drugs to achieve the desired therapeutic effect (**Figure 4.3**).[14–16] Recently, in 2022, as per new guidelines of WHO, a 6-month regime of BPaLM (BPaL regime + moxifloxacin)/BPaL has been recommended as the treatment of choice for eligible patients.[9]
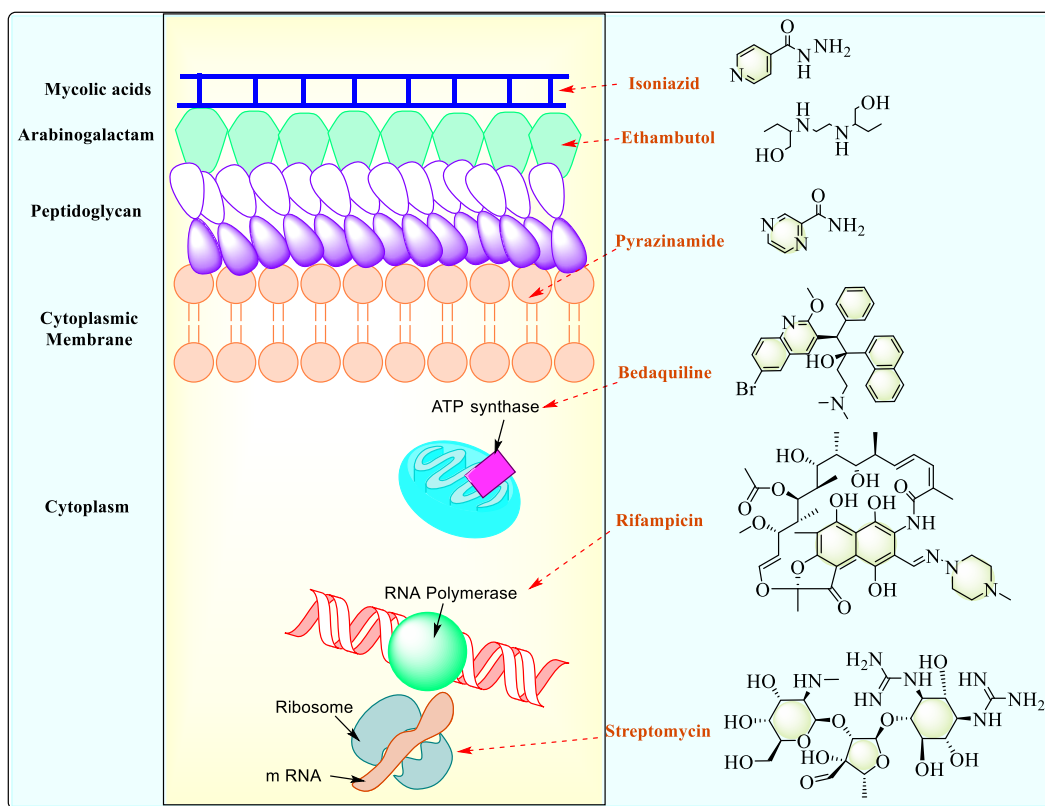
Figure 4.3. Mechanism of action of different antitubercular drugs on different regions of bacilli

However, the newly discovered anti-TB drugs are also ineffective against totally drug-resistant (TDR) TB (a type of TB which is resistant to more drugs than XDR).[17] Novel drugs have also been

developed, which are under clinical trials (**Figure 4.4**); nevertheless, the threat of emergence of resistance against the new drugs necessitates continuous efforts toward discovering novel anti-TB molecules and targets.[18]
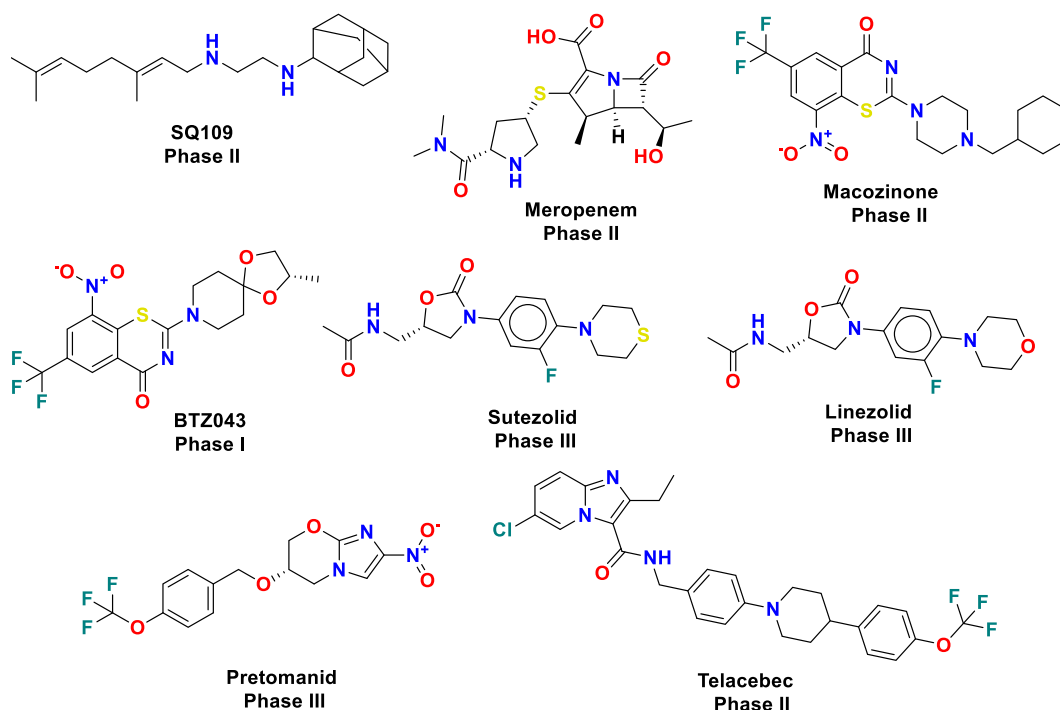
Figure 4.4. Antitubercular drugs under clinical trials

Proteolysis is an essential process in *Mtb* that maintains the required level and quality of the cellular proteins for optimum growth and virulence of the pathogen.[19] Recently, the proteolytic complex formed by the caseinolytic protease (Clp) chaperone-protease system has emerged as one of the potential anti-TB targets.[20] This protease system comprises of an oligomeric multi-subunit complex in bacteria containing the barrel-shaped heterotetradecameric proteolytic component (ClpP1 and ClpP2) and regulatory ATPase component. The hexameric ring-like ATPase subunit includes ClpX, ClpA, ClpC1 or 19S proteasome, known simply as unfoldases.[21] The ATPases recognize the targeted protein, unfold, and further translocate it to the proteolytic subunit of the complex to execute proteolysis. This multi-subunit system is involved in the degradation of cellular proteins to

maintain homeostasis and check the proteins specifically involved in the regulatory processes. Using the clustered regularly interspaced short palindromic repeats interference (CRISPRi)-mediated gene silencing approach, ClpC1 was found to be indispensable for the extracellular growth of *Mtb* and its survival in macrophages.[21]

4.2 GAPS IN EXISTING RESEARCH AND OBJECTIVES

1. The existing antitubercular drugs worldwide have lost their efficacy due to the development of resistance. Therefore, there is an urgent need to identify novel targets and develop new antitubercular agents.

2. The naturally occurring cyclic peptides, cyclomarin A (CymA), lassomycin, ecumicin, and rufomycin have shown potent activity against *Mtb* by inhibiting ClpC1.[22–26] However, peptides possess weak membrane permeability, thus are unable to reach the intracellular targets efficiently.[27] Peptides also have poor metabolic stability in addition to poor oral bioavailability.[28,29] Moreover, these molecules are too complex for chemical synthesis[30,31] and medicinal chemistry-based optimization. Therefore, these disadvantages limit the use of peptides in drug development. Thus, there is a scope to develop synthetically tractable small molecule inhibitors of ClpC1.

3. Systematic screening and SAR analysis of ClpC1 inhibitors based on bisquinolines.

4.3 RESULTS AND DISCUSSION

4.3.1 High throughput screening of compounds against ClpC1 (performed by our collaborators at THSTI)

To screen compounds against mycobacterial ClpC1, it was expressed and purified from *E. coli*, followed by an evaluation of its ATPase activity, as mentioned in the Experimental section. Simultaneously, the ClpX was expressed and purified, which was used as a control (**Figure 4.5A**).

As presented in **Figure 4.5A**, the ClpC1 exhibited relatively higher ATP hydrolysis (0.17±0.04 μM/Min/μM enzyme) in comparison to ClpX (0.04±0.001 μM/Min/μM enzyme), after 30 minutes of incubation with 180 μM adenosine triphosphate (ATP). Analysis of the kinetics of ATP hydrolysis further indicated ~3-fold higher V_{max} by ClpC1 compared to that observed with ClpX, possibly due to duplication of the ATPase domain (**Figure 4.5B**). Based on these preliminary experiments, the ATP hydrolysis activity of ClpC1 was targeted for screening of compounds.
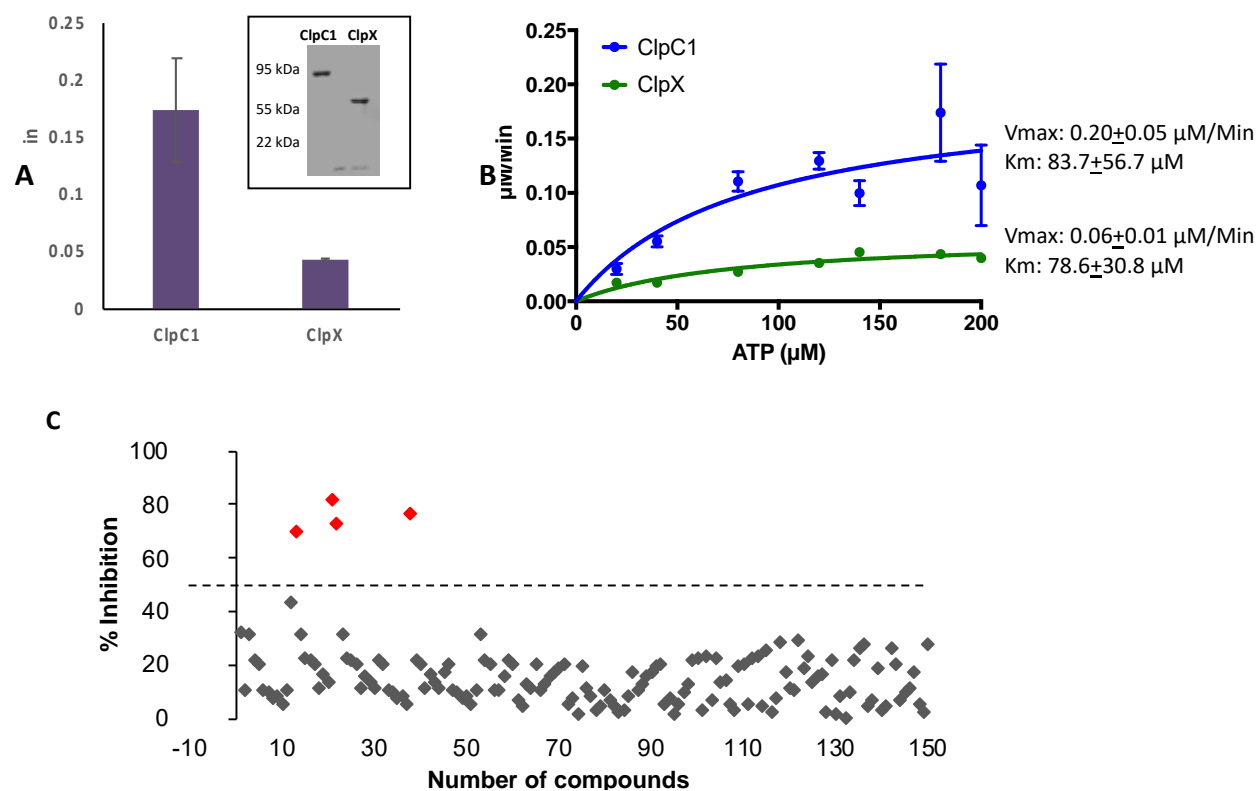
Figure 4.5. High throughput screening of compounds against *Mtb* ClpC1. A) Comparative analysis of the ATP hydrolysis activity of ClpC1 and ClpX. The status of the purified proteins on Coomassie Brilliant Blue-stained SDS-PAGE gel is shown in the inset. B) Enzyme kinetics of ClpC1 and ClpX. Shown is the kinetics of ATP hydrolysis by ClpC1 and ClpX unfoldases of *Mtb* using different concentrations of the substrate. C) Screening of small molecules for inhibition of ATPase activity of *Mtb* ClpC1. Enzymatic activity was zanalyzed in the presence of 100 μM concentration of the respective inhibitors. Molecules exhibiting an inhibitory effect above the baseline are shown by red dots. Data in (B) represent mean±s.d. of values from two biological repeats. These studies were performed in our collaborator's lab at THSTI.

Our collaborators at THSTI initially screened small libraries consisting of ~10,000 structurally diverse compounds[26] against *M. bovis* BCG, an attenuated vaccine strain of an *Mtb*-complex bacterium *M. bovis* [32, 33] (and unpublished data). This revealed that a set of 150 molecules inhibit in

vitro growth of BCG. Noteworthy to mention, they found that MIC_{99} of most of these molecules was similar against BCG and *Mtb* whereas some of them display differential activity against these bacteria.[32, 34] Further evaluation of these molecules for inhibition of the ATPase activity of *Mtb* ClpC1 led to the identification of a set of 4 molecules exhibiting substantial inhibition of the enzymatic activity of ClpC1 (**Figure 4.5C**).

4.3.2 Chemistry
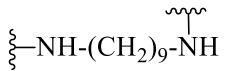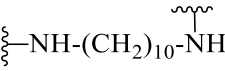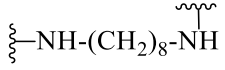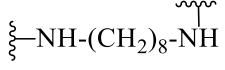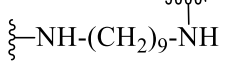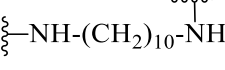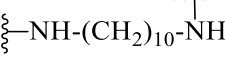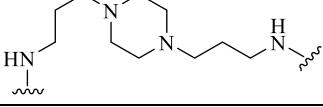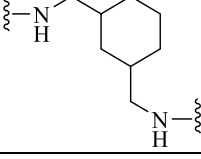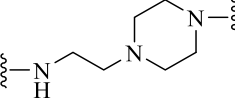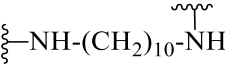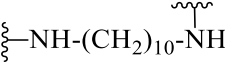
The target molecules were synthesized employing the well-known chemical reactions with slight modifications[35–38] as depicted in **Schemes 1** and **2**. The commercially available substituted 4-cholorquinolines were heated with different bis-amine linkers under microwave irradiation in the presence of *N,N*-Diisopropylethylamine (DIEA) base.
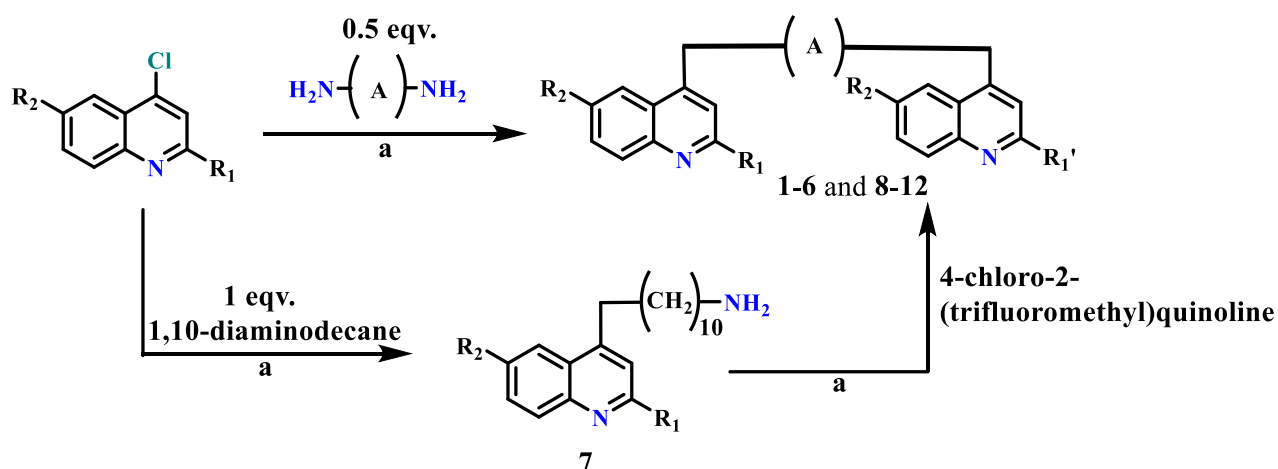
Scheme 4.1. Synthesis of bisquinolines. *Reaction Conditions: a) DIEA, 180 °C, 1hr, MW*

This one-step nucleophilic aromatic substitution protocol successfully yielded compounds **1-12** (**Table 4.1**) in good to moderate yields. For the synthesis of bisquinoline derivatives, an analogous procedure was used where different 4-choloroquinazolines were either heated (e.g., **13** and **14**) or stirred at room temperature (e.g., **15** and **16**) (**Table 4.2**) with 1,10-diaminodecane and DIEA to yield desired compounds.

Table 4.1. Description of linkers and substituents in compounds **1-12** synthesized using Scheme 1

Compound number	A (Cyclic or linear linker)	R_1	R_1'	R_2
1	$-NH-(CH_2)_9-NH$	$-CH_3$	$-CH_3$	$-OCH_3$
2	$-NH-(CH_2)_{10}-NH$	$-CH_3$	$-CH_3$	$-OCH_3$
3	$-NH-(CH_2)_8-NH$	$-CH_3$	$-CH_3$	$-OCH_3$
4	$-NH-(CH_2)_8-NH$	$-CH_3$	$-CH_3$	$-H$
5	$-NH-(CH_2)_9-NH$	$-CH_3$	$-CH_3$	$-H$
6	$-NH-(CH_2)_{10}-NH$	$-CH_3$	$-CH_3$	$-H$
7	$-NH-(CH_2)_{10}-NH$	$-CH_3$	$-CH_3$	-
8		$-CH_3$	$-CH_3$	$-H$
9		$-CH_3$	$-CH_3$	$-H$
10		$-CH_3$	$-CH_3$	$-H$
11	$-NH-(CH_2)_{10}-NH$	$-CF_3$	$-CF_3$	$-H$
12	$-NH-(CH_2)_{10}-NH$	$-CH_3$	$-CF_3$	$-H$
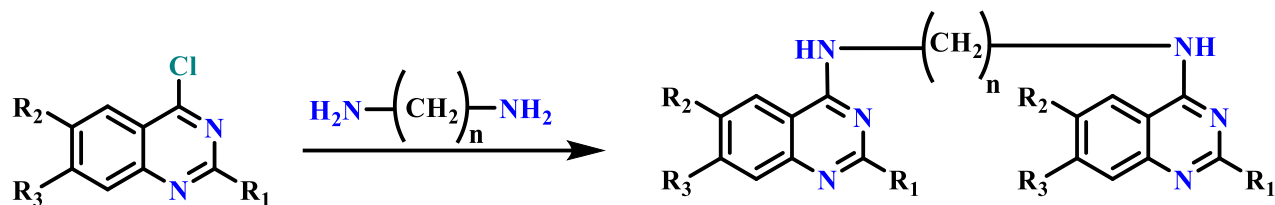
Scheme 4.2. Synthesis of bisquinazolines. *Reaction Conditions: DIEA, THF, 60 °C, 24hr*

Table 4.2. Description of linkers and substituents in compounds **13-16** synthesized using Scheme 2

Compound number	N (No of carbons in linker)	R₁	R₂	R₃
13	10	-Phenyl	-H	-H
14	10	-H	-OCH₃	-OCH₃
15	10	-Cl	-OCH₃	-OCH₃
16	10	-Cl	-H	-H

4.3.3 NSC10010 targets *Mtb* ClpC1

Revalidation of the 4 compounds confirmed NSC146771 and NSC10010 (referred to as **1**) to be the most promising candidates displaying >80% inhibition of the enzyme activity (**Figure 4.6A** and **Table 4.3**). Multi-dose kinetics of the inhibition further reveals that **1** inhibits the ClpC1's activity in a dose-dependent manner leading to 50% inhibition at ~ 40 μM concentration (**Figure 4.6B**). In contrast, the activity of ClpC1 is reduced by less than 40% in the presence of NSC146771, even at 80 μM concentration (**Figure 4.6C**). Further, bisquinoline **1** was evaluated for binding to ClpC1 using the Biolayer Interferometry (BLI) technique, which indicated its substantial association with ClpC1 with the K_d of 2.8$\pm$0.27 μM (**Figure 4.6D**).

Compound **1** is a small drug-like molecule with a symmetric structure that may be synthesized in a single step from commercially available building blocks, and displays significant inhibition of mycobacterial growth. Therefore, out of all the hit molecules compound **1** was chosen as the most promising candidate for further SAR study-based optimization.
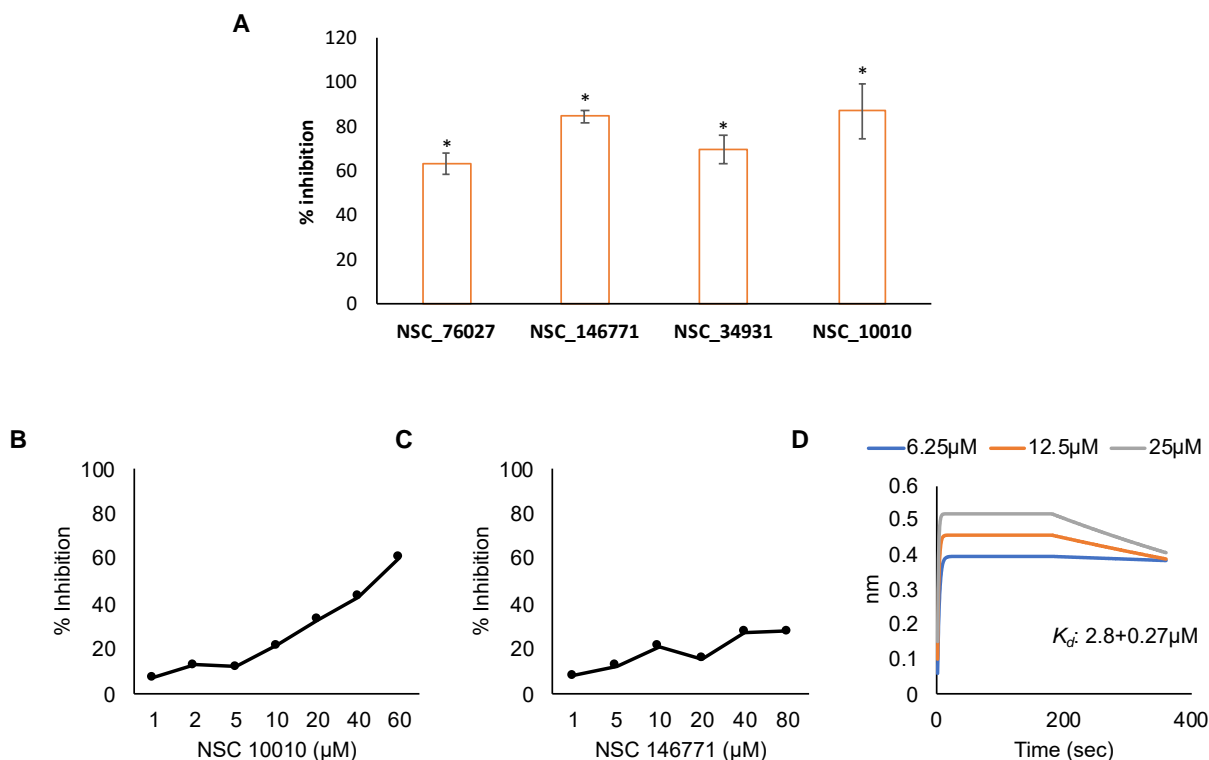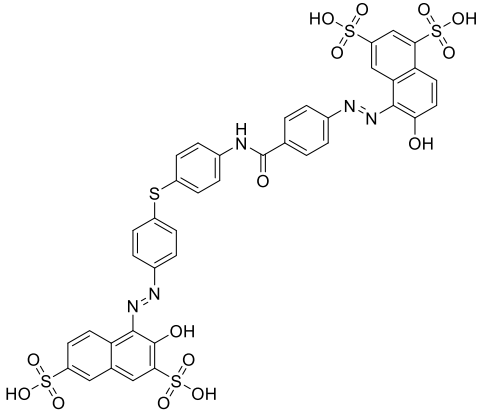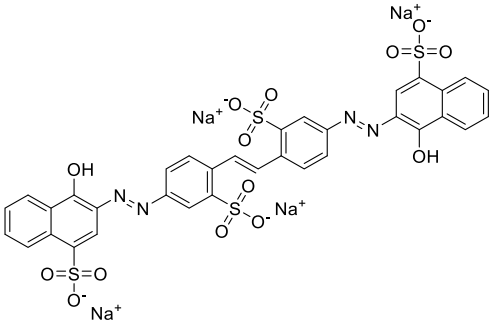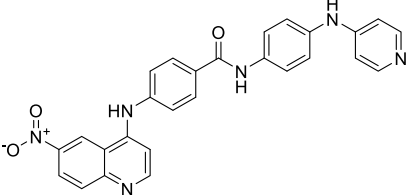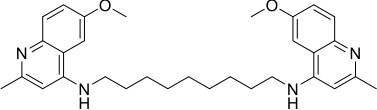
Figure 4.6. Identification of the top hit molecule targeting *Mtb* ClpC1. A) verification of the inhibitory activity of the top hit molecules against ClpC1. The select molecules were evaluated for their effect on the ATPase activity of *Mtb* ClpC1. **B-C)** Dose-dependent kinetics of enzymatic inhibition by **NSC 10010** (B) and **NSC 146771** (C). ATPase activity of *Mtb* ClpC1 was evaluated in the presence of various concentrations of inhibitors, and % inhibition with respect to activity in the absence of the drug is shown. **D)** Interaction of **NSC10010** with *Mtb* ClpC1. Interaction of *Mtb* ClpC1 with different concentrations of **NSC10010** was performed using BLI-OCTET, and the dissociation constant (K_d) was determined. Data in (A) represent mean$\pm$s.d. of values from two biological repeats.*: $p < 0.05$. (Work done by collaborators at THSTI)

4.3.4 SAR study

Initially, we resynthesized the NSC10010 (**1**) and revalidated the enzyme inhibition data with the pure (95% HPLC purity) sample of **1**. In addition to inhibiting the ClpC1 ATPase activity, the in-house synthesized compound **1** also shows ~60% inhibition of the proteolytic activity of ClpC1 at 50 µM concentration and 100% inhibition at 100 µM concentration, as evaluated by the fluorescein

isothiocyanate (FITC)-casein degradation assay described in experimental section (**Figure 4.7** and **Table 4.4**). The MIC$_{99}$ of compound **1** against *Mtb* was 12.5 µM (**Table 4.4**).

Table 4.3. The structures of top hit compounds inhibiting ClpC1 ATPase activity.

Compound Code	Structure	ClpC1 ATPase % inhibition (100 µM)
NSC 76027		63
NSC 34931		70
NSC 146771		85
NSC 10010 (1)		87

151
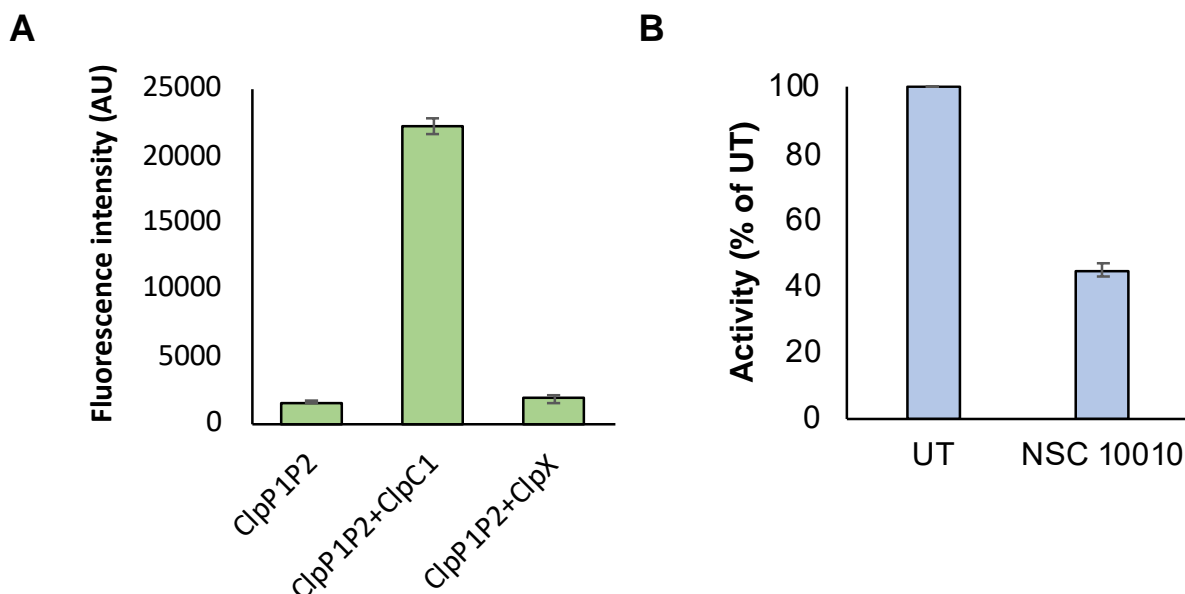
Figure 4.7. Effect of NSC10010 on the ClpC1-assisted proteolytic activity of Clp protease. A) Comparative analysis of proteolytic activity of different Clp protease complexes from *Mtb*. B) Effect of **NSC10010** on degradation of FITC-casein by ClpP1P2+ClpC1. The assay was set up in the absence (UT) or the presence of 50 µM inhibitor. Data in (A-B) represent mean±s.d. of values from two biological repeats. (Work done by collaborators at THSTI)

Compound **1** is characterized by two 6-methoxy-2-methyl-quinoline rings connected *via* a bisamine linker at position 4. Firstly, we studied the effect of changing the linker size between the two quinoline rings. The *Mtb* growth inhibition assay was kept as the primary screen to evaluate the new analogues. Increasing the size of the linker from 9 carbons in **1** to 10 carbons in **2** leads to the improvement in MIC against *Mtb* to 6.25 µM and retention of the proteolytic activity; however, ATPase activity is not affected much. On the other hand, analogue **3,** with a carbon less in its linker, maintains the MIC of 12.5 µM against *Mtb*. Removing the methoxy group from position 6 significantly increases the MIC across the different-sized linkers (e.g. **3** vs **4**; **1** vs **5**; **2** vs **6**). Compounds **5** and **6** do not retain ATPase inhibition activity, whereas compound **5** displays 80% inhibition of the protease activity. Together these data suggest that the methoxy group at position 6 is essential for the enzyme as well as *Mtb* growth inhibition. Removing one of the quinoline rings results in the complete abolishment of in vitro or cell-based activity (**6** vs **7**), thus, displaying the importance of the bisquinoline chemotype.
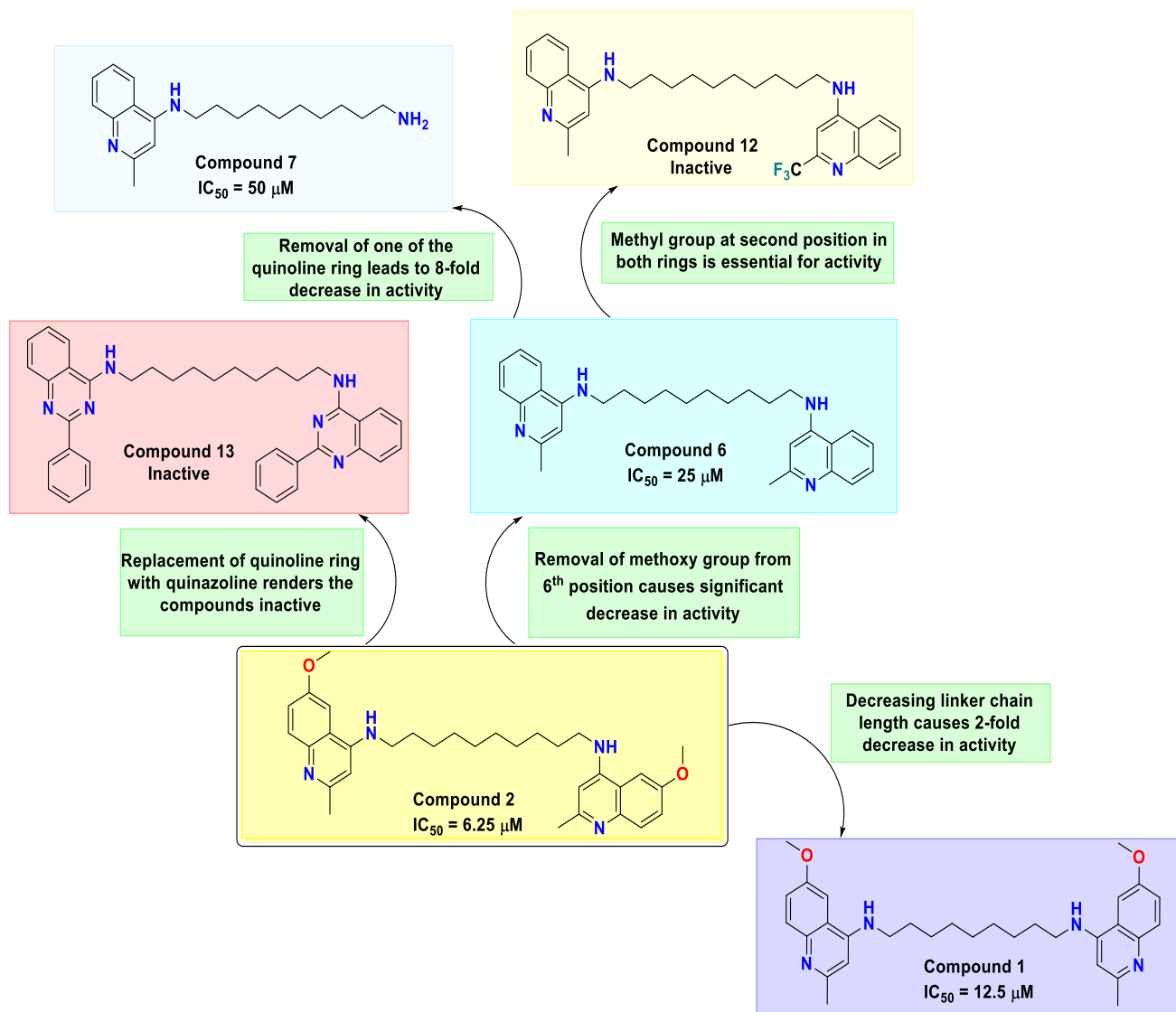
Figure 4.8. Effect of linker chain length and different substituents on bisquinoline activity

Next, we synthesized bisquinoline analogues **8-10** with linkers consisting of 6-membered rings to observe the influence of linker flexibility on compound activity. Among these, compound **8** is analogous to **6** in linker length and missing 6-methoxy substituents. Both **6** and **8** display similar antimycobacterial and enzyme inhibition activity, suggesting the linker's flexibility may not be an essential element in this series (**Figure 4.8**). Compounds **9** and **10**, with a short and rigid linker, show higher ATPase activity but poor *Mtb* growth inhibition. Replacing -CH$_3$ in **6** with CF$_3$ in **11** completely abolishes antimycobacterial activity, suggesting the detrimental effect of an electron-

withdrawing group at position 2. Similar results were obtained with compound **12**, where -CH$_3$ to -CF$_3$ replacement was done only in one of the quinoline rings.

Replacing the quinoline ring with the quinazoline ring and vice versa is often followed in medicinal chemistry optimization due to their similarity.[37–39] Hence, we synthesized different bisquinazoline analogues **13-16,** employing the readily available starting materials. The 10-carbon linker length between the rings was maintained in all analogues for comparison (**Figure 4.8**). Unfortunately, all bisquinazoline derivatives were devoid of ATPase or antimycobacterial activity, establishing bisquinoline scaffold as an indispensable pharmacophore of this series.

Table 4.4. Structures of the synthesized compounds and their activity.

Code	K_d (at 100 μM) (μM)	ClpC1 ATPase inhibition (% inhibition at 100 μM)	FITC-casein degradation (% inhibition at 100 μM)	MIC$_{99}$ (Against *Mtb* H$_{37}$Rv strain) (μM)	Glide Score	MM/GBSA (kcal/mol)
NSC10010 (**1**)	2.8+0.27	74	100	12.5	-4.1	-77.9
2	Shows binding	28	100	6.25	-3.9	-73.4
3	ND	ND	ND	12.5	-3.8	-66.5
4	ND	ND	ND	50-100	-3.6	-66.5
5	Shows binding	6.8	80	25	-4.5	-68.3
6	Shows binding	1	40	25	-4.0	-75.1
7	ND	0	ND	50	-3.4	-59.7
8	Shows binding	4.5	65	25	-3.5	-61.2

9	ND	41.7	85	50	-4.1	-58.2
10	450±260	45.4	63	50	-3.8	-52.3
11	ND	31.7	ND	No effect	-4.6	-59.9
12	ND	0	ND	No effect	-4.1	-62.6
13	ND	0	ND	No effect	-4.2	-73.3
14	ND	0	ND	No effect	-5.0	-74.5
15	ND	11.5	ND	No effect	-4.4	-74.9
16	ND	0	ND	No effect	-4.2	-73.9
Isoniazid	ND	-	ND	0.39	ND	-

ND: not defined

4.3.5 Molecular modelling

CymA and other cyclic peptides inhibit *Mtb* ClpC1 by binding to a large pocket in the N-terminal domain. Given the large and flexible nature of **1**, we hypothesized that the latter may also bind in the same pocket. Thus, CymA binding site was used for the docking studies to determine the plausible binding poses of the synthesized molecules. The *Mtb* ClpC1 complexed with the standard inhibitor CymA (PDB: 3WDC), and the Glide program of Schrödinger Suite was used for the docking studies.[40–42] The docking score is generally used to estimate the strength of ligand-protein binding. However, in our studies, K_d values for most of the molecules could not be determined due to poor binding kinetics except for compound **1**, making the comparison of experimental and modelled binding complicated.
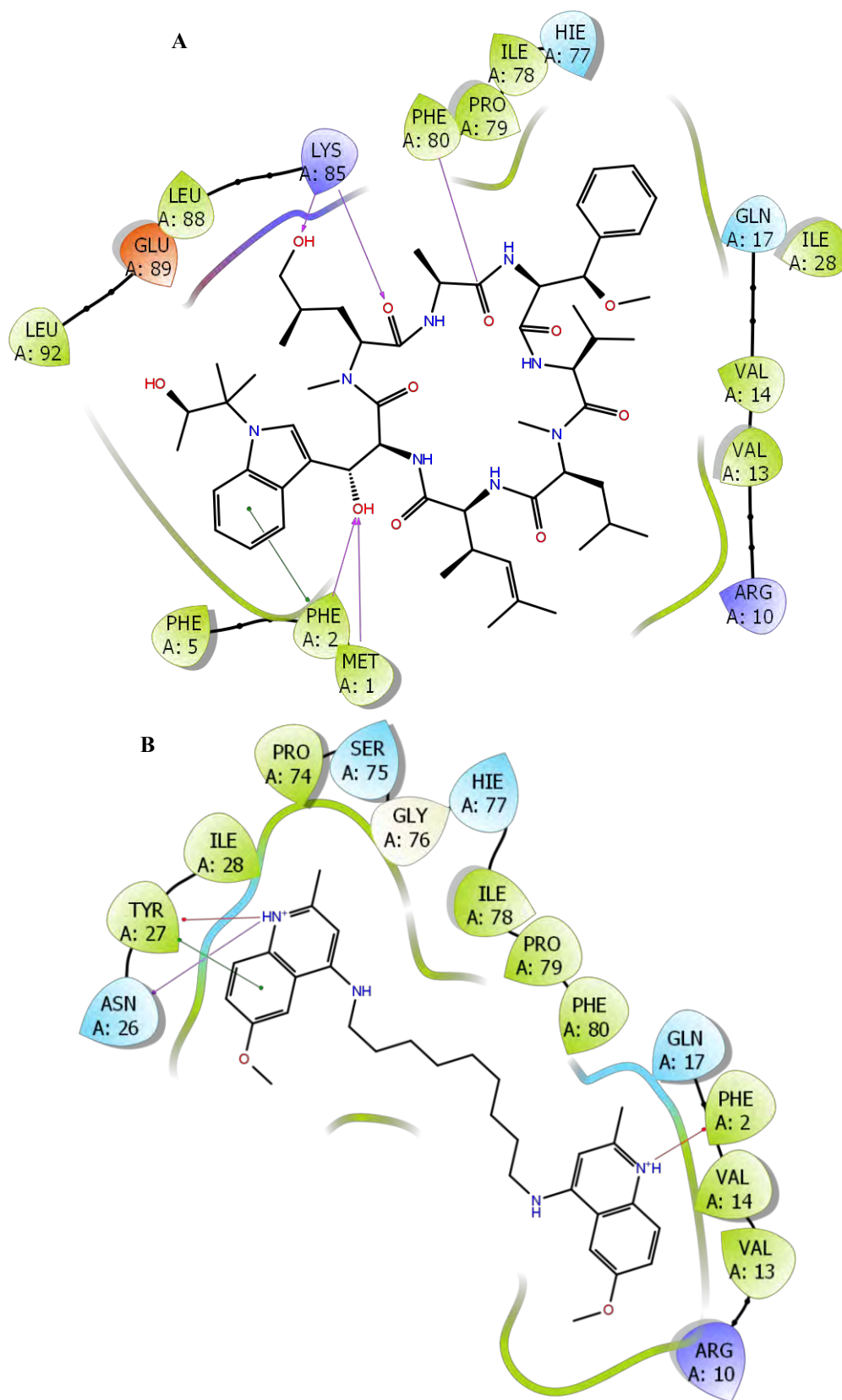
Figure 4.9. *In silico* **analysis of 2D interaction of CymA with ClpC1 by molecular modelling.** A) Interactions of CymA with *Mtb* ClpC1 (PDB 3WDC) B) predicted interaction of **1** with *Mtb* ClpC1.
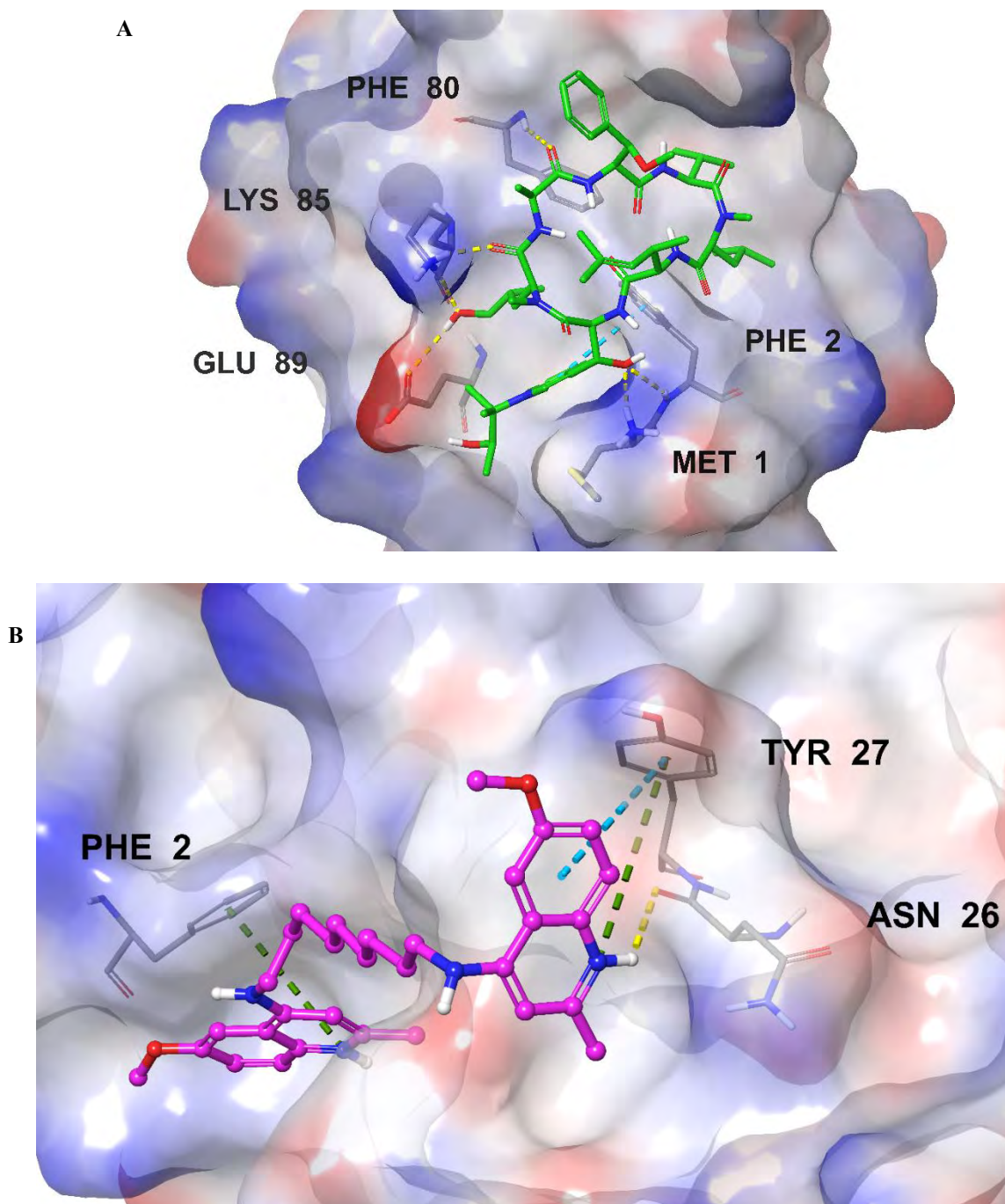
Figure 4.10. *In silico* analysis of 3D interaction of CymA with ClpC1 by molecular modelling. A) Overlay of the binding poses of CymA (green sticks) and **1** (pink sticks). B) 3D view of **1** showing key interactions with two different binding pockets of ClpC1. Yellow dashed lines represent H-bonds, pi-pi stacking by blue dashed lines, and pi-cation by green dashed lines.

Also, the docking score is calculated based on several approximations and rarely correlates with the experimental data. Nonetheless, the more accurate measure of modelled binding estimate is done using Molecular Mechanics/Generalized Born Surface Area (MM/GBSA) score.[43] Interestingly,

157

compound **1** shows the highest (most negative) MM/GBSA score, which is in line with its affinity towards ClpC1 and its enzyme inhibition activity compared to other analogues of the series.

A recent mutagenesis study suggests that residues Phe2, Phe80, and Glu89 contribute significantly to the CymA binding with ClpC1.[22] Mutation in Phe2 to Ala results in a rapid decline in binding by 300 times indicating Phe2 to be the most critical residue for binding followed by a mutation in Phe80 and Glu89 which exhibit approximately, 160 times and 10 times weaker binding, respectively. Comparing modelled pose of **1** with CymA binding pose reveals that both ligands interact with Phe2. CymA displays a T-shaped pi-pi interaction and an H-bond interaction with Phe2, one H-bond with residues Met1, Phe80, Glu89, and two H-bond interactions with Lys85 (**Figure 4.9A** and **4.10A**). Compound **1** makes pi-cation interaction with Phe2 through one of the protonated quinoline ring nitrogen (**Figure 4.9B** and **4.10B**). In the adjacent pocket, **1** also displays an H-bond with Asn26 through its second protonated quinoline ring. An additional pi-pi stacking and a pi-cation interaction between Tyr27 and the second quinoline ring are also observed. Thus, the basic character of the quinoline ring nitrogen seems to be essential for the ClpC1 binding. Although methoxy groups are not involved in direct interaction with the target, they are expected to increase the basicity of the ring nitrogen through resonance.[37,44] The importance of basic ring nitrogen is highlighted by the lack of activity of compounds **11** and **12** (**Table 4.4**). In these molecules, the electron-withdrawing nature of -CF_3 is expected to lower quinoline nitrogen's basicity, thus, diminishing binding affinity. Overall, the predicted pose and interactions of **1** with the ClpC1 binding pocket underline the importance of the quinoline ring and methoxy groups and agree with the SAR results.

4.4 CONCLUSION

In summary, we identified the bisquinoline scaffold as a potential inhibitor of *Mtb* ClpC1 ATPase activity. Initial screening by our collaborators against the enzymatic activity of ClpC1 and in vitro

growth of *Mtb* suggest compound **1** (NSC10010) to be the most promising. The SAR study suggests that chain length of 9-10 carbons is optimum to achieve inhibition of *Mtb* growth with reduced MIC. The quinoline ring seems to be indispensable as its basic nitrogen is predicted to be protonated and foster important interactions with the binding pocket residues. The preliminary SAR also suggests that the linker length rather than linker flexibility may have more influence on *Mtb* growth inhibition. The modelled pose of **1** displays highest MM-GBSA score, which is in line with its binding affinity and lower MIC compared to other analogues.

Overall, this is the first report on the systematic analysis of small molecule inhibitors of *Mtb* ClpC1 with high synthetic tractability. Future study is warranted to study the effect of diverse substituents and detailed SAR at different quinoline positions and to explore the potency of this series in the in vitro and cell-based assays.

4.5 EXPERIMENTAL

4.5.1 Cloning, expression and purification of *Mtb* unfoldases

To achieve expression of N-ter 6X His-tagged ClpX and ClpC1 in *E. coli,* our collaborators at THSTI amplified respective open reading frame (ORFs) from *Mtb* genome by polymerase chain reaction (PCR) and cloned in pET28b plasmid (Invitrogen) at Nde I and Hind III sites. For expression of mature ClpP1 lacking 6 aa (Δ6-ClpP1) and ClpP2 lacking 11 aa (Δ11-ClpP2) at the N-terminus, the respective ORF sequences without the stop codon were PCR amplified from *Mtb* genome and cloned in pET22b plasmid (Invitrogen) at Nde I and Hind III sites. Expression of N-terminal 6X His tagged ClpX and ClpC1, and C-terminal 6X His-tagged Δ6-ClpP1 and Δ11-ClpP2 was obtained in *E. coli* BL21 transformed with respective plasmids following overnight induction with 0.5 mM Isopropyl β-D-1-thiogalactopyranoside (IPTG) at 18 ˚C. The recombinant proteins were subsequently purified from *E. coli* by using Nickel-nitriloacetic acid (Ni-NTA) affinity

chromatography, as suggested by the manufacturer (Qiagen) followed by dialysis in a storage buffer containing 50 mM Tris pH 8.0, 100 mM NaCl and 10% Glycerol. The dialyzed proteins were stored at -80°C for further use.

4.5.2 Determination of ATPase activity

Release of inorganic phosphate (Pi) and subsequent colorimetric detection by malachite green assay was used to quantitate the ATPase activity, by our collaborators at THSTI, as described earlier.[45] The ClpC1 or ClpX protein (1 µM) was incubated with varying concentrations of ATP (0-200 µM) in the reaction buffer (Buffer C: containing 20 mM HEPES pH 7.5, 0.1 M KCl, 10 mM MgCl$_2$, 0.1 mM DTT and 5% glycerol) for 1 hr at 37 ˚C, followed by addition of 100 µl of malachite green substrate to stop the reaction. The reaction was incubated at room temperature for 30 minutes to develop the colour and absorbance at 630 nm was measured. Amount of Pi was calculated by using different known concentrations of phosphate standard.

4.5.3 FITC-casein degradation assay

Degradation of FITC-casein was performed by our collaborators at THSTI, as described earlier.[46,47] Reaction was set up in a 50 µl reaction volume by incubating 1 µM FITC casein (Sigma Aldrich) with 1 µM of mature protease subunits Δ6-ClpP1 and Δ11-ClpP2 in the presence of 0.5 µM ClpC1 or ClpX unfoldases, 5 mM ATP, 1 mM activator (Z-Leu-Leu), 0.1 mg/ml creatine kinase and 4 mM creatine phosphate in the buffer C. Reaction was stopped after 1 hr of incubation at 30 ˚C by adding 120 µl of 5% TCA. The undigested FITC-casein was allowed to precipitate for 1 hr at room temperature, followed by centrifugation at 12000 x rpm for 10 min. Fluorescence of the free FITC in the supernatant due to degradation of casein was estimated after neutralization with 0.5 M Tris-HCl, pH 8.8. Fluorescence was measured at the excitation wavelength of 490 nm and emission wavelength of 525 nm.

4.5.4 High throughput screening of inhibitors

For HTS, our collaborators at THSTI set up a reaction in a 96-well plate by incubating 1 µM ClpC1 (pre-incubated with 100 µM inhibitor for 10 minutes at RT) and 125 µM ATP for 30 minutes at 37 ˚C. A reaction without an inhibitor was simultaneously set as a control. After 30 min of incubation, 50 µl of malachite green substrate was used in each reaction to stop the reaction. The amount of Pi was calculated as described above. Percentage inhibition in the ATPase activity of ClpC1 was determined for each inhibitor with respect to the untreated control from two biological repeat experiments.

4.5.5 MIC$_{99}$ determination

Further, our collaborators, selected small molecule inhibitors that were serially diluted and incubated with equal volume of *Mtb* H$_{37}$Rv cultures in 7H9 containing 1X OADS (OD$_{600}$ of 0.01) in a 96-well plate. Growth was monitored after incubating the plate at 37 ˚C for 14 days without shaking. The minimum inhibitory concentration (MIC) to kill *Mtb* H$_{37}$Rv by 99% (MIC$_{99}$) was visually determined, as reported.[48]

4.5.6 Molecular docking studies

All the docking studies were performed using glide (version 2022-2). Crystal structure of ClpC1-N-terminal domain (NTD) in complex with CymA (PDB: 3WDC) was downloaded and prepared using Protein Preparation Wizard in Schrödinger to fill missing residues, minimize and delete waters and optimize H-bond assignments using default settings.[49,50] The ligands were prepared using the LigPrep function of Schrödinger to generate low-energy 3D structures and appropriate ionized forms.[51] For receptor grid generation centroid of workspace ligand option was selected (GRID CENTER x = -23.2, y = 13, z = -5.2).[40] SP mode was used to dock a rigid receptor and flexible ligand. For grid validation, the co-crystallized ligand (CymA) was re-docked with 3WDC using

shape constraints (CymA as a reference) to give a docking score of -10.06 with the root mean square deviation (RMSD) of 0.0225 Å with respect its bioactive conformation. The same protocol was followed for performing docking studies of the synthesized compounds. The OPLS-2005 force field implemented in Schrödinger Suite was used for all modelling work such as protein preparation, ligand preparation, glide grid generation, and molecular docking.[52]

4.5.7 General Chemistry Information

All starting materials were purchased from commercial sources and used without further purification unless stated otherwise. Thin-layer chromatography (TLC) was used to monitor the progress of the reactions and checked by pre-coated TLC plates (E. Merck Kieselgel 60 F254 with fluorescence indicator UV254). Components were visualized by irradiation with ultraviolet light (254 nm) or spots being visualized by iodine vapours. All compounds were purified over a silica gel (230-400 mesh) using the freshly distilled solvents. All final compounds were characterized by ^{1}H NMR spectroscopy using $CDCl_3$ or DMSO-d_6. ^{1}H NMR spectra were recorded on a Bruker Advance 400 MHz spectrometer and chemical shifts are given in parts per million (ppm). The mass spectra of compounds were recorded using Waters TQD system. Purity analysis for the synthesized compounds was performed using RP-HPLC (LC-2010HT, Shimadzu Corporation, Japan).

4.5.7.1 General Synthesis Procedure 1 (1-12). Different 4-chloroquinolines were heated with various diamines in the presence of DIEA at 180 °C for 1 hour in a microwave reactor. The reaction mixture was cooled to room temperature and poured carefully into water. The aqueous layer was extracted with dichloromethane (DCM) (3 × 30 mL), the organic extracts were combined, washed with brine and dried over anhydrous sodium sulphate. The solvent was removed *in vacuo* and the resulting residue was purified by silica gel chromatography (DCM : MeOH = 90:10) to yield the various target molecules.[53]

4.5.7.2 General Synthesis Procedure 2 (13, 14). A mixture of substituted quinazolines, 1,10-diaminodecane, DIEA and tetrahydrofuran (THF) was heated at 60 °C for 24 hours on an oil bath. The reaction mixture was cooled to room temperature and poured carefully into water. The aqueous layer was extracted with DCM (3 × 30 mL), the organic extracts were combined, washed with brine and dried over sodium sulphate. The solvent was removed *in vacuo* and the resulting residue was purified by silica gel chromatography (DCM : MeOH = 90:10) to yield the desired product.

4.5.7.3 General Synthesis procedure 3 (15, 16). A mixture of various substituted quinazolines, 1,10-diaminodecane, DIEA and THF was stirred at room temperature for 48 hours. The reaction mixture was cooled to room temperature and poured carefully into water. The aqueous layer was extracted with DCM (3 × 30 mL), the organic extracts were combined, washed with brine and dried over sodium sulphate. The solvent was removed *in vacuo*, and the resulting residue was purified by silica gel chromatography (DCM : MeOH = 90:10) to yield the desired product.

4.5.8 Purity Analysis. Ion pair reverse phase chromatography was used for purity profiling as the compounds were quite polar. The purity analysis of all the synthesized compounds was conducted by using a Shimadzu HPLC system (LC-2010HT, Shimadzu Corporation, Japan). The chromatographic data acquisition and integration for the experiments were recorded using Lab solution software. The chromatographic separation of the compound was performed at ambient temperature using stationary phase as Ascentis® C18 (50 mm × 4.6 mm, i.d. 3.0 µm) and mobile phase of Acetonitrile and 2.5 mM SLS buffer adjusted to pH 3.2 with formic acid. Isocratic mode with a flow rate of 1 mL/min was used for the analysis. [54,55]

4.5.8.1 Synthesis of N1,N9-bis(6-methoxy-2-methylquinolin-4-yl)nonane-1,9-diamine (1). **1** was synthesized from 4-Chloro-6-methoxy-2-methylquinoline (114 mg, 0.55 mmol), 1,9-diaminononane (51 µL, 0.28 mmol) and DIEA (72.10 µL, 0.41 mmol) according to general

procedure 1. White powder (yield 33 mg, 24%). ^{1}H NMR (400 MHz, DMSO-d_6) δ 7.69 (d, J = 9.1 Hz, 4H), 7.61 (s, 2H), 7.30 (dd, J = 9.1, 2.7 Hz, 2H), 6.42 (s, 2H), 3.88 (s, 6H), 3.49-3.46 (m, 4H), 2.48 (s, 6H), 1.71 – 1.66 (m, 4H), 1.41-1.34 (m, 10H); LCMS (+ESI): m/z calculated for $C_{31}H_{40}N_4O_2$: 500.3, found: 501.3 [M+H]$^+$. Purity 95.0% [Mobile Phase, ACN : Buffer (50:50) ; Rt 3.0 min]

4.5.8.2 Synthesis of N1-(6-methoxy-2-methylquinolin-4-yl)-N10-(7-methoxy-2-methylquinolin-4-yl)decane 1,10-diamine (2). **2** was synthesized from 4-Chloro-6-methoxy-2-methylquinoline (114 mg, 0.55 mmol, 1,10-diaminodecane (48 mg, 0.28 mmol) and DIEA (72.10 μL, 0.41 mmol) according to general procedure 1 Cream powder (yield 63 mg, 44%). ^{1}H NMR (400 MHz, DMSO-d_6) δ 9.22 (t, J = 5.7 Hz, 2H), 8.02 (s, J = 2.7 Hz, 2H), 7.90 (d, J = 9.2 Hz, 2H), 7.53 (dd, J = 9.2, 2.5 Hz, 2H), 6.71 (s, 2H), 3.93 (s, 6H), 3.51-3.44 (m, J = 6.9 Hz, 4H), 2.63 (s, 6H), 1.72-1.64 (m, 4H), 1.40-1.28 (m, J = 20.0 Hz, 12H); ^{13}C NMR (101 MHz, DMSO-d_6) δ 157.6 , 154.2, 152.2, 133.9, 124.2, 121.9, 117.4, 103.6, 98.2, 56.9, 43.2, 29.4, 29.2, 28.1, 26.9, 20.2; LCMS (+ESI): m/z calculated for $C_{32}H_{42}N_4O_2$: 514.3, found: 515.4 [M+H]$^+$. Purity 98.4% [Mobile Phase, ACN : Buffer (40:60); Rt 1.8 min].

4.5.8.3 Synthesis of N1,N8-bis(6-methoxy-2-methylquinolin-4-yl)octane-1,8-diamine (3). **3** was synthesized from 4-Chloro-6-methoxy-2-methylquinoline (114 mg, 0.55 mmol, 1,8-diaminooctane (48 μL, 0.28 mmol) and DIEA (72.10 μL, 0.41 mmol) according to general procedure 1. White powder (yield 49 mg, 37%). ^{1}H NMR (400 MHz, DMSO-d_6) δ 9.0 (bs, J = 5.7 Hz, 2H), 8.01 (s, J = 2.7 Hz, 2H), 7.89 (d, J = 9.2 Hz, 2H), 7.52 (d, J = 9.2, 2.6 Hz, 2H), 6.69 (s, 2H), 3.92 (s, 6H), 3.50-3.45 (m, 4H), 2.62 (s, 6H), 1.76-1.64 (m, J = 8.2, 7.5 Hz, 5H), 1.44-1.34 (m, J = 11.9 Hz, 8H); ^{13}C NMR (101 MHz, DMSO-d_6) δ 157.7, 154.3, 152.2, 124.4, 121.8, 117.3, 103.4, 98.3, 56.9, 43.3, 39.5, 29.1, 28.1, 26.9, 20.2; LCMS (+ESI): m/z calculated for $C_{30}H_{38}N_4O_2$: 486.3, found: 487.5 [M+H]$^+$. Purity 93.0% [Mobile Phase, ACN : Buffer (50:50); Rt 3.8 min].

4.5.8.4 Synthesis of N1,N8-bis(2-methylquinolin-4-yl)octane-1,8-diamine (4). **4** was synthesized from 4-chloroquinaldine (111 µL, 0.55 mmol), 1,8-diaminooctane (48µL, 0.28 mmol) and DIEA (72.10 µL, 0.41 mmol) according to general procedure 1. White powder (yield 42 mg, 36%). ^{1}H NMR (400 MHz, DMSO-d_6) δ 9.35-9.26 (m, J = 5.7 Hz, 2H), 8.63 (d, 2H), 7.98 (d, J = 8.4, 1.2 Hz, 2H), 7.88 (t, J = 8.4, 6.9, 1.1 Hz, 2H), 7.62 (t, J = 8.3, 6.9, 1.2 Hz, 2H), 6.75 (s, 2H),3.52 – 3.45 (m, J = 6.7 Hz, 4H), 2.65 (s, 6H), 1.75-1.63 (m, J = 7.4 Hz, 4H), 1.47-1.31 (m, J = 11.8 Hz, 8H); ^{13}C NMR (101 MHz, DMSO-d_6) δ 155.2, 154.2, 138.5, 133.5, 126.3, 123.7, 120.0, 116.2, 98.6, 43.3, 39.7, 29.2, 28.1, 26.8, 20.3; LCMS (+ESI): *m/z* calculated for $C_{28}H_{34}N_4$: 426.2, found: 427.3 [M+H]$^+$. Purity 88.0% [Mobile Phase, ACN : Buffer (50:50) ; Rt 4.2 min].

4.5.8.5 Synthesis of N1,N9-bis(2-methylquinolin-4-yl)nonane-1,9-diamine (5). **5** was synthesized from 4-chloroquinaldine (111 µL, 0.55 mmol), 1,9-diaminononane (51 µL, 0.28 mmol) and DIEA (72.10 µL, 0.41 mmol) according to general procedure 1. Yellow powder (yield 40 mg, 33%). ^{1}H NMR (400 MHz, DMSO-d_6) δ 9.41-9.34 (m, J = 5.7 Hz, 2H), 8.66 (d, J = 8.7, 1.2 Hz, 2H), 8.00 (d, J = 8.4, 1.2 Hz, 2H), 7.87 (t, J = 8.3, 6.9, 1.2 Hz, 2H), 7.60 (t, J = 8.3, 6.9, 1.2 Hz, 2H), 6.74 (s, 2H), 3.51-3.44 (m, 4H), 2.66 (s, 6H), 1.75-1.63 (m, J = 7.4 Hz, 4H), 1.42-1.24 (m, 10H); ^{13}C NMR (101 MHz, DMSO-d_6) δ 155.2, 154.1, 138.4, 133.4, 126.3, 123.8, 119.9, 116.1, 98.5, 43.3, 29.4, 29.2, 28.1, 26.9, 20.2; LCMS (+ESI): *m/z* calculated for $C_{29}H_{36}N_4$: 440.3, found: 441.3 [M+H]$^+$. Purity 99.0% [Mobile Phase, ACN : Buffer (55:45); Rt 7.7 min].

4.5.8.6 Synthesis of N1,N10-bis(2-methylquinolin-4-yl)decane-1,10-diamine (6). **6** was synthesized from 4-chloroquinaldine (111 µL, 0.55 mmol), 1,10-diaminodecane (48 mg, 0.28 mmol) and DIEA (72.10 µL, 0.41 mmol) according to general procedure 1. Brown powder (yield 46 mg, 37%). ^{1}H NMR (400 MHz, DMSO-d_6) δ 9.39-9.30 (m, J = 5.8 Hz, 2H), 8.64 (d, 2H), 7.99 (d, J = 8.4, 1.2 Hz, 2H), 7.87 (t, J = 8.3, 6.9, 1.2 Hz, 2H), 7.61 (t, J = 8.3, 6.9, 1.2 Hz, 2H), 6.74 (s, 2H), 3.50-3.44 (m, 4H), 2.65 (s, 6H), 1.73-1.63 (m, J = 14.8, 7.6, 6.9 Hz, 4H), 1.40-1.25 (m, 12H);

^{13}C NMR (101 MHz, DMSO-d_6) δ 155.2, 154.2, 138.6, 133.4, 126.2, 123.7, 120.1, 116.2, 98.5, 43.3, 29.4, 29.2, 28.1, 26.9, 20.3; LCMS (+ESI): *m/z* calculated for C$_{30}$H$_{38}$N$_4$: 454.3, found: 455.2 [M+H]$^+$. Purity 95.0% [Mobile Phase, ACN : Buffer (55:45) ; Rt 4.9 min].

4.5.8.7 Synthesis of N1-(2-methylquinolin-4-yl)decane-1,10-diamine (7). **7** was synthesized from 4-chloroquinaldine (500 mg, 2.80 mmol), 1,10-diaminodecane (967 mg, 5.62 mmol) and DIEA (981 µL, 5.62 mmol) according to general procedure 1. White powder (yield 322 mg, 37%). ^{1}H NMR (400 MHz, DMSO-d_6) δ 8.16 (d, *J* = 8.5, 1.3 Hz, 1H), 7.67 (d, *J* = 8.4, 1.2 Hz, 1H), 7.54 (t, *J* = 8.2, 6.7, 1.3 Hz, 1H), 7.32 (t, *J* = 8.2, 6.8, 1.3 Hz, 1H), 7.01-6.95 (m, *J* = 5.3 Hz, 1H), 6.32 (s, 1H), 3.28-3.19 (m, 2H), 2.45 (s, 3H), 1.72-1.61 (m, *J* = 7.3 Hz, 2H), 1.43-1.20 (m, 16H); ^{13}C NMR (101 MHz, DMSO-d_6) δ 129.2, 128.5, 123.5, 121.9, 42.8, 29.5, 29.4, 29.3, 28.3, 27.1; LCMS (+ESI): *m/z* calculated for C$_{20}$H$_{31}$N$_3$: 313.3, found: 314.1 [M+H]$^+$. Purity 98.0% [Mobile Phase, ACN : Buffer (50:50) ; Rt 1.7 min].

4.5.8.8 Synthesis of N,N'-(piperazine-1,4-diylbis(propane-3,1-diyl))bis(2-methylquinolin-4-amine) (8). **8** was synthesized from 4-chloroquinaldine (222 µL, 1.10 mmol), 1,4-Bis(3-amino propyl)piperazine (113.64 µL, 0.55 mmol) and DIEA (144 µL, 0.83 mmol) according to general procedure 1. Brown crystals (yield 82 mg, 31%). ^{1}H NMR (400 MHz, DMSO-d_6) δ 8.09 (d, *J* = 8.4, 1.3 Hz, 2H), 7.66 (d, *J* = 8.3, 1.3 Hz, 2H), 7.52 (t, *J* = 8.3, 6.8, 1.3 Hz, 2H), 7.31 (t, *J* = 8.3, 6.8, 2.6 Hz, 2H), 7.20-7.15 (m, *J* = 5.2 Hz, 2H), 6.33 (s, 2H), 3.31-3.27 (m, *J* = 5.7 Hz, 4H), 2.46-2.41 (m, 12H), 1.86-1.78 (m, *J* = 6.7 Hz, 4H); ^{13}C NMR (101 MHz, DMSO-d_6) δ 159.2, 150.5, 148.5, 129.1, 128.8, 123.4, 121.8, 117.9, 98.5, 98.4, 56.6, 53.5, 41.6, 25.8, 25.3; LCMS (+ESI): *m/z* calculated for C$_{30}$H$_{38}$N$_6$: 482.3, found: 483.2 [M+H]$^+$. Purity 99.9% [Mobile Phase, ACN : Buffer (50:50) ; Rt 2.8 min].

4.5.8.9 Synthesis of N,N'-(cyclohexane-1,3-diylbis(methylene))bis(2-methylquinolin-4-amine) (9). **9** was synthesized from 4-chloroquinaldine (222 µL, 1.10 mmol), 1,3-

Bis(aminomethyl)cyclohexane (84 µL, 0.55 mmol) and DIEA (144 µL, 0.83 mmol) according to general procedure 1. Brown powder (yield 61 mg, 26%). ^{1}H NMR (400 MHz, DMSO-d_6) δ 9.44-9.35 (m, J = 5.8 Hz, 2H), 8.72 (d, J = 8.5 Hz, 2H), 8.03 (d, 2H), 7.85 (t, J = 8.2, 6.9, 1.2 Hz, 2H), 7.56 (t, J = 8.2, 6.9, 1.2 Hz, 2H), 6.75 (s, 2H), 2.64 (s, 6H), 1.92-1.77 (m, 4H), 1.21-0.79 (m, 4H); ^{13}C NMR (101 MHz, DMSO-d_6) δ 155.3, 154.2, 138.8, 133.2, 126.1, 123.9, 120.2, 116.2, 98.7, 49.3, 36.5, 35.0, 30.7, 25.3, 20.4; LCMS (+ESI): m/z calculated for $C_{28}H_{32}N_4$: 424.3, found: 425.3 [M+H]$^+$. Purity 97.0% [Mobile Phase, ACN : Buffer (50:50) ; Rt 2.2 min]

4.5.8.10 Synthesis of 2-methyl-N-(2-(4-(2-methylquinolin-4-yl)piperazin-1-yl)ethyl)quinolin-4-amine (10).

10 was synthesized from 4-chloroquinaldine (222 µL, 1.10 mmol), N-(2-aminoethyl)piperazine (72.50 µL, 0.55 mmol) and DIEA (144 µL, 0.83 mmol) according to general procedure 1. Brown powder (yield 129 mg, 57%). ^{1}H NMR (400 MHz, Chloroform-d) δ 8.29 (d, J = 8.5 Hz, 1H), 8.05-7.97 (m, 3H), 7.67-7.61 (m, 3H), 7.46 (dd, J = 5.6, 2.7, 1.5 Hz, 1H), 6.77 (s, 1H), 6.26 (s, 1H), 3.61-3.54 (m, J = 5.7 Hz, 2H), 3.36-3.28 (m, 4H), 3.02-2.97 (m, J = 6.1 Hz, 2H), 2.94-2.87 (m, 4H), 2.77 (s, 3H), 2.70 (s, 3H); LCMS (+ESI): m/z calculated for $C_{26}H_{29}N_5$: 411.2, found: 412.3 [M+H]$^+$. Purity 99.0% [Mobile Phase, ACN : Buffer (50:50) ; Rt 2.4 min].

4.5.8.11 Synthesis of N1,N10-bis(2-(trifluoromethyl)quinolin-4-yl)decane-1,10-diamine (11).

11 was synthesized from 4-chloro-2-(trifluoromethyl)quinoline (128 mg, 0.55 mmol), 1,10-diaminodecane (48 mg, 0.28 mmol) and DIEA (96 µL, 0.55 mmol) according to general procedure 1. White powder (yield 42mg, 27%). ^{1}H NMR (400 MHz, DMSO-d_6) δ 8.34 (d, J = 8.4, 1.3 Hz, 2H), 7.89 (d, J = 8.5, 1.2 Hz, 2H), 7.76-7.68 (m, 2H), 7.56 (t, J = 8.3, 6.8, 1.3 Hz, 2H), 6.71 (s, 2H), 3.34-3.29 (m, 4H), 1.73-1.60 (m, J = 7.3, 6.8 Hz, 4H), 1.41-1.22 (m, J = 33.4 Hz, 12H); LCMS (+ESI): m/z calculated for $C_{30}H_{32}N_4F_6$: 562.3, found: 563.4 [M+H]$^+$. Purity 98.0% [Mobile Phase, ACN : Buffer (50:50) ; Rt 4.0 min].

4.5.8.12 Synthesis of N1-(2-methylquinolin-4-yl)-N10-(2-(trifluoromethyl)quinolin-4-yl)decane-1,10-diamine (12). **12** was synthesized from 4-chloro-2-(trifluoromethyl)quinoline (114 mg, 0.50 mmol, 194 (80 mg, 0.25 mmol) and DIEA (100 µL, 0.50 mmol) according to general procedure 1. White powder (yield 35 mg, 28%). ^{1}H NMR (400 MHz, Chloroform-*d*) δ 8.11 (d, *J* = 8.5, 1.2 Hz, 2H), 7.80-7.70 (m, 4H), 7.55 (t, *J* = 8.3, 6.9, 1.3 Hz, 2H), 6.75 (s, 2H), 5.27-5.20 (m, 2H), 3.73 (s, 3H), 3.43-3.35 (m, *J* = 7.2, 5.1 Hz, 4H), 1.85-1.76 (m, *J* = 7.3 Hz, 4H), 1.66-1.60 (bs, 4H), 1.54-1.35 (m, *J* = 13.9 Hz, 12H); LCMS (+ESI): *m/z* calculated for $C_{30}H_{35}N_4F_3$: 508.3, found: 563.4 [M+CH$_3$OH+Na]$^+$. Purity 89.4 % [Mobile Phase, ACN : Buffer (50:50) ; Rt 6.4 min].

4.5.8.13 Synthesis of N1,N10-bis(2-phenylquinazolin-4-yl)decane-1,10-diamine (13). **13** was synthesized from 4-chloro-2-phenylquinazoline (200 mg, 0.82 mmol), 1,10-diaminodecane (71 mg, 0.41 mmol), DIEA (418 µL, 2.46 mmol) and THF (10 mL) according to general procedure 2. Cream solid (yield 92 mg, 38%). ^{1}H NMR (400 MHz, DMSO-*d$_6$*) δ 8.54-8.46 (m, 4H), 8.31-8.28 (m, *J* = 5.5 Hz, 2H), 8.25 (d, *J* = 8.2 Hz, 2H), 7.80-7.71 (m, 4H), 7.53-7.42 (m, 8H), 3.66 (q, *J* = 6.6 Hz, 4H), 1.79-1.63 (m, *J* = 7.1 Hz, 4H), 1.40-1.22 (m, 12H); LCMS (+ESI): *m/z* calculated for $C_{38}H_{40}N_6$: 580.3, found: 581.5 [M+H]$^+$. Purity 100% [Mobile Phase, ACN : Buffer (50:50) ; Rt 5.4 min].

4.5.8.14 Synthesis of N1,N10-bis(6,7-dimethoxyquinazolin-4-yl)decane-1,10-diamine (14). **14** was synthesized from 4-chloro-6,7-dimethoxyquinazoline (184 mg, 0.82 mmol), 1,10-diaminodecane (71 mg, 0.41 mmol), DIEA (418 µL, 2.46 mmol) and THF (10 mL) according to general procedure 2. White powder (yield 60 mg, 28%). ^{1}H NMR (400 MHz, DMSO-*d$_6$*) δ 8.33 (s, 2H), 8.03-7.97 (m, *J* = 5.5 Hz, 2H), 7.62 (s, 2H), 7.07 (s, 2H), 3.88 (s, 12H), 3.52-3.49 (m, *J* = 6.5 Hz, 4H), 1.63 (p, *J* = 7.2 Hz, 4H), 1.33 – 1.27 (m, 12H); LCMS (+ESI): *m/z* calculated for $C_{30}H_{40}N_6O_4$: 548.3, found: 549.5 [M+H]$^+$. Purity 100% [Mobile Phase, ACN : Buffer (50:50) ; Rt 2.0 min].

4.5.8.15 Synthesis of N1,N10-bis(2-chloro-6,7-dimethoxyquinazolin-4-yl)decane-1,10-diamine (15). **15** was synthesized from 2,4-dichloro-6,7-dimethoxyquinazoline (500 mg, 1.90 mmol), 1,10-diaminodecane (166 mg, 0.96 mmol), DIEA (1 mL, 5.76 mmol) and THF (10 mL) according to general procedure 2. White powder (yield 174 mg, 29%). ^{1}H NMR (400 MHz, DMSO-d_6) δ 8.34-8.27 (m, J = 5.5 Hz, 2H), 7.61 (s, 2H), 7.06 (s, 2H), 3.88 (s, 12H), 3.47 (q, J = 6.6 Hz, 4H), 1.69-1.58 (m, 4H), 1.36-1.22 (m, 12H); LCMS (+ESI): *m/z* calculated for $C_{30}H_{38}N_6O_4Cl_2$: 616.2, found: 617.4 [M+H]$^+$. Purity 97.5% [Mobile Phase, ACN : Buffer (50:50) ; Rt 4.4 min].

4.5.8.16 Synthesis of N1,N10-bis(2-chloroquinazolin-4-yl)decane-1,10-diamine (16). **16** was synthesized from 2,4-dichloroquinazoline (500 mg, 2.62 mmol), 1,10-diaminodecane (225 mg, 1.30 mmol), DIEA (1.30 mL, 7.86 mmol) and THF (10 mL) according to general procedure 2. White powder (yield 210 mg, 32%). ^{1}H NMR (400 MHz, Chloroform-*d*) δ 7.80-7.70 (m, 6H), 7.51-7.44 (m, 2H), 6.04-5.98 (m, J = 5.6 Hz, 2H), 3.73-3.65 (m, J = 7.3, 5.5 Hz, 4H), 1.77-1.70 (m, J = 14.6, 8.0, 6.6 Hz, 4H), 1.45-1.28 (m, 12H); LCMS (+ESI): *m/z* calculated for $C_{26}H_{30}N_6Cl_2$: 496.2, found: 497.2 [M+H]$^+$. Purity 98.0% [Mobile Phase, ACN : Buffer (50:50) ; Rt 6.4 min].

4.6 REFERENCES

1.   Tuberculosis: Natural history, microbiology, and pathogenesis. Accessed May 28, 2023. https://www.medilib.ir/uptodate/show/8023

2.   Leung AN. Pulmonary tuberculosis: the essentials. *Radiology*. 1999;210(2):307-322. doi:10.1148/RADIOLOGY.210.2.R99JA34307

3.   Comstock GW. Epidemiology of tuberculosis. *Am Rev Respir Dis*. 1982;125(3 Pt 2):8-15. doi:10.1164/ARRD.1982.125.3P2.8

4.   Horsburgh CR, Rubin EJ. Clinical practice. Latent tuberculosis infection in the United States. *N Engl J Med*. 2011;364(15):1441-1448. doi:10.1056/NEJMCP1005750

5.   Smith GS, Van Den Eeden SK, Baxter R, et al. Cigarette smoking and pulmonary tuberculosis in northern California. *J Epidemiol Community Health (1978)*. 2015;69(6):568-573. doi:10.1136/JECH-2014-204292

6.	Bates MN, Khalakdina A, Pai M, et al. Risk of tuberculosis from exposure to tobacco smoke: a systematic review and meta-analysis. *Arch Intern Med*. 2007;167(4):335-342. doi:10.1001/ARCHINTE.167.4.335

7.	Sakamoto K. The pathology of Mycobacterium tuberculosis infection. *Vet Pathol*. 2012;49(3):423-439. doi:10.1177/0300985811429313

8.	Miggiano R, Rizzi M, Ferraris DM. Mycobacterium tuberculosis Pathogenesis, Infection Prevention and Treatment. *Pathogens*. 2020;9(5). doi:10.3390/PATHOGENS9050385

9.	WHO. Tuberculosis. Published October 14, 2021. Accessed June 10, 2022. https://www.who.int/news-room/fact-sheets/detail/tuberculosis

10.	Nahid P, Dorman SE, Alipanah N, et al. Executive Summary: Official American Thoracic Society/Centers for Disease Control and Prevention/Infectious Diseases Society of America Clinical Practice Guidelines: Treatment of Drug-Susceptible Tuberculosis. *Clinical Infectious Diseases*. 2016;63(7):853-867. doi:10.1093/cid/ciw566

11.	Hameed HMA, Islam MM, Chhotaray C, et al. Molecular Targets Related Drug Resistance Mechanisms in MDR-, XDR-, and TDR- Mycobacterium tuberculosis Strains. *Front Cell Infect Microbiol*. 2018;8(APR). doi:10.3389/FCIMB.2018.00114

12.	Dookie N, Rambaran S, Padayatchi N, et al. Evolution of drug resistance in Mycobacterium tuberculosis: a review on the molecular determinants of resistance and implications for personalized care. *J Antimicrob Chemother*. 2018;73(5):1138-1151. doi:10.1093/JAC/DKX506

13.	Kalscheuer R, Palacios A, Anso I, et al. The Mycobacterium tuberculosis capsule: a cell structure with key implications in pathogenesis. *Biochem J*. 2019;476(14):1995. doi:10.1042/BCJ20190324

14.	Märtson AG, Burch G, Ghimire S, et al. Therapeutic drug monitoring in patients with tuberculosis and concurrent medical problems. *Expert Opin Drug Metab Toxicol*. 2021;17(1). doi:10.1080/17425255.2021.1836158

15.	Black TA, Buchwald UK. The pipeline of new molecules and regimens against drug-resistant tuberculosis. *J Clin Tuberc Other Mycobact Dis*. 2021;25:100285. doi:10.1016/J.JCTUBE.2021.100285

16.	Peloquin CA, Davies GR. The Treatment of Tuberculosis. *Clin Pharmacol Ther*. 2021;110(6):1455-1466. doi:10.1002/CPT.2261

17. Maeurer M, Schito M, Zumla A. Totally-drug-resistant tuberculosis: hype versus hope. *Lancet Respir Med*. 2014;2(4):256-257. doi:10.1016/S2213-2600(14)70020-7

18. Huszár S, Chibale K, Singh V. The quest for the holy grail: new antitubercular chemical entities, targets and strategies. *Drug Discov Today*. 2020;25(4):772-780. doi:10.1016/J.DRUDIS.2020.02.003

19. Santra M, Farrell DW, Dill KA. Bacterial proteostasis balances energy and chaperone utilization efficiently. *Proceedings of the National Academy of Sciences*. 2017;114(13):E2654-E2661. doi:10.1073/pnas.1620646114

20. Leodolter J, Warweg J, Weber-Ban E. The Mycobacterium tuberculosis ClpP1P2 Protease Interacts Asymmetrically with Its ATPase Partners ClpX and ClpC1. Zeth K, ed. *PLoS One*. 2015;10(5):e0125345. doi:10.1371/journal.pone.0125345

21. Lunge A, Gupta R, Choudhary E, et al. The unfoldase ClpC1 of Mycobacterium tuberculosis regulates the expression of a distinct subset of proteins having intrinsically disordered termini. *Journal of Biological Chemistry*. 2020;295(28):9455-9473. doi:10.1074/jbc.RA120.013456

22. Vasudevan D, Rao SPS, Noble CG. Structural basis of mycobacterial inhibition by Cyclomarin A. *Journal of Biological Chemistry*. 2013;288(43):30883-30891. doi:10.1074/jbc.M113.493767

23. Schmitt EK, Riwanto M, Sambandamurthy V, et al. The natural product cyclomarin kills mycobacterium tuberculosis by targeting the ClpC1 subunit of the caseinolytic protease. *Angewandte Chemie - International Edition*. 2011;50(26):5889-5891. doi:10.1002/anie.201101740

24. Gavrish E, Sit CS, Cao S, et al. Lassomycin, a ribosomally synthesized cyclic peptide, kills mycobacterium tuberculosis by targeting the ATP-dependent protease ClpC1P1P2. *Chem Biol*. 2014;21(4):509-518. doi:10.1016/j.chembiol.2014.01.014

25. Gao W, Kim JY, Anderson JR, et al. The cyclic peptide ecumicin targeting CLpC1 is active against Mycobacterium tuberculosis in vivo. *Antimicrob Agents Chemother*. 2015;59(2):880-889. doi:10.1128/AAC.04054-14

26. Wolf NM, Lee H, Choules MP, et al. High-Resolution Structure of ClpC1-Rufomycin and Ligand Binding Studies Provide a Framework to Design and Optimize Anti-Tuberculosis Leads. *ACS Infect Dis*. 2019;5(6):829-840. doi:10.1021/acsinfecdis.8b00276

27. Zhu Q, Chen Z, Paul PK, et al. Oral delivery of proteins and peptides: Challenges, status quo and future perspectives. *Acta Pharm Sin B*. 2021;11(8):2416. doi:10.1016/J.APSB.2021.04.001

28. Wang CK, Craik DJ. Designing macrocyclic disulfide-rich peptides for biotechnological applications. *Nature Chemical Biology 2018 14:5*. 2018;14(5):417-427. doi:10.1038/s41589-018-0039-y

29. Wang L, Wang N, Zhang W, et al. Therapeutic peptides: current applications and future directions. *Signal Transduction and Targeted Therapy 2022 7:1*. 2022;7(1):1-27. doi:10.1038/s41392-022-00904-4

30. Barbie P, Kazmaier U. Total Synthesis of Cyclomarin A, a Marine Cycloheptapeptide with Anti-Tuberculosis and Anti-Malaria Activity. *Org Lett*. 2016;18(2):204-207. doi:10.1021/ACS.ORGLETT.5B03292

31. Lear S, Munshi T, Hudson AS, et al. Total chemical synthesis of lassomycin and lassomycin-amide. *Org Biomol Chem*. 2016;14(19):4534-4541. doi:10.1039/C6OB00631K

32. Kidwai S, Park CY, Mawatwal S, et al. Dual mechanism of action of 5-Nitro-1,10-phenanthroline against mycobacterium tuberculosis. *Antimicrob Agents Chemother*. 2017;61(11). doi:10.1128/AAC.00969-17/FORMAT/EPUB

33. Arora G, Gagandeep G, Behura A, et al. NSC 18725, a Pyrazole Derivative Inhibits Growth of Intracellular Mycobacterium tuberculosis by Induction of Autophagy. *Front Microbiol*. 2020;10. doi:10.3389/FMICB.2019.03051

34. Kidwai S, Bouzeyen R, Chakraborti S, et al. NU-6027 Inhibits Growth of Mycobacterium tuberculosis by Targeting Protein Kinase D and Protein Kinase G. *Antimicrob Agents Chemother*. 2019;63(9). doi:10.1128/AAC.00996-19

35. Vennerstrom JL, Ellis WY, Ager AL, et al. Bisquinolines. 1. N,N-Bis(7-chloroquinolin-4-yl)alkanediamines with Potential against Chloroquine-Resistant Malaria. *J Med Chem*. 1992;35(11):2129-2134. doi:10.1021/JM00089A025/ASSET/JM00089A025.FP.PNG_V03

36. Sundriyal S, Malmquist NA, Caron J, et al. Development of diaminoquinazoline histone lysine methyltransferase inhibitors as potent blood-stage antimalarial compounds. *ChemMedChem*. 2014;9(10):2360-2373. doi:10.1002/cmdc.201402098

37. Srimongkolpithak N, Sundriyal S, Li F, et al. Identification of 2,4-diamino-6,7-dimethoxyquinoline derivatives as G9a inhibitors. *Medchemcomm*. 2014;5(12):1821-1828. doi:10.1039/c4md00274a

38. Sundriyal S, Chen PB, Lubin AS, et al. Histone lysine methyltransferase structure activity relationships that allow for segregation of G9a inhibition and anti-Plasmodium activity. *Medchemcomm*. 2017;8(5):1069-1092. doi:10.1039/c7md00052a

39. Campbell SF, Hardstone JD, Palmer MJ. 2,4-Diamino-6,7-dimethoxyquinoline derivatives as alpha-1-adrenoceptor antagonists and antihypertensive agents. *J Med Chem*. 1988;31(5):1031-1035. doi:Doi 10.1021/Jm00400a025

40. Glide, Schrödinger, LLC, New York, NY, 2021.

41. Halgren TA, Murphy RB, Friesner RA, et al. Glide: A new approach for rapid, accurate docking and scoring. 2. Enrichment factors in database screening. *J Med Chem*. 2004;47(7):1750-1759. doi:10.1021/jm030644s

42. Friesner RA, Banks JL, Murphy RB, et al. Glide: A new approach for rapid, accurate docking and scoring. 1. Method and assessment of docking accuracy. *J Med Chem*. 2004;47(7):1739-1749. doi:10.1021/jm0306430

43. Sun H, Li Y, Tian S, et al. Assessing the performance of MM/PBSA and MM/GBSA methods. 4. Accuracies of MM/PBSA and MM/GBSA methodologies evaluated by various simulation protocols using PDBbind data set. *Phys Chem Chem Phys*. 2014;16(31):16719-16729. doi:10.1039/C4CP01388C

44. Rowlands GJ, Severinsen RJ, Buchanan JK, et al. Synthesis and Basicity Studies of Quinolino[7,8- h]quinoline Derivatives. *Journal of Organic Chemistry*. 2020;85(17):11297-11308. doi:10.1021/ACS.JOC.0C01428/SUPPL_FILE/JO0C01428_SI_002.CIF

45. Harder KW, Owen P, Wong LKH, et al. Characterization and kinetic analysis of the intracellular domain of human protein tyrosine phosphatase beta (HPTP beta) using synthetic phosphopeptides. *Biochem J*. 1994;298 (Pt 2):395-401. doi:10.1042/BJ2980395

46. Li M, Kandror O, Akopian T, et al. Structure and functional properties of the active form of the proteolytic complex, ClpP1P2, from Mycobacterium tuberculosis. *Journal of Biological Chemistry*. 2016;291(14):7465-7476. doi:10.1074/jbc.M115.700344

47. Akopian T, Kandror O, Raju RM, et al. The active ClpP protease from M. tuberculosis is a complex composed of a heptameric ClpP1 and a ClpP2 ring. *EMBO J.* 2012;31(6):1529-1541. doi:10.1038/EMBOJ.2012.5

48. Arora G, Tiwari P, Mandal RS, et al. High Throughput Screen Identifies Small Molecule Inhibitors Specific for Mycobacterium tuberculosis Phosphoserine Phosphatase. *Journal of Biological Chemistry*. 2014;289(36):25149-25165. doi:10.1074/JBC.M114.597682

49. Madhavi Sastry G, Adzhigirey M, Day T, et al. Protein and ligand preparation: parameters, protocols, and influence on virtual screening enrichments. *J Comput Aided Mol Des*. 2013;27(3):221-234. doi:10.1007/S10822-013-9644-8

50. Protein Preparation Wizard; Epik, Schrödinger, LLC, New York, NY, 2021; Impact, Schrödinger, LLC, New York, NY; Prime, Schrödinger, LLC, New York, NY, 2021.

51. LigPrep, Schrödinger, LLC, New York, NY, 2021.

52. Banks JL, Beard HS, Cao Y, et al. Integrated Modeling Program, Applied Chemical Theory (IMPACT). *J Comput Chem*. 2005;26(16):1752-1780. doi:10.1002/jcc.20292

53. Maurya SS, Bahuguna A, Khan SI, et al. N-Substituted aminoquinoline-pyrimidine hybrids: Synthesis, in vitro antimalarial activity evaluation and docking studies. *Eur J Med Chem*. 2019;162:277-289. doi:10.1016/j.ejmech.2018.11.021

54. Amin AS, Dessouki HA, Agwa IA, et al. Ion-pairing and reversed phase liquid chromatography for the determination of three different quinolones: Enrofloxacin, lomefloxacin and ofloxacin. *Arab J Chem*. 2011;4:249-257. doi:10.1016/j.arabjc.2010.06.03155.

55. Wright DH, Herman VK, Konstantinides FN, et al. Determination of quinolone antibiotics in growth media by reversed-phase high-performance liquid chromatography. *J Chromatogr B Biomed Sci Appl*. 1998;709(1):97-104. doi:10.1016/S0378-4347(98)00006-1

Chapter 5

Overall Summary & Future Prospects

5.1 PHYSICOCHEMICAL PROFILING AND PROPERTY SPACE CHARACTERIZATION OF ANTIMALARIALS

5.1.1. Summary

In summary, we have collated a large dataset of IN, MA, HA, ASAM, and oral drugs consisting of 7365, 6620, 10,557, 66 and 1954 molecules, respectively and obtained molecular descriptors like MW, HBA, HBD, Fsp^3, RB, Ar, #HetAr, clog P, TPSA, CarboAr, ArN, and BaN for these datasets. Comparison among the different categories of molecules was performed using various statistical parameters and hypothesis tests. Finally, descriptors essential for the antimalarial property space were identified, and a new descriptor, the sum of #BaN and #ArN (SBAN), was defined and used to scale various Lipinski's and Veber's properties. These results encouraged us to propose two new guidelines to characterize antimalarial property space. These analyses and recommendations should guide the discovery and optimization of future antimalarials while reducing the overall cost.

Table 5.1. Number of Molecules Compliant with the Specified Guidelines

Guidelines	Oral drugs (N = 1954)	ASAM (N = 66)	HA (N = 10,557)	MA (N = 6620)	IN (N = 7365)
Lipinski's Ro5	1786 (91%)	59 (89%)	8713 (83%)	5777 (87%)	6451 (88%)
Veber's rule	1647 (84%)	61 (92%)	8693 (82%)	5609 (85%)	5933 (81%)
Guideline-1 s-TPSA 5 to 65; s-RB ≤ 6; s-HBA ≤ 5; s-HBD ≤ 2	1338 (68%)	60 (91%)	8234 (78%)	4823 (73%)	4924 (67%)
Guideline-2 s-TPSA 5 to 65; s-RB ≤ 6; s-HBA ≤ 5; s-HBD ≤ 2; MW ≥ 235	1114 (57%)	60 (91%)	8090 (77%)	4639 (70%)	4418 (60%)

5.1.2 Future Prospects

A similar analysis of the physicochemical properties can also be done for the hits obtained in various phenotypic screens. The physicochemical profiling of hits vs the whole library can be performed to further validate the importance of these properties in determining antimalarial potency. To develop predictive models for the antimalarial activity, simple descriptors

described in this work, such as BaN, clogP, TPSA and MW can be used, which are relevant to the antimalarial chemical space. Also, newly discovered *Plasmodium* transporters should be characterized for their selectivity for the basic, lipophilic, and flat compounds.

5.2 SYNTHESIS AND EVALUATION OF BISQUINAZOLINE AND QUINAZOLINE BASED HYBRIDS AS POTENTIAL ANTIMALARIALS

5.2.1 Summary

To summarize, we synthesized 6 bisquinazolines and 21 quinoline-quinazoline hybrids. Based on initial screening, bisquinazolines were inactive in the in vitro assay, so in this study, we focused on 4-aminoquinoline and 8-aminoquinoline hybrids. Of the 4 aminoquinoline-quinazoline hybrids, **4a, 4c, 4d** and **5c** showed significant activity against the schizont stage of *Plasmodium* (3D7); therefore, these molecules were also tested against the resistant strains (C580Y). Moreover, we also developed a method to check the purity of the synthesized compounds using HPLC. The compounds **5c, 4a** and **4c** with $IC_{50} = 15$ nM, 28 nM and 21 nM against 3D7, respectively and $IC_{50} = 19$ nM, 16 nM and 16 nM against C580Y, respectively, were found to be the most active of the 4-aminoquinoline-quinazoline hybrids series. Similarly, in the 8-aminoquinoline-quinazoline series, 7 compounds were synthesized. The evaluation of these compounds against the ring stage of *Plasmodium* revealed **13c** and **14c** to be the most potent with IC_{50} (3D7) = 140.1 nM and 197.8 nM and IC_{50} (C580Y) = 243.3 nM and 249.5 nM, respectively. To investigate the mechanism of action of these compounds, we developed BHIA, and we found that most hybrids were more potent inhibitors of β-hematin formation than CQ. Therefore, a correlation between antiplasmodial activity and inhibition of β-hematin formation was observed in the case of a few molecules. However, these molecules are expected to hit *Pf*HKMT targets too.

Table 5.2. Showing most potent antimalarial compounds

S.No	Code	Formula	IC$_{50}$ (nM)		β-hematin IC$_{50}$ (μM)	Cytotoxicity HEK (% viability)
			Artemisinin sensitive (3D7)	Artemisinin resistant (C580Y)		
1	**4a**		28	16	NT	100
2	**4c**		21	16	29	64
3	**5c**		15	19	12	88
4	**13c**		140	NT	75	98
5	**14c**		198	NT	59	20
CONTROLS AND STANDARDS						
Piperaquine			27	22	55	89
Chloroquine			16	41	35	NT
Primaquine			9370	NT	>1000	NT
65			2 (66)	4.3	58	69

NT= Not tested

5.2.2 Future Prospects

Currently, it is challenging to isolate and purify predicted *Pf*HKMT proteins; hence, the synthesized molecules could not be screened against these epigenetic targets. However, recombinant forms of *Pf*HKMT might become available for screening recombinant forms of *Pf*HKMT might become available for screening. Also, these molecules may further be screened against different life stages of the parasite and analyzed for stage-specific activity. Further in vivo activity of these compounds remains to be studied.

Like CQ, most of the hybrid molecules possess two or more BaN and, thus, can achieve mM concentration in the FV of the parasite, as proposed recently by us.[1] Thus, these molecules may also be screened at high concentration against other protein targets present in FV, such as falcipains and plasmepsins. The toxicity observed in these compounds might be due to human G9a inhibition. In future, further modifications at positions 2 and 4 may be tried to segregate the antiparasitic and anti-G9a activity, which has been shown to be possible.[2]
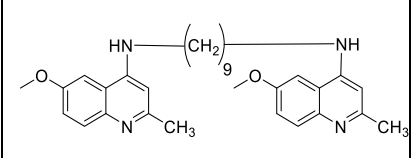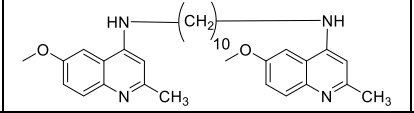
5.3 DISCOVERY OF BISQUINOLINES AS MYCOBACTERIUM TUBERCULOSIS CLPC1 INHIBITORS: SAR STUDIES AND ANTIMYCOBACTERIAL EVALUATION

5.3.1 Summary

Our collaborators at THSTI (Faridabad) performed initial screening of ~10,000 compounds and found compound **1 (NSC10010)**, a bisquinoline, to be the most promising scaffold targeting the ATPase activity of ClpC1 and proliferation of *Mtb* in vitro. For the SAR study, we synthesized 12 bisquinolines and 4 bisquinazoline compounds. Compound **2** was the most active with IC_{50} of 6.25 μM. Moreover, the preliminary SAR study suggested that bisquinoline with a chain length of 9–10 carbons is optimal for inhibiting *Mtb* growth with a reduced minimal inhibitory concentration (MIC). The quinoline ring appears indispensable, as its BaN is predicted to be protonated and facilitate crucial interactions with the residues in the binding

pocket. The preliminary SAR also implies that linker length may impact *Mtb* growth inhibition more than linker flexibility.

Table 5.3. Most potent anti-tubercular drugs

Code	Structure	ClpC1 ATPase inhibition (% inhibition at 100 µM)	FITC-casein degradation (% inhibition at 100 µM)	MIC$_{99}$ (Against *Mtb* H$_{37}$Rv strain) (µM)	Glide Score	MM/ GBSA (kcal/ mol)
NSC 100100 (1)		74	100	12.5	-4.1	-77.9
2		28	100	6.25	-3.9	-73.4

5.3.2 Future Prospects

This is the first systematic analysis of the synthetically tractable small molecule inhibitors of *Mtb* ClpC1. Future SAR analysis is needed to optimize the activity of this series in in vitro enzyme assay and antimycobacterial assay. For this, linkers containing heteroatoms may be employed, which were not part of the reported preliminary study. In addition, quinoline rings with diverse substituents at different positions can also be investigated to expand the SAR of this series.

5.4 REFERENCES

1.   Valluri H, Bhanot A, Shah S, et al. Basic Nitrogen (BaN) Is a Key Property of Antimalarial Chemical Space. *J Med Chem*. Published online June 25, 2023. doi:10.1021/ACS.JMEDCHEM.3C00206

2.   Sundriyal S, Chen PB, Lubin AS, et al. Histone lysine methyltransferase structure activity relationships that allow for segregation of G9a inhibition and anti-Plasmodium activity. *Medchemcomm*. 2017;8(5):1069-1092. doi:10.1039/C7MD00052A

APPENDIX

CHARACTERIZATION DATA FOR SYNTHESIZED COMPOUNDS

¹**H NMR** (400 MHz, DMSO-d_6) δ 9.34 (bs, 1H), 8.69 (bs, 1H), 8.50 (d, J = 9.1 Hz, 1H), 8.40 (d, J = 6.4 Hz, 1H), 7.90 (d, J = 2.2 Hz, 1H), 7.80 (s, 1H), 7.58 (dd, J = 9.0, 2.2 Hz, 1H), 7.31 (s, 1H), 6.68 (d, J = 6.5 Hz, 1H), 3.87 (d, J = 14.1 Hz, 6H), 3.62-3.48 (m, J = 25.2, 18.6, 5.8 Hz, 8H), 1.84 (s, 8H).

Figure A-1. 1H NMR spectra of N1-(7-chloroquinolin-4-yl)-N4-(6,7-dimethoxy-2-(pyrrolidin-1-yl)quinazolin-4-yl)butane-1,4-diamine (**5c**)

¹³**C NMR** (101 MHz, DMSO-d_6) δ 159.14 , 154.36 , 151.97 , 150.70 , 149.20 , 145.25 , 133.93 , 127.62 , 124.68 , 124.47 , 117.84 , 103.99 , 103.13 , 99.07 , 56.47 , 55.94 , 46.75 , 42.62 , 26.77 , 25.77 , 25.40

Figure A-2. ¹³C NMR of CN1-(7-chloroquinolin-4-yl)-N4-(6,7-dimethoxy-2-(pyrrolidin-1-yl)quinazolin-4-yl)butane-1,4-diamine (**5c**)

MS Zoomed Spectrum

MS Spectrum Peak List

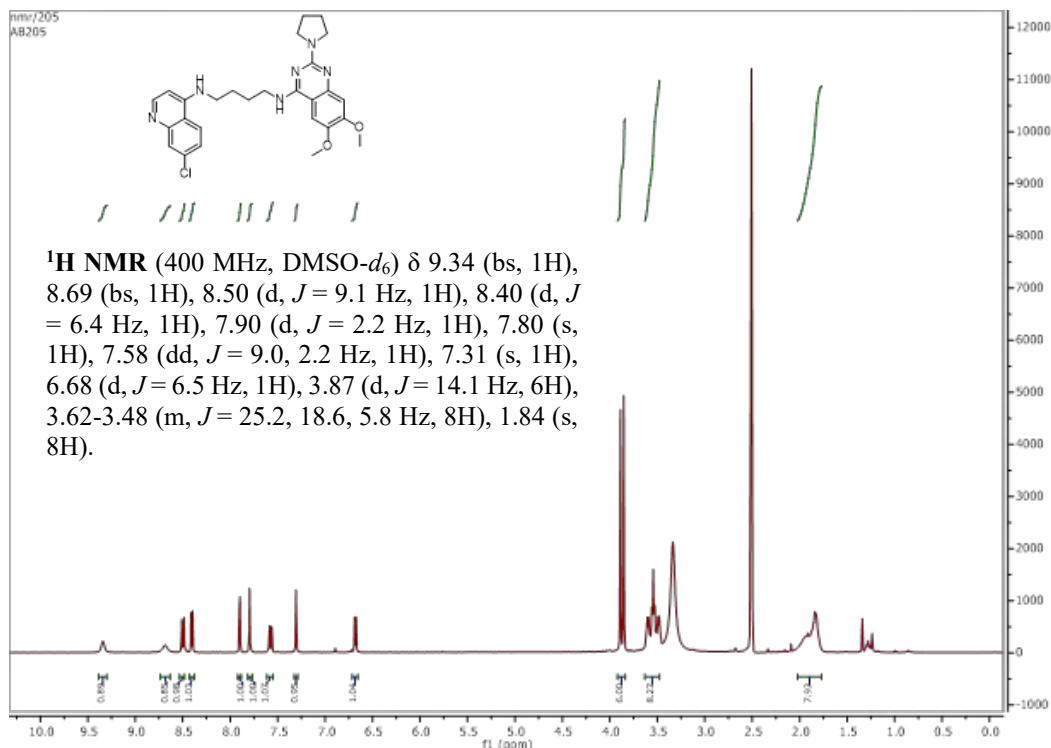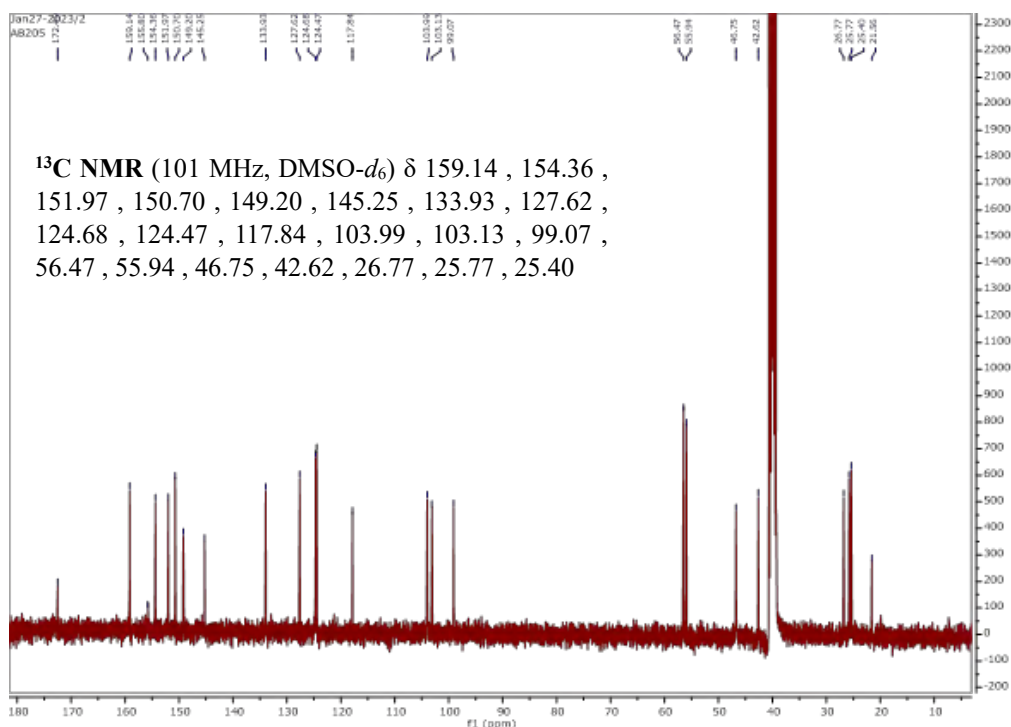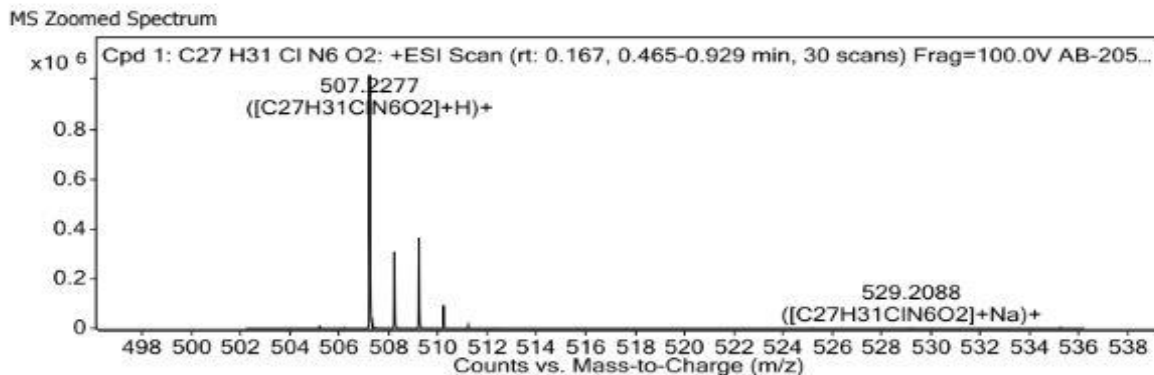| m/z	Calc m/z	Diff(ppm)	z	Abund	Formula	Ion
506.2147	506.2192	8.85	1	2888.83	C27H31ClN6O2	M+
507.2277	507.227	-1.35	1	1036598.88	C27H31ClN6O2	(M+H)+
508.2307	508.2299	-1.6	1	326809.39	C27H31ClN6O2	(M+H)+
509.2262	509.2253	-1.86	1	365598.25	C27H31ClN6O2	(M+H)+
510.2278	510.2275	-0.74	1	94260.04	C27H31ClN6O2	(M+H)+
511.2302	511.2301	-0.21	1	13449.96	C27H31ClN6O2	(M+H)+
512.2328	512.2327	-0.29	1	1490.81	C27H31ClN6O2	(M+H)+
529.2088	529.2089	0.16	1	2150.06	C27H31ClN6O2	(M+Na)+
530.2112	530.2119	1.2	1	698.27	C27H31ClN6O2	(M+Na)+
531.2067	531.2072	1.03	1	758.82	C27H31ClN6O2	(M+Na)+

Figure A-3. HRMS of CN1-(7-chloroquinolin-4-yl)-N4-(6,7-dimethoxy-2-(pyrrolidin-1-yl)quinazolin-4-yl)butane-1,4-diamine (**5c**). (ESI/Q-TOF) m/z: $[M + H]^+$ Calcd for $C_{27}H_{31}ClN_6O_2$ 507.2270; Found 507.2277

<Chromatogram>

<Peak Table>

PDA Ch1 254nm

Peak#	Ret. Time	Area	Area%	Theoretical Plates/meter(USP)	Tailing Factor	Resolution(USP)
1	4.642	376218	100.000	6701	1.747	--
Total		376218	100.000			

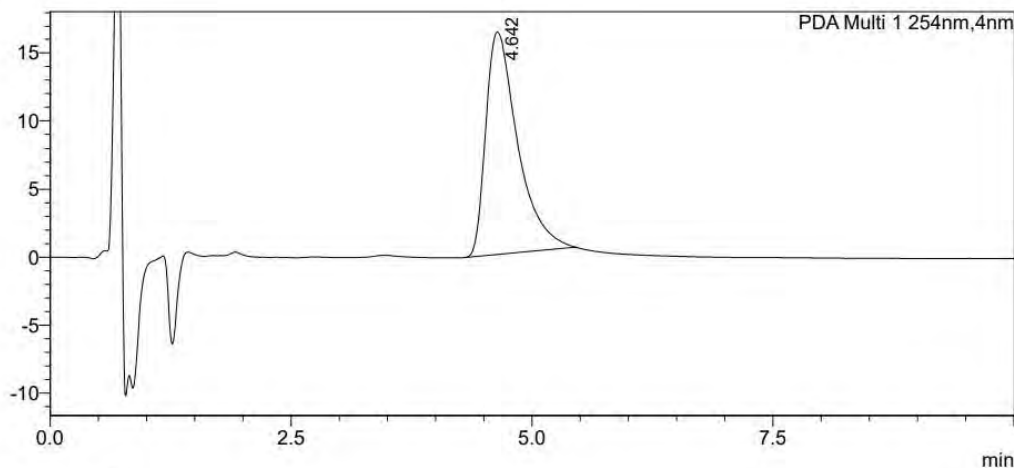**Figure A-4.** Purity profiling of CN1-(7-chloroquinolin-4-yl)-N4-(6,7-dimethoxy-2-(pyrrolidin-1-yl)quinazolin-4-yl)butane-1,4-diamine (**5c**). Purity 100% [Mobile Phase, ACN : Buffer (60:40) ; Rt 4.64 min]

¹H NMR (400 MHz, DMSO-d_6) δ 8.59-8.45 (m, J = 24.1, 8.1, 3.8 Hz, 3H), 8.41 (s, J = 5.4 Hz, 1H), 8.23 (d, J = 8.3 Hz, 1H), 8.15 (d, J = 9.0 Hz, 1H), 7.83-7.76 (m, 3H), 7.64 (t, 1H), 7.51 (m, J = 4.4, 3.9 Hz, 4H), 7.37-7.30 (m, J = 7.7, 5.2, 2.2 Hz, 1H), 6.77-6.70 (m, J = 5.0 Hz, 1H), 4.05-3.98 (m, J = 6.3 Hz, 2H), 3.75-3.65 (m, J = 6.3 Hz, 2H)

Figure A-5. 1H NMR spectra of N1-(7-chloroquinolin-4-yl)-N2-(2-phenylquinazolin-4-yl)ethane-1,2-diamine (**3a**)

¹³C NMR (101 MHz, DMSO) δ 160.49, 159.85, 152.00, 150.78, 150.35, 149.19, 139.16, 134.00, 133.29, 130.55, 128.71, 128.40, 128.33, 127.69, 125.87, 124.58, 124.44, 123.12, 117.86, 114.33, 99.16, 42.24, 40.60, 40.39, 40.18, 39.98, 39.77, 39.56, 39.35, 39.23.
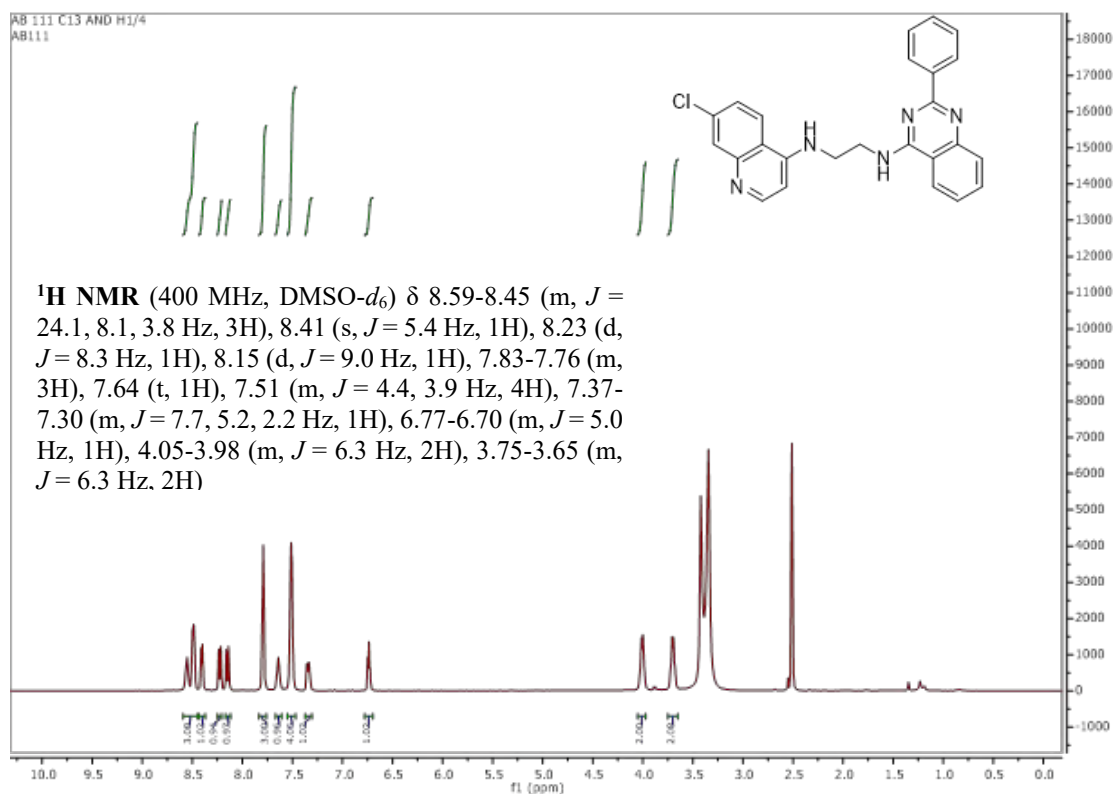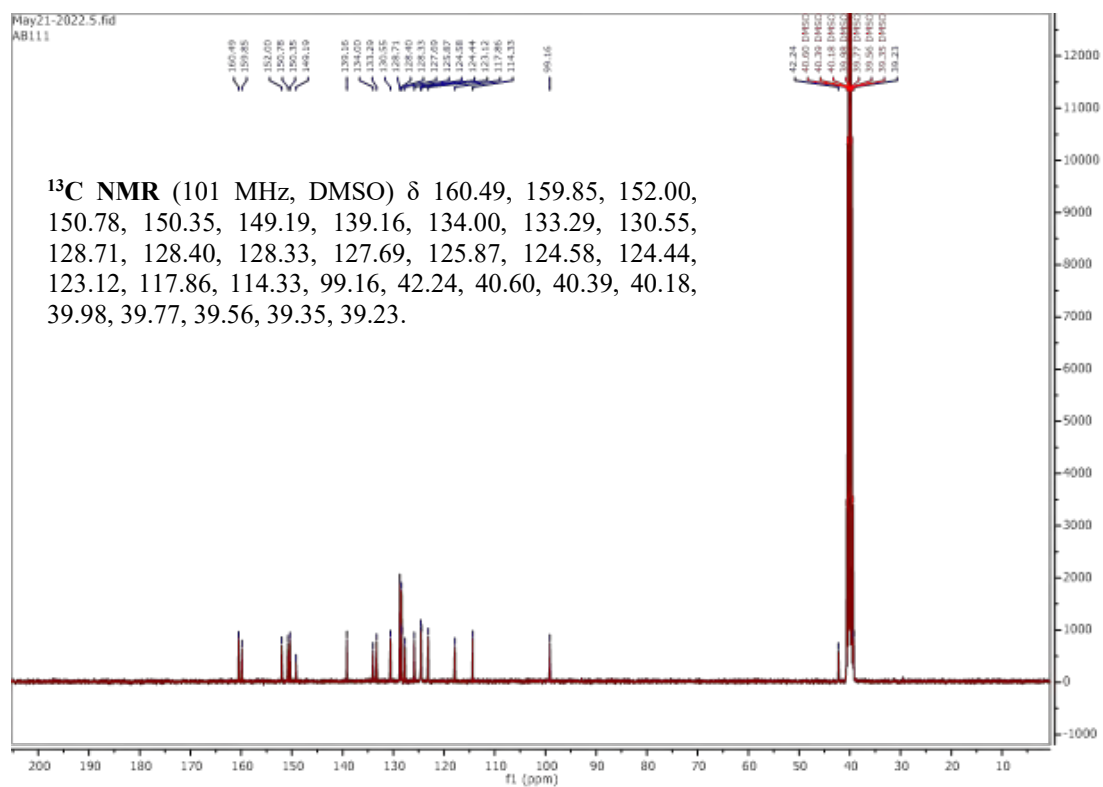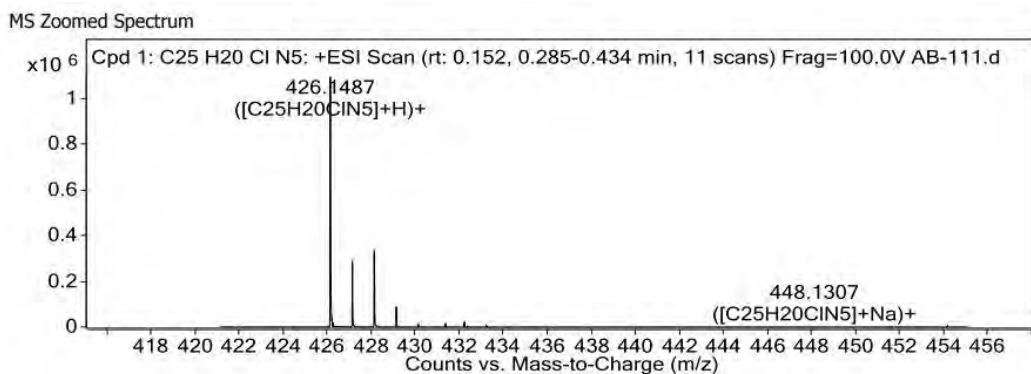
Figure A-6. ¹³C NMR spectra of N1-(7-chloroquinolin-4-yl)-N2-(2-phenylquinazolin-4-yl)ethane-1,2-diamine (**3a**)

MS Zoomed Spectrum

x10 6 | Cpd 1: C25 H20 Cl N5: +ESI Scan (rt: 0.152, 0.285-0.434 min, 11 scans) Frag=100.0V AB-111.d

426.1487
([C25H20ClN5]+H)+

448.1307
([C25H20ClN5]+Na)+

Counts vs. Mass-to-Charge (m/z)

MS Spectrum Peak List

m/z	Calc m/z	Diff(ppm)	z	Abund	Formula	Ion
425.1361	425.1402	9.56	1	528.84	C25H20ClN5	M+
426.1487	426.148	-1.68	1	1095750.96	C25H20ClN5	(M+H)+
427.152	427.151	-2.42	1	301484.75	C25H20ClN5	(M+H)+
428.147	428.1461	-2.1	1	340684.38	C25H20ClN5	(M+H)+
429.1487	429.1484	-0.72	1	89707.23	C25H20ClN5	(M+H)+
430.1514	430.1512	-0.48	1	10669.99	C25H20ClN5	(M+H)+
431.1539	431.154	0.29	1	968.23	C25H20ClN5	(M+H)+
448.1307	448.1299	-1.6	1	680.9	C25H20ClN5	(M+Na)+
449.1332	449.1329	-0.72	1	224.84	C25H20ClN5	(M+Na)+
450.1266	450.128	3.17	1	267.63	C25H20ClN5	(M+Na)+

Figure A-7. HRMS of N1-(7-chloroquinolin-4-yl)-N2-(2-phenylquinazolin-4-yl)ethane-1,2-diamine (**3a**). (ESI/Q-TOF) m/z: [M + H]+ Calcd for $C_{25}H_{20}ClN_5$ 426.1480; Found 426.1487

\<Chromatogram\>
mAU

PDA Multi 1 254nm,4nm

2.272

\<Peak Table\>
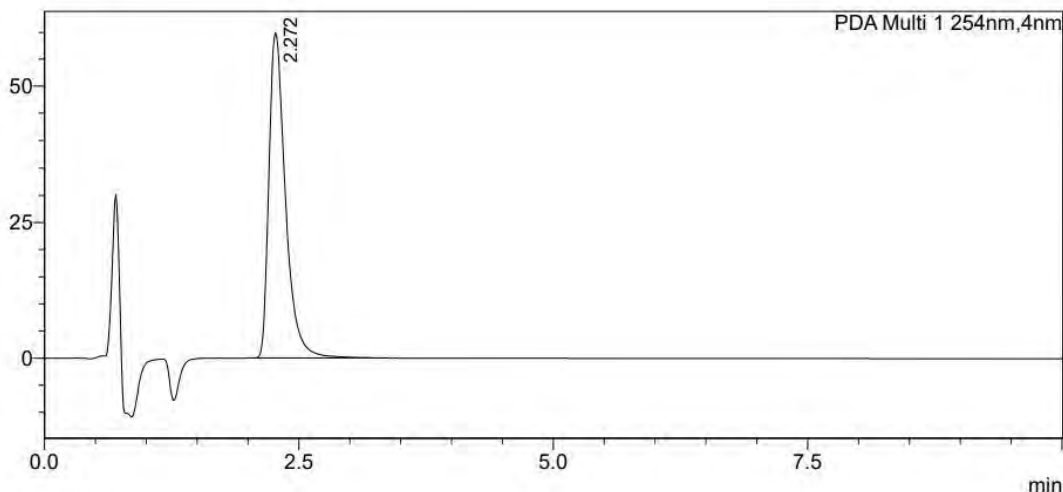
PDA Ch1 254nm

Peak#	Ret. Time	Area	Area%	Theoretical Plates/meter(USP)	Tailing Factor
1	2.272	679208	100.000	6206	1.527
Total		679208	100.000		

Figure A-8. Purity profiling **of** N1-(7-chloroquinolin-4-yl)-N2-(2-phenylquinazolin-4-yl)ethane-1,2-diamine (**3a**). - Purity 100% [Mobile Phase, ACN : Buffer (60:40) ; Rt 2.27 min]

¹H NMR (400 MHz, Chloroform-*d*) δ 8.68-8.53 (d, 4H), 7.93 (d, *J* = 8.3 Hz, 2H), 7.72 (t, *J* = 8.4, 6.8, 2.8 Hz, 2H), 7.59-7.42 (m, 8H), 7.35 (t, 2H), 5.85 (t, *J* = 5.8 Hz, 2H), 3.97-3.86 (m, *J* = 6.7, 6.1 Hz, 4H), 2.03-1.90 (m, 4H).
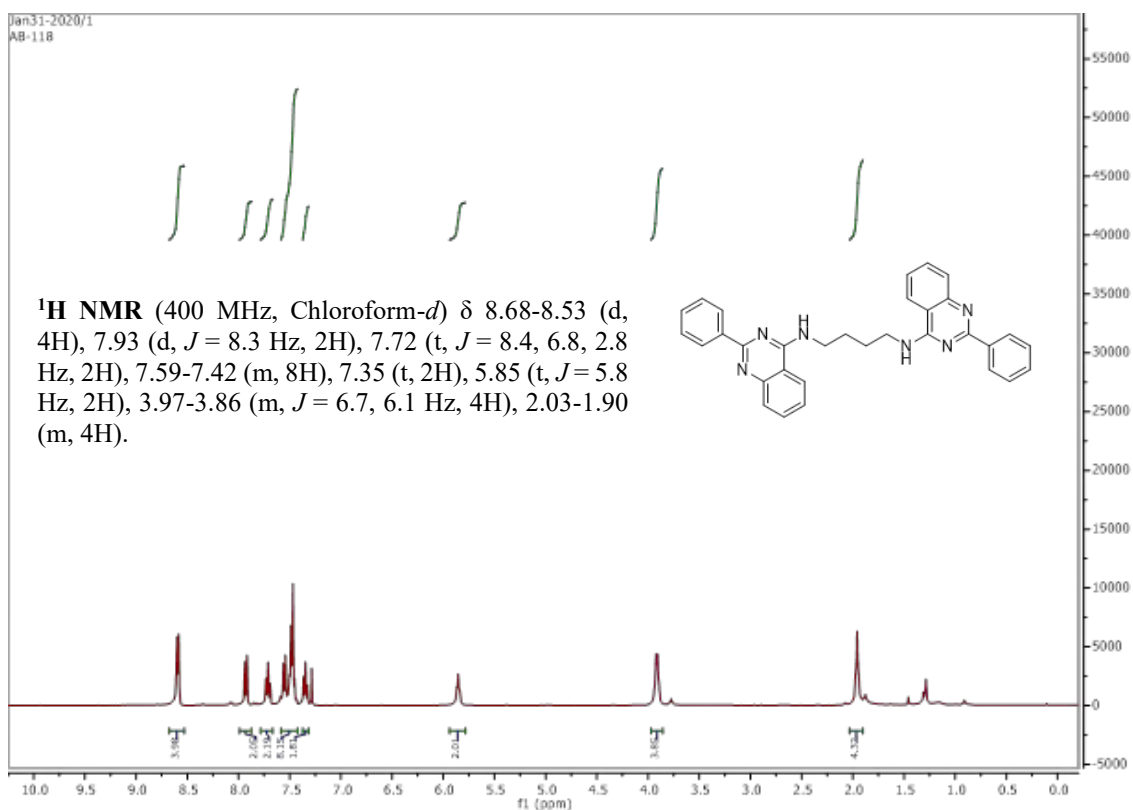
Figure A-9. ¹H NMR of N1,N4-bis(2-phenylquinazolin-4-yl)butane-1,4-diamine (**8c**)

¹³C NMR (101 MHz, CDCl₃) δ 160.51, 159.65, 150.48, 139.08, 132.49, 130.11, 128.82, 128.33, 125.41, 120.42, 113.63, 77.36, 77.05, 76.73, 40.71, 26.73.
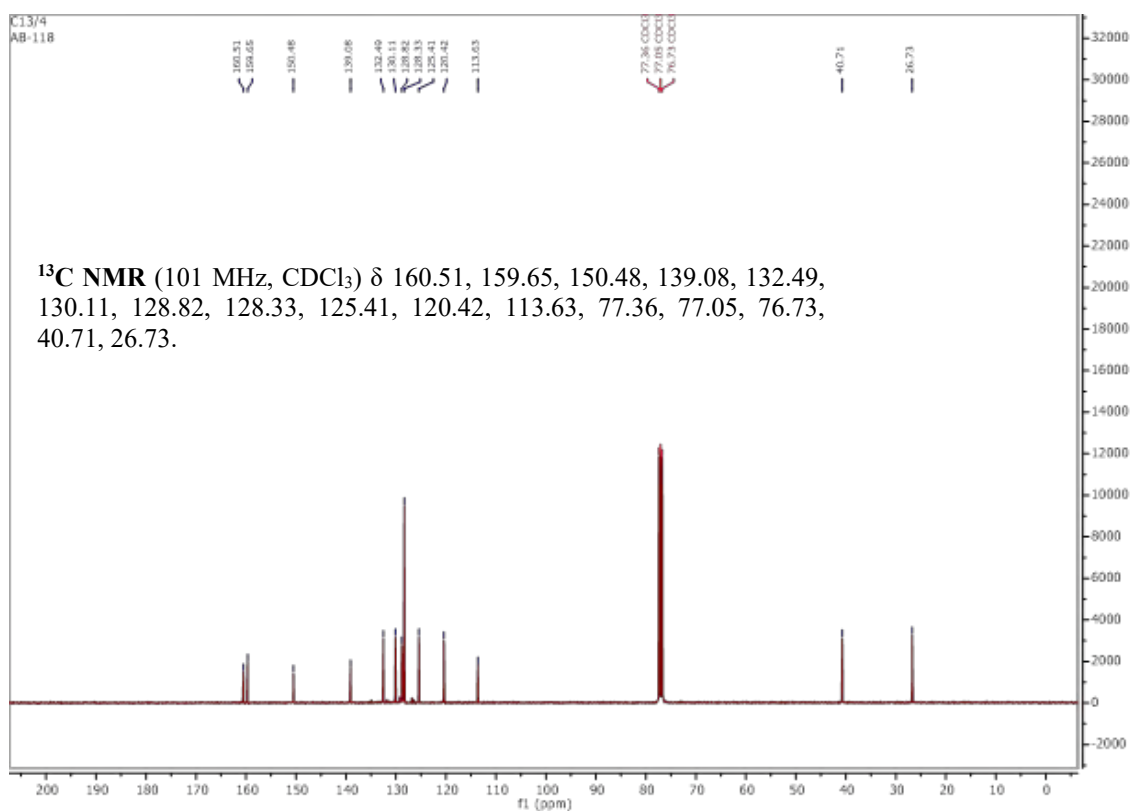
Figure A-10. ¹³C NMR of N1,N4-bis(2-phenylquinazolin-4-yl)butane-1,4-diamine (**8c**)

Cpd 1: C32 H28 N6: +ESI Scan (rt: 0.136, 0.302-0.467 min, 12 scans) Frag=100.0V AB-118.d

497.2436
([C32H28N6]+H)+

x10 6
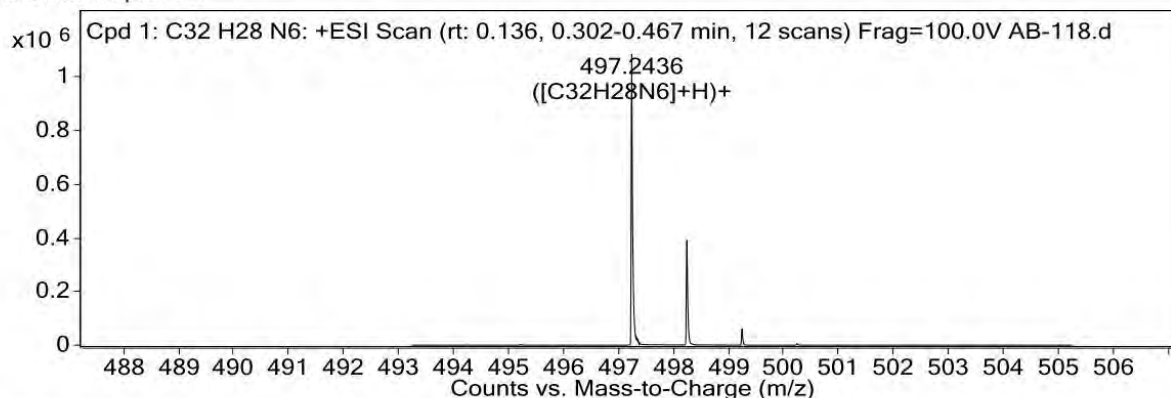
MS Spectrum Peak List

m/z	Calc m/z	Diff(ppm)	z	Abund	Formula	Ion
497.2436	497.2448	2.48	1	1089491.44	C32H28N6	(M+H)+
498.2469	498.2478	1.95	1	392312.67	C32H28N6	(M+H)+
499.2493	499.2508	3.07	1	61015.06	C32H28N6	(M+H)+
500.252	500.2538	3.56	1	6094.32	C32H28N6	(M+H)+
501.2558	501.2568	1.99	1	609.71	C32H28N6	(M+H)+

Figure A-11. HRMS of N1,N4-bis(2-phenylquinazolin-4-yl)butane-1,4-diamine (**8c**). (ESI/Q-TOF) m/z: [M + H]+ Calcd for $C_{32}H_{28}N_6$ 497.2448; Found 497.2436
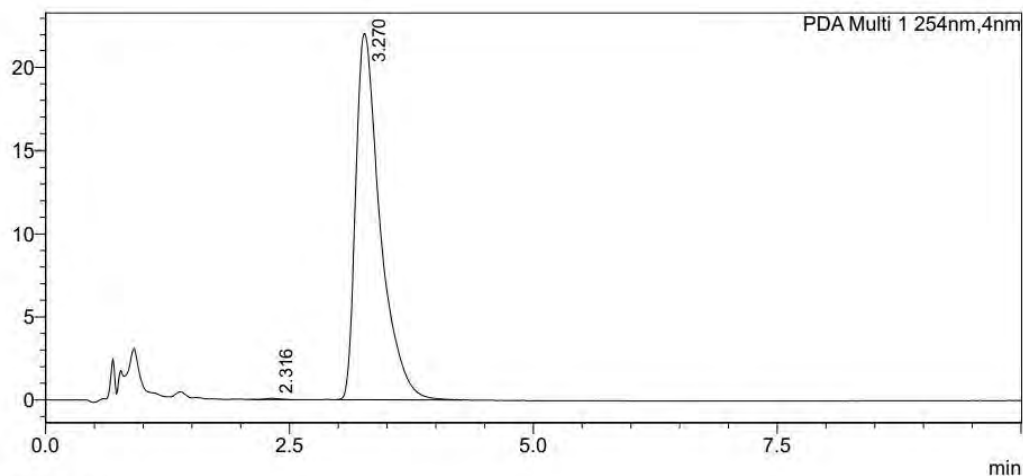
\<Chromatogram\>

mAU

PDA Multi 1 254nm,4nm

3.270

2.316

\<Peak Table\>

PDA Ch1 254nm

Peak#	Ret. Time	Area	Area%	Theoretical Plates/meter(USP)	Tailing Factor	Resolution(USP)
1	2.316	621	0.161	7722	1.338	--
2	3.270	384959	99.839	5953	1.754	2.688
Total		385580	100.000			

Figure A-12. Purity profiling of N1,N4-bis(2-phenylquinazolin-4-yl)butane-1,4-diamine (**8c**). Purity 99.83% [Mobile Phase, ACN : Buffer (60:40) ; Rt 3.27 min]

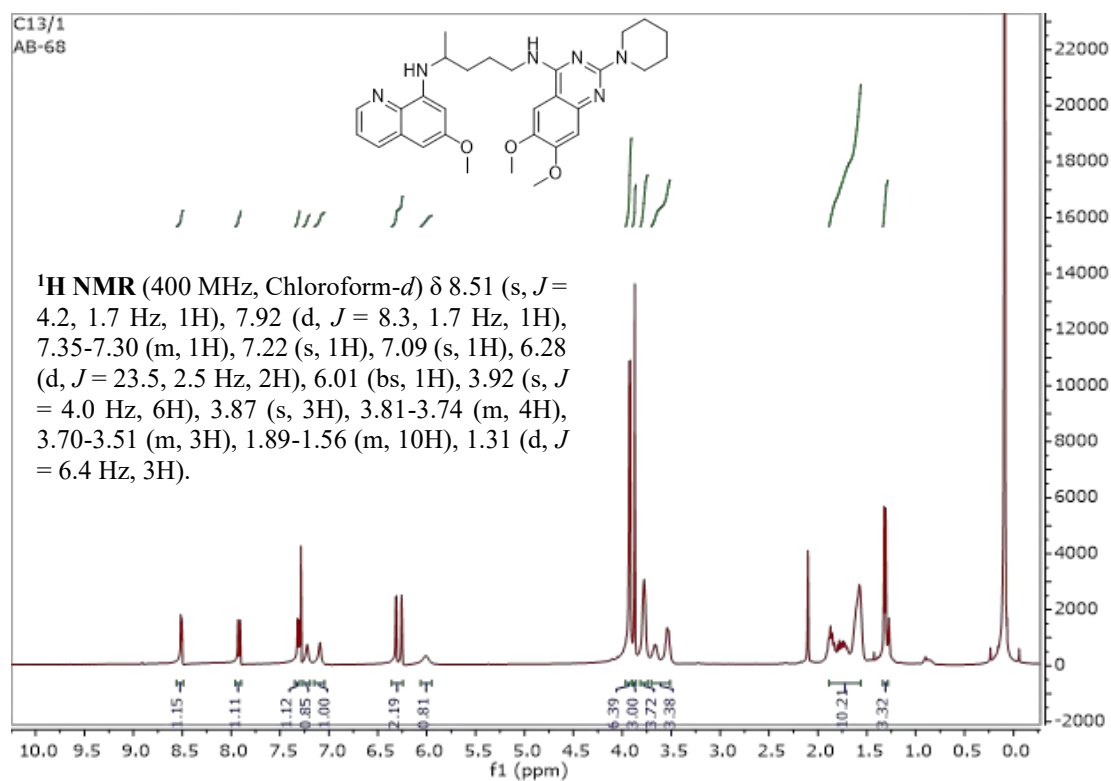**¹H NMR** (400 MHz, Chloroform-*d*) δ 8.51 (s, *J* = 4.2, 1.7 Hz, 1H), 7.92 (d, *J* = 8.3, 1.7 Hz, 1H), 7.35-7.30 (m, 1H), 7.22 (s, 1H), 7.09 (s, 1H), 6.28 (d, *J* = 23.5, 2.5 Hz, 2H), 6.01 (bs, 1H), 3.92 (s, *J* = 4.0 Hz, 6H), 3.87 (s, 3H), 3.81-3.74 (m, 4H), 3.70-3.51 (m, 3H), 1.89-1.56 (m, 10H), 1.31 (d, *J* = 6.4 Hz, 3H).

Figure A-13. ¹H NMR of N1-(6,7-dimethoxy-2-(piperidin-1-yl)quinazolin-4-yl)-N4-(6-methoxyquinolin-8-yl)pentane-1,4-diamine (**13c**)

¹³C NMR (101 MHz, CDCl₃) δ 159.40, 158.54, 154.33, 146.17, 144.87, 144.25, 135.31, 134.77, 129.88, 121.84, 102.62, 96.79, 91.57, 77.34, 77.03, 76.71, 56.40, 56.20, 55.16, 47.84, 46.27, 41.51, 34.07, 25.65, 25.41, 24.48, 23.96, 20.54, 1.03.
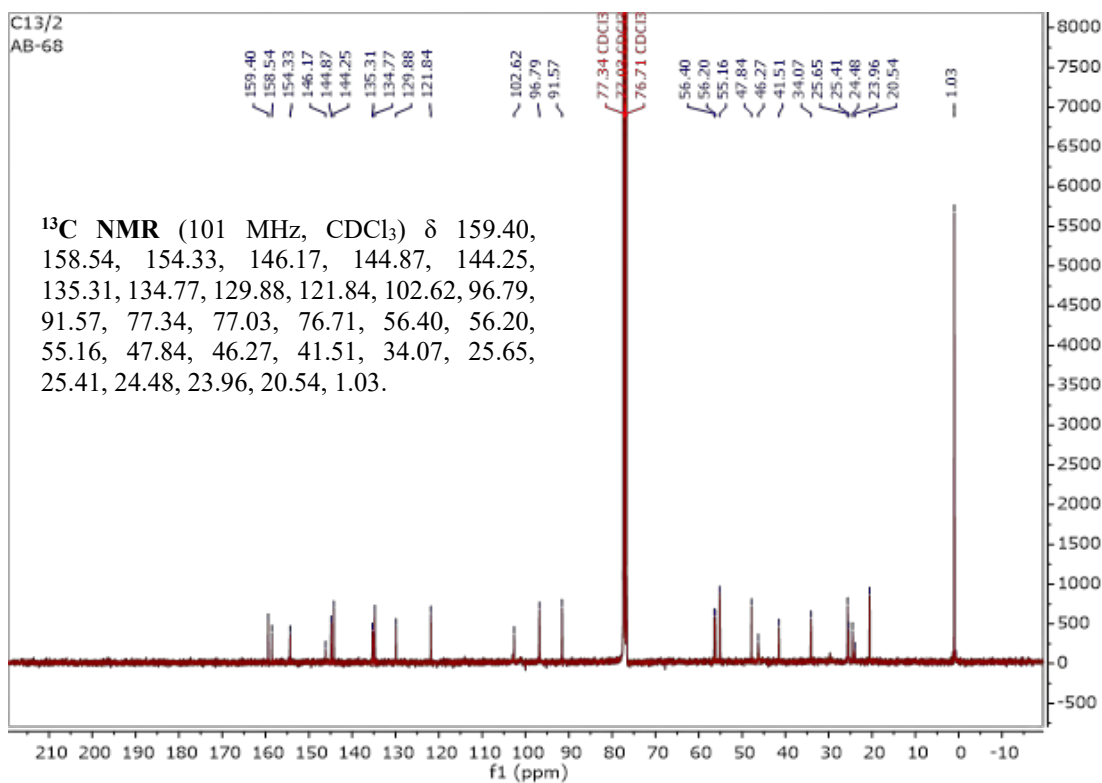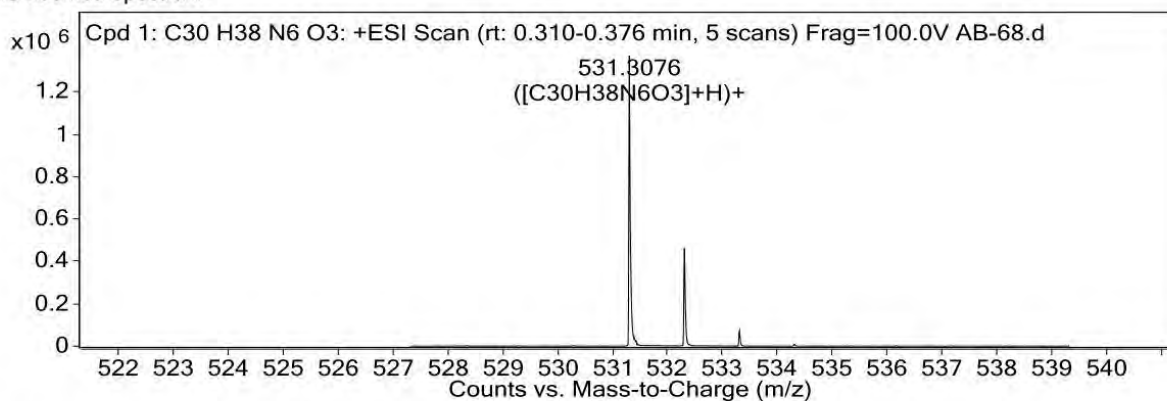
Figure A-14. ¹³C NMR of N1-(6,7-dimethoxy-2-(piperidin-1-yl)quinazolin-4-yl)-N4-(6-methoxyquinolin-8-yl)pentane-1,4-diamine (**13c**)

MS Zoomed Spectrum

Cpd 1: C30 H38 N6 O3: +ESI Scan (rt: 0.310-0.376 min, 5 scans) Frag=100.0V AB-68.d

531.3076
([C30H38N6O3]+H)+

MS Spectrum Peak List

m/z	Calc m/z	Diff(ppm)	z	Abund	Formula	Ion
531.3076	531.3078	0.38	1	1374556.32	C30H38N6O3	(M+H)+
532.311	532.3108	-0.31	1	461264.01	C30H38N6O3	(M+H)+
533.3132	533.3136	0.87	1	72850.77	C30H38N6O3	(M+H)+
534.3157	534.3164	1.15	1	8649.2	C30H38N6O3	(M+H)+
535.3211	535.319	-3.84	1	1043.9	C30H38N6O3	(M+H)+

Figure A-15. HRMS **of** N1-(6,7-dimethoxy-2-(piperidin-1-yl)quinazolin-4-yl)-N4-(6-methoxyquinolin-8-yl)pentane-1,4-diamine (**13c**). (ESI/Q-TOF) m/z: $[M + H]^+$ Calcd $C_{30}H_{38}N_6O_3$ 531.3076 found 531.3078

<Chromatogram>

PDA Multi 1 254nm,4nm

<Peak Table>
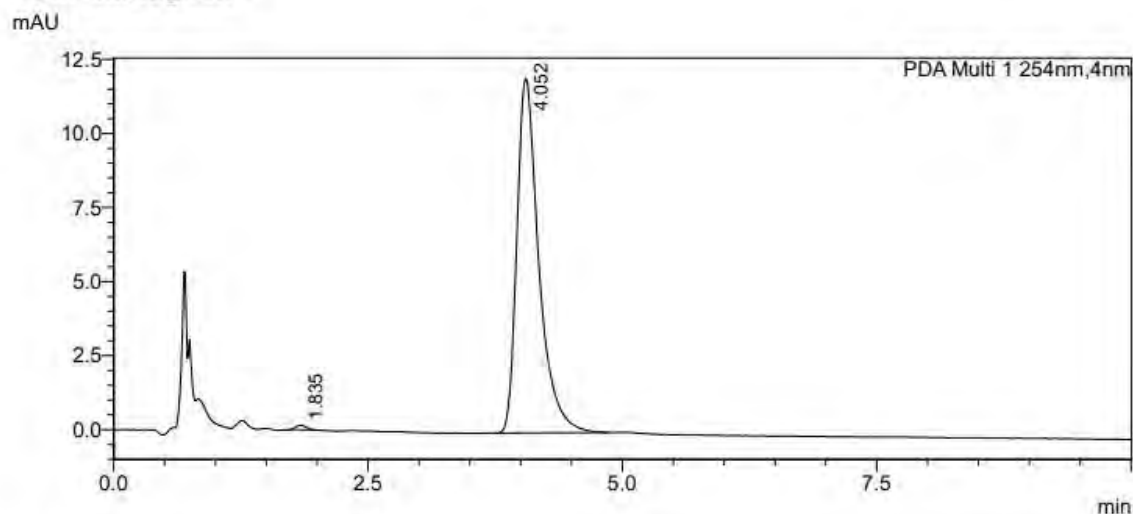
PDA Ch1 254nm

Peak#	Ret. Time	Area	Area%	Tailing Factor	Resolution(USP)	Theoretical Plates/meter(USP)
1	1.835	1128	0.624	1.296	--	8009
2	4.052	179739	99.376	1.521	7.446	11892
Total		180867	100.000			

Figure A-16. Purity profiling of N1-(6,7-dimethoxy-2-(piperidin-1-yl)quinazolin-4-yl)-N4-(6-methoxyquinolin-8-yl)pentane-1,4-diamine (**13c**). Purity 99.4% [Mobile Phase, ACN:Buffer (60:40) pH4.2; Rt 1.52 min]
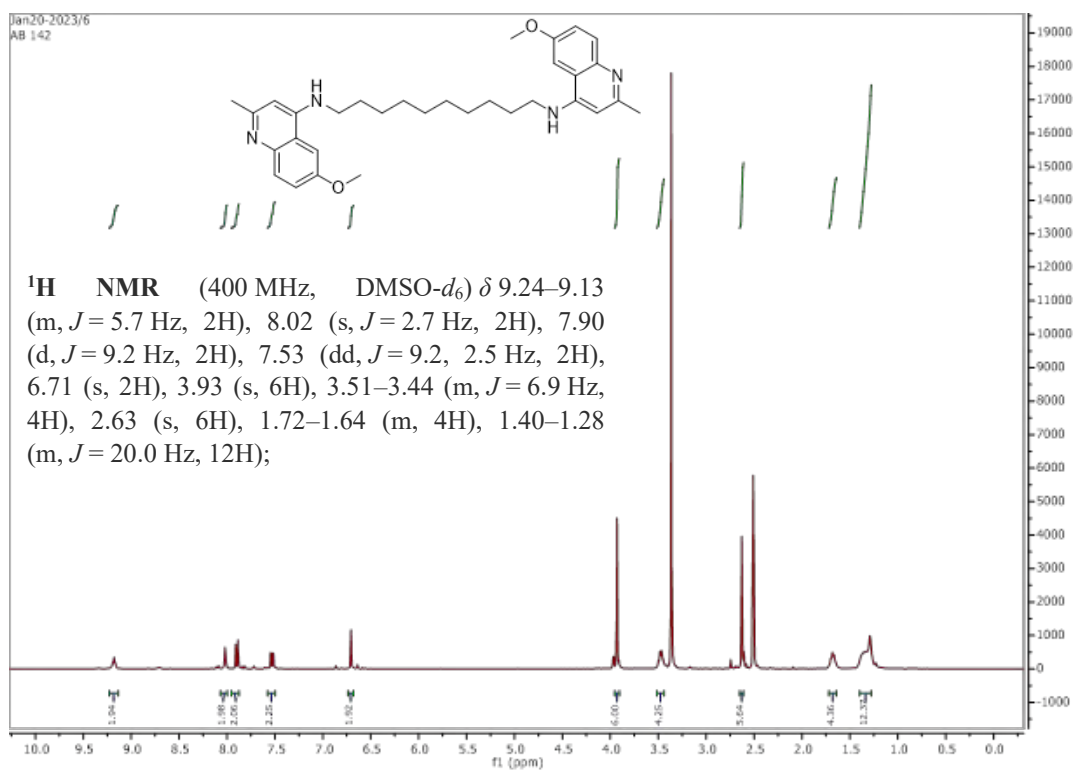
Figure A-17. ¹H NMR of N1,N10-bis(6-methoxy-2-methylquinolin-4-yl)decane-1,10-diamine (**2**)
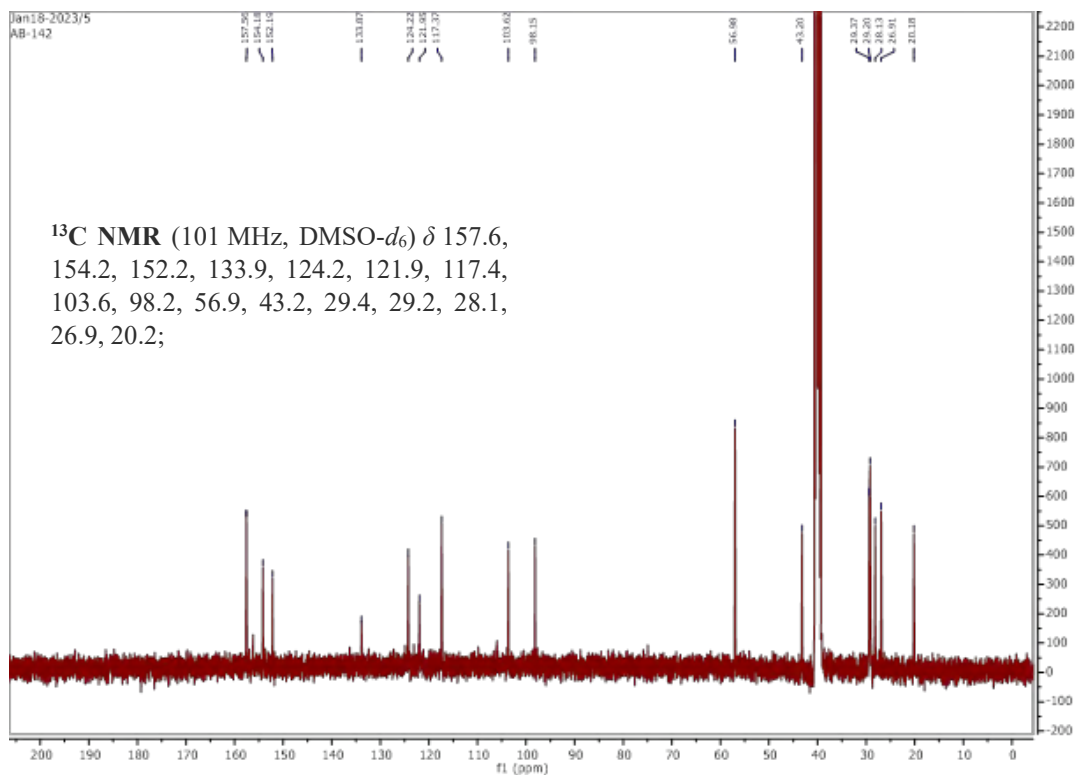
¹H NMR (400 MHz, DMSO-d_6) δ 9.24–9.13 (m, J = 5.7 Hz, 2H), 8.02 (s, J = 2.7 Hz, 2H), 7.90 (d, J = 9.2 Hz, 2H), 7.53 (dd, J = 9.2, 2.5 Hz, 2H), 6.71 (s, 2H), 3.93 (s, 6H), 3.51–3.44 (m, J = 6.9 Hz, 4H), 2.63 (s, 6H), 1.72–1.64 (m, 4H), 1.40–1.28 (m, J = 20.0 Hz, 12H);

Figure A-18. ¹³C NMR of N1,N10-bis(6-methoxy-2-methylquinolin-4-yl)decane-1,10-diamine (**2**)

¹³C NMR (101 MHz, DMSO-d_6) δ 157.6, 154.2, 152.2, 133.9, 124.2, 121.9, 117.4, 103.6, 98.2, 56.9, 43.2, 29.4, 29.2, 28.1, 26.9, 20.2;
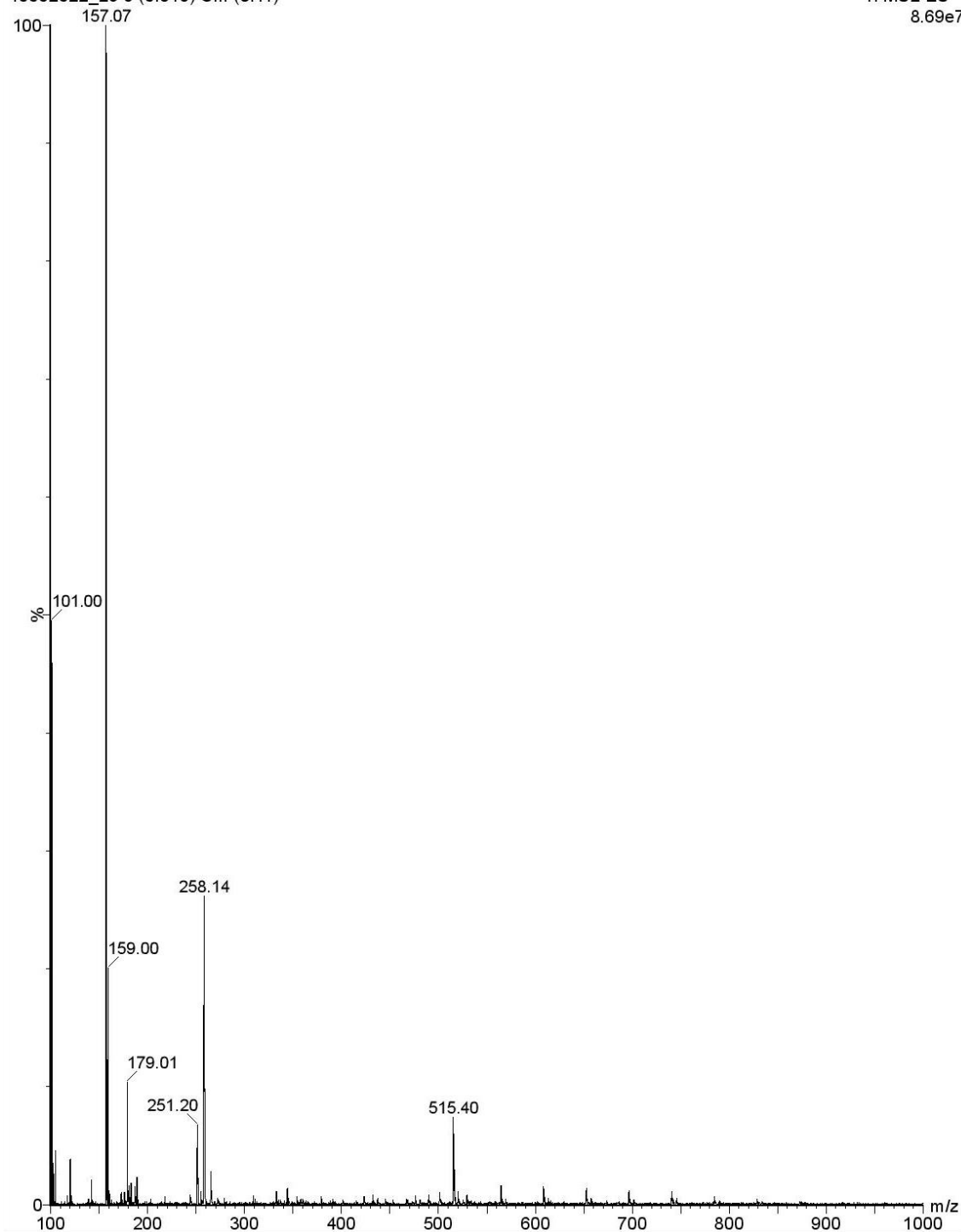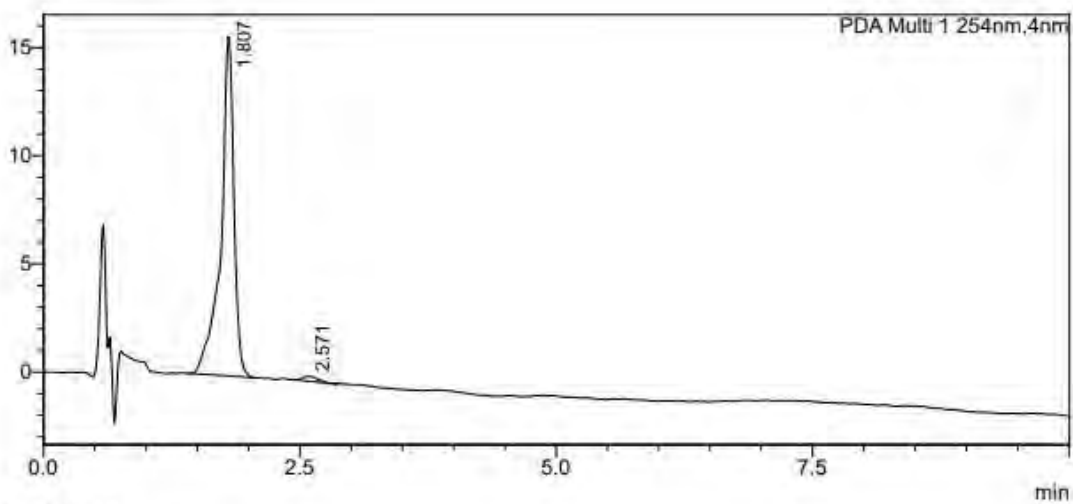
188

Figure A-19. LCMS of N1,N10-bis(6-methoxy-2-methylquinolin-4-yl)decane-1,10-diamine (**2**). (+ESI): m/z calculated for $C_{32}H_{42}N_4O_2$: 514.3, found: 515.4 $[M+H]^+$. Purity 98.4% [Mobile Phase, ACN: Buffer (40:60); Rt 1.8 min].

<Chromatogram>

mAU

PDA Multi 1 254nm,4nm

<Peak Table>

PDA Ch1 254nm

Peak#	Ret. Time	Area	Area%	Theoretical Plates/meter(USP)	Tailing Factor	Resolution(USP)
1	1.807	138508	98.417	7512	0.745	--
2	2.571	2228	1.583	8984	1.677	3.084
Total		140736	100.000			

Figure A-20. Purity profiling of N1,N10-bis(6-methoxy-2-methylquinolin-4-yl)decane-1,10-diamine (**2**). Purity 98.4% [Mobile Phase, ACN: Buffer (40:60); Rt 1.8 min].

ANNEXURE

Publications

Bhanot A, Sundriyal S. (2021) Physicochemical Profiling and Comparison of Research Antiplasmodials and Advanced Stage Antimalarials with Oral Drugs. ACS Omega. 2021 Feb 25;6(9):6424-6437. doi: 10.1021/acsomega.1c00104. PMID: 33718733; PMCID: PMC7948433.

Bhanot, A., Lunge, A., Kumar, N., Kidwai, S., Singh, R., Sundriyal, S., & Agarwal, N. (2023). Discovery of small molecule inhibitors of Mycobacterium tuberculosis ClpC1: SAR studies and antimycobacterial evaluation. Results in Chemistry, 5, 100904. https://doi.org/10.1016/J.RECHEM.2023.100904

Valluri H, Bhanot A, Shah S, Bhandaru N, Sundriyal S. (2023). Basic Nitrogen (BaN) Is a Key Property of Antimalarial Chemical Space. Journal of medicinal chemistry. 10.1021/acs.jmedchem.3c00206.

Kesharwani S, Raj P, Paul A, Roy K, Bhanot A, Mehta A, Gopal A, Varshney U, Gopal B, Sundriyal S. (2023) Crystal structures of non-uracil ring fragments in complex with Mycobacterium tuberculosis uracil DNA glycosylase (MtUng) as a starting point for novel inhibitor design: A case study with the barbituric acid fragment. European Journal of Medicinal Chemistry, 2023, 115604, ISSN 0223-5234, https://doi.org/10.1016/j.ejmech.2023.115604.

Patent

Quinazoline Based Compounds and Pharmaceutical Compositions Thereof, Sundriyal, Sandeep, Bhanot, Amritansh, Pandey, Kailash C, Prashar, Cherish, Chitkara, Deepak, Reena, application number PA. NO: 20231100266

Poster presentation

Presented poster at "Recent Trends and Challenges in Drug Discovery" on 3-4 March, 2023 at BITS Pilani, Pilani Campus, Pilani.

Biography of Candidate

Amritansh Bhanot is a research scholar working in the Medicinal Chemistry lab of Dr. Sandeep Sundriyal in the Department of Pharmacy at BITS, Pilani. He has obtained his Master's degree in Pharmaceutical Chemistry from Punjabi University, Patiala. He has qualified national level entrance exam GPAT 2012 and GPAT 2013. He has published articles in international peer-reviewed journals. He has also applied for patent of his thesis work vide application number 202311002668.

Biography of Supervisor

Sandeep Sundriyal is an Assistant Professor in the Department of Pharmacy, Birla Institute of Technology and Science - Pilani (BITS-Pilani), Rajasthan, India. He received his doctoral degree in Medicinal Chemistry in 2008, for which he was awarded Eli-Lilly Asia Outstanding Thesis Award. Dr. Sundriyal gained ~ 8 years of postdoctoral experience at different USA and UK institutes, including one as a Marie Curie International Incoming Fellow at Imperial College London. He is also a 'Fellow of the Higher Education Academy (FHEA)' of UK. During his postdoctoral stints, he designed and synthesized ligands for various therapeutic targets, including histone lysine methyltransferases (HKMTs) inhibitors as antimalarial and anticancer agents. His current research interest includes antimicrobial and antiparasitic drug design. Dr. Sundriyal's lab employs computational and synthetic chemistry to further the goals of the ongoing projects. He has over 30 research publications in international peer reviewed journals and has presented his work in several conferences. His current research is funded by several Indian Government agencies, such as DST-SERB, ICMR, and DBT. He is currently supervising and co-supervising 9 PhD students.